FROM:

Mr. Pierre Albert Mandel B.S. M.S.
11232 Via Carroza
San Diego, CA. 92124 USA
SS: 469-68-4339
CA. Lic: N8228713
US Patent Pending #08/248506
US Patent Examiner #2506
Date: 06-03-2009
pmandel@ucsd.edu
pierre9ecc1@hotmail.com

The Five Dimensional Obelus Universe Unit and The Time-Warp Theorems.

By: Pierre A. Mandel

The Five Dimensional Obelus Universe Unit and The Time-Warp Theorems.

By: Pierre A. Mandel

ABSTRACT:

This work pertains to, and expounds upon, Einstein's theory of special relativity, and explores, extends, and supports Einstein's laws with theoretical and astronomical subject matter; consolidates relativised gravitational tensor systems, along with the relativised kinetic time-energy, and rest-mass time-energy. Einstein's total energy equations, are re-invented and developed to include inertial, gravitational, and rest time-warp; time-energy kites are for the first time unveiled in this article, and the Lorentz factor is made obsolete with the development of another, more useful polar function. The orthonormal, meta-normal, and para-normal trajectors of time and energy have as component terms three types of energy, which are associated with three types of time-warp, inertial, gravitational, and rest time-warp. These are examined differentially and as functions of space-time-energy, respectively. Proposed are more examples of unified field special relativity equations, and unified singularity time-energy equations, as well as, along with new temporal causality time-energy laws which further special relativity to a new level. Unified singularity theory is proposed and examined. The omni-directional relativised spaces, and meta-normal and orthonormal natures of energy are discussed as well. New subjects of length expansion in a gravitational field, the matter-anti-matter sources for this, as well as the source of the time-expansion effect of gravitation. Classical relativity is explained as sub-set to special relativity; slow and fast light, blue and red-shifted spectral theory, special astronomical objects, post-singularity Doppelganger time regions, and the periodic nature of the Lorentz time-warp factor equation are all examined and explained. Doppelganger subjects (post-singularity quasars, black-hole jetties), are discussed at length. Big-Bang theory has been completely refuted. Observed K.E. is from

debits in rotational and residual G.P.E.; are responsible for and explains fully cosmogonic motion; and is of two types of K.E. both from G.P.E. debits. Residual G.P.E. is dominant; will always be observed as receding velocity K.E. due to gravitational time-space centrism expansion, is represented by the 4th dimenisonal; is noticable as apparent directionally receding K.E. for all subjects with debits in gravity; i.e. away from the galactic core of another galaxy. The arcing of the galaxies is due to the first half of total gravitation, as commonly known. Debits in potential energy are also responsible for the outward spiral effect of the arms, observed in the celestial photographic record. Forming heavier elements, as stellar fusion does, over time produce greater density, hence the predicted debits in G.P.E.; will appear as (+)K.E., receding away from any other similar object, in addition to the revolution component as arcing across the background sky. Cosmogonic motion is for two kinds, both half of total G.P.E.; hence the trend for apparent stellar and galactic inertia is a compilation basically two of balanced permutations of a similar force. Gravitation is as the source for all cosmic motion. The four forces and their four fields of inertia, gravitation, electrical and magnetic correspond to the four bosons, respectively. The previous theories of special relativity extend to 3 dimensions, instead of only one, as previously thought.

The Five Dimensional Obelus Universe Unit and The Time Warp Theorems

By Pierre A. Mandel

Introduction - Overview:

Benjamin Franklin's discovery of electricity in the 18th century, propelled mankind from the Iron age to the Power age. Einstein's developements led mankind to the Nuclear Power age. Newtonian physics, modified by Einstein, necessitated including the obelus of the velocity of light for proper interpretation of the physics of motion, first proposed by Galileo who introduced the physics of moving frame references, compared with stationary ones. In this article the time warp conservation theorems are developed which explains further the receding nature of the galaxies. Attributes of micro and macro temporal displacement (time travel) theory are found to be a function of the relations pioneered by W. Heisenberg, A. Einstein, and Pauli. Also in this article are the theoretical mathematical proof for Einstein's laws. In addition a periodic function for the Lorentz transform is also developed. Causality and Supercausality are also explained and incorporated into the formulary of special relativity. It has been well known that the modern particle accelerators operate according to the Heisenberg principle, the mathematical theory of which is now complete in this article. and is presented in the text. The former will be used to explain and formulate an matter anti-matter reactor to produce an aerospace engine, powered by particle jetties from MAM (matter anti-matter) gamma-ray oscillator decay products.

The Big-Bang, Steady-State, and the receding of the galaxies are in review in this article. Classical relativity is already explained as sub-set to special relativity; slow and fast light, blue and red-shifted spectral theory, special astronomical objects, post-singularity Doppelganger time regions, and the periodic nature of the Lorentz time-warp factor equation are all examined and explained. Doppelganger subjects (post-singularity quasars, black-hole jetties), are re-developed and discussed at length. Big-Bang theory has been completely refuted; rotational K.E. and receding/acceding K.E. from debits/credits in G.P.E. and 4th dimensional dilation effects of time and distance; is a 3 dimensional effect and responsible for and explains fully cosmogonic motion. Proposed and discussed are the sources for the receding/acceding natures of the galaxies as observed in the spectral shifts seen in the celestial photographic record.

Gravitation is as the source for all cosmic motion. The four forces, and their four fields of inertia, gravitation, electrical, and magnetic correspond to the four bosons, respectively. The previous theries of special relativity extend to 3 dimensions, instead of only one, as previously thought. Also discussed is the phenomenon of spectral ’blue-shift’. Additionally, the concepts of both "fast-light" and "slow-light", are under review and explained. The constructs of classical relativity are explained as subsets of discrete special relativity; are found also to be time-warp related.

From this first law of A. Einstein, the calculation of c is possible. The speed of light is easily derived from this first law as: $E = h\,\nu$. From the pre-amble to the second law c is shown to be the greatest velocity possible by taking the minimum path in time; thus becomes the obelus by which all the other velocities measured by.

Hence between any two reference systems, the second law becomes the conversion - warp factor. Einstein’s first part of the second law, is easily derived from the latter part of the second law, when c is coupled with the obelus of warp factors for both length contraction and time contraction for moving frames of reference. It will be shown that a quantitative conservation laws of space-time warp stem from Einstein's laws; discourse on the nature of the causal past and supercausal future along with the differential time-conservation equations are debued for the first time in this document.

According to Newton's first law of thermodynamics, how an infinite space-time system renews itself, given cooling and eventual heat death implicit in adiabatic systems, is not clear. But from figures 7 - 7k, this is cleared up. For reason that residual gravity with Eqs. 2-3, from related figs. 7-7k, it becomes clear that orthonormal (rest-mass) formation will occur predictably and is accompanied by a net decrease in energy; as hypotneuse is longer than side, rest mass formation is accompanied by a net decrease in total gravitational energy from that of naked gravity alone forms a greater potential energy. This is true for positively biased gravitational time-warp, as well as for inertial energy; added rest-mass leads to a lesser/greater energy, as the sign of the Pythagorean hypotneuse would dictate. Related paranormal components exist as features of time-warp geometry is as depicted in figs. 2-2dii and figs. 7-7k., e.g. with K.E. as normal and *R.W.* as paranormal commonly is associated with orthonormal specially relative rest mass-energy. The "Why" of modern physics understanding needs first to explain the origins of matter as a function of time-energy. This document does that. Is the universe a closed set, by what dimensional set? Where does the first hot stem from. Could there be other universes? Can time-fissures exist? Can time-spacee bubbles exist which, by analogy, would occur as with common blown glass?

There are two realms of time sheets and are depicted in fig. 2; shows how time-dilation varies for the moving frame (moving clock). Thus: $\frac{d\,(x_{lgt})\lambda_{wf}}{d\,(\Lambda_0)\lambda_{wf}} = c\ (1)$. Adding the co-factor expression still doesn't change the local velocity of light, but rather supports Einstein's first law of special relativity. The indeterminate form for this co-factor is still equal to 1, at $v = c$. Regarding the The analysis of the singularity at c typically involves the Sandwich and Cauchy theorems, in the approach to accommodate the terminus there when at zero rank. The proposed method requires the adoption a new definition, namely the concept of a "Super-Origin" (+/- infinity).

The five dimensional Universe Unit theory is based on the proposition that there exists three states of velocity: that velocity at 0; that velocity at less than c; that velocity at c; and that velocity greater than c, (if that were possible). This corresponds to the three time-warp or moving frame time conditions, namely: $\Delta\Lambda' \leq 1$; $\Delta\Lambda' = 0$; and $\Delta\Lambda' \geq 1$. where $\Delta\Lambda_0$ is an earthbound observatory time's clock rate, and $\Delta\Lambda'$ is the moving clock rate. Time warp is defined as the ratio of these time-rates. Gravitational tensors are negative in direction to those of vectors. Energetically this is the case with gravity. This always increase time rates; with decreases in gravity (i.e. orbit) time slowing would occur until reaching 0g, which occurs with escape velocity, e.g. is why an astronaut's watch ticks slower than that of one on Earth, when in orbit. Time's tick would continue slowing until the inertial scalar for time reaches almost 0, but being bound by the minimum that the nature allows, i.e. considering Heisenberg Uncertainty, introducing quantum mathematics - minima of time-energy momentum-span couplets. The mutual obelus of one of the partners of time-distance induces obelus warping equally in 3D space. These themes are explained in greater detail in this document. The fact that the light speed constant is the greatest velocity, becomes the function by which all the others are measured by, hence is used in the obelus fraction of Einstein's second law as an implementation of the the light constant in the previously reported Galilean moving frame transform. The dual nature of light is further developed as a geometrically described effect; is Pythagorean by nature of the trigonometry between K.E. and R.E. and solves the dual nature of light (particle and wavelet as R.E., K.E.). For the first time the geometry is developed and explored fully in the appendices of this document. The figures attached accompany and reveal the analytical geometric properties are as new theorems and academic mathematica. The velocity of light: c, as constant is fully explained as a local effect, from another reference points differences arise, but in any one reference frame the are all alike, will measure light as c. The local cancellation of time and space warps makes this so. The light record is known due to Doppler shift in frequency, to exhibits equally red and blue spectral shifts. Also due to obelus cancellation the Doppler shifts are in general immune to the effects of special relativity. Luckily this means the Doppler red-shifts and blue-shifts can be used to measure directly relative velocity.

Furthernmore these effects stem from physical laws of nature. It is true that the same causal laws are at work in PEP accelerator MAM rings is true also for wire coils, they react from electrical and magnetic field minor interactions. Two sample designs are depicted in figs. 5a, 5b, and 5c, of the illustrations. The main idea behind them involves the use of a mandrake in a particle stream; produces a pull force ortho-normal to the energetic charge-flow time-warped areas (figs. 5a-5d). Rigging with a central magnet, toroidal ones elevate by pulling a craft upward; the linear ones pull their way along.

This theoretical claim can be proven experimentally, connecting a bicycle wheel to a digital bathroom scale at the axle; depending upon which way the wheel is rotating, the torque force vector from rotation will affect the measured weight. This torque force vector acts as a stand-alone jetti-propulsion type expulsion from a single axial source, thus an object is easily propelled using essentially only electricity, as from a nuclear pile as a pseudo-voltaic effect as an energy source e.g. using solar cells with radiactivity as a battery charger; could propel a rocket by ion accelerators of all kinds, up to and including left-hand ruled MAM particle accelerators time-warp induced propulsion. Electrical sourced engines could power crafts in this way one day and they are far cleaner than SRM technology, and would act as a back-up propulsion system, only. Since half-lives of nuclear piles last an extremely long-time. A nuclear electrical engine could stand extended service times; even Tokomaks have service times which would be extended once special relativism is taken into account.

The sources of the production of mass and answering the question of where does the first particle come from are not readily apparent. It may never be known how the first mass is produced. Two main causes come to mind, energy’s cooling vs. energy’s decay as occurs in nature. The fact remains, because one mass unit can occur implies another can occur also. Beyond star formation, thermodynamic heat death theory normally confounds theorists of adiabatic Steady State. Beyond this there has only been LaPlace’s nebular theory; not much more was known. But in this document new theories are proposed, which are rigorous and easy mathematically. Methods of mass production include also, through gamma ray decay and are also explained and re-inforces MAM production through what is in essence a cooling/conversion of the photon to mass. Methods of separation, and particle generation/collection/concentration without clumping nor annihilation in MAM technology, are more the subject of the task for today.

Recently blue-color shift in the astronomical emmision spectra are in actuality Doppelganger-realm objects. They are predicted by the theories proposed within this document; are termed "defective" cross-overs since they defect to Doppelganger realms. They appear blue-shifted due to the acceding 4th dimensional velocity. The graphs of which depict and explain the mathematical consideration of special relativity first proposed by Albert Einstein et al., used in this document to elaborate upon the structure of the universe. The quadrants of fig. 2a, the slopes, and their periodic then hyperbolic functions, are reproduced in figs. 2ci, 2di. Many new laws governing these phenomena are re-derived which fuly explain the anomalies of the physics apparent; is much as Copernicus’ influence over Ptolomy’s view. Also held in review is Big-Bang theory, which is a non-relativistic and insufficient view of cosmogony. The physics of special relativity is more accommadating and comforting this way. As such, the facts presented in this document are easily deducible using today’s mathematics.

The lambda factor as used here is defined as the Lorentz nucleus to the (+) half power, thus for the distortion is according to: $\lambda_{wf} = (1 - \frac{v_x^2}{c^2})^{½} = \frac{\Delta\Lambda'}{\Delta\Lambda_0}$. Generally speaking momentum and energy vary with velocity accordingly: $E_{rel_{K.E.}} = \int v_{rel} dp \approx \frac{(f(m v^2))}{g(v^2)½}$. Also regarding energy: $E_{rel_{K.E.}} \approx \int f(v\,dp) = \int f(p\,dv)$; becomes: $E_{rel_{K.E}} \approx \int \frac{f(v\,dp)}{g(v^2)½}$.

Relativised momentum-distance is central to relativism and when integrated yields K.E., thus relativsed once according to known algebraic rules. The relativised energy comes from a product rule integration by parts (Green's Theorem), as the inertial frame has velocity components i.e. the force differential quartet. The v_{rel} is mounted in the following kinetic energy differential is as: $dE = \frac{dp\,dx'}{d\Lambda'} = \frac{dp\,dx\,(i)\lambda_{wf}}{d(\Lambda_0)(i)\lambda_{wf}}$. The same is true of the velocity of light.

If the causal past time dilation factor is considered to be the nucleus of the famous Lorentz factor, thus: $(i)\lambda_{wf}\Delta\Lambda_0 = \Delta\Lambda'$. This repeats itself in length contraction of spaces as: $(i)\lambda_{wf}\Delta X_0 = \Delta X'$. When added to the momentum expression, and then integrating the total inertial relativistic energy is calculated, as in Eqs. 1a, 1b, 1c, and 1d. When the relativistic gravitational energy is added, Eqs. 2-3 result. The property characterizes Unity as that point where from which one may access any point in space simultaneously. The speed of light is a type of pipe to infinity, and is the limiting point for inertial frames due to the central obelus validity in the physics. Thus for inertial frames this point constitutes also an end point of a string. The harmonic node formation that occurs at that time extinction point of c, is reflected in fig. 2a, the inertial frame graph. The gravitation interpreted as potential energy holds a negative value in the central Eqs. 2, 2a, and 3. The derivative of the inertial warp is calculated, and graphed in fig. 2c, 2d. The sign negative of fig. 2c, is 2d. When these time warp pictograms are superimposed an energy - time-warp conglomerate emerges as fig. 2e.

The nature of the special relativism of the light point and the bi-partite temporal nature of the universe, is made knowable when through the proposal of a "Super-Origin", O_∞, the nature of the light point singularity, becomes clear, as indicated in figs. 2ci, 2di. The Super-Origin implies reaching a source for maxima in integers both positive and negative. The switch over occurs as that for the decimal origin. In figs. 2ci, 2di, and 2ki, there is implied also a free-fall condition (in this case time-dilation) from what was formerly considered a "pike" maxima. It is more realistic a consideration thus tool, than the Hermitian alternative. The former serves to explain the latter, symbolically. Also, one may be substituted at any time when encountering maxima of any type.

If: $(i)\lambda_{wf}$ is the nucleus of the Lorentz factor as: $\frac{1}{(i)\gamma}$, and if $\Delta\Lambda_0\,(i)\lambda_{wf} = \Delta\Lambda'$, then the $\Delta\Lambda'$ is the moving frame's slower clock. If the Einstein obelus factor of $\frac{v}{c}$ is decomposed, the elements permute to $\frac{\Delta X_{vel}\Delta\Lambda_0}{\Delta X_{lgt}\Delta\Lambda_0}$; or $\frac{\Delta X_{vel}\Delta\Lambda'}{\Delta X_{lgt}\Delta\Lambda'}$; or $\frac{\Delta X_{vel}\Delta\Lambda_0}{\Delta X_{lgt}\Delta\Lambda'}$; or $\frac{\Delta X_{vel}\Delta\Lambda'}{\Delta X_{lgt}\Delta\Lambda_0}$; when the two permutations of Λ equate and cancel the quotient becomes: $\frac{\Delta X_{vel}}{\Delta X_{lgt}}$. These two even permutations of the obelus set the stage for what is to come regarding the remaining theoretical developments of this digest. In that case of even time tense the derivative can be computed with respect to v, yielding figures 1b, 2a, 2b, 2c, and 2d. Another law of Unity pertains to c being the fastest velocity possible in the universe. Considering the above quotient, it follows that the mass-less propagation of an E-M field front functions naturally as a function of a photon's field amplitude-energy, it's frequency and it's frontal propagation velocity particular to the medium. If the E-M field front of common energy is considered as occurring in the moving time frame Λ'; and if the constant c is as $2.998x10^8$ m/sec, the relativised time frame velocity would by comparison be ∞ m/sec. In general for the pre-singularity causal past-universe, gravitational objects can stem from inertial ones inertial ones; can evolve gravitationally through mass dilation.

Time hyper-red environments occur for both inertial and gravitational subjects, and are part of the photographic record of central regions near the cores of galaxies; already at sub-light galactic cores exhibit the gravitational bluing predicted; is readily noticed among the largest of the stellar objects there. To another galaxy the core unit appears to them, as a red-shifted, object, due to the direct reaction to the residual G.P.E., showing a net reactive residual K.E. Observed K.E. is primarily from residual G.P.E.; is responsible and explains fully cosmogonic motion; and is of two types of K.E. from G.P.E. Residual G.P.E. is dominant; first observed as receding velocity K.E., as stated, proved in this document, is solely due to the gravitational time-space expansion, noticed in the photographic record as receding from any other similar gravitational object. The arcing of the galaxies is due to the first half of total gravitation, is already known. Debits in potential energy are also responsible for the outward spiral effect of the arms, observed in the celestial photographic record. Forming heavier elements, as stellar fusion does, over time produce greater density, hence the predicted debits in G.P.E.; will appear as (+)K.E., receding away from any other object, on top of revolution and arcing aross the background sky. Big-Bang theory has been completely refuted; rotational K.E. and receding/acceding K.E. is from residual G.P.E. 4th dimensional dilation effect of time and distance; is a 3 dimensional effect, is responsible for and explains fully cosmogonic motion; is proposed and discussed as the source for the receding/acceding natures of the galaxies observed in the celestial photographic records. From forming heavier elements, over time are known to produce and burn heavier elements, which change the gravitation as well. Thus, the trend to debit G.P.E., showing from time dilation as receding (+)K.E. Thus from debits in G.P.E. comes the apparent receding nature, from credits in G.P.E. comes acceding appaent motion. Thus cosmogonic motion is explained as two fold, i.e.

rotation, and/or receding/acceding natures. The effects of gravitation as the source of all cosmogonic motion. The goal for man-made time/space warp producing designs is with space propulsion in mind. The previous theories of spcial relativity did not extend to 3D; were commonly thought to be planar in effect. Interferometry by coincidence has proven that the planar view of special relativity is false, since no planar distortion is observed.

Did light create the metric, or the time? Or, did the time develop for light to propagate through? It seems counter-intuitive that the light energy is related to time, differently than to mass. However, it seems that light spans the entire metric. Photon path studies of light near or about Dark-Matter reveals that time-distortions from gravity would still exist around such non-luminescent objects, as theory would necessitate. It is a mythological event that theoretically released from formlessness all things. This would fulcrum from a point where space-time sets and energy-momentum sets unit. Another view-point maintains that first the metric, then time, and then E-M (light) were in that order created for the latter to be contained by the former. From another viewpoint, light which supra-cedes time and could thus be reasoned to separate the temporal regions, thus in turn creates a channel in time to self-propagating through, thus is in part responsible for dimensionality (3D). (See fig 5. - Creation Plate (circa 1610)). How would astronomers ever clear up this theoretical controversy conclusively one way or another? If the sepals of events-consequences are preceded by the petals of time, would the unfolding lay in the center of the flower-candle of the real?

The relativistic conversion of the mass-less self-propagating E-M fields into de Broglie momentum was set into stone through the use of constants of proportion throughout, Planck - Heisenberg constants. Thus the inverse proportionality in the $E\,\Lambda \longleftrightarrow GPE\,\Lambda \longleftrightarrow P\,X$, where Λ is the variable for time. The fact that these are equate using an inequality implies minima and maxima of the factors.

For similar reasons light and their nucleonic counterpart influenced by magnetic and electric fields. The effect of electrical voltage upon a magnetical field is by drag responsible for the different velocities of electromagnetic waves through different media. Snell's refraction and the Fermat effect for all of EM and light is as wave phenomena act and is essentially only a re-iteration of Einstein's first law: $E = h\,\nu = \frac{h\,c}{\lambda_{wv}} = p\,c$. Since the velocity of EM is always constant, naturally higher frequency light takes a shorter path due to the increased non-sympathetic electric drag from the greater changing electric fields of higher frequency wavelets upon the waveform; induces the curtailed change in path. This type of magnetically induced electric field drag affects the larger wavelength less since the changing electric fields are less in longer wavelength photons, hence take the longer path. The former is more hindered, hence takes a shorter path to make up for increased clock time from induced stearic ion-field hinderance; keeps velocity constant. Refraction of path has its parallel with refraction of time per the the Doppler effect; spectral shifts from a moving frame are due to the increases/decreases in distances-time and the frequency changes associated with the moving frame. If the velocity changed instead of the frequency, there would be no refraction nor Doppler effect in any scenario.

When the doubling of $(i)\,\lambda_{wf}$ is taken into account, the equation assumes interesting proportions. Yes, it would be nice to have such a system, such that when rest energy is subtracted, the total energy becomes the remaining kinetic energy as per Eq. 1. This lends support to theoretical concerns regarding placement of galaxies in a sea of time; would by special relativity be measured by their depth in time dilation, as determined by their gravity compared to another galaxy; a quasar would thus decrease in mass due to Doppelganger time hyper-red conditions, fig. 2m. Such Doppelganger subjects are both associated by spans greater than that of c, and by decreases in energy once over the spike form excessive backwards racing in time. The relativism of a galactic spiral is a function of the potential energy of the galactic core, and it's component stars. Quasars that occult reach and then exceed the summit of c at "sea level" by analogy; they jump from sub-light to another sub-light - time-hyper-red Doppelganger temporal areas. The isomorphism at c and its implications in time-energy are the focus of this document.

Physicists need to prove or disprove whether in light of the "Background Radiation" vs. Gaian release theory. If the background radiation is an echo of a greater, a more majestic super-alternate expansion, was there a Big Bang, through an Mega-Super Nova? A greater burn of time expansion seems more apt, as no Mega-Nova remnant has been found. However the back-ground radiation may point to a greater nebula if its source is cosmogonic instead of mere cosmic radiation energy. Still the four fields and the four boson energies are simple sums and remains a sophomoric challenge to reproduce these equations; steering our view of common astro-mechanics toward a dual differential treatment, e.g. Heisenberg's uncertainty equations.

To re-iterate if: $\frac{1}{(i)\,\lambda_{wf}} = (i)\,\gamma$, then $(i)\,\lambda_{wf}$ represents the discriminant nucleus of the causal past Lorentz factor, the other being the causal length contraction factor: $(i)\,\lambda_r$. The work-up of the Galilean inertial frame incorporates a central obelus as: $\frac{v}{c}$. This leads to: $\sqrt{(c^2 - v^2)}$ for a general relativity statement comparing any moving object's velocity to that of light. In orbiting systems, one could conceivably measure relativistic gravity's influence by differences in clock performances as well as that for inertial objects.

What is at hand is the general time-space of 3 dimensions vs. Energy of 3 kinds. As gravitational force is potential, when added with rest energy, forms the bottom triangle of a half-kite of right triangles; the inertial being the top triangle of fig. 7. A similar triangle half kite ortho-normalization occurs for time-warp as well, fig. 7a. In this arrangement there is rest time-warp and meets the in situ condition. As a term in the energy equations this occurs as a product of rest energy and local time. Meta-normality occurs between kinetic energy and gravitational energy. The rest warp and rest energy forms a second meta-normal rest 2-vaned diameter is as paranormal to the orthonormal K.E. (fig. 7c). Congruent to Einstein's amble to the second law, and represented here in this document as λ_{wf} represent length contration and time contraction concurrently. The inverse arrangement of these constitute a type of zone of time inhibition - exclusion in the time-space coordinate continuum; lie disjoint from each other, (See Type III, Type IV high-energy cross-overs).

Expressions of engineering efficiency, the energy time-warp formula develops as: $\frac{2\,\Delta P_0\,\Delta X'}{\Delta E_0\,\Delta\Lambda'} < 1$; if the terms are equated the obelus becomes a line rather than an area. In the case of inequalities, each one constitutes one of the two areas either above or below the line of the equality. Since there are three types of energy, there are three constants of proportion associated with them. For gravity, there are four sign changes, distributed over two terms. Thus the reversal in time-warp, is typical tensor in general. In parallel with the inertial, there exists an equivalent gravitational expression for Heisenberg constant, or: $(-)\bar{h}$. This comes from the gravitational equivalent for time-energy, thus: $(-)\Delta\, G.P.E. < \left(\frac{2\,\bar{h}}{(-)\,\Delta\,\Lambda'} \right)$, becoming: $(-)\Delta\, G.P.E. < \left(\frac{(-)2\,\bar{h}}{(+)\,\Delta\,\Lambda'} \right)$. Differentially this appears as: $(-)\,d\,(G.P.E.) < \left(\frac{(-)2\bar{h}}{(+)\,d\,(\,\Lambda'\,)} \right)$. This construction proves two things. First, if the negativity for values of Λ' for gravity (< 0 as in fig. 2), the sign negation migrates to the Heisenberg constant, in so doing renders the time-warp positive in value. As a general rule, as pertains to the time part of time-gravity the following function applies: $\Lambda' = \Lambda_0\, r_t cos\,(\,\varepsilon\,)$, for $\varepsilon > \frac{\pi}{2}$. Time-energy of any kind, is always positive, however differential time-energy is always negative. This is true for time-gravity as well. The universe runs primarily on differential time-energy. Thus kinetic energy from gravitation, or from man-made jetti-propulsion always shifts from greater differential time-energy to lesser differential time-energy. This is true always and is as a general law of conservation for differential time-energy. When the relation $(i)\lambda_{wf}$ is examined at the terminus, it becomes zero; but $\frac{(i)\lambda_{wf}}{(i)\lambda_{wf}}$ remains equal to 1. This is true for the proposed polar function as well. The derivative of this quotient, however is as expected equal to zero. The gravitational singularity is as a tensor; switches to being a vector at 0g, and is non-trivially tied to escape velocity. Thus at that point inverting and becoming a vector for any orbiting system of masses. The reason for occultation is clear. Far red stem from far short UV; Doppler shifts continue in object evolution until from the invisible to the invisible; extreme UV $\rightarrow$ extreme infra-red shifted status, thus occult. Since the time warp factor reaches terminus, the energy we receive on earth reaches terminus, too (See Eqs. i-viii later in this text). Beyond this lay the Doppelganger post-singularity regions of time. As such, they bear unique mathematical attributes.

Theoretically one should be able to measure "double-caduceus" electric and magnetic fields and their propagation reticulation and velocity; thus measures the span of light's components to us on Earth comes to us in terms of un-relativised distance in relativised time. Thus for light, $p\,c = h\,\nu$; furthermore from this the field relations of Maxwell are briefly as: $\nabla \cdot (\vec{E} \times \vec{B})$.

The slowing effect of a photon also changes the path and trajectory in response to the velocity difference of light through molecular solid/liquid media, taking the shorter path which occurs and corresponds to a slower velocity, thus taking the shorter path makes up for the longer elapsed time; hence the wavelet remains at c-level in time-dilation. However the cause is in extrema shows as the short-wave UV's effect in translucence-refraction $\rightarrow$ in the average crytalline earth.

But Fermat's principle - the refracrion law; is often mistakenly interpreted as a time dilation effect, but that is not quite true. It is actually an ionic stearic effect usually crystalline media. The time dilated effect pertains to the Doppler formula and involves moving frames. Snell’s and Fermat’s laws and rhe refraction phenomenon as a whole are path adjustments that EM makes due to the frequency induced drag on the wavelet that the media introduces. Thus for cyclical funtions that feature changing sinusoidal electric and magnetic fields, that: $d(\sin(\theta)) = \cos(\theta)$ and, $d(\cos(\theta)) = (-)\sin(\theta)$. This is what characterizes the crystalline lattice ion-interference effect.

Through any media and for any wavelet, the velocity of the an EM-front is always constant. As stated , if the velocity changed it would be measured instead of the frequency change; the frequency would remain constant. This is true for the Doppler effect as well; frequency changes instead of the velocity of the wavelet due to the differences that a moving frame introduces. Otherwise, spectral shift would not occur if the velocity of the light changed to accomodate the moving frame. This is not the case, due to the primacy of c for any reference frame, that fact is attibuted to the obelus cancellation with of space warp with that of time. These concepts is explored and developed, in this document, for both matter and anti-matter.

Still another example of this lay in the paradox of the pre-amble of Einstein’s second law. The conflict between general relativity and special relativity, concerns the fact that two photons (wavelets) traveling in opposite directions; will one measure the other as twice the speed of light relative to the first? Why this does not occur is as simple as the Doppler effect for reason. Again, by Einstein’s first law, the frequency of the passing wavelet is greater, not the velocity of each wavelet relativie to the other. They will still measure each other as at c.

Another example of electrical charge affecting wavelet velocity, can be seen to occur and is easily demonstrated in a simple experiment. If a magnetic compass is exposed to a fully charged battery, the needle will swing. If the same magnetic compass is exposed to an empty battery the needle will not swing. Thus polar stearic considerations always effect the velocity of EM through any medium; hence transparent vs.

translucence vs. opacity common to many crystalline elements. This was first noticed by E. Hall, as the Hall effect.

More evidence lay in the fields of the optical rotatory and chemical stereoisomerism of common organic chemistry (polarimetry), to support the view that these are stearic, polar, and are handed phenomena in nature. The solution to the controversy would be to generate transparent/translucent levo, dextro, and racemic prisms of a suitable solute to research further the nature of refraction.

Generally time-warp is always a function of the inertial, the gravitational, or the rest energy. The aforementioned is an example of the velocity of light integrity as a constant, and is additionally coupled with a unity law for time-warp. Describing both involves taking basic functions to their limits, from which we wish to explain Einstein's three laws seen in the macro/micro photographic record of nature.

It is easy to conceive that the velocity point of c is portal to time travel but that is only half the story. There is also the gravitational to account for. The analogy for time travel pertaining to special relativity plays much as Aesop's tortoise vs. hare on a time-race track. The tortoise is the sub-light time traveler and the hare moves forward at earth's rate of time. The hare naturally advances beyond the tortoise on the track of time, but upon return to the hare's time-realm of Earth, finds he cannot return to the point where he began. The third generation hare is far displaced into the future; and as such, would naturally have long forgotten about the race with the original astronautical tortoise, who would also naturally win the race. That's why it is important not to visit the high bias time-warp environment. One easily runs out of time, compared to one who does not. Knowing this would naturally appreciate the idea of space travel, as an average astronaut would last longer than an average Earth man, and would give rise to the idea of finding one's "time-legs", in space travel. As we will see, such things also exists in the cosmos.

If a skew tensor of 180 degrees is applied around the origin of fig. 2a, one can easily see that at the pinnacle point in time occurs at light speed; the most efficient way of travel is at the top of the rotated figure (c). Analytically hyper-c inertial conditions would bring a traveler nearer to their goal, but would be less efficient than at c, where time passage stops entirely. The notion is also that at hyper-c another temporal bay which is predicted and broached in the mathematical derivations of Eqs. 1-3, and of figs. 2b, 2c, 2ci. How is this significant?

The isomorphism in time-sheets of fig. 2a, is quantitatively asymmetric, but qualitatively shows two sheets or bays of the temporal and the changing time rate bias. The time function undergoes a discontinuity through a sign change of the time-ordinate as dictated by the Heisenberg constant's limits upon time-space, and energy-momentum, which the graph-set shows. A negative dilation at hyper-c as displayed in figs. 1a, and 1b, translates to a positive time compression or time warp for the traveler. Due to the fact of time-contraction, energy expands, and increases-bloats. Beyond c, Doppelganger warp factors become time-mached values: ($\partial t' > 1$); past/future time-travel ensues. Doppelganger energies decrease due to these expanded time values. The subjects also become blue-shifted.

To conserve momentum a slightly heavier object would move at a lesser velocity, and the converse is true too. For the moving object, in their time frame, experiences mass constriction (weighs less), by a factor of 1/10th in mass at 99.5% light speed. This appears to us in the laboratory/ observatory as a mass increase of ten times. The clue is to consider what happens to the element of time. The integral of the momentum for the inertial K.E. is solved differently than for the gravitational time-energy. One is solved using the by parts approach; half the gravitational energy is exchanged as kinetic to the total for that mass determined system of variables, half remains; (fig. 2q).

The integration by parts solution to the area of any time-energy trapezium has for any inertial frame occurs for us here as a solution to the total time-energy goal. The quartet generated the integral of the force is equivalent to the total inertial energy. Briefly, and in review: $\vec{F}\,\Delta\,\Lambda_0 = \vec{P}$, is for momentum, as $\vec{F}\,\Delta\,\vec{X} = E$, is for energy. Overall the relation stems from the general form for these two initially inertial items, which adjoins as follows: $\nabla^n\, E\, \nabla^n\, \Lambda' = \nabla^{(n-1)}\, F = \nabla^n\, P\, \nabla^n\, X$. For common gravitational rotation, the Jacobian of gravity's potential force is used with a coordinate translation from rotational to rectangular energy, for any orbiting system of masses. The famous Einstein energy equation is expandable by this method of mathematica. If half the gravitational potential energy is kinetic, as rotational energy; in terms of the G.P.E. half is used, and half remains as residual - gravitational-energy; a time-energy kite can be used for these exchanges. Symbolically we can solve for the total time-energy of any system by calculating the double line integral (circumference), of the two half-kites (figs. 7, and 7a.); evolves into Eq. 9a.

How would time warp accommodate light for greater than non-time-relativised spans for light, is also under review in this document. The flow of time toward the future implies the temporal potential nature of the future; however contrary to intuition, this also implies the sign nature of the past that which occurred becomes time-spent vs. the future as that which may occur as causal potentials in time. This is true for time-energy in general; is always positive. It can be said that time is as a kind of pile (potential); as such is is positive and is related to also to positive energy; and both tend from greater to lesser per Isaac Newton. The future is related to lower time-energy. This is true for time-warp as well.

For: $(i)\,\lambda_{wf} > 1$, is necessarily associated with a decreased energy which occurs with increasing gravitation. When: $(i)\,\lambda_{wf} < 1$, as pertains to the inertial frames. The latter is thus always associated with greater energies. the former with higher sign opposite time-gravity. Thus, the change in potential energy as: $\Delta G.P.E = (-)\left[G.P.E._f - G.P.E._i \right] = (+)Work = (+)\Delta K.E. = \int (+)F\, dx$. A typical gravitational object (quasar) easily proceeds from causal time regions to Doppelganger ones upon reaching activation energy; is an exothermic, then endothermic, process. Naturally, with enough debits in gravity, a typical star nebula of formation will self-ignite upon accumulating enough mass.

There are two types of gravitational cross-overs. The Doppelganger and Sublight reflexive sign considerations in time-energy along with their differentials - permutaions, are detailed in Table 1. Time as covaribale with energy, permutes mathematically to develop into the Heisenberg relations. As a preview, is fig. 2e, appears to be composed of a "high-hat" of gravitational time-warp in canceling the low-hat of inertial time-warp. This does not take into account doubling theory, but rather is that of singly as: $(i)\,\lambda_i$. Considering fig. 2-2l this fraction is explored mathematically using modern calculus per the by parts solutions to a tri-variable product. If the gravitation is added to Eq. 1, becomes Eqs. 2, 2a, and 3. These time-warp phenomenon are due to the doubling effect appearing as the difference between the singly moving frame time warps vs. energy considerations which uses the same factor as denominator. Above the obelus of c, lay the outer regions of potential-past. The inertial vessel based radii find their potential in Doppelganger regions, lower energtically creating a net work output, can be produced by particle stream technology and eventually as a useful electrically produced jetti-propulsion system; design are presented here. More will be said of this later.

One analogy of the span maker of time states that past and future are as cantilevers upon the fulcrum point of light. Still another analogy would state that time is as a sextant whose arc would be the spans would be scaled by the yoke radius of time. The radius of which would act much as the measure of time-warp (centered at c). Thus also metric contraction is predicted by thus time-warp reduced arc-lengths. Another way of looking at metric contraction due to special relativistic effects, are by example likened and seen in the transcept join per arched cathedric archectiture, is a 3D spce effect, stemming from the trajector of time which is master over the causal parsimonious contraction of 3D space radiant from a center, e.g. spherical lentgh radius to 3D contraction - expansion.

From this Doppelganger hyperbolic radii extensions also exist; unfold to hyperbolic latea and direcirix. The effect this has on the metric is by analogy, likened to a 4-vane vaulted archway; the distances contract, and the time contracts; the two types of vaults join at the pinnacle point of c. The moving frame, distance and time contract in a similar way, specially relative to light's obelus placement in the Galilean transform. Einstein knew well to place it there, being as denominator to velocity. From $E = h\nu = p\,c$ and is an already relativised product equal to Eqs. 1- 1c.; from this light's constant velocity is determined (Einstein's first law }.

Yet, another analogy states the light point is as a zenith to the span of universe, is true for c-level regarding special relativity; as such forms a special decimal physical measurable origin for relativised 3D bound space around any change in time. Harnessed as a foil as featured in this document will represent a new chapter in the fundamental physics the soecial relativuty regarding time and space.

Noteworthy is the fact that the distances spanned at $\Delta\Lambda' \gg 1$ are much greater than at $\Delta\Lambda' \ll 1$, As such warp-travel yielding high returns in travel in little time. represents new considerations in differential time-energy and time gravity; represents as a new way to cross greater distances through advanced time-induced propulsion regarding the future of space travel (sub-light and super-light); reprsents also opening the door-way for galactic as well as intergalactic travel as potential, is from this document, is feasable and realizable. Additionally time-warp travel in this fashion will be shown to be energetically facile, both macro and micro, in situ, as well as for an in-vivo astronaut in the depths.

The 4th dimension (time), is dependent upon the 5th dimension - energy is king in the sub-light causal sphere, time as the slave, but king to 3D-space, slave to the former. Thus light's time-point a type of minima and acts as constant of division. The denominator dimension of time thus has fallacy of obelus applied as a result; teaching us that the Universe revolves around such an obelus of a division; thus would become a reference for time and diameter of the 3D spaces. This implies the subtending of two temporal bays; thus light is pinnacle to between the two temporal "halves" of the universe, reaching through contraction of all points in space by arresting time's passage altogether; reaches a summit in time's moving frame contraction; applies as same divisor - denominator to all 3D.

If the Jacobian integral is formed for the total time-energy stacks of future sets, is equated to the set of past sets, they reach an equilibrium of past with future; pointing to the need to consider the SuperCausal sources (strings) for the integral of the totals of future and past sets of time-energy. The expansion of the universe is a function of, and can be derived from the above consideration. The background radiation has been explained as the dispersive echo of the ripple of this expansion. Once the total time-energy of the universe system is calculated, the determination for the value for this expansion can also be derived.

The proposition that there was a Big-Bang is now in doubt for two reasons. First it does not take into account the differing time frames of the galaxies (Big-Bang theory is a dilation dead theory); secondly without a massive central remnant, as evidence for the fact of such an event is flirtatious and un-true. Steady-State theory on the other hand could be modified to include a time dilation factor to repair that theory to accommodate time-dynamic equilibrium; if the heat energy wound down to zero it could explain the inconvenient notion of heat death, due Newton's Laws of Thermodynamics - Gibbs Free Energy flowing and decreasing one way. If all major energy is a remnant of Big Bang, would there also be an epicenter as the background radiation would suggest? At what inertial time environment would it exist. Just where would we begin to look for the Mega-Star remnant. Could it have gone out (where would a dark Mega Star remnant exist)? So far, if none has been thus far detected, if it will ever be found is not certain, if it hasn't been discovered as of yet. Secondly, if there were a Big Bang all of the galaxies would be receding at the same rate, and clearly they're not, confirmed from the spectral data. Tertiarilly, there would be an expansive large scale remnant nebula of formation associated with this event. The same can be said of the lack of a remnant nebula of formation regarding the solar system; but cosmogonically between the galaxies is this also true?

i). why is there so much empty space between the galaxies?
ii). why are there no nebulae of formation between the galaxies?
iii). why of which is there no evidence of this to date.
iv). why does the matter volume vs. space's volume
ratio << 1, cosmogonically?

Similarly the rings of Saturn were more likely a collision of two moons, rather than any kind of gravitational force stress or strain, as moons in orbit are in a state of free-fall; thus the centripetal gravity is equal to twice the inertial centrifugal force, thus forms a perpetual equilibrium that persists as long as the gravity persists. Gravity in a typical unlit star persists in-spite of being dark matter.

The apparent image of a time-hyper-red object is actually a ghost-image that is from the past. We receive their record as it trickles down from their time hyper-red reference frame, to ours on Earth. The fact that they disappear from view means they reach the event horizon velocity of c, thus singular and free-falling in time and contracted in dimension to dim(2). They are predicted to re-appear as blue-shifted highly inertially aspected subjects where emission spectra are concerned. This is true for the Super-

Particle as well, they to achieve occultation from time-warp terminus (time-free-fall). Super-Particle occultation is due to crossover defection; depending upon their energy will make their re-appearances in the past and/or future time-frame, as well. Whether they are defectors or direct will depend upon further energy applied to make them excellent Doppelganger subjects for scientists to learn from, once it is better known how to track them.

Crossing from one temporal bay to the other involves traversing that pinnacle point of c in time-space. If a galaxy were in this condition-state how would the astronomical-photo record appear; why do time-occulted subjects re-appear? Does the slow-down occur in hyper-c time environments - does it reverse itself? Does this violate Einstein's second law? Einstein's three laws are fully explained; the anomalies, precepts, and conditions are represented in full by the central equations in this document. Proposed and developed in this text is the concept of a Super-Origin: O_∞. This origin changes sign the same as the decimal origin does, upon passing through it. That is why and how the isomorphism at c exists. When the graphs of this isomorphism, are plotted using O_∞, instead of the decimal origin, O_0, then the physics of this will be much easier to comprehend, (figs. 2ci - 2di). Does the fact that these objects traverse into the spans of the infinite alter what Einstein said, regarding the speed of light as being the maximum velocity? The receding of the galaxies is generally dependent upon the comparative masses of two objects; are both Newtonian reactions to velocity pointed to the center of the greater mass. With naturally occuring debits in gravity, both report the other as receding. The idea of a receding galaxy at c, slowing down would be preposterously unnatural, but this is the tip of iceberg of time hyper-red theory. Furthermore ravitational Doppelganger subjects can become inertially blue-shifted if when credits in gravitation occur, with and decreasing kinetic energy, blue-shifted Doppelganger objects congrue to the sign of the slope in each quadrant in the graph of fig. 2.

The acceding distances covered by blue-shifted Doppelganger objects are often confused with sub-singular gravitational objects. Note that as $\Lambda' \gg 1$ then $\Delta X_{obj} \gg \Delta X_{lgt}$. Now we know how to interpret these results; and the explanation of these phenomenon coincides and operates in such a way as to be predicted by the formulary as well. The relativistic time-energy vortex of gravity operates opposite in sign to that of the inertial. This is true of gravitation's tensor property.

Electromagnetic energy seems endogenous to this "Universe Unit" and is a factor of frequency as well as by wavelength. Conceivably one should be able to come up with a Carnot-like time engine such as an particle accelerator would operate according to principia that claims that an induced timme-warp will propel an assembly from the diffrences in local said time-warp. Said force pulls craft(s) in the direction ortho-normal to the particle charge flow and warp (figs. 5a-5d, Eqs. 9, 9i). Said pull is shown to be electrically powered form of aeronautic-astronautic jetti-propulsion that can operate with long service cycles in the vagaries and vacuum of space. Said time-warp induced propulsive force follows the Heisenberg sextet; can be seen using thermal neutrons over mandrake gold-leaf roller test assemblies. Ideally, in particle electrical charge needs balance using charged particle nuclei (alpha). Such rings also have successful by theory MAM assembly potential. If true, their locally useful man-made time-energy differences would work as the stars also do - propelling them by their differences in, always positive, time-energy.

With the concept of a Super-Origin proposed, is where orbiting objects disappear from view (figs. 2ci - 2ki) for two reasons. First, inertial objects become infra-red.invisible. Black-hole candidates become blue-shifted all the way to the x-ray invisible spectral level. The ideal concept of a point such as the Super-Origin proposed here and elsewhere is defined as the theoretical central maximum of integers both positive and negatives; where negative infinity is united with positive infinity, and defined as the joining point of at least 3 independent vanes. These special ideal points include such mathematical special quotients as the indeterminate forms, or zero divided by zero, infinity over infinity, and empty set diveded by empty set. These considerations are necessary when studying the light constant, the obeluses in time-warp, and Einstein's preamble to the second law. Specific applications from the derivation to the proof for the existence of a mathematical concept so dubbed: SuperOrigin, or O_∞, is proposed here; the evaluation of such occurs as the derivative form of the following: $\lim_{v \to c} d\,(\,(i)\,\lambda_{wf}\,)$. The derivative of this expression, is calculated and graphed as in figs. 2a, 2b, 2c, 2d, 2ci, 2di.

Mathematical Derivations and Results:

The derivative of the momentum in any system with respect to time yields the derivative of energy with respect to distance. The force to move a mass by changing the velocity, or dynamic system, is solved mathematically in this volume. The relativised momentum involves time dilation; mass dilation also originates in the latter. This is represented as: $p_{\,rel} = \dfrac{m_0 \Delta X_0}{\Delta\,\Lambda_0\,(i)\,\lambda_{wf}}$. The expansion of the force expressions generate the Heisenberg functions as: $\int F\,dx = \int \dfrac{dp\;dx}{d\Lambda_0} = v\;dp = \Delta\,K.E.$. This energy expression is actually only part of a greater by parts integral. The inertial energy derivation is ordinarily treated using the product rule (Green's Theorem), and the differential of the energy develops into a Stokes relation as: $\int d\,(\,m \times v \cdot v\,)$, becoming: $\int d\,(\,pv\,) = \int 2p\;dv = \int v^{\,2}\;dm = pv$. If the nested differential for momentum e.g. $d\,(\,m\;v\,)$ is expanded, the expression becomes: $\int d\,(\,m\;v\;v\,) = \int 2\,mv\;dv = \int v^{\,2}\;dm = \dfrac{2\,mv^{\,2}}{2} = m\;v^{\,2}$. Once the intervals for the integral are added with the relativism factor, the total inertial relativitic energy of a system is easily computed; see eqs. $\Theta 1 - \Theta 19$. These delineate the applications of the combinations of differential time-energy couplets; introduces leads to the conservation laws for differential time-energy in Sublight and Doppelganger regions (See Table 1).

Since the triple vector product can be assembled either way; the product of: $d\,m \times (d\,v_i \cdot d\,v_j)$, is by identity, the same as $d\,m \cdot (d\,v_i \times d\,v_j)$, describes the energy describes the energy cube; a Stokes geodesic energy cube can be expressed as a triple pyramid. Twice the energy cube is the same as a sextuple array of Stoke's pyramids, the center point of which is called the Chief Center Point, thus:

$$\iiint (dm_0 \times (dv_i \cdot dv_j)) \cdot \mathbf{n}\, d\sigma = (2) \int\int\int (dm_0\, dv_i\, dv_j) =$$

$$\iiint (dm_0 \cdot (dv_i \times dv_j)) \cdot \mathbf{n}\, d\sigma = (2) \int\int\int (dm_0\, dv_i\, dv_j) = B\,h = (p\,v) = 2\,½\,m\,v^2$$

This would hold true considering that the "bout" integral degenerates as to a "neutrino inclusion". As such the former and main derivative set of the maomentum and mass can be expressed as the also as the derivative of the product of volume and density: $dm = d(V\,D)$; D density and V for volume. As such a six energy pyramid assembl can be created and results as: $(\frac{6\,B\,h}{3}) = (2\,B\,h) = (2\,p\,v)$. The indefinite integral for this is a mapping of a similar but more general vector form: $\iiint \nabla \times ((dm_0 \times (dv_i \cdot dv_j)) \cdot \mathbf{n}\, d\sigma) = \iiint \nabla \times (\nabla \cdot E)\, dV$. The converse vector product arrangement is also, by identity, true. A full integration by parts of the relativistic momentum, gives a full energy expression, thus: $E_{rel} = \int \frac{d(m_0 \times v_i \cdot v_j)}{(i)\,\lambda_{wf}} = \int \frac{v}{(i)\,\lambda_{wf}}\, dp + \int \frac{p}{(i)\,\lambda_{wf}}\, dv = 2 \int\int\int \frac{(dm_0\, dv_i\, dv_j)}{(i)\,\lambda_{wf}}$. The Heisenberg kinetic energy relation is, however, equal to: $(\Delta E_0\, \Delta\Lambda')_E = (2\,\Delta E_0\, \Delta\Lambda')_{K.E.} = (2\,\Delta P_0\, \Delta X')$. Hence: $(\Delta E_0\, \Delta\Lambda')_{K.E.} = (\Delta P_0\, \Delta X')$.

When relativised, and rest energy added becomes the familiar total relativistic energy of Einstein, (Eqs. 1-1d). When the time-warp factor is applied to the momentum work-up, the following complement occurs: $\int_0^c m_0\, dv = m_0\, c = R.P. = P_0$, then: $\int_0^c \frac{m_0\, dv}{(i)\,\lambda_{wf}} = m_0\, c\,(\sin^{-1}(\frac{v}{c})) - 1 = I.P. = P'$. The time factor is expressed as the ratio of clock rates, such that: $(i)\,\lambda_{wf} = \frac{\Lambda'}{\Lambda_0} = \left[1 - \frac{{v_{x_0}}^2}{c^2}\right]^{½}$. More basic physics facts:

$$\Theta\, 1).\;\; F = m\, a = \frac{P_0}{d\,\Lambda'}$$

$$\Theta\, 2).\;\; \int F\, d\underline{x} = m\, v^2 = m\, a\, x = m\, g\, h$$

$$\Theta\, 3).\;\; \int F\, d\,(\underline{dx}) = ½\, m\, v^2$$

$$\Theta\, 4).\;\; \int dG.P.E. = \int (-)F\, dx = \int m\, g\, dx = \iint G.P.F.\; r_0\, dr d\theta = \int (-)P_0\, dv = \int (-) v\, dP$$

$$\Theta\, 5).\;\; F = \int dE = \int d\,(\frac{(m_0\, v\, v)}{(i)\,\lambda_{wf}}) = \iiint \frac{dm\, dv\, dv}{(i)\,\lambda_{wf}} = \int \frac{P_0\, dv}{(i)\,\lambda_{wf}} = \int \frac{v\, dP}{(i)\,\lambda_{wf}}$$

$$\Theta\, 6).\;\; \int d\,(m\, v\, v) = \int_0^c mv\, dv + \int_0^p v\;\, dp \;\rightarrow\; \int_0^c 2\, mv\;\, dv = E_{rel}$$

$$\Theta\, 7).\;\; \int_0^p \frac{v}{(i)\,\lambda_{wf}}\, dp + \int_0^c \frac{p}{(i)\,\lambda_{wf}}\, dv = \int_0^m \frac{v^2}{(i)\,\lambda_{wf}}\, dm = E_{rel}$$

$$\Theta\, 8).\;\; \int dE = \int_0^c \frac{mv}{(i)\,\lambda_{wf}}\, dv + \int_0^p \frac{v}{(i)\,\lambda_{wf}} dp \;\rightarrow\; \int_0^c \frac{2mv}{(i)\,\lambda_{wf}}\, dv = \int_0^m \frac{v^2}{(i)\,\lambda_{wf}}\, dm$$

$$\Theta\, 9).\;\; \int_0^c \frac{2\,p}{(i)\,\lambda_{wf}}\, dv = \frac{m_0 c^2}{(i)\,\lambda_{wf}} - m_0 c^2 = E_{rel}$$

$$\Theta\, 10).\;\; 2\,\Delta P_0\, \Delta X' = \Delta E_0\, \Delta \Lambda'$$

$$\Theta\, 11).\;\; \Delta P_0\, \Delta X' = \Delta K.E.\; \Delta \Lambda'$$

$$\Theta\, 12).\ \int E_0\, d\Lambda' = \int \Lambda'\, dE_0$$

$$\Theta\, 13).\ \frac{G.P.E._0\, d\,\Lambda'}{d\,X'} = \frac{G.P.E._0}{v}$$

$$\Theta\, 14).\ \frac{2\,P'\,d\,X_0}{E'\,d\,\Lambda_0} = \frac{2\,P_0\,v}{E_0}$$

$$\Theta\, 15).\ 2\,(+)\,\Delta\,E_0\,(+)\Lambda' = (-)\,\Delta\,G.P.E._0\,(-)\Lambda' = 4\,(+)DELTA\,P_0\,(+)X'$$

$$\Theta\, 16).\ 2\,(+)\Delta\,E_0\,(-)d\Lambda' = (-)\Delta\,G.P.E._0\,(+)d\Lambda' = 4\,(+)\Delta\,P_0\,(-)dX'$$

$$\Theta\, 17).\ 2\,(+)d\Delta\,E_0\,(+)\Lambda' = (-)d\Delta\,G.P.E._0\,(-)\Lambda' = 4\,(+)d\Delta\,P_0\,(+)X'$$

$$\Theta\, 18).\ 2\,(+)d\Delta\,E_0\,(-)d\Lambda' = (-)d\Delta\,G.P.E._0\,(+)d\Lambda' = 4\,(+)d\Delta\,P_0\,(-)dX'$$

The product rule requires the parametric form for the embedded variables of the momentum couplet, in order to solve. The treatment of this function with embedded variable employs the power rule to treat the differential itself as a variable under exponent and under the integral; this works remarkably well, and shows no exception to the power rule, with exponents of -1, as exists with the more frequent, non-differential, full variables. The symmetry generated in the Heisenberg relations establishes new credibility in the mathematica of the physics. The trapezia of time-space, and energy-momentum symmetrically equate in this system of relations. The gravity portion involves a differential of a cube of twice the size of the same cube of kinetic energy. The kinetic energy is viewed as a triangular half of a diagonal cut 6-sided cube of a greater Jacobian of gravity. The energy estimate of any system of these differential products, forms from a Jacobian for area; has a common degenerate to an integral of circumference; applied to an orthonormal set of vectors, and tensors (Fubrini).

Another way of looking at the differential quartet and their relativistic partners which do also form a Jacobian time-energy trapezium; concerning orbiting systems gravity's contribution is twice the K.E. noting first that (-)P.E. = (+)K.E.; when added with rest energy become total energy, or (K.E. + P.E. + R.E.) = T.E. When the rest energy when added, a Pythagorean sum quickly develops. The two part momentum function has the effect of halving the Heisenberg constant ordinarily used to describe energy.

The Jacobian product for energy and time warp are characterized as a double right triangles for each model. The line integrals are multiplied (fig. 9a) and the two sets of two right triangles sharing one side, evolve to generate a full kites figure (fig. 7b, 7c). The double line integral of these two areas are always in dynamic equilibrium common to in mass-time-energy-gravity systems. This is due in part to the conditions for orbit, however they general reckon to be, when centripetal force equals the centrifugal one, orbit equilibrium point is still achieved; is also true with special relativity.

For the mathematical astronomical analysis of the ideal conditions of space, one way to measure energy is to measure that of light empirically as a function of wavelength and velocity of light as measured empirically (Plank's law). The mathematical model of Einstein et al. involves summaries of energy involving mass and velocity. The two are then equated once gravity's influence is added. One solution stems from two applications of the product rule (Green's Theorem), for the embedded variable p. Thus: $\int_0^p 2v\,dp = \int_0^m v^2\,dm = E_{tot}$. With special relativity taken into accout using the relativism factor, $(i)\,\lambda_{wf}$, the following product rule development occurs: $\int dK.E._{rel} = \int_0^p \frac{2v}{(i)\,\lambda_{wf}}\,dp = \int_0^c \frac{2p}{(i)\,\lambda_{wf}}\,dv = \int_0^m \frac{v^2}{(i)\,\lambda_{wf}}\,dm.$

As a digression, as an example, if a hypothetical space ship were to leave from Earth, orbit the moon and return, the distance is calculated as approximately 500,000 miles by mission control. The paradox is that after the space ship completes the trip and returns home, the log reads a traveled distance of approximately 250,000 miles and records half the time of the earthbound clock (the Earthbound clock records an elapsed time of 1 hour). If the same time interval (1 hour of the moving clock time) the distance traveled doubles to 1,000,000 miles for an hour of time on the relativised (moving frame) clock. Thus, this testifies to the metric contraction of the metric distance as a function of time contraction of the inertial frame, i.e. the metric contraction is the identical phenomenon of length contraction. Since the fourth dimension of time is affected, the distortion would be carried by all 3 space dimensions equally, (spherical distortion); thus structural integrity for any object is constant and maintained. This was not well known for some time. The spherical remnant, would still be time positive, even at the minimum time segment. Type I, and Type II defector cross-overs occur also at singulairty and each type is by analogy and operate much as a Magnetic Space Wheel child's toy, by tracking inside the metal rail, then rolling over loop-wise tracking outside the metal rail. Similarly, an extended heavy-quasar with higher K.E. from residual G.P.E. would roll-over the same way, at c, moves in a similar way along a Doppelganger time-track. The velocity warp factor is carried by both numerator and denominator equally, and cancels as per time-space radius: R_i. The kinetic direct Type III crossover, is seen in nature as high K.E. time-hyper-red Doppelganger blued particle jetties. They present with credits in potential energy $(+)\Delta G.P.E.$; are also endothermic and cross large distances. These jetties are reproducible in the laboratory and are claasified as Super-Particles. They also show the crossover nodal area or zone of occultation; are visibly seen in the photographic record as polar oriented streams of matter that top many black-hole star candidates (jetties).

In attempting to answer this question, one encounters eventually an indeterminate form: $\lim_{v \to c}\left(\frac{(i)\,\lambda_r}{(i)\,\lambda_{wf}}\right)$. The original function for the indeterminate form shares the same value as the derivative obelus, as the one above, thus will be (1) more strongly, for being the same function. The outcome in the evaluation is the same for both, also. The definition of Unity as such reproduces in physical application of special relativity thus the concept of a SuperOrigin O_∞, holds disjoint worm-holes from black-holes. This is due to the radically large magnitude of sign difference in comparative energy. Due to the meeting in tensor with vector, the two energies lay distinct and time space realm lay disjoint; as evidenced by necessity and discontinuity from the change in sign of the time ordinate from (-)infinity to infinity (gravitational vs. inertial energy $(-/+)\infty$). From Cauchy's theorem the symbolic form of: $\frac{(i)\lambda_{wf}}{(i)\lambda_{wf}} = \frac{d\,(i)\lambda_{wf}}{d\,(i)\lambda_{wf}} = 1$, as a rule always converges to unity sustaining the causal past universe's conjoint motif with the supercausal future; is in each case energy specific.

The energy flux is solved for represented in Eqs. 1i - 9i. The lambda factor becomes the governor of the relativistic energies (inertial, gravitational, but not rest energy). The difference in time readouts are easier to use to compute velocity, instead of conventional distance-time estimates.

As Einstein noted, time ticks faster in gravitational fields. K.E. reverses this effect. The inertial time-warp obelus is depicted in graph 2a. Each kind of time-warp derivatives are graphed in figs. 2c, 2d, and 2e. The degeneration of the kernel which occurs at {+/-}c is often described as a Hermitian isomorphic singularity. The gravitational singularity is the same but reverse phenomenon, both can cross-over (flop-over) with enough momentum, to Doppelganger regions in time-space. There are many examples of this with man-made devices (Super-Particles), as well as that seen in the astronomical record.

By definition and as choice of the causal past time-warp variable is as: $\frac{\Delta\Lambda'}{\Delta\Lambda_0} = (i)\lambda_{wf}$; this warp factor is used instead of the more common gamma function. The nucleus of the Lorentz factor $(i)\lambda_{wf}$, is described here as the causal past inertial frame (moving frame) function stemming from the Galilean physics for any moving frame of reference. The application of 3-dimensional special relativity introduces a certain intuitive level of an arbitrary kind of ambiguity to space-travel, because it begins with considering differences in distance vs. time-span between any 2 reference points, but often includes a 3rd as an orthonormal rest mass such as a star or planet, remembering that this argument always distills to any two (2) reference points. When we consider special relativity one must also remember to consider the special relativism in terms of energy-momentum, space/time; is carried by all 3-dimensions of space.

As such, for inertial frames of reference the lambda factor quickly becomes an obelus thus governor of the kinetic set. Also when the function becomes sign changed, as in the case of gravity, the $(i)\,\lambda_{wf}$ function changes quadrant (fig. 2). Increases in energy show up differential decreases in time warp and thus time-well formation ensues, (figs. 2-2di.). The degeneration of the kernel occurs at {+/-}c and the Hermitian isomorphism takes hold for the rest of what is essentially an imaginary that reverses the time slowing condition that develops with inertial moving frame systems. The limits of these derivatives and the time-well graphs associated with them are the same limits for derivatives in general.

The two paths to the total energy equation are reconciles mathematically with product rule as applied to the linear systems. The formulation of the Jacobian for the Heisenberg relation is preferred for the solution to the relativistic gravitational component of total time-energy. The resulting pair of relations have the characteristics of an indefinite integral in their solution due to their embedded nature. Time remains positive for all velocities. Reducing and collecting terms, one achieves new temporal conservation and causal - supercausal total energy equations. This introduces new hope for new forms of electro-anti-gravitational jetti-propulsion, and new uses for the toroidal based particle generators (PEP rings). By feeding the PEP ring products into linear accelerator pods would generates a useful local pulling force as when a mandrake is introduced in a particle ion flow; would induce a net thrust; pushing upon the mandrake tail, ortho-normal to the charge flow induced time-warp, i.e. toward lower differential time-energy (figs. 5a-

5d). The idea is the same operationally for the entire cosmos. The time-foil as presented, acts as propulsion by inducing a $\Delta\lambda_{wf}$ using a charge lubed mandrakes in a similarly charged (dual Tandem Van de Graffe - induced) particle streams. From differential time-energy, the assembly shifts toward lower differential time-energy, moving the (vessel) with it. Sample designs are predented as figs. 5a, 5b, and 5c. The equations for this and others are presented here as unified field Time-Energy-Gravity equations:

$$Eq.1.\quad \Delta E_{rel} = \Delta\left[\frac{m_{r_0}c^2}{(i)\lambda_r}\right]$$

$$Eq.1a.\quad \Delta E_{rel} = \Delta\left[\frac{m_{r_0}c^2}{(i)\lambda_r}\right] - \Delta\left[(\frac{\Delta\Lambda'}{\Delta\Lambda'})m_{r_0}c^2\right]$$

$$Eq.1b.\quad \Delta E_{G.P.E._{rel}} = (-)\,2\left[\Delta\left[\frac{m_{r_0}c^2}{(i)\lambda_r}\right] - \Delta\left[(\frac{\Delta\Lambda'}{\Delta\Lambda'})m_{r_0}c^2\right]\right]$$

$$Eq.1c.\quad \Delta E_{rel_{tot}} = \Delta\left[\frac{m_{r_0}c^2}{(i)\lambda_r}\right] - \Delta\left[(\frac{\Delta\Lambda'}{\Delta\Lambda'})m_{r_0}c^2\right]$$

$$-2\left[\Delta\left[\frac{m_{r_0}c^2}{(i)\lambda_r}\right] - \Delta\left[(\frac{\Delta\Lambda'}{\Delta\Lambda'})m_{r_0}c^2\right]\right]$$

$$= (-)\left[\Delta\left[\frac{m_{r_0}c^2}{(i)\lambda_r}\right] - \Delta\left[(\frac{\Delta\Lambda'}{\Delta\Lambda'})m_{r_0}c^2\right]\right] = ½\,\Delta G.P.E._{rel} = (-)\,\Delta K.E._{rel}$$

$$Eq.1d.\quad T.E._{rel} = (-)\left[\left[\Delta\left[\frac{m_{r_0}c^2}{(i)\lambda_r}\right] - \Delta\left[(\frac{\Delta\Lambda'}{\Delta\Lambda'})m_{r_0}c^2\right]\right] + \Delta\left[(\frac{\Delta\Lambda'}{\Delta\Lambda'})m_{r_0}c^2\right]\right]$$

$$= \Delta T.P.E._{rel} - \Delta R.E. + \Delta R.E. = (-)\,(\Delta T.E._{rel} + \Delta R.E. - \Delta R.E.\ )$$

This reduces to: $\Delta E_{rel} = \Delta\left[\frac{m_{r_0}c^2}{(i)\lambda_r}\right]$. This is akin by analogy, to the problem involving the time- energy of a cherry. If the fruity flesh is the relativistic K.E. of an object, the pit is then considered to be the rest time-energy; the relativistic kinetic time-energy is the flesh of the cherry minus the pit; when the pit is added, the sum is the total cherry (total relativistic time-energy). Not surprisingly, there is no cherry without first the pit. With the potential energy of gravity included, the total energy expression functionally becomes: $\left[E_{rel} - P.E._{grav_{rel}} - R.E._{rest}\right]$. And thus: $(E_{tot_{rel}})^2 = (E_{rel} - G.P.E._{rel_{grav}})^2 - (R.E._{rest})^2$; energy for any gravitational system can be expanded to this general formula e.g. in the case of a galactic system of solar masses in pinwheel orbit about its core and among any given local group, evolves to: $\left[E_{glx_{rel}} - P.E._{glx_{core_{rel}}} - R.E._{rest}\right]$. The equivalent Jacobian integral of gravitational force yields the net P.E. when added to $E_{rel}{}'$, yields half the total iteration for gravitational energy. What remains is: $\int \frac{G\,M\,m\,dr}{r_g^2} \rightarrow \int\int \frac{G\,M\,m\,r_g dr\,d\theta}{r_g^2} = \int\int \frac{G\,M\,m\,dx\,dy}{1}$. In general and converting the rectangular coordinates, the P.E. becomes $(\Delta K.E. - \Delta(G\,M\,m\,\theta \ln r_g)) = (\Delta K.E. - \Delta G.P.E.) = \Delta(-)K.E.$ If the area of the square represents the differential for relativistic G.P.E. then the sign negative half of it represents the relativistic K.E.; a sign negative square is added to a sign positive K.E. triangle, when, for comparison purposes the circles of rest energy cancel once, what remains is half of relativistic gravitational energy or, the sign negative of the triangle of K.E. relativised gravitational potential energy square remains; the $½(-)G.P.E_{P.E._{rel}} = (+)E._{rel}$ remains. Gravitational force is an empirical expression and the gravitational energy formula and measurements from such us as an already relativised host. As such, any appearance of $(i)\lambda_{wf}$, (the time-warp factor), can occur as a doubly type of construction when incorporated with the expressions of Eqs. 1-1d. A typical galaxy exhibits two types of motion, i.e. inertial and rotational. Relative to another galaxy; the energy would be analyzed in a similar way (two reference frames).

The square of this classical text-book case Jacobian represents for summing up the relativistic rotational gravitational potential energy gone into orbital kinetic energy reaches an equilibrium as orbiting freefall dictates, and thus establishes an equilibrium with the relativistic linear energy of the greater (e.g. Milky-Way) galaxy, in relation to a closest neighbor a the local group partner vs. a furthest distance partner such as a quasar, by comparison. In equations 1-3, what is fundamentally a time-dilation phenomenon leads to relativistically higher energies for time-warp factors of $(i)\lambda_{wf} < 1$; (figs. 2c, and 2d). For high integer Doppelganger time-warps where: $(i)\lambda_{wp} > 1$, this leads to gravitational objects becoming relativistically Doppelganger inertial subjects, developing lower residual potential energies, with increases in arc-span, and develop blue shifted emission spectra. Observed K.E. is primarily from residual G.P.E.; is responsible and explains fully cosmogonic motion; and is of two types of K.E. from G.P.E. Residual G.P.E. is dominant; first observed as receding velocity K.E. due to gravitational time-space expansion, is noticed toward the gravitational center, receding in direction K.E.; i.e. away from the galactic core of another galaxy. The arcing of the galaxies is due to the first half of total gravitation, as commonly known. Debits in potential energy are also responsible for the outward spiral effect of the arms, observed in the celestial photographic record. Forming heavier elements, as stellar fusion does, over time produce greater density, hence the predicted debits in G.P.E.; will appear as (+)K.E., receding away from any other object, on top of revolution and arcing aross the background sky.

This method of using relativistic time jacketing of the classical energy equations is not unique, yet now well understood. The physics leads us to another popular energy relation being expanded to include gravitational energy in the time frame lattice, so that the Einstein total energy relation evolves for objects in orbit. What evolves is the Pythagorean sum of squares of kinetic, potential, and rest energy producing the total energy hypotenuse. The measured phenomena at the observatory level are fattened by the obelus with the causal past Lorentz nucleus or $(i)\lambda_{wf}$; the time-space warp factor lambda. This Pythagorean averaging occurs mathematically, is conserved both in time-warp and energetically and the notion of time-warp changes are related to energy changes and vice versa. The receding of the galaxies is related strictly to gravitation and is reconciled using W. Heisenberg’s expression as applied to conservation of momentum vs. conservation of energy, these diatomics explain at their limits, Pauli displacement. At c, the momentum that reaches nearly nil due to time being warped in Earth time-frame to large scale amounts, thus the decrease in apparent momentum, and the exclusion which occurs through physical displacement; resuming physical appearance are although blue-shifted in emission spectra.

Doubly adjusted figures of the relativistic complexes are true for the gravitation too; the complexes of T.I.E. and T.P.E. are also both already adjusted as per Eq. 3, which simplify to simple special relativistic values of Eqs. 1-1d. The discord occurs when a summa is performed over the sides to the trapezium with components of relativistic momentum and velocity, as: $p\,dv$ and $v\,dp$; one has an embedded product and the other does not. The Jacobian has a degenerate energy cube forming a differential square $dr\,d\theta$, in polar dim(2). Naturally a conversion/translating matrix and its determinant form from $dx\,dy$. When the double line integrals are calculated and expanded, (figs. 7-7c). Ensuing a total time-energy Fubrini. The full kite energy time-warp trapezium involves the line integral of the line elements of figs. 7b and 7c, are also functions of Eq. 9, 9i, 9a, and 9ai. The reticulation and reciprocation of these elements are discussed at length in appendices A-V and toward the end of this manuscript.

In orbiting systems the absolute total relativistic energy (the inertial relativistic kinetic energy added to the absolute value of the relativistic gravitational energy), gives a glimpse into the meaning of the cancellation part by subtraction of time-warps (fig. 2e); as opposed to the cancellation by division of the reciprocal part. The former implies time-warp equilibria; the latter implies a type of time-warp reflexive inversion. The former neutralizes by subtraction; the latter by division, reduces the doubly complex into a singly. This repeats itself laterally for each type of energy, with the exception of rest energy, which remains in local time. This would imply energy and momentum conservation laws are subset to that of time-warp equilibrium and conservation ones.

The time-warp adjusted explanation of Einstein's energy full kite, fig. 7b and 7c, fit observations and calculations in accordance with mathematical conservation laws of time and energy, (Eqs. Ω 1–20, and Eqs. i-viii). Additionally, as pertains to this set of equations the search for a common denominator naturally could also involve rest mass. The indeterminate form would naturally apply, thus thus the relativistic momentum's special relativism would cancel with that of energy. This is true for gravitation too. This speaks also to the cancellation of the Lagrangian multiplier for rest-energy and rest-warp special relativity, as well. In other words, if: $\lim_{v \to c} f\left(\frac{(i)\lambda_{wf}}{(i)\lambda_{wf}}\right) = 1$, then: $\lim_{v \to c} f'\left(\frac{(i)\lambda_{wf}}{(i)\lambda_{wf}}\right) = d(1) = 0$. But if: $\lim_{v \to c} \frac{d\,(i)\lambda_{wf}}{d\,(i)\lambda_{wf}} = \frac{0}{0} = \lim_{v \to c} \frac{(i)\lambda_{wf}}{(i)\lambda_{wf}} = 1$. Thus, in this instance the, obelus of the derivatives is not the same as the derivative of the obelus. In general then: $\lim_{f(x_{i,j}) \to 0} d\left(\frac{f(x_i)}{f(x_j)}\right) = d(1) = 0$ Thus from Cauchy analysis, it can be shown that for any two functions $\lim_{f(x_{i,j}) \to 0} f(x)$ and $\lim_{g(x_{i,j}) \to 0} g(x)$ that if $\frac{f(x)}{g(x)} = \frac{0}{0}$, and $\frac{f(x)'}{g(x)'} = 1$, then the obelus of the two functions equals the obelus of the two functions themselves, then $\frac{0}{0} = 0^0 = 1$ thus when evaluated the indeterminate form converges to 1, in both cases. This is also the result for empty sets; and their derivatives; their obelus also equals 1. It is necessary to comprehend this when studying time-space warps.

Since the species of the terms are the similar in kind; the result is weighted more than other variable, other exponential, or other derivative cross-specie obelus. If $f(x_i) = f(x_j) = f((i)\lambda_{i,j})$, then: $\lim_{v \to c} d\left(\frac{(i)\lambda_{wf}}{(i)\lambda_{wf}}\right) = 1 - 1 = 0$. In the case of simple velocity: $\lim_{dx = dt \to 0} v = \frac{d(x)}{d(t)} = 1$, and the derivative of this equals 0. From l'Hôpital's rule the indeterminate form which occurs at c, is also a known solution to this expression.

For the change in time form, $\Delta\Lambda_{i,j}$ is used. The change of the quotient of time readouts is: $\Delta\Lambda = \Lambda_{final} - \Lambda_{initial}$. This becomes evident with gravitational time-energy as the tensor trajectory is inwardly bound toward a center of mass. Specially relativity explains the occultation of an inertial along with that of the gravitational black holes. The interpretation of the mathematica and the proposition of a SuperOrigin, "rolling" Pauli exclusion-inclusion, involve the four modes of encounter with accessing the extrema of this Universe Unit.

$$Eq.2.\ \Delta E_{rel_{tot}} = \Delta \left[\left(\frac{p_{glx_{i,j}} c}{(i)\lambda_{wf}} \right) - \left(\frac{(G\, M_{glx_{i,j}}\, m_{glx_{i,j}} \theta_{i,j} \ln r_{\,g_{i,j}})}{(i)\lambda_{wf}} \right)_{glx_{i,j}} \right] ((i)\lambda_r\, \Delta\Lambda_{0_{i,j}}) - \Delta \left[m_{rst_{glx_{i,j}}} c^2 \left(\frac{\Delta\Lambda_{0_{i,j}}}{\Delta\Lambda_{0_{i,j}}} \right) \right]$$

$$+ \left[\sum_{k,l=0}^{k,l=\infty} \left[\Delta_{k,l} \left[\left(\frac{p_{orb_{k,l}} c}{(i)\lambda_{wf}} \right) - \left(\frac{G\, M_{glx_{Core_{k,l}}}\, m_{orb_{k,l}} \theta_{k,l} \ln r_{\,g_{k,l}}}{(i)\lambda_{wf}} \right) \right] ((i)\lambda_r\, \Delta\Lambda_{0_{k,l}}) - \Delta \left[m_{rst_{k,l_0}} c^2 \left(\frac{\Delta\Lambda_{0_{k,l}}}{\Delta\Lambda_{0_{k,l}}} \right) \right] \right] \cos(\eta_{glx_{k,l}}) \sin(\zeta_{glx_{k,l}}) \right]$$

$$Eq.2a.\ \Delta E_{rel_{tot}}{}' \cdot \Delta\Lambda_{i,j}{}' = \Delta \left[\left(\frac{p_{glx_{i,j}} c}{(i)\lambda_{wf}} \right) - \left(\frac{G\, M_{glx_j} m_{glx_i} \theta_{i,j} \ln r_{\,g_{i,j}}}{(i)\lambda_{wf}} \right)_{glx_{i,j}} \right] ((i)\lambda_r\, \Delta\Lambda_{0_{i,j}}) - (\Delta\, m_{rst_{i,j0}} c^2 \Delta\Lambda_{0_{i,j}})$$

$$+ \left[\sum_{k,l=0}^{k,l=\infty} \left[\Delta_{k,l} \left[\left(\frac{p_{orb_{k,l}} c}{(i)\lambda_{wf}} \right) - \left(\frac{(G\, M_{Core_{k,l}} m_{orb_{k,l}} \theta_{k,l} \ln r_{\,g_{k,l}})}{(i)\lambda_{wf}} \right) \right] ((i)\lambda_r\, \Delta\Lambda_{0_{k,l}}) - \Delta \left[m_{rst_{orb_{k,l}}} c^2 \Delta\Lambda_{0_{k,l}} \right] \right] \cos(\eta_{glx_{k,l}}) \sin(\zeta_{glx} subk, l) \right]$$

The forms of K.E. are associated with the gravity of any planet or star. Orbital K.E. comprises the half the total time-energy of any system of gravitation. Linear motion K.E. of the entire system is due to the residual gravitational potential energy’s effect upon the time-warp. The Oranus effect (Uranus) is seen cosmologically and is due to time-energy’s arbitrary nature to fall toward lower P.E. in 3D. Such a response also is thought to regulate barred spiral development from ellipticals. In orbiting systems, planetary spin, and other rotational energy as a law, always moves toward lower potential energy, reactive to gravitation. Such angular momentum and the like, is considered miniscule comparing to planetary residual G.P.E. of the greater system of orbiting objects. The Uranus effect is no exception. The greater sentiment of lies in the fact that orbital energy and linear K.E. are both gravitationally derived.

Doppelganger re-appearance show increased arcs in travel distance covered by ordinary light. The related blue-shift in the spectra re-iterate, and represent comparative differences from credits/debits in gravity between two gravitational subjects are, with respect to differential time-energy, That omni-directionality of expansion/contraction is opposite to what happens at the core; they undergo contraction/expansion respectively. Thus the comparative masses determine 4th dimensional relativism, as: $M_1\ vs.\ M_2$ where $(-)G\,(M_1 - M_2)\,m_0$. Depending upon mass conversion over time, two stellar reference points will always show receding nature, and local contraction of sphere. Due to the normal evolution of both stars and galaxies there will be more receders than acceders. At least 1 out of 10 galactic objects are of the Doppelganger acceding type.

The effect upon the astro-physical problem is as such; if differential time-energy is represented as a mole-hill with as top, and a galaxy is as to a golf-ball, then depending on the mass they will tend to roll down in an omni-directional way. All galactic gravitational evolution behaves in this way, depending upon the time-space topology of their local continuum. Further figures of these constraint functions and their permutations are listed as: (see figs. 2b, 2ci, 2di, 2e, 2f, 2g, 2i, 2j, 2k, 2ki, and 2q). The free fall point in P.E. (at c) and is a topic of much speculation, and is depicted by figures 2ci, 2di, and 2ki; invoking the concept of a Super-Origin, is necessary to describe the isomorphism at c; many mathematical blunders are overcome, and a new Origin is developed. Doppelganger subjects are thus also explained, and such things as galactic evolution, also.

Transit times for smaller objects regarding orbiting systems of masses will show when checked, transit pre-appearance to that dead-reckoned calculated, the correction is easily calculated from Eqs. 2, 2a, and 3. To that of an Earth bound observer, the two are not always equal. Because the value for transit appearance is both a function of $d(i)\lambda_{wf}$, the slowed time-field for performance of the velocity of light in a gravitational field is balanced by the increased distance covered; the two are in balance. The path is a generally reckoned curved surface; the hyperbolic paraboloid (saddleback) surface occurs first in energy (G.P.E.), influences time, then similarly influences the 3D radii of space, as a gradient; this occurs for both for inertial objects as well as gravitational time-wells. The apparent image is a type of virtual image from a hyperbolic-paraboloid surface as illustrated in the graphs that follow the appendices. Accurately predicting transit appearances are more usably possible. The product and sum ratios of these two time-foils, (inertial and gravitational) are also depicted in the included graphs (figs. 2c, 2d, 2cii, 2dii).

The implication is that the Super-Ordinate, Super-Number, { 1 prime }; has, by definition, the special and special property of being prime which all other numerical prosodies are derived, as per the number theory. Looking at graph 1a, and 1b, we see plotted the expression: $\frac{\Delta\Lambda'}{\Delta\Lambda_0}=\frac{\Delta X'}{\Delta X_0}=((i)\lambda_{wf})$. The formula for the supercausal is a simple derivation, occuring as: $(1-((i)\lambda_{wf})^2)=(\frac{\Lambda'}{\Lambda_0})^2$. Also: $(1-\cos^2(i)\varepsilon)=(\frac{\Lambda'}{\Lambda_0})^2=(\sin^2((i)\varepsilon))$, as fig. 2a. The composite figure of causal with supercausal temporal phenomena and the temporal conservation laws are as: $\Omega 9-\Omega 20$, remain depicted as fig. 2a.

R is the normal matter (momentum) and normal space-time radius causality constant (offered as a obelus of division). This factor dubbed here as a measure of the "linkage-disequilibrium" of normal space-time; often occurs and has the value of 1. This expands Green’s and Stokes theorems to include the normal of time-warp applied space, and found them to vary similarly and in lock-step. When both are taken into account, new symmetry issues arise, and the notion of linkage dis-equilibrium for each; the hyper-red conditions i.e. when: $\sqrt{1-k^2}$ as: $k \lesseqgtr 1$. The the ratio of the distance radius with time is define here as: $\mathbf{R}_i = \frac{r_r{}'}{r_t{}'}$. For anti-matter, anti-momentum, note the reverse in reciprocal order in the division obelus for velocity. $\mathbf{R}_\alpha = \frac{r_t{}'}{r_r{}'}$.

From the polar form comes the polar nature with their associated maximas, minimas, and hyperbolic extensions. This mathematical description of the terminus is more complete than the Lorentz form; renders the Lorentz form obsolete; explains sign attributes more succinctly in all cases of time-energy. As such the hyperbolic cosine yields two roots; one positive and one negative, four forms of time travel are implied in one relation. Both the singularities surrounding gravity and inertial kinetic energy have with their accounting regarding higher time slewed conditions surround the consideration of the energy at terminus of c, with the time-warp at terminus is explained using these formulae.

This thus unifies singularity theory, as fig. 2a, depicts the singularity of gravity (the black-hole), which evolutionally proceed as sub-singularity short-wave UV-shifted objects, evolving into x-ray emitters, culminate by total occultation in the crossover to infrared shifted subject-matter; form from a type of special relativity free-fall. Considering the terminus condition, both quasar occultations and black-hole occultations are both permutations of similar singularities, but involve two differing phenomenon; they both occult light due to infrared conditions; both involve space-time warp phenomena. Does this also mean their momentum decreases to Heisenberg levels, then displace to an inverted sign opposite, differentially changing time sheet? It seems energy of the system reaches a local top before "rolling" into a non-inhibited crossover or decolletage to another time-warp bay. The Pauli exclusion of the singularity of c is overcome by the cline of time; is dependent upon time-permitivity, yet is non-destructive. These topics have come-up before but were greatly mis-understoood. Said fig. 2a, clearly shows a join, but these results must consider the limits of these physical constants; appear mathematically as well-defined.

This is notable caveat that must be observed; are nearly impossible to graph, especially symbolically. Thus at singularity a gravitation black-hole joins a Doppelganger time-region after a non-inhibitory, non-destructive, exclusion from the causal. The typical defects from inertial cross-over is labelled Type I crossover-decolletage. The latter gravitation is classified as Type II; occurs with gravitational objects. This is discussed further in this document, in (Eqs. i-viii).

Time-energy trapezia generally are always positive, including that of time-gravity, as well as that of rest time-energy. The bias of time can be either in forward or reverse direction. Doppelganger time-energy trapezia operate in oppositely affected ways compared to their sub-light, sub-terminus, counter-parts. Furthermore, from figs. 4-4c, we now know that unified singularity theory declared inertial worm-holes are opposite singularity phenomena to that of black-holes. Thus introducing the science of special temporal relativity; Ψ, Ξ, theory will broaden the understanding of physicists regarding temporal based phenomena as a whole (figs. 4-4c). With knowable quantities of time-warp, it is a simple excersize to calculate velocity, arrival times, and distances. Doppelganger regions, both future travel and past travel are predicted and now proven mathematically; are seen analytically for the first time, in this document. The consideration of Doppelganger conditions involves the mathematical imaginary co-factor and as such extends the time-radius of > 1, results in the same distortion for all dimensions of space equally. The fourth dimension od time occurs as the obelus with 3D space. Hence triple vector products must be used for any computation.

If the Universe Unit's access exists for the first (involvement). then it could be that another could exist, as this one does. Each would by necessity exhibit similar parsimony both in principle, and in reflex, consistent with the principia inherent to any particular Universe Unit. How "Top" would be accessed, in the dualistic universe's case is not readily known; but would imply orbit in time (time free-fall) to succeed in being independent of the two. Thus the case where kinetic worm-hole terminus at c, is the opposite to that of a black-hole terminus must be central to this Universe Unit's principle and mode (Eqs. i-viii). So far, mankind has made little progress in the astro-physics, other than that of the set theory logos.

The mathematical notion of warp doubly, can occurs in both the numerator and the denominator, for both inertial frames and in the sign reversed gravitational ones: $\frac{(i)\lambda_{wf_i}}{(i)\lambda_{wf_i}(i)\lambda_{wf_j}}$, and $\frac{(i)\lambda_{wf_j}}{(i)\lambda_{wf_i}(i)\lambda_{wf_j}}$. This construction becomes in form a measure of time-warp acceleration (unit-wise). The graphs of this additive effect shows the double fat of the denominator is trimmed once by the numerator presented in figs. 2m-2o. The net is an increase in elapsed time for the moving frame events compared to that of Earth. If this effect is measured at the planetary level it could be reproduced at the laboratory accelerator level. Another form of doubly lay in the numerator of the following as: $\frac{\Delta X_{lgt}\,((i)\lambda_r)^2}{\Delta\Lambda_0\,(i)\lambda_t} = c\,(i)\lambda_r$; is also a form of: $\frac{\Delta X_{lgt}\,r_r\cos^2((i)\varepsilon)}{\Delta\Lambda_0\,r_t\,cos((i)\varepsilon)} = c\,r_r\,cos((i)\varepsilon)$.

Delving into some more mathematics of the time-energy physics, one comes across the Planck's time-energy as equated with the Heisenberg time-energy; the time-warp becomes doubly multiplied, the $(i)\lambda_{wf}^2$ time warp factor function suddenly becomes a measure of acceleration, as the denominator becomes $(secs^2)$ seconds squared. The concept and implications of the doubly function shows how time-warp can reciprocates and reticulates in each formula, to follow. The indeterminate function develops when v = c; while the periodic previously developed would explain this better, essentially when evaluated the energy becomes infinite at $\frac{\pi}{2}$, (See fig. 2).

This Universe Unit is typified by both the infinite and the finite. Mathematically, both are produced i.e. SuperOrigin, and decimal origin. In accordance with LaPlace's

Nebular Theory most stars have in most abundance the organic and mineral elements also found most commonly on Earth, namely: (Lithium, Beryllium, Boron, Carbon, Oxygen, Nitrogen, Hydrogen, Sulfur, and Phosphorus). Thus from the ecliptic alignment this form of planetary evolution is plausible; becomes also a function of recombinations of these eight main elements; the spectral record shows this as well. The nuclear valences grow according to: $(Deuterium)_m^p \cdot 2^n \, (n = 0, 1, 2, 3...)$. The closest packing of the larger nuclei, often does so hap-hazardly; clustering like this is causal for the weak force fission. Also known are polarity driven instabilities, releasing neutrinos often accompany activation complexes of nuclear events. The strong force rest-energy conversion acts much as a venturi for energy release, seen in all fusion fired stars. The valence theory for this nuclear joining has been worked out in great detain with the advent of quark physicists.

While the other elements are also present only to a lesser extent. Planetary evolution can thus be tied to common stellar evolution, and hence other Earth class planets must also exist, by virtue of the former statement being true. As stellar furnace objects they naturally produce heavier elements, increase in mass, from this temperature as well increases, over time. Gravity gradually thus also intensifies. The time-energy varies indirectly as the couplet is attached to a constant. If a gravitational field affects the velocity of light by any local measurement the velocity can only be c, since the metric is both time distorted metric distorted the same way, in reference to any second point. As pertaining to the general reckoning of light through a increasing gradient in time-warp, acts to distort the space in a concave way, yielding a virtual image view of a planetary transit; the metric varies as a function of $(-)d\left(\frac{ln(r)}{(i)\lambda_{wf}}\right)$. Curiously a new more practical form of Einstein’s total energy form exists for time-warp, namely when: $(-)d\left(\frac{ln(r)}{(i)\lambda_{wf}}\right) = d(i)\lambda_{wf}$. When the latter is equated to the former, yields: $E_{rel}{}' = \lim_{v \to c}\left(\frac{m_0 v_x^2}{r_t cos(\varepsilon)}\right) - m_0 c^2$. An application of the imaginary factor as in: $r_t cos((i)\varepsilon)$, becomes the hyperbolic cosine for Doppelganger values, as previously stated. This occurs naturally in the time-warp $(i)\lambda_{wf}$ expressions; which also is much more handy than Einstein's form. Naturally, this leads to degrees of sub-light time-warp, and radii of time-hyper-red warp. Re-writing expressions 1-1d, yields:

$$Eq.1i. \quad \Delta E_{rel} = \Delta \left[\frac{m_{r_0} c^2}{r_t cos((i)\varepsilon)_E} \right]$$

$$Eq.1ai. \quad \Delta E_{tot_{rel}} = \left[\Delta \left[\frac{m_{r_0} c^2}{r_t cos((i)\varepsilon)_E} \right] - \Delta \left[\left(\frac{\Delta \Lambda'}{\Delta \Lambda'} \right) m_{r_0} c^2 \right] \right]$$

$$Eq.1bi. \quad \Delta E_{G.P.E._{rel}} = (-)\,2 \left[\Delta \left[\frac{m_{r_0} c^2}{r_t cos((i)\varepsilon)_E} \right] - \Delta \left[\left(\frac{\Delta \Lambda'}{\Delta \Lambda'} \right) m_{r_0} c^2 \right] \right]$$

$$Eq.1ci. \quad \Delta E_{tot_{rel}} = \left[\Delta \left[\frac{m_{r_0} c^2}{r_t cos((i)\varepsilon)_E} \right] - \Delta \left[\left(\frac{\Delta \Lambda'}{\Delta \Lambda'} \right) m_{r_0} c^2 \right] \right]$$

$$+(-)\,2 \left[\Delta \left[\frac{m_{r_0} c^2}{r_t cos((i)\varepsilon)_E} \right] - \Delta \left[\left(\frac{\Delta \Lambda'}{\Delta \Lambda'} \right) m_{r_0} c^2 \right] \right]$$

$$= (-) \left[\Delta \left[\frac{m_{r_0} c^2}{r_t cos((i)\varepsilon)_E} \right] - \Delta \left[\left(\frac{\Delta \Lambda'}{\Delta \Lambda'} \right) m_{r_0} c^2 \right] \right] = ½\, \Delta G.P.E._{rel} = (-)\, \Delta K.E._{tot_{rel}}$$

$$Eq.1di. \quad T.E._{rel} = (-) \left[\left[\Delta \left[\frac{m_{r_0} c^2}{r_t cos((i)\varepsilon)_E} \right] - \Delta \left[\left(\frac{\Delta \Lambda'}{\Delta \Lambda'} \right) m_{r_0} c^2 \right] \right] + \Delta \left[\left(\frac{\Delta \Lambda'}{\Delta \Lambda'} \right) m_{r_0} c^2 \right] \right]$$

$$= \Delta T.P.E._{rel} - \Delta R.E. + \Delta R.E. = (-)\,(\Delta T.E._{rel} + \Delta R.E. - \Delta R.E.)$$

For pre-singular events, the implied radius is 1, and the time relation is the arc cosine, the event time-angle is between 0, and 2π. For Doppelganger events the radius is > 1, and the time angle relation is the hyperbolic arc cosine, whose two roots correspond to past-future bifurcation, which speaks to affirm causal past equilibria as pre-singularity and post-singularity temporal phenomena for energy and time, are as orthogonal relatives. Past sets form from future sets as actualization occurs. If this begets that, vertex for a myriad other events is opened.

For MO fans this expression can also be modified to include the use of the Planck's relation for energy then if the period is converted by dividing by 2π radians/cycle; the Heisenberg sextet comes about, yielding new relativistic time-energy relations. The transit images we receive are a residual composite of these two. Navigationally, and astronomically it becomes clear the choice falls between either the straight-on dead-reckoning of slow light, i.e. according to: $d\,(i)\lambda_{wf}$, or the general arc-reckoning of the path of normal light-speed light, i.e. according to path: $(-)d\,(\frac{ln\,(r)}{(i)\lambda_{wf}})$. Using the periodic function developed earlier yields: $d\,r_t cos\,(\,(i)\varepsilon\,)$; the general arc-reckoning of the path of normal light-speed light, i.e. according to path: $(-)d\,(\frac{ln\,(r)}{r_t cos\,(\,(i)\varepsilon\,)})$.

$$Eq.2i.\;\; (\Delta E_{tot_{rel}}{}')_{csl} = \Delta\left[(\frac{p_{glx_{i,j}}c}{r_t\,cos\,(\,(i)\,\varepsilon\,)_{i,j}}) - (\frac{(G\,M_{glx_{i,j}}\,m_{glx_{i,j}}\theta_{i,j}\ln r_{\;g_{i,j}})}{r_t\,cos\,(\,(i)\,\varepsilon\,)_{i,j}})_{glx_{i,j}} \right] (\,r_r\,cos\,(\,(i)\,\varepsilon\,)_{i,j}\,\Delta\Lambda_{0_{i,j}}) - \Delta\left[m_{rst_{glx_{i,j}}}c^{\,2}(\frac{\Delta\Lambda_{0_i},j}{\Delta\Lambda_{0_{i,j}}}) \right]$$

$$+\left[\sum_{k,l=0}^{k,l=\infty}\left[\Delta_{k,l}\left[(\frac{p_{orb_{k,l}}c}{r_t\,cos\,(\,(i)\,\varepsilon\,)_{k,l}}) - (\frac{G\,M_{glxCore_{k,l}}\;m_{orb_{k,l}}\theta_{k,l}\ln r_{\;g_{k,l}}}{r_t\,cos\,(\,(i)\,\varepsilon\,)_{k,l}})\right](\,r_r\,cos\,(\,(i)\,\varepsilon\,)_{k,l}\,\Delta\Lambda_{0_{k,l}}) - \Delta\left[m_{rst_{k,l\,0}}c^{\,2}(\frac{\Delta\Lambda_{0_{k,l}}}{\Delta\Lambda_{0_{k,l}}})\right]\right]\cos(\eta_{glx_{k,l}})\sin(\zeta_{glx_{k,l}})\right]$$

$$Eq.2ai.\;\; (\Delta E_{tot_{rel}}{}'\,\Delta\Lambda_{i,j}{}')_{csl} = \Delta\left[(\frac{p_{glx_{i,j}}c}{r_t\,cos\,(\,(i)\,\varepsilon\,)_{i,j}}) - (\frac{G\,M_{glx_j}m_{glx_i}\theta_{i,j}\ln r_{\;g_{i,j}}}{r_t\,cos\,(\,(i)\,\varepsilon\,)_{i,j}})_{glx_{i,j}} \right] (\,r_r\,cos\,(\,(i)\,\varepsilon\,)_{i,j}\,\Delta\Lambda_{0_{i,j}}\,) - \Delta\left[m_{rst_{i,j\,0}}c^{\,2}\Delta\Lambda sub0_{i,j}\right]$$

$$+\left[\sum_{k,l=0}^{k,l=\infty}\left[\Delta_{k,l}\left[(\frac{p_{orb_{k,l}}c}{r_t\,cos\,(\,(i)\,\varepsilon\,)_{k,l}}) - (\frac{(G\,M_{Core_{k,l}}m_{orb_{k,l}}\theta_{k,l}\ln r_{\;g_{k,l}})}{r_t\,cos\,(\,(i)\,\varepsilon\,)_{k,l}})\right](\,r_r\,cos\,(\,(i)\,\varepsilon\,)_{k,l}\,\Delta\Lambda_{0_{k,l}}\,) - \Delta\left[m_{rst_{orb_{k,l}}}c^{\,2}\Delta\Lambda_{0_{k,l}}\right] right)\cos(\eta_{glx_{k,l}})\sin(\zeta_{glx_{k,l}})\right]$$

The supercausal portion becomes:

$$Eq.2aii.\;\; (\Delta E_{tot_{rel}}{}'\,\Delta\Lambda_{i,j}{}')_{scsl} = \Delta\left[(\frac{p_{glx_{i,j}}c}{r_t\,sin\,(\,(i)\,\varepsilon\,)_{i,j}}) - (\frac{G\,M_{glx_j}m_{glx_i}\theta_{i,j}\ln r_{\;g_{i,j}}}{r_t\,sin\,(\,(i)\,\varepsilon\,)_{i,j}})_{glx_{i,j}} \right] (\,r_r\,sin\,(\,(i)\,\varepsilon\,)_{i,j}\,\Delta\Lambda_{0_{i,j}}\,) - \Delta\left[m_{rst_{i,j\,0}}c^{\,2}\Delta\Lambda_{0_{i,j}}\right]$$

$$+\left[\sum_{k,l=0}^{k,l=\infty}\left[\Delta_{k,l}\left[(\frac{p_{orb_{k,l}}c}{r_t\,sin\,(\,(i)\,\varepsilon\,)_{k,l}}) - (\frac{(G\,M_{Core_{k,l}}m_{orb_{k,l}}\theta_{k,l}\ln r_{\;g_{k,l}})}{r_t\,sin\,(\,(i)\,\varepsilon\,)_{k,l}})\right](\,r_r\,sin\,(\,(i)\,\varepsilon\,)_{k,l}\,\Delta\Lambda_{0_{k,l}}\,) - \Delta\left[m_{rst_{orb_{k,l}}}c^{\,2}\Delta\Lambda_{0_{k,l}}\right] right)\cos(\eta_{glx_{k,l}})\sin(\zeta_{glx_{k,l}})\right]$$

It is interesting to note that classical relativity fits in as a subset to the special relativity. Thus, for inertial frames the velocity of light is faster due to time slowing. Locally, however the velocity of light is the same. Also due to length expansion in a gravitational field, there is length expansion as also of this field. How gravitational time warp affects time-space is explaned; also how classical sums and differences would produce such phenomena as fast and slow light, are also explained in this document. According to Einstein's 1st law every frame of reference will report measuring light's velocity as c. Are the conflicts in report due to the consideration of more than one reference point?

The speed of light is locally always measured at c. Gravitational reference frames are also all similar, to each other. A new correlate to Einstein's second law is found to apply for all values of and permutations for time-energy, time-gravity, and momentum-span; Doppelganger subjects included. The local time-warp function, $r_t cos((i)\varepsilon)_0$, is positive for all time-warps, $\Delta\Lambda'$, with this change in formulary, expands the parsimony of Einstein's laws to include gravitation, momentum, and relativistic warp. (Eqs. 2, 2a 3, 3a., figs. 2a, 2b, 2c, 2d, 2ci, 2di, 2e).

$$Eq.3.\ \ (\Delta E_{tot_{rel}}{}'\Delta\Lambda_{i,j}{}')^2_{csl} = \Delta\left[\left(\frac{F_{glx_{i,j}}c}{(i)\lambda_{wf}}\right)-\left(\frac{G\,M_{glx_{i,j}}\,m_{glx_{i,j}}\theta_{i,j}\ln r_{i,j}}{(i)\lambda_{wf}}\right)_{glx_{i,j}}\right]^2((i)\lambda_r\,\Delta\Lambda_{0_{i,j}})^2-\Delta\left[(m_{rst_{glx_{i,j0}}}c^2\Delta\Lambda_{0_{i,j}})\right]^2$$

$$+\left[\sum_{k,l=1}^{k,l=\infty}\left[\Delta_{k,l}\left[\left(\frac{F_{orb_{k,l}}\,c}{(i)\lambda_{wf}}\right)-\left(\frac{G\,M_{Core_{k,l}}\,m_{orb_{k,l}}\theta_{k,l}\ln r_{k,l}}{(i)\lambda_{wf}}\right)\right]^2((i)\lambda_r\,\Delta\Lambda_{0_{k,l}})^2-\Delta\left[(m_{rst_{orb_{k,l}}}c^2\Delta\Lambda_{0_{k,l}})\right]^2\right](\cos(\eta_{glx_{k,l}}))^2(\sin(\zeta_{glx_{k,l}}))^2\right]$$

These three equations are in time-tense identical to each other no matter what time-frame is used i.e. moving reference frame vs. local reference frame. That is how Einstein's 2nd law of special relativity becomes true. By the same notion all gravitational reference frames are also identical. This leads the third corollary; the inertial is meta-normal to the gravitational; thus K.E. = (-)P.E.; and I.W = (-)G.P.W. It is a ubiquitous feature and parsimoniously identical to any other, moving or not. The permutations and combinations bear examining however, particularly among them is the bi-lateral: $(i)\lambda_{wf_i} \neq \frac{1}{(i)\lambda_{wf_j}}$. Except for one instance they are distinct functions. The exception is evident in the Doppelganger regions of velocity, where energy crosses over with time-warp, evident in figs. 2j, and 2k.

$$Eq.3i.\ \ (\Delta E_{tot_{rel}}{}'\Delta\Lambda_{i,j}{}')^2_{csl} = \Delta\left[\left(\frac{F_{glx_{i,j}}c}{r_t\,cos\,((i)\varepsilon)_{i,j}}\right) - \left(\frac{G\,M_{glx_{i,j}}\,m_{glx_{i,j}}\theta_{i,j}\ln r_{i,j}}{r_t\,cos\,((i)\varepsilon)_{i,j}}\right)_{glx_{i,j}}\right]^2 (r_r\,cos\,((i)\varepsilon)_{i,j}\,\Delta\Lambda_{0_{i,j}})^2 - \Delta\left[(m_{rst_{glx_i}},j_0 c^2\Delta\Lambda_{0_{i,j}})\right]^2$$

$$+\left[\sum_{k,l=1}^{k,l=\infty}\left[\Delta_{k,l}\left[\left(\frac{F_{orb_{k,l}}\,c}{r_t\,cos\,((i)\varepsilon)_{k,l}}\right) - \left(\frac{G\,M_{Core_{k,l}}\,m_{orb_{k,l}}\theta_{k,l}\ln r_{k,l}}{r_t\,cos\,((i)\varepsilon)_{k,l}}\right)\right]^2 (r_r\,cos\,((i)\varepsilon)_{k,l}\,\Delta\Lambda_{0_{k,l}})^2 - \Delta\left[(m_{rst_{orb_{k,l}}}c^2\Delta\Lambda_{0_{k,l}})\right]^2\right](\cos(\eta_{glx_{k,l}}))^2(\sin(\zeta_{glx_{k,l}}))^2\right]$$

The supercausal portion becomes:

$$Eq.3ii.\ \ (\Delta E_{tot_{rel}}{}'\Delta\Lambda_{i,j}{}')^2_{scsl} = \Delta\left[\left(\frac{F_{glx_{i,j}}c}{r_t\,sin\,((i)\varepsilon)_{i,j}}\right) - \left(\frac{G\,M_{glx_{i,j}}\,m_{glx_{i,j}}\theta_{i,j}\ln r_{i,j}}{r_t\,sin\,((i)\varepsilon)_{i,j}}\right)_{glx_{i,j}}\right]^2 (r_r\,sin\,((i)\varepsilon)_{i,j}\,\Delta\Lambda_{0_{i,j}})^2 - \Delta\left[(m_{rst_{glx_{i,j0}}}c^2\Delta\Lambda_{0_{i,j}})\right]^2$$

$$+\left[\sum_{k,l=1}^{k,l=\infty}\left[\Delta_{k,l}\left[\left(\frac{F_{orb_{k,l}}\,c}{r_t\,sin\,((i)\varepsilon)_{k,l}}\right) - \left(\frac{G\,M_{Core_{k,l}}\,m_{orb_{k,l}}\theta_{k,l}\ln r_{k,l}}{r_t\,sin\,((i)\varepsilon)_{k,l}}\right)\right]^2 (r_r\,sin\,((i)\varepsilon)_{k,l}\,\Delta\Lambda_{0_{k,l}})^2 - \Delta\left[(m_{rst_{orb_{k,l}}}c^2\Delta\Lambda_{0_{k,l}})\right]^2\right](\cos(\eta_{glx_{k,l}}))^2(\sin(\zeta_{glx_{k,l}}))^2\right]$$

The third law of Einstein is described by Eqs. 1-1d, 1i-1di, 3, and 3a, to follow. These are expanded to include not only gravitational and rest energy reference frames and their respective normalized time-warp components; their orthogonal geometry in sums and differences, is featured also later in this document. The variables for time can be and are easily interchangeable, but the reference frames remain the same. The time warp factor of fig. 2, and 2a, can be expressed now in three ways; as an inertial, rest, and gravitational time-energy. The nucleus, $r_t cos\,((i)\varepsilon)_{wf}$, corresponds also to the clock ratio readings. In cases where $\Lambda' \approx \Lambda_0$; or when v << c, then relativistic kinetic energy is just the "slim" version: $½m_0 v_{x_0}{}^2$. The same is true of gravity. At zero-gravity, the time bias differential is at zero; similarly at zero velocity, the inertial time bias differential is also at zero, (See fig. 2). Subtracting inertial time-energy from the gravitational time-energy, can be used as a practical application and mode for the calculation of orbital time-energy that would be necessary to achieve orbit and thus zero gravity in any system. Employed in the construction of said equations 1-3(i), are the two types of meta-normal time-energy couplets and their terms; the inertial rest, and gravitational. The rest time-energy remains local in all reference time-energy frames and are also all mathematically and mutually independent in rank, as per figs. 7, 7a, 7b, 7c.

For all values, consider the definitive relativistic axioms below:

a). Inertial-Energy - I.E. or K.E.

b). Gravitational Potential Energy - G.P.E.

c). Rest Energy - R.E.

d). Total Inertial Energy - T.I.E.

e). Total Gravitational Potential Energy - T.G.E.

The three types of time-warp associated with the 3 types of energy
are as follows:

f). Inertial Time Warp - I.W.

g). Gravitational Potential Time Warp - G.P.W.

h). Rest Time Warp - R.W.

i). Total Inertial Warp - T.I.W.

j). Total Gravitational Potential Time Warp. T.G.W.

This is subject is further developed in appendix T, and U.

It should also be noted that $\dfrac{(i)\lambda_r\,(i)\lambda_{wf}}{(i)\lambda_{wf}^2}$ represents the greater complex of energy per second squared relation is a form of energy / time-warp acceleration, relating 3 things together. The equivalent exists for the polar version of this function: $\dfrac{r_r\, cos(\,(i)\varepsilon\,)\, r_t\, cos(\,(i)\varepsilon\,)}{r_t \cos^2(\,(i)\varepsilon\,)}$. They are re-iterations of the same function only used in reciprocal ways. In this case the time warp function is identical to that of the constraining energy function, only in doubly form. The sign specificity is also a determinant factor over three forms of energy. Gravity’s component is 180 degrees phase negative (meta-normal), to that of the kinetic (inertial) energy, throughout the complexes. This product is of the reciprocal function and the product cancellation is two fold leaving rest time-energy lone, as it is orthonormal to normal.

Additionally, if: $\int_0^c m_0\, dv = m_0\, c = \int_0^c \dfrac{E_0}{dv} = m_0\, c = R.P. = P_0$, then total relativised inertial momentum is as: : $\int_0^c \dfrac{m_0\, dv}{\lambda_{wf}} = m_0\, c \sin^{-1}(\dfrac{v}{c}) = I.P.$. If: $(\,T.I.P.\,)^2 = (\,I.P.\,)^2 + (\,R.P.\,)^2$, then: $\left[(\,m_0\, c\,)(\,\sin^{-1}(\dfrac{v}{c}) - 1\,)\right]^2 + (\,m_0\, c\,)^2 = (\,T.I.P.\,)^2$. This essentially introduces new terms for relativised inertial and rest momentum.

These basic and universal equations constitute a second law of eight laws of time-energy dynamics. A new law of time-energy dynamics as proposed states that an object on one time-line will either remain on that time line, until otherwise disturbed by constructive or destructive interference along from the past event horizon to the present. A Newton-like third law states that every action has its equal and/or opposite reaction in space-time, and that time’s vector, or positive trajectory, is always from the past toward the future in direction; is either moving forward or moving backward, or is at stand-still, (see figs. 2a 2p). A typical event horizon’s geodesic can be expressed as a quadric set up as a difference of squares equal to zero; in this case would become: $\left[\dfrac{v^2}{c^2} + (\dfrac{\Lambda'^2}{\Lambda_0^2})\right] = (+/-)\,1$. The asymptotic cone can be derived from the same formula, when set equal to zero, yields: $\left(\frac{v^2}{c^2} + (\frac{\Lambda'^2}{\Lambda_0^2}) \right) = 0.$

One can easily substitute to obtain the general form by simple permutations of $v = \frac{\partial(+/-)\, x_0}{\partial(+/-)\, t_0}$, At light speed $c_{rel} = \infty$. Borrowing from number theory one can easily discern that $½\infty = 2\,\infty$ and $\infty^2 - \infty^2 = \infty$. Thus Einstein's second law is in this way proven and was accepted as a new fact. The gravitation however needs to be added, acting as equal and opposite to the inertial. In figs. 2ci and di, the inertial time vortex is the derivative of the inertial time-advance fig. 2, and 2a, graphs. The gravitational time vortex is depicted in fig. 2d, and is the negative of the two previous graphs. This is in keeping with central equations 1-3.

Classical relativity was replaced by special relativity since E-M from the standpoint of special relativity, spans an infinite distance, in zero time. If fig. 2a, is inverted, the point of c easily becomes summit in time dilation. Being immersed in the temporal all other points are slower. The Unity point is independent of temporality, thus divides the meta-normal while conjoining causal and supercausal folds of each the 4th dimensional Λ as specie. There also exists and as alluded to withing the text, the notion of time permittivity for free space default as one-to-one belus feature. Also implied is a quantum time specie, also the maximum amount of time is described and computed.

The riddles of occultation reports as two in kind; formeally the Doppler frequency shift can vary as per red-shift for 4th dimensional receders, and blue-shift for the 4th dimensional acceders. These kind have to do with the notion of a "cross-over point" in time-gradient sheet, reaching time-free fall kind occultation. They as Doppelganger candidates, re-appear but bear blue-shifted spectral reports, and such 4th dimensional subjects are reckoned to have energetically flopped to lesser G.P.E. time-hyper-red realms, super-passing the time free-fall singularity, without Pauli destructione to rest-energy, nor destructive disclusion. As unified singularity theory proposes, black-hole singularities are distinct from worm-hole singularities; the two forms of time-ordinate are disjoint; separated by a cross-over nodal zone of inhibition; is seen also in the laboratory as Super-Particle extinction-occultation.

In nature the actual is often concealed in the observed. The underlying truth must always explain observation. Even heat dead stars still bear mass and relativistic energies of both kinds, still distort the space-metric in opposing ways, though emitting little or no light, nor heat. From the set of two meta-normal time-energy vanes write a new chapter in the search for the causal past relationship between rest mass and rest time-warp, figs. 7-7c. It is true that light is a relativised subject, thus spans all distances through near nulls in time's advance. Another fallacy of division occurs with Einstein's obelus; if one is to accept division by c, then the equations presented in 1905 and here hold true and will predict detectable differences in the time-energy attributes of all kind of rocket propelled satellites and their astronautic corollaries. It would naturally follow that these theoretical conclusions (Einstein's 3 laws) and their premises proposed by Einstein, be tested for truth or fallacy.

An observer's reading of time Λ_0 Is, by definition, the earthbound "clock on the wall" time reading. According to figures 1a, and 1b, there exists a point of $v_{rel} = 0$ where minimum dilation occurs; this is also the point from which all other time clocks are compared, and represents a reference point for earthbound observations. The second ideal point is the proposition of a Super-Origin or O'_∞. The third point - the unity point (velocity of c), pipes into the Super-Origin Superset - O'_∞.

The question arises of whether or not there would exist a danger of not having enough fuel to fire the slow-down or to fire a retro-rocket. Would this result in "China-Man's Warp", (being stuck in time jump with no way of exiting that modality)? Another concern, lay in the case of a "time wake" that theoretically would never dissipate. One popular theory of space travel purports that matter anti-matter reactions generate a thrust given enough emission, however light flux emission from the annihilation only results in a momentum change of, per photon: $p = \frac{h\nu}{c}$. As iso-spin physics/mathematics has shown, not only do matter anti-matter reactions produce high energy EM (gamma rays), but also that the reverse reaction is also true, namely, high energy photons (gamma burst) can be artificially induced using high energy oscillators as sources for gamma rays; activated x-tal catalyzed gamma-decays into MAM particle pairs; gamma-ray producers can be derived from energtic sensitive decay x-tal catalyzers could trigger gamma decay process if they utilize the right doping; forming matter/anti-matter is natural stemming from decreased K.E. needing an activition energy-comlex to do so. Cascades from doped x-tals do this naturally, much as activated carbons would in their tight structural channels. Such candidates include synthetic production x-tal oxides of Beryllium, Lithium, Boron, and Aluminum. Both matter anti-matter pairs can be laser-beam sorted, selected, collected, and accelerated in bi-level matter anti-matter (MAM) multi-ringed, directionally opposed, separate MAM accelerator ring assemblies. Initialization is accomplished by venting their corridors, to achieve the absolute vacuum of space. In this way, both matter and anti-matter can be handled using opposite polarity of their electromagnetically guided walls and corridors. Their beams' forces would add-in sympathetically; one task would be to create aerially dynamic yet controllably stable landing/take-off engine-body chassis designs. Ringed-type space jetti-propulsion systems have been possible since 1965; could lead to space-craft based upon this propulsion modality. Incorporating a central core magnet would enhance this Joule-induced torque force effect; would put MAM derived electro-magnetic non-flame jetti-propulsion systems as classically suited for long-range space-travel. The right-hand rule applies for matter, the left-hand rule applies for anti-matter; noting that there permutations, and combinations of these two cross product pneumonics are diverse and algorithmic in number.

While progress has been made, the light flux could be used in conjunction with Eq. 7 as a catalyst for time-particle producing time-crystals. Ideally, a temporal time-travel effect could be noticed and used if matter can be brought to time travel through beam-crystal irradiation and directed flux. Such time-crystals most likely would be grown synthetically from in-organics with (or without) the impurities which cause cascades in the electron shells such as that seen in lasers. Semi-quartz or radioactive bi-crystals could also lend themselves to produce time-particles. Their photo-electric activity to laser light and/or nucleon beam may produce a real or pseudo-Compton time-particle effect. For example, figs. 4a, and 4b, detail the crystal-collector assembly using isotopic Boron-12 goshenides, or bromolides and can be used as a platform for weak-force derived plasmas. Coordinate complexes for naturally with radio-meric isomers which upon irradiation produce high-energy weak-force plasmas. High energy alpha fluxes upon slow thermal neutron irradiation, and could be produced easily form a high energy particle plasma cascade with the correct combination(s). As an example, radio-isomeric isotopes of Boron(12) with a beryllium deuteride coated outer layer contained within a goshenide host crystal in coordinate bond would naturally form synthetically and transparence can be had through skull melt(s) - thus naturally show more promise. When enough them are formed they could act together with sufficient flux to serve as a method of amplification for a plasma producing instrument. Yet another scenario for Boron(12), could utilize a central Cobalt (II,III)-Boron(12) ion in the development of coordinate compounds, as high-energy alpha emitting energy sources.

As an example of a newly time relativised we turn to the photo-electric effect and the energy necessary to eject an electron from the atom’s light shell plasma. The energy of the scattered particle after an in-elastic collision with a photon is as we know, the kinetic energy minus the work function ϕ, the latter is defined as that energy needed to overcome the work needed to free it from the electronic shield of the atom. The photon thus releases its energy to the particle, upon absorption. Depending upon the energy of a particle with its relativistic complexes; when multiplied by the relativistic time-warp, produce a dual application of the $(i)\lambda_{wf}$. The double Jacobian line integral for total time-energy is computed. Since the terms are bi-linear and independent the Fubrini comes about. Furthermore the integral's definite limits are expanded to include from 0 to c, then again from c to infinity. When the two half-kites of figs. 7, and 7a are juxtaposed, the full kite of relativistic energy time-warp ensues, as per Eq. 7b.

Symbolically, this begins with the treatment of the following expression, as: $\frac{m_0 \, v_{x_0}}{(i)\,\lambda_{wf}}$, and the residual kinetic energy is $pc + \phi$; thus $E_t - \phi_i = K.E.$ The rest energy of the particle remains $m_{r_0} c^2$ and when added to the K.E. the total time-energy expression forms. When the relativistic time jacket is applied in the same way to already well accepted energy formulae one can see an old energy expression with the time dimension re-introduced: The relativistic Compton's Photo-Electric Formula - becomes also the pseudo-effect for charged particles. From: Eqs. 4, 5, and 7 these are described more fully.

$$Eq.4.\ \ \Delta E_i = \Delta\left[h\,\nu_j - h\,\nu_i\right] = \Delta\left[(p_j\,c + \phi_j) + (m_j\,c^2)\right] - \Delta\left[(p_i\,c + \phi_i) - (m_i\,c^2)\right]$$

$$Eq.5.\ \ \Delta E_j = \Delta\left[h\,\nu_k - h\,\nu_j\right] = \Delta\left[(p_k\,c + \phi_k) + (m_k\,c^2)\right] - \Delta\left[(p_j\,c + \phi_j) - (m_j\,c^2)\right]$$

The relativised Planck's Energy is thus:

$$Eq.6.\ \ \Delta E\,'\,\Lambda'\,(i)\lambda_{wf} = \Delta\,h\,\nu\,\Lambda' = \Delta\,(p\,c\,\Lambda')$$

The Compton's energy by virtue of this same process, similarly translates into:

$$Eq.7.\ \ (\Delta E_{rel_{i,j}}\,'\,\Delta\Lambda')^2_{csl} = \sum_{i,j=1}^{i,j=\infty} \Delta\left[\left[\left(\frac{p_{i,j}\,c + \phi_{i,j}}{(i)\lambda_{wf}}\right) - \left(\frac{p_{i,j}\,c + \phi_{i,j}}{(i)\lambda_{wf}}\right)\right]^2\right]\left(((i)\lambda)_r\,\Delta\Lambda_{0_{i,j}}\right)^2$$

The polar substution yields an equivalent specie:

$$Eq.7i.\ \ (\Delta E_{rel_{i,j}}\,'\,\Delta\Lambda')^2_{csl} = \sum_{i,j=1}^{i,j=\infty} \Delta\left[\left[\left(\frac{p_{i,j}\,c + \phi_{i,j}}{r_t\,cos\,((i)\,\varepsilon)_{i,j}}\right) - \left(\frac{p_{i,j}\,c + \phi_{i,j}}{r_t\,cos\,((i)\varepsilon)_{i,j}}\right)^2\right]\right]\left(r_r\,cos\,((i)\varepsilon)_{i,j}\,\Delta\Lambda_{0_{i,j}}\right)^2$$

The supercausal portion becomes:

$$Eq.7i.\ \ (\Delta E_{rel_{i,j}}{'}\Delta\Lambda{'})^2_{scsl} = \sum_{i,j=1}^{i,j=\infty}\Delta\left[\left[(\frac{p_{i,j}\,c+\phi_{i,j}}{r_t\,sin((i)\varepsilon)_{i,j}})-(\frac{p_{i,j}\,c+\phi_{i,j}}{r_t\,sin((i)\varepsilon)_{i,j}})^2\right]\right](r_r\,sin((i)\varepsilon)_{i,j}\,\Delta\Lambda_{0_{i,j}})^2$$

The relativistic Doppler equation proves its independence from special relativity thus its usefulness, becomes:

$$Eq.8.\ \ \nu^2 = \frac{\left[(\lambda_{wv}\pm\Delta X_{obj})\Lambda_0\right]}{\left[(\Lambda_0\pm\Delta X_{lgt})\lambda_{wv}\right]}\nu_0^2$$

With the periodic, yields:

The relativistic Lorentz Time-Energy-Magnetism-Gravitation formula proceeds from Eq. 7 to become:

$$Eq.9.\ \ (\Delta E_{rel_{i,j}}{'}\Delta\Lambda{'})^2_{csl} = \sum_{i,j=1}^{i,j=\infty}\left[\Delta\left[((\frac{q_{i,j}\,d_{i,j}\,\vec{E}\,c}{(i)\lambda_{wf}}+\frac{q_{i,j}\,v_{i,j}\,d_{i,j}\,\vec{B}\sin(\rho)\,c}{(i)\lambda_{wf}}))-(\frac{G\,M_{i,j}\,m_{i,j}\theta_{i,j}\ln r_{i,j}}{(i)\lambda_{wf}})\right]^2((i)\lambda_r\,\Delta\Lambda_{0_{i,j}})^2-\left[\Delta\Lambda_{0_{i,j}}\,\Delta E_{rst_{i,j}}\right]^2\right](\cos(\eta_{i,j}))^2(\sin(\zeta_{i,j}))^2$$

The equivalently periodic substituted form yields:

$$Eq.9i.\ \ (\Delta E_{rel_{i,j}}{'}\Delta\Lambda{'})^2_{csl} = \sum_{i,j=1}^{i,j=\infty}\left[\Delta\left[((\frac{q_{i,j}\,d_{i,j}\,\vec{E}\,c}{r_t\,cos((i)\varepsilon)}+\frac{q_{i,j}\,v_{i,j}\,d_{i,j}\,\vec{B}\sin(\rho)\,c}{r_t cos((i)\varepsilon)}))-(\frac{G\,M_{i,j}\,m_{i,j}\theta_{i,j}\ln r_{i,j}}{r_t\,cos((i)\varepsilon)})\right]^2(r_r\,cos((i)epsilon)\Delta\Lambda_0)^2-\left[\Delta\Lambda_0\Delta E_{rst}\right]^2\right](\cos(\eta_{i,j}))^2(\sin(\zeta_{i,j}))^2$$

The supercausal portion becomes:

$$Eq.9ii.\ \ (\Delta E_{rel_{i,j}}{'}\Delta\Lambda{'})^2_{scsl} = \sum_{i,j=1}^{i,j=\infty}\left[\Delta\left[((\frac{q_{i,j}\,d_{i,j}\,\vec{E}\,c}{r_t\,sin((i)\varepsilon)}+\frac{q_{i,j}\,v_{i,j}\,d_{i,j}\,\vec{B}\sin(\rho)\,c}{r_t sin((i)\varepsilon)}))-(\frac{G\,M_{i,j}\,m_{i,j}\theta_{i,j}\ln r_{i,j}}{r_t\,sin((i)\varepsilon)})\right]^2(r_r\,sin((i)\varepsilon)\Delta\Lambda_0)^2-\left[\Delta\Lambda_0\Delta E_{rst}\right]^2\right](\cos(\eta_{i,j}))^2(\sin(\zeta_{i,j}))^2$$

The total time-energy for any system is as follows:

$$\text{Eq. 9a. } \oint(x-y)\cdot dx\,dy = (u_i v_i)^2(u_j v_j)^2\left[\frac{((u_i v_i)^2-(u_j v_j)^2)}{2}\right]$$

Where:

$$x_{csl} = (\Delta E_{d\sigma_i}{}' \cdot \Delta \Lambda_{d\sigma_i}{}')^2 = (u_i v_i)^2 = \Delta \left((\frac{p_i c}{(i)\lambda_{wf_i}}) - (\frac{G M_i m_i \theta_i \ln r_i}{(i)\lambda_{wf_i}}) \right)^2 ((i)\lambda_{r_i} \Delta \Lambda_{0_i})^2$$

And where: $y = (\Delta E_{rest} \Delta \Lambda')^2 = (u_j v_j)^2 = (\Delta E_0 \Delta\Lambda')^2$

Where:

$$x_{csl} = (\Delta E_{d\sigma_i}{}' \cdot \Delta \Lambda_{d\sigma_i}{}')^2 = (u_i v_i)^2 = \Delta \left((\frac{p_i c}{r_t \cos((i)\varepsilon)_{wf_i}}) - (\frac{G M_i m_i \theta_i \ln r_i}{r_t \cos((i)\varepsilon)_{wf_i}}) \right)^2 (r_r \cos((i)\varepsilon)_{wf_i} \Delta \Lambda_{0_i})^2$$

The translation matrix of partial derivatives for this Jacobian are as follows:

$$\Pi = \begin{vmatrix} (2 u_i v_i^2)(2 u_j^2 v_j) \\ (2 u_j v_j^2)(2 u_i^2 v_i) \end{vmatrix}$$

The polar version of the above relation goes accordingly as follows:

Eq. 9ai. $\oint (x - y) \cdot dx\, dy = (u_i v_i)^2 (u_j v_j)^2 \left(\frac{((u_i v_i)^2 - (u_j v_j)^2)}{2} \right)$

Where:

$$x_{csl} = (\Delta E_{d\sigma_i}{}' \Delta \Lambda_{d\sigma_i}{}')^2 = (u_i v_i)^2 = \Delta \left((\frac{p_i c}{r_t \cos((i)\varepsilon)_{wf_i}}) - (\frac{G M_i m_i \theta_i \ln r_i}{r_t \cos((i)\varepsilon)_{wf_i}}) \right)^2 (r_r \cos((i)\varepsilon)_{wf_i} \Delta \Lambda_{0_i})^2$$

The supercausal portion becomes:

$$x_{scsl} = (\Delta E_{d\sigma_i}{}' \Delta \Lambda_{d\sigma_i}{}')^2 = (u_i v_i)^2 = \Delta \left((\frac{p_i c}{r_t \sin((i)\varepsilon)_{wf_i}}) - (\frac{G M_i m_i \theta_i \ln r_i}{r_t \sin((i)\varepsilon)_{wf_i}}) \right)^2 (r_r \sin((i)\varepsilon)_{wf_i} \Delta \Lambda_{0_i})^2$$

Where: $y = (\Delta E_{rest} \Delta \Lambda')^2 = (u_j v_j)^2 = (\Delta E' \Delta\Lambda')^2$

The determinant of this is: $\det(\Pi) = 0$, pointing to the independence of six terms of time and energy, confirming their perpendicularly related nature and linear independence; gravity meta-normal with the inertial, both being then also orthonormal to the rest energy and rest time warp. a translation matrix is therefore not necessary. The Jacobian degenerates into the Fubrini form of the expression.

Multiplying by time-warp becomes what we see at the observatory level and is the warp normalized function. The Kepler's values are the actual phenomenological values which are reflected as the Pythagorean square root of the T.I.E. complex. For this reason the time-environment must always be considered before assessing the status of kinetic and/or gravitational objects. Objects in gravitational freefall such as an orbiting planet are described by their remaining potential energy and the rest energy only, due to subtraction-cancellation. Below is a listing for the definitions of the variables involved:

$\vec{P} = \vec{p} = m\vec{\mathbf{u}}$ The Lorentz Momentum.

$q =$ Charge of the Fermionic specie.

$\phi =$ The work function for the Compton's photo-electric effect.

$c =$ Speed of light constant.

$d_i =$ Distance of each particle's travel through the field.

$\lambda_{wv} =$ The de Broglie wavelength of

the scattered light wave.

$(i)\lambda_{wf} = \frac{1}{\gamma} = (1 - \frac{v_x^2}{c^2})^{½}$. The Lorentz Factor Nucleus.

$\frac{\Delta\Lambda'}{\Delta\Lambda_0} = (i)\lambda_{wf}$: The Time warp factor clock ratio.

$r_t cos((i)\varepsilon) = \frac{1}{\gamma} = (1 - \frac{v_x^2}{c^2})^{½}$. The identity time-warp factor nucleus, in polar form.

$r_r cos((i)\varepsilon)_r = \frac{1}{\gamma} = (1 - \frac{v_x^2}{c^2})^{½}$. The identity space-warp factor nucleus, in polar form.

$\frac{\Delta\Lambda'}{\Delta\Lambda_0} = r_t cos((i)\varepsilon)$: The Time warp factor clock ratio, using a periodic function.

$v =$ Speed of the Fermionic specie.

$G =$ The Gravitational constant.

$M_1 =$ The primary mass of a system of 2 masses.

$m_2 =$ The lesser secondary orbiting object or mass.

$r_0 =$ The distance between any system of 2 masses.

$\eta_{glx_{i,j}} =$ The primary torque angle i in velocity direction j.

$\zeta_{glx_{i,j}} =$ The secondary torque angle i in velocity direction j.

$\rho =$ Angle of beam refraction.

$\vec{E} =$ Coulomb's Electric Field.

$\vec{B} =$ Lorentz Force Magnetic Field.

$\bar{h} =$ Heisenberg Constant.

$h =$ Planck's Constant.

$r_r =$ The radius of distance.

$r_t =$ The radius of time.

$r_{t_{csl}} = r_t cos((i)\varepsilon)$ The causal past time-radius for sub-singular time warp.

$r_{t_{scsl}} = r_t sin((i)\varepsilon)$ The supercausal future time-radius for supercausal time-warp.

$\nu_i =$ Frequency of emission.

$\nu_0 =$ Initial Doppler frequency of light.

$T^2 = (\frac{(4\pi^2)}{GM})r_g^3 =$

The Elliptical orbits and rotation period.

Discussion:

The Lorentz time-energy as formulated from the Lorentz force is useful for time particle energy calculations to be used in conjunction with the Time-Warp factor. Building a detector that can detect the geneology and evolution of a time-particle's correct energy and temporal position, is an easier task now. Detectors for hyper-light time jump would pick up these particles somewhere in the future by decreasing time-energy as a function of reverse time-dilation. Experiments prove this everyday i.e. for any event that alters course or speed for any time-mass-energy-gravity relativistic object, points to the consequence part of the causal universe. Testing this phenomenon could easily be designed. Due to the gravity tensor, the warp in time occurs opposite to that of inertial energy. Instead of a decreasing time rate, there occurs an increasing time rate in a gravitational filed. Mathematically, there are two sign negatives spread over three terms, i.e. gravity, time-warp, and the Heisenberg constant. The two sheets of time; in particular generate a 3D mathematical curve representing the shape of the space warp and that of the similarly shaped time warp (black hole inverted becomes a worm-hole). In hyper-c territory the particle actually loses energy, while gains in span may break records, from the time hyper-red point of view, this is to be expected. While, in the sub-light regions, the opposite is true; decreasing time bias is accompanied by higher energy.

The "Lazarus Corridor" as a concept, could by allusion stem from that area where the function of time is undefined; pertains to the indeterminate form, and specifically refers to those points between sheets in time's Λ function such that $1 > \Lambda_0 > -1$, of fig. 1a. This concept would invoke values between the two Heisenberg constants: $(+/-)\,\bar{h}$. Considerations of simultaneity, polarity, total charge, velocity, frequency of nuclear events, and the durations of their consequent activated interactive complex; their outcome, are also involved. At the quantum level particles are always time dependent, also. The Pauli exclusion principle more properly concerns the occupied time-energy states of the smaller set greater meaning set of sub-atomic particles and their various quantum numbers associated with energy state, need to be expanded to include all the other terms. This may require anti-symmetric systems of quantum numbers to describe the nuclear derivatives, until their conditions, can be ore fully inventoried and described. Often one nucleon transforms into another via weak force interactions, collisions and/or fusion, it always shifts the set of quantum numbers to account for the change of state-time. Hence it could be more useful to regard Fermions as multiple states of the same nucleon, in some systems, existing as such differing only in time position. In quark theory it became necessary to adopt the gluon quantum variable of Color to maintain quark anti-symmetry as it pertains to Pauli's spin statistic theorem. The same is true of time line integrity, positioning, and relative persistence (fatigue-ability), described earlier in this document. This leads to a Newton like first law of time-dynamics which describes the destructive and/or constructive interference of the dynamics of any matter-time-energy arrangement. This combines four concepts of Huygens, Isaac Newton, Einstein, and Pauli. Proper time-lines and time-line sets normally join their pasts with their futures, through their present. Thus the set of futures depends upon the set of past events, and their outcomes. Expected antecedent-outcomes from an ordered set of variables; are polynomially related. When predicting closed set of polynomial rules has always been the temptation of any science inquiry. Given identical variables and values, the same outcomes can be reproduced mathematically if our models are parsimonious enough.

Thus length contraction for Doppelganger inertial objects, would be opposite in sign to the length expansion for gravitational objects. Sub-singularity inertial objects, are similarly placed relative to their Doppelganger counterparts. The qualifying criteria is the polarity in sign of the differential to the warp factor itself. In this document a new warp co-efficient is developed, and the obelus of normal time-space warp and mass is introduced as namely: **R**. For anti-matter and its detailed realm is as: $\mathbf{R}_{\alpha}$.

These are the essentials to convert from tensor world anti-matter to that of normal vector matter; more commonly known as the proof for the right-hand rule; and the corollary proof of the left hand rule for anti-matter; varies and co-varies as a double obelus of division and sign reversal.

The former thus explains the Stokes geodesic for relativised distance and relativised time. The volume of a geodesic pyramid follows the general formula: $V = \frac{B\,h}{3}$, and $6\,V = 2\,(B\,h\,)$, where B is the area of the base (e.g. $(\,v^{\,2}\,)$), and $h_i = m_0$. Six of these pyramids when assembled, coincide with twice the volume of the cube containing any one. The same is true for a lower normal pyramid as well if joined at the base. When arranged, the six pyramids naturally form hexa-vertexed cube of chief-cornerstones (joined at the tips). The greater cube defines a greater spherical distortion field of influence; occurs as 3D gradient of special relativity is an extension of any time-space radius is represented as X' contravariant for the moving frame, and defines the Volumes as the areas and volumes of a time-space sphere, with a six-pyramid cube inside, touching at the corners, with the former's extension.

The surface area of the sides L are such that $L = P\ s$, when P is the perimeter of the base and s is the slant height of that point on the side measured from the base. This calculation for volume equals exactly the 1/3 the volume of a cube of same base and height. Other considerations are the diagonals and the octahedral arrangements with time-gravity as a lower pyramid. The momentum-distance forming an upper pyramid; the time-gravity as lower pyramid, forms a time-gravity pyramid (figs. 4-4c). The sums of the sum of squares form a tertiary total temporal time-energy kite circumferences/areas as well. Proposed also is a time-energy equilibrium constant for the universe, using this knowledge.

One result of this examination of special relativity could be the generation of the first Universe Time-Dilation Topical Relief Map. Such topology of the universe; the permittivity of space are always a function of depend on the fourth dimensional time-disortions, i.e linkage-disequilibrium. Could be used to explain the chute or luge effect of the galaxy concentrations which occurs cosmogonically. Certainly any such map would have two topi-spheres, conjoined at the mathematical time free-fall c-point. Since gravitational fields expand time-space, this kind of distortion and output would naturally be be repsonsible for the spiral formation as well. In such a charting scheme, each galaxy would have a pipe associated at its base; the length of which could represent the time frame bias for individual object galaxy determined by spectral red-shift. Generally, from resdual G.P.E., a galaxy's maximum gravity is 4 times its kinetic energy, can also equate as: $\Delta K.E. = \frac{\Delta(-)G.P.E._{tot}}{4}$. Gravity debits/credits are alone to amply explain cosmogonic motion. The residual K.E. is two-fold; the trend inward (pointed toward the center) and the receding trend. Both are figments of the same phenomenon. Thus the K.E. from the galactic core debits in G.P.E. are the same K.E. responsible for the apparent motion inward. The receding of the galaxies, as stated previously, is generally dependent upon the comparative masses of any two objects; are both Newtonian reactions to velocity pointed toward the center of the greater mass. With naturally occuring debits in gravity, The inward motion becomes prominent and pronounced with phenonmena such as black-holes. Which factor to use will in large part always be lead by the fact that debits in G.P.E. always result in positive changes in kinetic energy. For Doppelganger, the opposite is true. They always have large decreases in K.E. in exchange for credits in gravity. While in the causal universe, debits in gravity occur with matter accretion, are UV shifted, i.e. the black-hole, are reversed in role for Doppelganger regions, they dispell matter, and are red-shifted subjects, while moving backward in time. A galaxy in causal time-space will always appear to recede, extend outward its stellar arms (pinwheel effect), be red-shifted in spectra; while a Doppleganger galaxy will be blue-shifted, appear to accede, and its stellar arms actually tighten-up into an ellipse.

The "quartermain form" is a formula for cosmogony as well as one for navigation; pertains to all orbiting cosmology; embodies advanced energy induced time-warp mechanics. This rule is reflected as a triad for new constants per: $\frac{(-)h}{\pi}$ for time-gravity, $\frac{h}{2\pi}$ for time-energy and $\frac{h}{4\pi}$ for momentum-spaces. Concerning residual K.E. from residual gravity as a propulsion system (from Eq. 9); the gravity tensor is reactive and generates a group K.E., that is residual to residual gravity. Typically as: $(\,(+)K.E.\,)_{res.}$), so that $(-)\,4x\,(+)K.E.\,)_{res} = G.P.E$, or the total gravity of an object. The residual time-gravity is as: $\frac{(\,(-)\,\Delta\,G.P.E.\;(+)\,\Delta\Lambda'\,)}{2} < (-)\,\bar{h}$. The Riemann infinite series is as:

$\frac{((-)\,\Delta\, G.P.E.\ (+)\,\Delta\,\Lambda')}{4} = \frac{((+)\,\Delta\, K.E.(-)\,\Delta\,\Lambda')}{2} = (((+)\,\Delta\, K.E.\ )_{res}\ (-)\,\Delta\,\Lambda')\ \cdots.$ The residual the K.E. to that of residual time-gravity is deduced as system inertia, becoming: $\frac{((-)\Delta\, G.P.E.\ (+)\Delta\,\Lambda')}{8} = \frac{(\ (+)\Delta\, K.E.\ \Delta\,(-)\Lambda')}{4} = \frac{((\,\Delta\, K.E.\ )_{res}\ \Delta\,\Lambda')}{2}\ \cdots.$ This Green’s/Riemann infinite series reciprocates in a similar way as Occam’s razor; operates as geometrically recursive, and after a few iterations, converges.

Conceivably MAM particle accelerators could serve as jetti-propulsion engines (See figs. 5a, 5b, and 5c). Even a minimum warp in time produces a catapult effect in space displacement, that once in space, will perform from small but workable time-warping streams of particles which induce an elevating force. Predicted by Eq. 9; is easily reproduced as commonly seen with speaker coils, wire coils with a centrally positioned yet attached ringed magnet will easily rise off the bench even with spikes of rectified DC Voltage. More-over the pseudo-Compton effect can be rigged to make essentially similar arrays of particle induced photo-voltaic effect battery re-chargers, using the same photo-cell panels. With the power of nuclear electricity, deep space systems can be designed; using cylindrical Tokamak’s and/or Plutonium radioactivity; time-warp producing engines could easily empower deep space voyages. It becomes a sophomoric exercise to convert the conservative output of a (9600 x 4) x 2 array of nautical screw-turning, electricity producing, Tokamak and/or (Pu) nuclear-powered engines can be used for electron volt (eV) energy generation.

Theoretically 2 x 4 linear MAM propulaion systems run by having particle matter circulation on one side with anti-matter particle circulation in the adjacent accelerator tandem tube-assemblies. so that the force vector of each sympathetically aligns as right-hand rule and left-hand rule would predict; matter and anti-matter respectiviely. Such a system would work much as a laser does, only in reverse; pods that could collect and circulate/accelerate particle matter along side ones for anti-matter both fed by a gamma ray catalized emitter/decay source for magnetic sorter systems would feed linear 4 x 4 MAM assembly coil particle accelertaor systems. Both produce net torque force vectors from EM-MAM electricital power sources. Such energy conversion to jetti-propulsion is of the day. One technology mutually serves the other.

Theoretically if the Big Bang story is correct then there would be a center point where it occurred, within this dilation mapping of the time-space topi-sphere. The subject of time-space strings draws to mind what natural strings do; namely generate harmonic topi-spheres as strings do. Schrödinger node formation dictate resonance and also cancellation. In the case of the Tokomak reactors, regarding their inability to stabilize their plasma clouds; the plasma stabilizes readily by using rail magnets down the sides of cylindrical reactors. These rail magnets act as geodesic plasma guides resulting in resonance geodesics, which in turn form high temperature nodes within these geodesics. Additionally, the cylindrical Tokomak designs will achieve this goal much more readily than the toroidal ring type, which should only be used as storage rings and/or collectors. Particularly a V-twin Tandem cylindrical design would work by one plasma pre-igniting the other, or from yet other still un-conceived burn scenarios. In order for the space movement to be able to use nuclear fuel as an SRM technology (solid rocket motor) conceivably would involve fusion reactions however this would necessitate strong force capable bomb reactor units (similar in use to those of chemistry laboratories regarding chemical protocols only as adapted for the nuclear space fuels industry); these could utilize an input hatch with a solidified thruster-escape plasma conic nodule. The energetic burst would be temporary; the plasma would act in primarily accordance with Newton’s third law of motion (action-reaction), i.e. sub-light velocities. The reactor unit would be necessarily be dependent upon the durability of the mantle walls e.g. Uranium(238), the cooling/coolant properties used, the heats of vaporization, choice based upon overall strength in being impervious to vaporizing. As a distant goal, a new substance could be produced and utilized, from a triple helium fusion-reaction as substrate, as seed mixed for the polymer element formed is as: Carbonomium $C({}^{6}_{12})^{n}$, for (n = 1,2,3...n); inter-mixed with Nitrogen(12)-C(60) form a intra-atomic-ploymer-sheet as a nuclear ladder; using Boron(12)-Nitrogen(12) as a fluxing agent and an arc-welder's arc, modified to include thermal neutron flow could reach suitable temperatures for formation. Releasing the high-energy alpha from the B(12) should form the proposed "Carbamide" bi-element strand. Polymerized Carbonomium when produced in sheets can be used to form formidably indestructible hulls, shields, and shelters; designs of all kinds that utilize solid moldings are possible. A well equipped science could easily reach daylight in the development of Carbamide space hull design systems; in the real and very near future.

Also the aforementioned considerations help answer the temporal paradox of meeting one's Doppelganger; if future time travel were the mode of the day, would they annihilate or never meet due to differing quantum time reference frames or time-stereoisomerism? Furthermore, would assigning time-line quantum numbers solve this time paradox? How would one prove, or disprove, this would occur, or be a factor. The weak interaction electronic and the Schrödinger resonant oscillation of electron wavelets and how wavelets confine regarding a minimum quantum time interval; the smallest quantum interval implies a minimum measurable interval, as the Heisenberg law predicts. With equations i-vi, this becomes easily predictable.

Still other designs utilize laser mediated fusion within a Uranium(238) bomb-mantle. Still other designs could operate using weak-force in thermal neutron/proton exposure generating a cascading particle effect, within a radiomeric crystalline mantle. Radiomeric centered, electricity producing, synthetic conductive X-tals, could be used as powerful particle emitters, and may surpass the dirty high-radioactive waste radiomeric fuels of this day. Also these through the use of ring-collectors high energy plasmas can develop. The forces generated can easily be used for lift and propulsion.

The 4-point time-energy (Real + Doppelganger) Energy Star is related to the Time-Warp Star as pictured as: figs. (figs. 2ci, 2di, 2e, 2j, 2k, and 2ki). The vortex shape is re-iterated in Doppelganger portions. At singularity the isomorphism appears, and the ends reach to apparent infinity. The proposed Super Origin, O_{∞} takes care of this condition providing an alternate and opposite logos to the decimal origin.

With respect to un-controlled boson release, as it pertains to the development and use of super-fuels, their burn statistics, their end-products, their intermediates, the reactants, fireball size, catalysis, and reactor coolants; solving how to handle the excessive temperatures will be essential to progress in this field. How should time quantum numbers be scripted? As a rule of thumb, a particle's starting point and end point in time are the two special points for any event-outcome expression using these forms. The rest are events along the way, including EMT emission, whose time event horizon is dependent upon its energy. Time-warp free-fall occurs in the laboratory as well, with SuperParticles. These too, experience Pauli temporal "rolling" into a non-inhibited inclusive - crossover-decolletage; after a gap of short occultation-extinction; Doppelgangers should be quick to re-appear. The key is in their being locally at lower energy, and appear further down the track, at a later point in time.

As already stated, the apparent receding is evidence that increasingly gravitational objects have decreases in P.E. that are associated with increases by their inertially aspected reactive time-warp. The equivalent in momentum results is as the follows: $((+)2\Delta P_0(+)\Delta X')$. The opposite is true for $d(\Delta X')$, at the differential level, the net time-energy is as: $((+)2d(\Delta P_0)(-)d(\Delta X'))$. The tensor negation of energy also generates a negative inertial time warp, thus doubly negating. This explains mathematically the receding nature of most galaxies. As the graphs dictate,

goes further to predict the acceding kind, too.

Fast/Slow light as a current fad could actually be a clipping wave cresting in any Huygen wavelet, slow light if known, could simply be an ebbing and illusory effect, better explained by poor man's lab error. The more theories there are regarding this subject, the less they have to do with time-space warp cancellation true for fundamental special relativity. Thus what is true for all waves, more usefully described by frequency differences, as the velocity for wave phenomena will always be constant for their media substrate. This is true for all waves, e.g. their crests, their wave-front, their ebb, their flow, as captured by the webbing of time-space in Earth's gravitational field. Both time and metric distortion stems ultimately from time distortion, when they cancel as in any typical obelus of velocity, does so also per 3D. The the modular integrity of any object with velocity is thus always maintained. This occurs for all velocities. From the Heisenberg sextet, the following occur:

i). $\uparrow d\, E_{K.E._0} \downarrow d\, \Lambda' \approx \downarrow d\, G.P.E._{res_0} \downarrow d\, \Lambda' \approx \uparrow 2\, dP_0 \downarrow d\, X' > \bar{h}\, d(1)$

ii). $\downarrow d\, E_{K.E._0} \uparrow d\, \Lambda' \approx \uparrow d\, G.P.E._{res_0} \uparrow d\, \Lambda' \approx \downarrow 2\, dP_0 \uparrow d\, X' > \bar{h}\, d(1)$

iii). $d\dfrac{(h\nu)}{2\pi}\, d\Lambda' = (\dfrac{d(pc)}{2\pi}\, d\Lambda') > \bar{h}\, d(1)$

iv). $\Delta\dfrac{(h\nu)}{2\pi}\Delta\Lambda' = \Delta\dfrac{(pc)}{2\pi}'\Delta\Lambda_0 = \Delta\dfrac{(pc)}{2\pi}(i)\lambda_{wf}\Delta\Lambda_0 = (2\Delta P_0\Delta X') = 2\Delta P_0(i)\lambda_{wf}\Delta X_0 = (\Delta P'\Delta X_0) > \bar{h}$

v). $\Delta\dfrac{(h\nu)}{2\pi}\Delta\Lambda' = \Delta\dfrac{(pc)}{2\pi}(r_t cos((i)\varepsilon))\Delta\Lambda_0 = (2\Delta P_0\Delta X') = 2\Delta P_0\, r_t cos((i)\varepsilon)\Delta X_0 = (\Delta P'\Delta X_0) > \bar{h}$

vi). $\dfrac{1}{\Delta E_{K.E._0}\Delta\Lambda'} = \dfrac{1}{\Delta G.P.E._{res_0}\Delta\Lambda'} = \dfrac{1}{2\Delta P_0\Delta X'} < \dfrac{1}{\bar{h}}$

vii). $\dfrac{1}{\Delta E_{K.E.}{}'\Delta\Lambda_0} = \dfrac{1}{\Delta G.P.E.'_{res}\Delta\Lambda_0} = \dfrac{1}{\Delta P'\Delta X_0} < \dfrac{1}{\bar{h}}$

viii). $(\dfrac{1}{\Delta E_{K.E._0}\Delta\Lambda'})^n = (\dfrac{1}{\Delta G.P.E._{res_0}\Delta\Lambda'})^n = (\dfrac{1}{2\Delta P_0\Delta X'})^n < (\dfrac{1}{\bar{h}})^n$, for: $n = (1,2,3...)$

Sublight vs. Doppelganger Time-Energy and Differential Time-Energy Results:

Table 1.

Type I - Defector Kinetic Time-Energy Cross-Overs.

$K.E._S \, \Lambda_S{}' = (+\,+)$	$K.E._D \, \Lambda_D{}' = (-\,-)$
$K.E._S \, d\Lambda_S{}' = (+\,-)$	$K.E._D \, d\Lambda_D{}' = (-\,-)$
$dK.E._S \, \Lambda_S{}' = (+\,+)$	$dK.E._D \, \Lambda_D{}' = (+\,-)$
$dK.E._S \, d\Lambda_S{}' = (+\,-)$	$dK.E._D \, d\Lambda_D{}' = (+\,-)$

Type II Defector Gravitational Time-Energy Cross-Overs.

$G.P.E._S \, \Lambda_S{}' = (-\,-)$	$G.P.E._D \, \Lambda_D{}' = (+\,+)$
$G.P.E._S \, d\Lambda_S{}' = (-\,+)$	$G.P.E._D \, d\Lambda_D{}' = (+\,+)$
$dG.P.E._S \, \Lambda_S{}' = (-\,-)$	$dG.P.E._D \, \Lambda_D{}' = (-\,+)$
$dK.E._S \, d\Lambda_S{}' = (-\,+)$	$dK.E._D \, d\Lambda_D{}' = (-\,+)$

Type III Direct Kinetic Time-Energy Cross-Overs.

$K.E._S \, \Lambda_S{}' = (+\,+)$	$K.E._D \, \Lambda_D{}' = (-\,+)$
$K.E._S \, d\Lambda_S{}' = (+\,-)$	$K.E._D \, d\Lambda_D{}' = (-\,+)$
$dK.E._S \, \Lambda_S{}' = (+\,+)$	$dK.E._D \, \Lambda_D{}' = (+\,+)$
$dK.E._S \, d\Lambda_S{}' = (+\,-)$	$dK.E._D \, d\Lambda_D{}' = (+\,+)$

Type IV Direct Gravitational Time-Energy Cross-Overs.

$G.P.E._S \, \Lambda_S{}' = (-\,-)$	$G.P.E._D \, \Lambda_D{}' = (+\,-)$
$G.P.E._S \, d\Lambda_S{}' = (-\,+)$	$G.P.E._D \, d\Lambda_D{}' = (+\,-)$
$dG.P.E._S \, \Lambda_S{}' = (-\,-)$	$dG.P.E._D \, \Lambda_D{}' = (-\,-)$
$dK.E._S \, d\Lambda_S{}' = (-\,+)$	$dK.E._D \, d\Lambda_D{}' = (-\,-)$

Noteworthy of discussion are the differences between the product of differentials and the differential of the product of: $d(E_0\Lambda')=dE_0\Lambda'+E_0\,d\Lambda'$ vs. $dE_0 d\Lambda'$. thus: $dE_0\Lambda' = E_0\,d\Lambda'$. The conservation principle works exactly as any equilibria problem taking the product of differentials noting differential time-energy transfers in the following way: G.P.E. gives rise to K.E., and momentum in orbiting systems: $\frac{(-)dG.P.E.\,(+)d\Lambda'}{2} \rightarrow (+)dK.E.\,(-)d\Lambda' \rightarrow 2\,(+)dP_0\,(-)dX'$. For example, for Type I, II 4th dimensional subjects, a dual-natured futuristic vessel were to have two pedals, energy would be the master pedal and time would be the slave, for the causal universe. These roles reverse itself for Doppelganger time-realms. For Doppelganger gravity these two are reversed, i.e. time-distance decreases and occurs with increases in gravity (credits). They appear to accede, and have blue-shifts. 3D space is easily represented by a cartesian cube inside a and a sphere of inertial/gravitationsl contravariant radii in time-space.

Time-space radii extend from the center to the corners of the momentum-energy cube, touching the 3D gravitational sphere syncitially positioned along a time-space well. Experimentally, this can be proven through gravitational structural interferometry, measuring the lengths of a typical perfectly square assembly using monnochromatic laser light, checking for any change in frequency, wave-length, and apparatus (number of laser light crests to 1/20th wave). This test would need a parallel apparatus-experiment-data collection in the free-fall (0g) of the ISS space-staion to collect experimental control data, for comparaison. Length expansion as a function of time dilation would or would not be a 1D dimensional and vector dependent vs. 3d in effect and not vector related, is the question. If length expansion were one-dimensional it would show up in the vertical measurement but not while the set-up is in the horizontal position (lying flat). Thus, if the interferometry results record no-difference in time of travel, nor distance of travel, and without change in the laser frequency, then the time-warp effect of length contraction is 3D, with no loss to structural integrity to mass, which would occur, and which is not what the record of events of astronautics current and known to man, but has not been well understood by fundamental physicisists of the day.

For review, the Heisenberg Uncertainty Principle as it applies to time yields already familiar laws. Concerning non-simultaneity, object(s) cannot be of the same space at the same time, nor may they be of different place but same time, nor of same place but of different time, nor of same time but of different place; of not less than $\bar{h}$, and not greater than $\frac{1}{\bar{h}}$. If Pauli exclusion occurs for values $< \bar{h}$, then at values $\frac{1}{\bar{h}}$ Pauli's exclusion would also inverse, hence inclusion would occur. This is true for like species of energy. However exclusion occurs for differing species of energy (gravity is excluded from the inertial). Super-simultaneity of Doppelgangers, has to do with the non one-to-one causal-supercausal correlates; beyond the crossover-decollatge lay the supercausal-decolletage in both Doppelganger inertial- future, and Doppelganger gravitational-past, superceding the causal equivalents, (See fig. 2).

The case for SuperOrigin O_∞ is defined by (1) one double positive quadrant of infinity; is balanced with one double negative quadrant of infinity. The other two balance each other as well, with two having a (+/-) sign aspect quadrant of infinity that is balanced by the other's opposite numerical sign arrangement; just as the decimal Origin does. Whether crossover(s) can occur as Type I, (inertially aspected (red-shifted) gravitational objects which cross the singularity at c in a defective low-energy way, become blue-shifted inertial 4th dimensional subjects as blue-shifted gravitational quasars. Thus, Type II subjects also cross-over the nodal zone of inhibition-occultaion, and also disappear from their ensconced position in the cosmos, fall far into the future, thus removed from view (occulted). Type IV direct mode high-energy cross-overs occur when graviaitonal black-holes fall into their past becoming subjects in reverse time. As a general rule, blue-shifted objects can also mean that they are Doppelganger acceders, figs. 3a, 3b. These are depicted in figs. 2a, 2ci, 2di, 2cii, and 2dii. Also extreme UV level blue-shifts, are also seen with black-hole formation, fig. 5f.

Some galaxies show an acceding nature. From observation these occur in at most 1 in 6 instances and should be catalogued in the astronomic record; the rest are recede from the Milky Way galaxy. Conservation laws for time are related to those concerning energy. Acceders are generally blue-shifted and occur with credits in gravity and with Doppelganger subjects. Receding time-warp implies increasing kinetic energy, acceding time-warp implies decreasing kinetic energy. Generally speaking time-warp values vary inversely with energy for sub-singularity values; Doppelganger time-warp values also can vary inversely with energy, but are reverse in order. Type I, and Type II cross-overs are simple and bi-directional, but Type III and Type IV, are possible only when enough gravitational/inertial energy is present due to the sign differences in the time ordinate. Thus energy in Type III, and Type IV cross-overs involve an extreme inertial differential time sign changes and are possible only with enough energy compared to the low-energy Type I, and Type II defectors.

In figs. 2, and 2a, if $\frac{v}{c} = sin((i)\varepsilon)$, then $(\frac{c^2 - v^2}{c^2})^{½} = cos((i)\varepsilon)$. If $cos((i)\varepsilon)^2 + sin((i)\varepsilon)^2 = (\frac{c^2 - v^2}{c^2}) + (\frac{v}{c})^2 = \frac{c^2}{c^2} = 1$. Furthermore, if $v_r\, cos(\theta) = v_x = \frac{\partial X_0\, r_r\, cos((i)\varepsilon)}{\partial \Lambda_0\, r_t\, cos((i)\varepsilon)}$; then said that: $\frac{m_0\, v_x\, r_r}{\Lambda_0} = m_0\, c^2$. The "Rosetta Stone" relation is pursuant to the following development: $\frac{(-)d\, ln(r_r)}{(i)\lambda_{wf}} = d\,(i)\lambda_{wf}$, yielding: $\frac{m_0\, c}{r_r\, \sqrt{c^2 - v^2}} = \frac{m_0\, v_x}{c\, \sqrt{c^2 - v^2}}$. The two may be equated by chaining the differential as: $\frac{d}{dr} * \frac{dr}{d\Lambda_0}$. With substitution $r_t{}' = \frac{\Delta\Lambda_0}{r_t cos((i)\,\varepsilon)}$, and for space distortion: $r_r{}' = \frac{\Delta X_0}{r_r\, cos((i)\,\varepsilon)}$, where $r_r = 1$. The event-horizon cone forms a time-foil; from this time distortion creates a 3-D gradient and constitutes a phenomenon that repeats itself throughout nature. Any time hyper-red "hyper-c" object could be charted by its progress along the second dilation sheet, of figs. 1b, and 2a both show the node singularity at c. The two temporal bays are joined at the light point. The Poisson's modulus can be applied. The stress/strain ratio can be adopted to explain any "linkage dis-equilibrium" of space/time distortions of the continuum at any given point, and implies topological viscosity based upon this ratio, calculated by the quotient / ratio of: $\frac{r_r}{r_t} = \mathbf{R} \lesseqgtr 1$. For anti-matter this is expressed as: $\frac{r_t}{r_r} = \mathbf{R}_\alpha \lesseqgtr 1$. This can also occur with gravitational objects as well, particularly in regard to breaks in the space-time fabric due to the ultra heavy mass of a galaxy (e.g. M87 - fig. 5b). Perhaps nuclear ion-stars exist, stripped of their electrons (Pulsars). It is a law of Unity that the point of Unity conjoins the causal past, with the supercausal future, a any point in the present. The supercausal future is always nmeasured by and as causal evernt potentials. The causal past, always brings us to the present, always extending into the future, where Newton's laws of motion apply. The same is true for the gravitional realm. The causal gravity is conjoined with the super-causal gravity; at singularity, reflexing in time bias there. However, these two energy species (i.e. inertial vs. gravitational) are held completely disjoint from each other by being oppositely pointed, as tensor is to vector.

$$Eq.\ \ \Omega 1.\ \ E_{rel} = \int_0^c \left(\frac{p\, dv}{r_t \cos((i)\varepsilon)} \right) + m_0 c^2 = \frac{m_0 c^2}{(i)\lambda_{wf}} = \left(\frac{m_0 c^2}{r_t \cos((i)\varepsilon)} \right)$$

When the differentials of energy and time-warp are equated (See. fig. 7-7k), these relations become:

$$Eq.\ \ \Omega 2.\ \ (d(K.E.) - d(G.P.E.))^2 + (d(R.E.))^2 = (d(T.I.E.))^2 = (d(G.P.W.) - d(I.W.))^2 + (d(R.W.))^2 = (d(T.W.))^2$$

However both gravitational and inertial time-warp at or near zero occurs as a near-mathematical conjoining type of terminus as depicted in figs. 2, and 2a. It is not certain how quasar occultations occur but that they re-appear, thus Pauli exclusion would have to be re-considered upon approach to the time terminus region.

The Heisenberg couplets, and their relativistic partners sufficient as tools to predict and explain these physical phenomena. The Planck constant is of a class of constants of proportion; the partner constant, or the Heisenberg constant appears as two constants, as the inverse is also considered. The replacement of the Lorentz warp factor is accomplished as: $(i)\lambda_{wf}$ by: $r_t cos((i)\varepsilon)$, which occurs in: $\Omega 1$; is a derived function later in the text. The terminus point can be described using either $(i)\lambda_{wf}$, or as $(i)\varepsilon$ the latter being more complete than the former form; the periodic accommodates the sign criteria of the singularities surrounding gravity of relativistic proportion, as well as those for kinetic energy, at c. Both types of time-hyper-red Doppelganger conditions (gravitational and inertial) are also fully described by the hyperbolic arc cosine function. If the discriminant of the casual is as: $\varepsilon_{csl} \leq\geq 0$, then certainly: $r_{t_{csl}}' = r_t cos(\frac{(i)\pi}{2}) = 0$, for $r_t = 1$. This represents a new route to total relativistic time-energy (Einstein's 1st law); essentially affixes total energy equation links to time-warp with the circular / periodic functions, (figs. 2a 2p). When the equations turn imaginary the periodic in the denominator, predicts the $(i)\lambda_{wf}$ factor's embedded time-radii both as a function of cosine, and as a function of the sine which occurs for any temporal energy equation; becoming predictably hyperbolic for Doppelganger values, thus: starting with the causal, then supercausal time-angle moments and time-radii: If $((i)\lambda_{wf})^2 = 1 - r_t \sin^2((i)\varepsilon) = r_t \cos^2((i)\varepsilon)$. The identities surrounding these temporal causality expressions become laws and have components of familiar polar forms, are presented and form Pythagorean orthonormal right triangles for energy and time and are in and of their own right, both unique and of a kind, (figs. 4-4c vs. those of figs. 7-7c). In general, the cosine describes the temporal past, the sine describes the future; along with their hyperbolic analogs both occur in the causal and supercausal parts comprising this Universe Unit. Thus, these two total time-energy temporal causality equations add and define an additional supercausal component to the causal equations of A. Einstein, and W. Heisenberg; are new to mankind, and advance and expand the potential of the physics of special relativity. They are as follows:

$$Eq.\ \Omega 3.\ (\Delta\Lambda_0 r_r \cosh(\varepsilon)_{csl})^2 - (\Delta\Lambda_0 r_r \sinh(\varepsilon)_{scsl})^2 = (\Delta\Lambda_{tot})^2$$

$$Eq.\ \Omega 4.\ (\Delta X_0 r_t \cosh(\varepsilon)_{csl})^2 - (\Delta X_0 r_t \sinh(\varepsilon)_{scsl})^2 = (\Delta X_{tot})^2$$

$$Eq.\ \Omega 5.\ (\Delta\Lambda_0 r_r \cos((i)\varepsilon)_{csl})^2 + (\Delta\Lambda_0 r_r \sin((i)\varepsilon)_{scsl})^2 = (\Delta\Lambda_0 r_r \cosh(\varepsilon)_{csl})^2 - (\Delta\Lambda_0 r_r \sinh(\varepsilon)_{scsl})^2 = (\Delta\Lambda_{tot})^2$$

$$Eq.\ \Omega 6.\ (\Delta X_0 r_t \cos((i)\varepsilon)_{csl})^2 + (\Delta X_0 r_t \sin((i)\varepsilon)_{scsl})^2 = (\Delta X_0 r_t \cosh(\varepsilon)_{csl})^2 - (\Delta X_0 r_t \sinh(\varepsilon)_{scsl})^2 = (\Delta X_{tot})^2$$

$$Eq.\ \Omega 7.\ (\frac{E_0}{r_t{}'})^2_{csl} + (\frac{E_0}{r_t{}'})^2_{scsl} = E_t^2$$

$$Eq.\ \Omega 8.\ ((\frac{r_r \cos((i)\varepsilon)_{csl}}{r_t \cos((i)\varepsilon)_{csl}})^2 + (\frac{r_r \sin((i)\varepsilon)_{scsl}}{r_t \sin((i)\varepsilon)_{scsl}})^2) = (\mathbf{R}_{tot})^2$$

$$Eq.\ \Omega 9.\ (r_r \cos((i)\varepsilon)_{csl})^2 (r_t \sin((i)\varepsilon)_{scsl})^2 + (r_t \cos((i)\varepsilon)_{csl})^2 (r_r \sin((i)\varepsilon)_{scsl})^2 = (\mathbf{R}_{csl})^2 + (\mathbf{R}_{scsl})^2 = (\mathbf{R}_{tot})^2$$

$$Eq.\ \Omega 10.\ (r_r \cosh(\varepsilon)_{csl})^2 (r_t \sinh(\varepsilon)_{scsl})^2 + (r_t \cosh(\varepsilon)_{csl})^2 (r_r \sinh(\varepsilon)_{scsl})^2 = (\mathbf{R}_{csl})^2 + (\mathbf{R}_{scsl})^2 = (\mathbf{R}_{tot})^2$$

$$Eq.\ \Omega 11.\ ((\frac{r_t \cos((i)\varepsilon)_{csl}}{r_r \cos((i)\varepsilon)_{csl}})^2 + (\frac{r_t \sin((i)\varepsilon)_{scsl}}{r_r \sin((i)\varepsilon)_{scsl}})^2) = (\mathbf{R}_{\alpha_{tot}})^2$$

$$Eq.\ \Omega 12.\ (r_t \cos((i)\varepsilon)_{csl})^2 (r_r \sin((i)\varepsilon)_{scsl})^2 + (r_r \cos((i)\varepsilon)_{csl})^2 (r_t \sin((i)\varepsilon)_{scsl})^2 = (\mathbf{R}_{\alpha_{csl}})^2 + (\mathbf{R}_{\alpha_{scsl}})^2 = (\mathbf{R}_{\alpha_{tot}})^2$$

$$Eq.\ \Omega 13.\ (r_t \cosh(\varepsilon)_{csl})^2 (r_r \sinh(\varepsilon)_{scsl})^2 + (r_r \cosh(\varepsilon)_{csl})^2 (r_t \sinh(\varepsilon)_{scsl})^2 = (\mathbf{R}_{\alpha_{csl}})^2 + (\mathbf{R}_{\alpha_{scsl}})^2 = (\mathbf{R}_{\alpha_{tot}})^2$$

$$Eq.\ \Omega 14.\ (\mathbf{R}_{tot})^2 = \left[(R_{csl} \cos((i)\varepsilon))^2 + (R_{scsl} \sin((i)\varepsilon))^2\right]$$

$$Eq.\ \Omega 15.\ (E_{tot\,\Lambda'}{}')^2 = \left[(m_0 c^2)^2 \left[(R_{csl} \cos((i)\varepsilon))^2 + (R_{scsl} \sin((i)\varepsilon))^2\right]\right]$$

$$Eq.\ \Omega 16.\ (E_{tot}{}')^2 = \left[(m_0 c^2)^2 ((\frac{1}{(R_{csl} \cos((i)\varepsilon))^2} + \frac{1}{(R_{scsl} \sin((i)\varepsilon))^2}) - 2)\right] + 2(m_0 c^2)^2$$

$$Eq.\ \ \Omega 17.\ \ (\Delta X_0\, r_t{}')^2_{csl} + (\Delta X_0\, r_t{}')^2_{scsl} = (\Delta X_{tot})^2$$

$$Eq.\ \ \Omega 18.\ \ (\Delta \Lambda')^2_T = (\Delta \Lambda_0\, r_t\, cos((i)\varepsilon))^2_{csl} + (\Delta \Lambda_0\, r_t\, sin((i)\varepsilon))^2_{scsl}$$

$$Eq.\ \ \Omega 19.\ \ (\Delta E\, \Delta \Lambda)^2_{\mathbf{T}} = \left(\frac{\Delta E_0}{(R_{csl}\, cos((i)\varepsilon))}\right)^2 + \left(\frac{\Delta E_0}{(R_{scsl}\, sin((i)\varepsilon))}\right)^2$$

$$Eq.\ \ \Omega 20.\ \ (\Delta E\, \Delta \Lambda)^2_{\mathbf{T}} = \left(\frac{\Delta E_0\, \Delta \Lambda'}{(r_t\, cos((i)\varepsilon))}\right)^2_{csl} + \left(\frac{\Delta E_0\, \Delta \Lambda'}{r_t\, sin((i)\varepsilon)}\right)^2_{scsl} > 2(\bar{h})^2 = \left|(\bar{\mathrm{Y}})\right|^2_T$$

For gravity $\left|(\bar{\mathrm{Y}})\right|_{\mathbf{G}} = \left|(2\sqrt{2}\,\bar{h})\right|$. For total energy: $\left|(\bar{\mathrm{Y}})\right|_{\mathbf{E}} = \left|(\sqrt{2}\,\bar{h})\right|$. For K.E.: $\left|\frac{(\sqrt{2}\,\bar{h})}{2}\right|$. The inverse of the time warp factor $\frac{1}{r_t cos((i)\varepsilon)_{wf}}$, is the constraining relation for energy, as per Eqs. 2a, 3. The resulting bloating in energy is entirely due to the constraint of time contraction for the moving frame. The derivative of the inverse time warp factor is as fig. 2f; the sign negative is fig. 2g. The time-warp factor is defined in this document as the explicit form; the periodic nucleus of the Lorentz function. Furthermore, grouping inertial energy with gravitational potential energy yields: $\frac{G\, M\, m\, dr\, d\theta\, r_r cos((i)\varepsilon)}{r_g * r_t cos((i)\varepsilon)}$.

For orbiting systems, there remains a net (-)half P.E. of gravitational potential energy; this becomes a net (+) in time-energy, after double negation of at the differential level: $d(G.P.E.)\, d\Lambda' \rightarrow (--)$, thus the residual time-gravity is accompanied by residual K.E. The latter is a function of a 4 obelus sign cancellation, when including the negative Heisenberg constant for gravity. Mathematically space or length expansion in a gravitational system, shows as $(\frac{G\, M\, m\, dr\, d\theta}{r_g * r_t cos((i)\varepsilon)})\Lambda_0\, r_r cos((i)\varepsilon)$. Due to the inverse of radius, the scale of the sum (integral) of the P.E. is logarithmic; is already known. Upon distribution of the cosines the effect manifests itself as increased distance or radius, and increased time. On a more intuitive note, if an energy vector contracts time (for the moving frame

), then a gravity tensor will have the opposite effect on time, expanding it. Similarly a sign-negative residual time-gravity tensor has this also as a reverse effect. These facts are doorway to resolving resolutely the question of the receding of the galaxies for orbiting systems of masses, without having to delve into the vagaries of Big Bang theorists. Similarly, if the gravitational energy were not negated in sign by the negative warp of time, the galactic record would show only galaxies receding at high velocities. While clearly not the case for most, some actually do, due to residual gravity's sign its motion can be in fundamentally in two entirely different directions. The rotational constitutes half of the energy; the remainder is the residual energy, which constitutes linear apparent motion component as residual reactive K.E.; the latter is best described using double dose of the LaGrangian double dyad multipliers; the apparent receding motion is a function of: $(\cos(\eta_{glx_{k,l}}))^{n}(\sin(\zeta_{glx_{k,l}}))^{n}$, for (n = 1,2,3); diagrammed angles between two galaxies. The square, and cube of this function would naturally extend from the former consideration's coordinate system.

This can lead to a complex product of $(i)\lambda_{wf}$ factors, thusly: $\left(\frac{(i)\lambda_r}{(i)\lambda_r\,(i)\lambda_{wf}}\right)(\Lambda_0\,(i)\lambda_r)$. This type of doubling also occurs as: $\left(\frac{(i)\lambda_{wf}}{((i)\lambda_{wf})^2}\right)(\Lambda_0\,(i)\lambda_r)$. It is vital to remember that in the final denominator the singly function prevails as $\frac{(i)\lambda_r}{(i)\lambda_{wf}}$. These are depicted in figs. 2-2m. The orthonormal development of this takes the form of: $\left(\frac{((i)\lambda_r)^2}{(i)\lambda_r\,(i)\lambda_{wf}}\right)^2$. It would be a challenge at the experimental level to look for validatation of doubly theory.

Three more relations that are necessary for any full discussion of time and energy. They are represented in the formulary of: Eqs. $\Omega 17-20$. They represent the three additional laws of Einstein's special relativity; are accompanied by three additional Universal constants for the total time-energy of any system. Also of note that: $r_{r_{csl}}' = r_r\,cos((i)\varepsilon)$, and: $r_{r_{scsl}}' = r_r\,sin((i)\varepsilon)$, for: $r_r = 1$, and are as per figs. 2, and 2a, suggest. Also for time:

$r_{t_{csl}}{}' = r_t cos((i)\varepsilon)$,

and: $r_{t_{scsl}}{}' = r_t sin((i)\varepsilon)$, for: $r_t = 1$, and as a measure of linkage dis-equilibrium for these two parameters is for normal matter defined by: $(\frac{r_r{}'}{r_t{}'})^2 = (\mathbf{R})^2$; is as a new warp constant; individually may be negatively potent for two principal reasons i.e. the specie of the energy, and the nature of the state are either pre-singularity objects or post-singularity 4th dimensional subjects; are as per fig. 2 suggests This graphs the orthonormality of the causal past with the supercausal future, which exists for this universe unit's time function. If one subtracts the past from the total time basin, only the future remains. Similarly and also, if one subtracts the future from the total time basin, the past leading up to the present only remains. This completes unified time theory for causal and the supercausal components of this universe unit. Further simple substitution yields the familiar energy expression: $E_{rel} = \frac{m_0 c^2}{r_t cos(\frac{(i)\pi}{2})} = \infty$. This polar form, and its supercausal superpartner sum represent the total relativistic time-energy of Einstein; were listed in the Ω table of equations.

One form of temporal causality is represented as a typical "hourglass" event-horizon and outcome cone. In the case of the Jacobian for dE, $d\Lambda_0$ with respect to energy and time, two Jacobians are formed. As stated the approach involves first using a definite line integral for the time portion from 0 to c, and the other half involves another indefinite line-integral from c to ∞. If the past sets double line integral is subtracted from the future set's double line integral, keeping the same the line integral for energy, (as computed by the two total temporal energy right triangles), the total time-energy for the universe is thus composed and becomes discernable. Each of the triangles from figs. 7-7k and figs. 4-4c. by aligning the total energy hypotenuses of the four respective right triangles of time, space, energy, and momentum, (K.E. and G.P.E. can be switched by sign change), form when juxtaposed with any two base warp triangles of figs. 4-4c, new temporal causal/supercausal super-pyramids; each has a 4-sided square base and 4-triangular side elements. The grand total temporal time-energy Stokes pyramids also have a chief-cornerstone with vertex: *h*. This is identical to the Riemann Tensor; from the Divergence Theorem - Kelvin Stokes:

Eq. $\omega 1.\ \iiint (\boldsymbol{\nabla} \cdot \mathbf{F})\, dV = \iint (\nabla \times \mathbf{F}) \cdot \mathbf{N}\, d\sigma$

Eq. $\omega 2.\ \mathbf{F} = \boldsymbol{\nabla} \cdot \mathbf{E}$

Eq. $\omega 3.\ \iiint ((\nabla \times (\nabla \cdot \mathbf{E})))\, dV = \iint ((\nabla \times \mathbf{F}) \cdot \mathbf{N})\, d\sigma$

Eq. $\omega 4.\ \mathbf{G} = \boldsymbol{\nabla} \cdot \mathbf{G}_E$

Eq. $\omega 5.\ \iiint ((\nabla \cdot (\nabla \cdot \mathbf{G}_E)))\, dV = \iint ((\nabla \cdot \mathbf{G}_E) \cdot \mathbf{N})\, dx\, dy$

Eq. $\omega 6.\ \int \mathbf{N}_\alpha\, d\sigma_i = \oint \mathbf{G}_E \cdot N_\alpha\, dS$

Eq. $\omega 7.\ \iiint ((\nabla \times (\nabla \cdot \mathbf{E})))dV = \iint ((\nabla \times \mathbf{F}) \cdot \mathbf{N})\, d\sigma$

Eq. $\omega 8.\ \mathbf{E}_{tot} = 2 \iiiint\!\!\iint (\boldsymbol{\nabla} \times (\boldsymbol{\nabla} \cdot \mathbf{E}))\, dV = (-) \iiiint\!\!\iint (\boldsymbol{\nabla} \cdot (\boldsymbol{\nabla} \cdot \mathbf{G}_E))\, dV = 4 \iiiint\!\!\iint ((\nabla \times (\nabla \cdot \boldsymbol{\Gamma})))\, dV$

Eq. $\omega 9.\ \boldsymbol{\Gamma} = \boldsymbol{\nabla} \cdot \mathbf{P} \ \rightarrow\ 2 \iiint (\boldsymbol{\nabla} \cdot \boldsymbol{\Gamma})\, dV = \iint (\nabla \times (\nabla \cdot \mathbf{P})) \cdot \mathbf{N}\, d\sigma_i$

Eq. $\omega 10.\ \int \mathbf{N}_i\, d\sigma_i = \oint d\, \mathbf{R}_i$

The treatment of the normals are as an obelus of division: $\mathbf{N}_i = \dfrac{\mathbf{n}_r}{\mathbf{n}_t}$. For the anti-set the anti-diameter(s), are as: $\mathbf{N}_\alpha = (-)\,\dfrac{\mathbf{n}_t}{\mathbf{n}_r}$, noting that both are always positive. Also true that the span/space is the numerator - normal to the surface as: $\mathbf{n}_r$, lying in the numerator. The inner normal is as: $\mathbf{n}_t$ becomes the denominator. Also note: $\mathbf{curl}\, E = \mathbf{n}_r$, and $(-)\,\mathbf{curl}\, E = \mathbf{n}_{r_\alpha}$. For the normals for time: $\mathbf{curl}\, \Lambda = \mathbf{n}_t$, and $(-)\,\mathbf{curl}\, \Lambda = \mathbf{n}_{t_\alpha}$. For space and anti-space, time and anti-time, their position occurs as: $(\frac{\mathbf{N}_{csl}}{\mathbf{N}_{scsl_\alpha}}) = (\frac{\mathbf{n}_r}{\mathbf{n}_t})(\frac{\mathbf{n}_{\alpha_t}}{\mathbf{n}_{\alpha_r}})$. Their positions often bond and coincide and/or can also often annihilate. Thus separation into quarkonium MAM can be used as a propulsion system. Large plumes of MAM annilhilation products are and can be used as thrust producing, given a suitable reaction chamber/engine with proper mixing for a controllable burn. Note that it is also true that both obeluses of subtraction/addition, and that of reciprocal division are used to manipulate/convert vector/tensor radii of MAM systems.

Eq. $\omega 11.$ $\iint (\nabla \times (\nabla \cdot \mathbf{E})) \cdot (-) \frac{1}{\mathbf{N}_\alpha} d\sigma_{i_\alpha}$

Eq. $\omega 12.$ $\int (-) \frac{1}{\mathbf{N}_\alpha} d\sigma = \oint d((-) \frac{1}{\mathbf{R}_\alpha}) = \int \mathbf{N}_i \, d\sigma_i = \oint d\, \mathbf{R}_i$

Eq. $\omega 13.$ $\int \mathbf{N}_\alpha \, d\sigma = \oint d(\mathbf{R}_\alpha) = \int (-) \frac{1}{\mathbf{N}_i} d\sigma_i = \oint (-) d \frac{1}{\mathbf{R}_i}$

Eq. $\omega 14.$ $\iiint ((\nabla \cdot (\nabla \cdot \mathbf{G}_E))) dV = \iint ((\nabla \cdot \mathbf{G}_E) \cdot \mathbf{N}) dx\, dy$

Eq. $\omega 15.$ $\int \mathbf{N}\, d\sigma_i = \oint \mathbf{G}_E \cdot N$

For anti-matter, anti-time, and anti-gravity, this becomes:

Eq. $\omega 16.$ $\int (-) \frac{1}{\mathbf{N}_\alpha} d\sigma = \oint \mathbf{G}_E \cdot (-) \frac{1}{N_\alpha} dS$

When the moving frame $\Delta\Lambda'$ becomes nearly zero in rank for velocity at c, the moving frame time-energy would need only reach a maximum on the order of: $(.94825x10^{34} J{-}secs^{-1})$; ultimately crossing over into the Doppelganger time regions; are of Type I, or Type II only; Type III, or Type IV test the Super-Origin; energy limiting. As such raises the mathematical concern and thus necessitates the concept of a bi-axial Super-Origin: O_∞. The SuperOrigin has a single time axis and a single distance axis for the purposes shown here. For the physical universe, the scalar product: $\nabla V_{\max} \approx (\frac{1}{2\, \nabla P\, \nabla X'})^3 < (\frac{1}{\bar{h}})^3$, and is calculatable as a maximum volume; occuring as the triple scalar product, suggested by:

$$\Delta V_{\max} = \Delta V_A \times (\Delta V_B \cdot \Delta V_C) \approx (\frac{1}{\Delta X'})^3 < (\frac{2\, \Delta P_0}{\bar{h}})^3 = (2\, \Delta P_0)^3 \, (0.862068\, x\, 10^{102}) (\frac{kg \cdot m}{Joule\ sec^{\,2}})^3$$

The absolute minimum volume involves the triple scalar product of spaces as:

$$\Delta V_{\min} = \Delta V_a \times (\Delta V_b \cdot \Delta V_c) \approx$$

$$(\Delta X')^3 > (\frac{\bar{h}}{2\, \Delta P_0})^3 > (\frac{(1.16\, x\, 10^{-34})}{2\, \Delta P_0})^3 = (\frac{1.5608\, x\, 10^{-102}}{2\, \Delta P_0^{\ 3}}) (\frac{kg \cdot m}{Joule\ sec^{\,2}})^3$$

For the physical universe, the scalar product: $\nabla \Lambda_{\max} \approx (\frac{1}{\nabla E\, \nabla \Lambda'})^3 < (\frac{1}{\bar{h}})^3$, and is calculatable as a maximum time interval; occurs as the triple scalar product, suggested by:

$$\Delta \Lambda_{\max} = \Delta \Lambda_A \times (\Delta \Lambda_B \cdot \Delta \Lambda_C) \approx (\frac{1}{\Delta \Lambda'})^3 < (\frac{\Delta E_0}{\bar{h}})^3 = (\Delta E_0)^3 \, (0.862068\, x\, 10^{102}) (\frac{Joule}{Joule\ sec})^3$$

The absolute minimum time interval involves the triple scalar product of spaces as:

$$\Delta \Lambda_{\min} = \Delta \Lambda_a \times (\Delta \Lambda_b \cdot \Delta \Lambda_c) \approx$$

$$(\Delta \Lambda')^3 > (\frac{\bar{h}}{\Delta E_0})^3 > (\frac{(1.16\, x\, 10^{-34})}{\Delta E_0})^3 = (\frac{1.5608\, x\, 10^{-102}}{\Delta E_0^{\ 3}}) (\frac{Joule\ sec}{Joule})^3$$

For the gravitational physical universe, the scalar product: $\nabla\, G.P.E._{\max} \approx (\frac{1}{\nabla \Lambda_0\, \nabla G.P.E.'})^3 > ((-) \frac{1}{2\, \bar{h}})^3$, and is calculatable as a maximum gravitational interval energy; occurs as the triple scalar product, suggested by:

$$\Delta G.P.E._{\max} = \Delta G.P.E._A \cdot (\Delta G.P.E._B \cdot \Delta G.P.E._C) \approx$$

$$(\frac{1}{\Delta G.P.E.\,'})^3 < ((-) \frac{\Delta \Lambda_0}{2 \bar{h}})^3 = (\Delta \Lambda_0)^3 (0.080083 \, x \, 10^{102}) (\frac{sec}{(-) \, Joule \; sec})^3$$

The absolute minimum time interval involves the triple scalar product of spaces as:

$$\Delta G.P.E._{\min} = \Delta G.P.E._a \cdot (\Delta G.P.E._b \cdot \Delta G.P.E._c) \approx$$

$$(\Delta G.P.E.\,')^3 > (\frac{(-) 2 \bar{h}}{\Delta \Lambda_0})^3 > (\frac{((-) 2.32 \, x \, 10^{-34})}{\Delta \Lambda_0})^3 = (\frac{(-) 12.487 \, x \, 10^{-102}}{\Delta \Lambda_0{}^3}) (\frac{(-) \, Joule \; sec}{sec})^3$$

When these values and formulations of the Heisenberg time-energy are composed and computed the minimaxes of volume(s), and time are now computed for this Universe Unit touches the limits and tests the boundaries of the minima(s) and maxima(s) for the aformentioned. The trajectors for time and volume are found to increase or decrease around these known parameters. Once again, the essential effects upon astro-physical systems is as time-energy re-iterate as Stokes cubes and Stokes pyramids; some end-up as residual ones. This is as likened to a golf ball rolling down a mole-hill; a galaxy is as to a golf-ball, then depending on the mass they will tend to naturally form the depression-distortion in the fabric of space-time such that they roll down in a natural but omni-directional way. Colliding galaxies are thus readily explained. The Big-Bang theory does not account for this sufficiently well. The reaction to this warp is one opposite in direction; is a result of time-warp’s inertia. Hence, the barred spiral quandary is thus explained, also. Singularity crossover-decrochment decolletage-libre-de-temps, recrochement-apres-temps-future; is easily feasible and understood after reading this document. The evidence presented here is in full never unscrupulous in witness to nature; can predict its course as adducial to the theory presented therein.

Data tracking virtual images of warped time-space could easily be measured through a system laser-emitting satellites, (one orbiting Earth, one orbiting the Moon, and one orbiting Mars), comes to mind as one scenario of testing our theory of the time-space distortions generated by planetary gravity. The expanded form of the hyperbolic cosine involves the natural exponent as: $\frac{e^{x_i} + e^{-x_i}}{2} = r_t cosh(x_i)$. For the hyperbolic sine, the exponential form becomes: $\frac{e^{x_i} - e^{-x_i}}{2} = r_t sinh(x_i)$. The exponential form is sometimes easier to compute than the polar form. The solution to the differential would naturally employ both these natural logarithm identities (l'Hôpital's rules in exponent form).

As a rule when gravitational objects approach gravitational terminus, the Poisson time-space stress/strain ratio can be adopted to explain these breaks in the fabric of the time-space continuum. Although this subject lay un-noticed by physicists, this phenomenon is not the first for non-ideal special relativity, One need only look to the galactic record to confirm this. The only qualm lay by the disqualification of such, per Einstein's second law. Scientists will have to now ponder the kinds of non-ideal space-time physics. Much as a glass blower forms bubbles by stretching the glass leads us to larger time-anomalies, i.e. a proposed "lac d'rien" syndrome, If so, running into such would be ruinous to any space vessel hull. With no-mass these rips in the fabric of time, form hardened space-time bars. The nature of these as phenomenon has to do with the fabric-like real nature of space and time; the proposed obelus of zero(s) of space and time when indeterminate, helps explain, if not predict the occurrence of these types of time-space phenomena. Beyond this theory lay another theory, namely: anomalous containment of the obelus of non-zero nullities of space-time occurs, forming these proposed null-bars; if correct is not yet well known, however the correct one allows photons flow over such, where the space-time is defined. The time-space bar phenomena are detected by light extinction close up. Once discovered, would necessarily mean charting their position also.

The moon shot did offer a glimpse into this subject, recording differences in time's measure which arose from the differing inertial and gravitational time-warp environments from the moving frame astronauts. Astro-robots could easily record these subtle differences in time, as an alternative. In the case of the Moon astronauts, basically they experience a two fold warp environment; that of Earth, and that from the capsule's inertia, among other considerations, i.e. Earth's inertial warp, and those of the Sun.

If an un-maskable interruption occurred in the present, the future could be suddenly cut short. For example, should a hypothetical pilot encounter along one timeline his disappearance from the helm vs. an alternate timeline where he does not; it should be noted that the pre-occurrence of a temporal disaster to come were one user event vs. any alternate user-involvement event were to occur; such a decision nexus in the pilot's decision tree would depend upon chromatic events from the pilot's point of view of the consequences to any decision or action. This essentially describes common and recurring (eddy-like) anomalies in time.

This is particularly annoying when trouble occurs. i.e when a destructive event occurs; the nexus choice in time-lines would ideally fore-warn the pilot of decisions, acts, and their causal consequences, if they are trained for such. It should be clear by now that hyper-red time is not the same as hyper-red space, but the two vary sympathetically. In hyper-c conditions time's passage is quickened. The same is true of hyper-red space. What appears as non-Euclidian is actually an error in interpretation. There is hyper-time, but it is both inclusive and Euclidian. The decreasing function's change-over suddenly changes to an increasing function, i.e. inertial Doppelganger time-warp space-warp. The opposite is true of gravity, and Doppelganger gravity.

As an alternate route of use of nuclear fuels; a space industry plank should be the next logical step. Creating laws with this in mind could not only preserve the races but extend man's understanding and further the colonization ideal. At the very least these fuels could prove useful as last-ditch mode of exodus from an atomic war on earth should man-kind and their leaders be so tempted to in the future. As a policy it should be the goal of mankind and the league of nations, to insure that these mechanisms of destruction never be used against mankind. Ideally nuclear laws need to be passed proscribing non-nuclear nations from experimenting with design and manufacture of the WMD instruments of destruction for military advantage. The proscription should be parsimonious and only clean nuclear nations will have the right to engage in this science, then such nation could only use these materials for space and aeronautics programs; then eventually those that are non-military; or that which would enhance security. Such nations would jointly install planks recognizing each other's right to exist, then also a co-existence plank.

Any freelance flirtation would be quickly extinguished by those pillars of force already in place, i.e. (mendacious threat assessment). Installing safeguards should be a goal to prevent such an eventuality through the United Nation's Atomic Energy world-policy. The problem of non-aligned nations gaining the technology is inclusive in the debate. How can this be policed or enforced? Compliant nations would be rewarded with trade; non-compliance would bring trade sanction penalty, and austerity, only basic necessities to withhold starvation of an indigenous populous. Other issues include the down-sizing of MIRV warhead tips and nuclear safety; could they be stored in nearby bunkers in 3-stage build down to vaults that could not be re-opened without take time difficulty, be a goal? Shifting some of the ballistic missile buildup into a stored, no-load, state could win politically. Project "Holster" befits the idea that nuclear tip removal and storage as National Space Agency fuels would permit. Already other G-9 nations have already de-nuclearized their defenses.

Adopting then a 45-day cooling off period in a 3-tier re-mounting moth-balled storage process, seems feasible if the Super-Power nations could join hands as an "Alliance" Super-Partnership Treaty; any threat or otherwise terror/warlike barbarian nation quickly surfaces to fore-ground. League, or Partner nations would, under this scenario, have primary no-first-strike agreements, as well as non-aggression pacts; all agreements contingent upon separation of church and state which must appear first in their respective constitutions, atomic nuclear science and nuclear electricity, should be banned for such nations; solar-geo-wind should make suitable alternatives for peaceful power development. Ideally the advent of these newer, low-radioactivity-waste, photo-voltaic clean-atom methods and models are already in use in this day, and soon be replace nuclear power in western nations as well.

The "House" of the Nation and its occupants would be safer; the trust among them would increase; the chances for "MAD", e.g. an abrogation of detente - mutually assured destruction, would decrease. Particularly for the Super-Power nations the peace base would be realized after this mutual motion for stability, is in place. Cold storage of these "hot-potatoes" in this way could ensue, once political acceptance and protocols are ironed out for bilateral un-loading, (trust but verify). This particularly concerned the larger weapons of mass destruction. Still, a ready-force of nuclear weaponry would make sense in the event of "other-world" organism emergencies; mankind would naturally unite around defeating a common xeno-philic enemy.

Such nuclear ordnance would have to be up-graded to more forgiving and less destructively capable (N-bomb vs. H-bomb). For TGF (tres grande force) caisson directed against an obdurant opponent; H-bomb deuterides of lithium, and/or beryllium pre-ignite the carbon-carbon materials, readily leading to a fusion burn cascading element formation, potentially reaching burn temperatures to 40-50 million, degrees C., as absolute hot is defined. Provided the pressures are great enough, and temperatures high enough, ignition of a carbon fusion cycle can ensue. Such temperatures are doorway to the quarkonium state.

Formation of such carbo-myte devices could render invincibility to any army that could accurately deliver it (proximity or direct-hit). A hull of any substance known or yet unknown would be reduced quickly to quarkonium soup. Such a devices would especially utilize "bucky-balls" of Carbon-60, as cores. But to ignite this, one would need to be mixed with Cyanogen (CN), Nitrogen12 (N12), Boron(12), Lanthanum (La), Vanadium (V), and Zirconium (Zr) core elements are critical for the carbon-carbon cycle commencement fusion. A 3D effect of fig. 6a’s layout, would involve an arrangement of 24 surrounding fusion devices, in an octagonal cube arrangement which in turn has a 25th as Main Core, (fig. 6a, appendix V.).

Such a devices could be useful as doomsday devices, or extra-terrestrial planet killers should such deleterious scenarios come about. Such "MakMammoth" carbo-myte devices, can be built up to 5-tier assembly configurations as well. These devices fall into the type-S carbon burning fusion class (Super-Giant star temps.); type-K, and type-M class have Cyanogen and oxides of Calcium as fusion fuels, at their cores. Alternatively, as part of terra-forming science these can be deployed as man-made stars. These types of devices could serve the Homeland to destroy a comet that could be on a collision course with the Earth or the Moon, (Cometary Demolition Project). Additionally were such a collision to occur, certain fragments could cause tsunami and or climate changes, ice ages, lasting an Epoch or two, e.g. Dinosaur extinction. Venus, and Mars could also be fragmented by such a collision. Furthermore, these two are still minor planets, thus a collision conceivably could make eccentric their orbit; pose a danger to Earth. The must be proscribed for any other use in observance and in concordance with AEA policy.

Presumably new weak-force mediation of a fusion via irradiated crystal ignition could be rapidly utilized. Low temperature catalysis could be an advantage. Still lower radioactive profile weaponry would serve as cleaner weapons should a limited exchange break out. For those outside the zone of destruction it would be easier to recover and clean-up from, in the neighboring areas; (countries - states - cities). Destabilization would naturally ensue given the human nature of the leaders of the nations. Any kind of alien-world presence with superior technology could easily tilt the leaderships from cold-war neurosis into a full 1st strike elimination psychosis. Given the psychic numbing surrounding this subject, introduction of a superior element could easily destabilize any Alliance or Treaty, between the member nations. Additionally, once nuclear power is phased out (replaced with wind power or weak-force x-tal derived plasmas); dirty nuclear fuels would be relegated to only space industries; the age of both Tokomaks and conductive x-tal mediated power plants (even photo-voltaic Solar-power farms), would be available to countries that would seek electrical technology, but be forbidden nuclear knowledge, and the purview of the Atomic Energy Agency would similarly shift to follow the modernization.

Reaching a balance between ready vs. stored forces; and what leadership and oversight organizations are considerations that come to mind. For the stored force concept make necessary an instituted a "cooling off" period while forces could still be readied in time of war should that be necessary. Such forces could be readied only after a certain time, being un-mounted in war-head. In the mean time, the terrorist threat from sabotage is essentially thus eliminated. Furthermore nuclear stock-piles could easily be commandeered by a rogue administration. Strategic policy could shift from detente, to one advocating MAD. One administration may not honor previous previous agreements-laws, made under previous administrations, as their political objectives may differ. Mothballing nuclear warheads alone should enhance the peace especially since Soviet communism has been outlawed for nearly 18 years. Ideally, the former measure seems more paletable; timely bilateral un-loading should be done, with the goal of safer storage of the caisson of nuclear weaponry.

A strike force's ability to strike is directly related to technological superiority and secondarily by the ability to damage their hulls. This would make Alternatively the threat from asteroid e.g. an Icarus asteroid, or cometary collision is another constant and real threat. Such objects are easily scaled by a landing, or even in proximity to, can be destroyed by such caisson as with a carbo-myte device. A formation such as an octagonal cube of carbo-myte could render convincing destructive power to any Icarus project to perform in a resolute way the obliteration of a collision course cometary object, of would be devastating proportion to the Homeland or Earth in general. This has occurred before, and has been filmed to occur on Jupiter with comet Russel-Hale.

Since the age of Discovery and the Renaissance, occurring in the late 1400's - 1500's with Copernicus proposing his proof for the heliocentric solar system, later reiterated by Galileo, applying Jan Lippershey's telescopic lens arrangement, to peer up at the celestial heaven charting Jupiter and its moons, among other celestial bodies. Now, 500 years later mankind will for the first time in this human colony's history, be able to time travel using conventional fission - fusion nuclear fuels, { Lithium-Deuteride and Lithium-Triteride }. If nuclear rocketry begins with smaller nuclear fires, they may be more likely to be able to be controllable (< 1 mole/hr.); or lead man to use a hydrogen plasma from linear Tokamak systems; can be used as an electric power generating system.

Running on minute rod pellet Lithium Deuteride; the engine would operate as a fusion engine with a burn-cool-eject type of cycle. Such technology that will overcome the "engine melt" hurdle, (particularly true of the nozzle of a typical rocket engine). The thermal conditions of space would make the cool cycle short, and reliable thermal-electronic igniters could even be converted for such as use. The successful treatment of dealing with the extremes of heat in a fusion engine will be critical in their future development. An example of such a nuclear pulsed engine thruster layout design is displayed in figure 6. The octagonal of an ennea-thruster array system of fig. 6 and the geometric relations displayed in fig. 6, show potential for an alternating (2 x 2), or (4 x 4), firing of the array, followed by cooling, and waste-pellet discard after the thrust cycle. The engine in the middle should be reserved for return flight as a fail/safe backup system flight engine.

One proposal in this text includes plans for miniature forms of fusion from Lithium Deuteride as gas could form few-atom fusion using radio-centered filled x-tals. The mantle region is in the middle, of a prototype crystalline boule. Exclusion-Inclusion-imperfection points could act as mantles for such, also. Cores of weak-force driven radio-isomers could also ignite small amounts of Deuteride fuel internally at the level between the internal layer and the external layer. Tests will have to be made. The micro-fusion fusion unit thus can attain stand alone self definition; self-containment is achieved with an internal weak-force ignition system. This method would have a non-radioactive by product (Helium), also. Power lasers could provide the heat necessary for heat of activation, alternately low thermal protons, or particle streams from an ion-laser producing high-energy alpha streams could work also, and is a more practical design in regards to activation energy.

Still other ideas come to mind concerning the previously elucidated facts concering MAM confinement. From the study of time-space moments of inertia-time represents easily the laws of form concerning quark assemblies for all matter. The mathematical treatment of the time-space normals reveal that through high-energy NMR treatment of a matter sample could deconfine (decrochement) the matter from anti-matter. If done in a controlled way, could be a pathway for matter anti-matter spearation-collection. In the worst case, this high-energy NMR cis-bis feedback led resonance could be a method that would lead towarrd an un-controllable chain reaction of MAM deconfinment, accompanied by gluon release. These devices are termed here "Tronomyte Devices".

As regards inertial time-warps from kinetic particle beams such as those on Earth; they too will reveal distortions in time, and experiments can be set up to record this fact. The proof for this lay in the mathematics. As from Eqs. 1-3, the gravitational energy term can be substituted for the kinetic energy term, if the former is first divided by 2. Such a switching of couplets, one for the other, transposes the function into different variables, e.g. transposes the K.E. into an identical function composed of ($M\,m\,r$) for variables. When time warp is added, it becomes clear that such a temporal effect will show up as a function of radius from the inertial particle beam. If this is true, then in space, there would be a reactive kinesis to that inertial time-warp with any modern, but space-bound accelerator. Such a device could prove to be valuable in space travel.

Surely fusion engines would make this trip quicker if nuclear space fuels could be handled; seemingly less would be better, with heavy-water fuels. Matter-antimatter reactions imply quark annihilation, too. Such high outputs of light may be useful in weaponry. To gain kinetically the fusion method may be a more likely method for achieving large scale relativistic velocities, again with smaller amounts. Another method of thrust as once stated, could occur via weak-force mediated ion jetti-propulsion using high output energy radio-topic crystals which would belch out radioactive plasma products once when irradiated with slow thermal protons or neutrons. Conceivably one could ignite a fusion fuel, by this method.

There are three more questions which remain which must be researched.

1. Does dilation occur as a planar trapezoid or does time-contraction
effect space three-dimensionally (at relativistic velocities); will
such space distortion be viable for an astronaut?
2. Would an astronaut age faster or less
at relativised velocities?
3. Do trapped surfaces occur? Concerning cross-over events,

does the trapped-sruface at c act as a two-way time mirror?
How would one test this theory through structural
integrity tests?

Another downfall to fusion involves dealing with the extreme heat and maintaining the reaction, restarting and shutdown, which continues to plague these crude but effective space fuels. As a starting point, smaller may be better in handling the nuclear rocketry. Designing modular stand alone flight and return engines will be one hurdle to cover; non-radioactive Uranium-Rhenium hull designs could be built alternatively, for their high heats of vaporization temperatures, higher densities, and greater sturdiness with heat obduracy in mind; backup systems, fail safe systems would meet danger assurance standards, sortie hulls of all kind can be designed; of particular interest as a hull substance would entail the an annealing process whereby carbon is fused with carbon nuclei. While this is essentially the same nuclear reaction the carbo-myte device is designed for; the fusion product of that reaction results in a new material as an end product which when coated with a de-localized electron tetrahedral $\sigma\pi^3$ electron bonding with central C-C nuclear bonded planar-layered nuclear polymer; is a new metallic material that cannot be melted, is non-brittle, is completely indestructible, by nuclear WMD, or any other heat / pressure driven instrument. While neutrons can be joined in this way, the product is brittle. Such a fusion product metals branch of study needs to be created, to advance this field further. Again a shield or hull could sustain the highest temperatures e.g. even a WMD would not penetrate a hull built of this material, and would prove invincible in battle.

Geometrical Derivations:

To begin with, regarding the geometric laws presented; the lengths of the terms are all positive, but the values of the terms can be negative, i.e. meta-normal terms. By virtue of the similarity in models, relativistic energy vs. time-warp; one is not independent of the other but the actual relationship between these two is clarified in this manuscript. and why this occurs. This pertains also to the Fubrini developed as Eq. 9a. With regard to the line sums and their multiplication, Eq. 9a solves this. As such, and within the mathematical treatment to follow, developed are two sets of quadra-obelus time-energy hyperbolic equations. The equation which has a quadric surface associated with it, is discerned and generates both hyperbolae as well as parabolic curves composing the hyperbolic paraboloid cone for energy, and one for time-warp. The latter is completely dependent upon the former. Described within is the symbolic development of a new total energy time-warp model with reproducible results.

The fundamental surface involved is discovered and the isolation of the hybrid axes is performed. The cone of parabolas and hyperbolas is also evaluated and illustrated. This geometric cone manifests as a hyperbolic function of three variables. As is often the case, when two or more variables are combined and squared, a quadric surface often ensues. The hyperbolic paraboloidal energy cone is isolated and the curves generated are both sets of the parabolic, mixed with the hyperbolic; the former being different in cross section geometrical than the latter, upon the same conic. Although the results from cross sectioning are similar, the cone is deficient of circles or ellipses in the cut, atypical to those commonly generated.

The features of this model have principally to do with the incorporation of the general symbolic geometric solution to the typical two right triangle with perpendicular drawn to base problem should have caught the attention of early geometry mathematicians, and are reproduced here. Within this document six new laws governing the dynamics of the double triangle with base drawn problem are listed. The solution to the geometry yielded six new geometric laws; isolating the correct graph rewarded the promised hyperbolic paraboloid. Isolated was a function that generated contours of a trapped parabolic operator which opened and closed with variation in the other two terms. Within the daughter formula is a related quadric, was another quadric cone that acted as a generator to both parabolics and hyperbolics, as predicted. (7)

Summary of the Problem:

A general relation should involve variables of K.E, G.P.E, and R.E., As angles of incidence and exit angle attainable through common means of reduction, result in the double right triangle model of fig. 7. Holding *K.E.* constant, the two tangents composed of *K.E.* and *R.E.* are complimentary Pythagorean components of the energy triangle. In the bottom triangle the G.P.E. is subtracted from the K.E., but as for the geometry, all the lengths must be positive. Afterwards, the sign substitution may be applied. As such $\gamma_c = \frac{\pi}{2} - \gamma_m$. The hypotenuses compile to Total Kinetic Energy (T.I.E.), and Total Gravitational Potential Energy (T.P.E.) segments.

In obtaining the difference of squares relation equal to one, That operation yields a two-dimensional segment of a hyperbola of one sheet, shown here as equation B12 of appendix B., (fig. 8) and its fundamental hyperbolic paraboloid quadric is in this case, C8, of appendix C, or (figs. 8, 9, 10, 10a). The proofs, (appendices A-J), show the derivation of a hyperbolic formula governing the reticulation of two adjacent right triangles and the quadric functions associated with this R^2 geometric model. The saddle-point of the quadric of figs. 9, 10, 10a. (fig. 10 is the root plot of fig. 9), and lies at (.8603, .8603) radians, representing a point in the cross section of the midsection of a hyperbola of one sheet, with the minimax shifted along the hybrid linear axis, i.e. the $\theta = \gamma$ axis of fig. 10a. The two roots correspond to two solution lines, which make diagonals across the original quadric surface. The trigonometric square cosine factor of equation B12, produces one of the two independent root lines seen in fig. 10. Through symbolic rearrangement and functional analysis the root-lines are separated and the results are displayed in equation Eq. 16, (figs. 8, 9, 10, and 10a). The units cancel in all cases. The figures are presented in radians, although degrees may be used with equal success. Cartesian coordinates are preferred in this case over polar ones (due to the obelus triploidy).

Description of the Geometric Model:

Theoretically, a geometric solution in the tri-modal reticulation of similar right triangles can be derived from the model. The general solution, is without constraint; applies for any value of the three variables, θ, *R.E.*, and fixed *K.E.* Initially, as the bottom angle θ increases and the top angle γ varies directly or inversely with θ, respectively. Secondarily, γ, is a dependent variable, in *K.E* and *R.E.* are the two sides. These first two movements are depicted in fig. 9, and 10, and are axial solution sets to the original equation's (C8) hyperbolic paraboloid. Tertiarily movement is where the R.E. line moves along the y-axis as per fig. 7, reducing to two minor formulas, (E11, I8). The useful contour is generated by the secondary, inverse variation in the adjacent angles of the triangle model, and is a function of θ, *K.E.*, and *R.E.*

As review, triangle < K.E.,T.I.E.,R.E. > and triangle e < G.P.E.,T.P.E.,R.E. >, are similar but not congruent, with the R.E. and perpendicular angles being common. From proportionality, the three-way angle equality A2 can be formulated, which leads to B3 and B4 being substituted into B5; which is the Pythagorean triple used in the subsequent derivation of the two formulae. Notably axiom A2 is revisited as C8. (appendices A, B, and C).

In expression A6, and of fig. 7, the δ is composed of the segment difference between one K.E. along the length *T.I.E.*, and σ. That small segment is δ, which varies with *K.E.* and γ directly. σ is the remainder such that $\delta + \sigma = K.E.$ Subtract *K.E.* from *T.I.E.* to obtain the z that is double substituted for, in the Pythagorean right triangle B1, B3, and B4, which once completed, leads to B6; (see appendix B, and fig. 7). No condition is made on the z, which varies directly with the angle γ, which in turn varies with θ any of two ways, as stated. A more important key lies in the extra *K.E.* in expression B2, which leads to a perfect square relation in expression B6, and B8. Re-arranged the perfect square leads to the Hyperbolic Cosine Energy Formula, a difference of squares relation equal to one; which is an expression of an already reduced number of independent variables: *K.E.*, and *R.E.*, and θ; displayed in expression B12, The graph of B12 is fig. 8, is constrained by the square cosine factor in the denominator; and is factored out, yields the backbone function to the parent equation to B12, Eq. 24; (figs. 17, and 18). The Pythagorean triple is used in equation C3; and then the trigonometric C7 is employed to finalize the proof yielding the predicted quadric C8, (1).

Geometrical Analysis and Discussion:

The hybrid solution axes or roots to the equation, the hyperbolic cosine formula function are simple to comprehend. The linear root corresponds to the angle pair in direct variance, the other is a function of a trapped parabolic variable in an hyperbolic equation. Since this is a function of an angle and two sides it would be wise to convert the angle to linear rectangular coordinates through the conversion: $(k\,\theta_m)^2 = 4\,p\,R.E.$ If theta is an incident angle, the angle of reflection would equal the incident angle, and the sum would equal θ*model*. That is one way the two angles vary, and yields the linear root. If by fixing the cosine remnant of B12 to be equal to 1 at all times, the result is equation 16; the child is process to the parent function B12. Also the point values differ for the child process than for the parent equation B12; although the saddle-point remains the same. Regarding the dynamic analysis pertaining to the geometry of the triangle with base model; these six new laws contained here add to that known regarding the former. Thus in equation 16, that isolated cone generates both the parabolas and the hyperbolas (fig. 11), and the planar harmonics of such are similar to that generated by the general quadratic equation, the cone differs in shape from those normally seen as the cross section results are deficient in generating circles and ellipses.

With K.E. fixed the R.E. varies up to the minimum K.E./R.E. ratio of 1.16233, leaving θ to vary bi-linearly with the two sides, in the double obelus construction. The partial derivative of Eq. 16 is completely linear with respect to θ, as one would suspect, and the two first order partial differentials vary according to fig. 2c, 2d. As already noted, the quadric in question has implicit a periodic and re-iterations of the other two variables. If one obelus actually degenerates, the result will be the parabola. If one is dependent or is chained formulated, the result is the hybrid axes conglomerate displayed in figs. 2a 3, and 4. The general form of a hyperboloid of one sheet is as follows in Eq. 10.

$$Eq.10 \quad \frac{x^2}{a^2} + \frac{y^2}{b^2} - \frac{z^2}{c^2} = 1$$

Equation 10, breaks down into three component combinations of two-dimensional parts, namely Eqs. 11, 12, and 13:

$$Eq.11 \quad \frac{x^2}{a^2} + \frac{y^2}{b^2} = 1$$

$$Eq.12 \quad \frac{x^2}{a^2} - \frac{z^2}{c^2} = 1$$

$$Eq.13 \quad \frac{y^2}{b^2} - \frac{z^2}{c^2} = 1$$

Equation 2, is an ellipse, or circle. Equations 3, and 4, are both two dimensional, two sheet, hyperbolic components. Together they compose the whole, or three-dimensional hyperbola of one sheet. Since the Hyperbolic Cosine Energy Formula equation is also two termed, by contrast, produces figs. 8, 9, 10, and 10a; the application of quadric tests can be performed as well. In the general quadric equation Eq. 5, the quadric discriminant, Eq. 15 could be useful in determining the minimax of C8, of figs. 8, and 9. The isolated hybrid axes displayed in figs. 10, and 10a, are generated by Eq. 7; the cone associated with this equation could later prove valuable to astronomy buffs, but this quadric law that generates both and only hyperbolas and parabolas which stem from a the slices to this cone in the xy and xz axes. This is a new cone and the cross-sections are easier to generate than in the traditional "hour-glass" conic. This hyperbolic equation generates a refreshing solution to an age old problem; namely that of the reticulation and reciprocation of the components to two similar right triangles associated with the geometric model.

In table A, some common values are presented from the parent equation B12. For a point to be a minimax, the quadric must obey the above condition; where $K.E._{xx} = \dfrac{\partial^2 (K.E.)}{\partial (x)^2}$. When the symbolic quadric test is applied to the Eq. C8; the minimax, (.8603, .8603), of fig. 9, 10, and 10a, the result is -5.4335; thus confirming that that point, (.8603, .8603), is the true minimax. For the hyperbolic paraboloid of figs. 9, 10, and 10a, shows a relative minimum occurs at $\theta = 0$, and at the maximum R.E. of 20. This was determined from the discriminant after the partials were generated; this same conic however, has no saddle-point.

$$Eq. 14 \;\; Ax^2 + Bxy + Cy^2 + Dx + Ey + F = 0$$

$$Eq. 15 \;\; K.E._{xx}\, K.E._{yy} - K.E.\,^2_{xy} = \begin{vmatrix} K.E._{xx} & K.E._{yx} \\ K.E._{xy} & K.E._{yy} \end{vmatrix}$$

$$Eq.15a \quad K.E._{xx}K.E._{yy} - K.E._{xy}^{2} < 0$$

$$Eq.16 \quad \frac{\gamma^2}{\theta^2} - \frac{K.E.^2}{R.E.^2} = 1$$

From the drawings and throughout the discussion, it is clear that the cosine factor of B12 is responsible for the double root. Through functional analysis, setting θ equal to zero, such that $\cos^2(\theta) = 1$, the net result is a decoupled fundamental equation whose eccentricity and discriminant show parabolic and hyperbolic features depending on the view or slice, without participation from the linear component. Accordingly, the partial derivative is linear for θ, confirming potential bi-linearity, as predictable from the form. As was stated earlier a constant would be valuable to convert the principle angle, θ to linear coordinate values. A linear coordinate transpose matrix could further un-tangle the analytical knot.

In accordance with Snell's law, when parallel light from a star or distant light source is collected by a concave surface and the angle of the displacement of that ray is equal to twice the tangent angle at the surface. The linear coordinate translation for the theta, or x-axis, of fig. 10, is such that: $R.E.' = (k \times \theta)$. For this graph $k = 14.79924...$, in respective length units per radian. After transposing the minimax the parabolic latus rectum can be computed. For review the latus rectum is $lr = 4p$, where $p = 11.6233$, and $K.E. = 2p$; and plugging into yields: $(k\theta)^2 = 2K.E.\ R.E.$

Geometrical Results:

Table A.

1).	$\theta_m = 90$	$R.E._1 = \infty$	$\frac{K.E.}{R.E.}\ ratio = 0$	$\gamma_m = 0$	$G.P.E._1{}' = \infty$
2).	$\theta_m = 75$	$R.E._2 = 61.3288$	$\frac{K.E.}{R.E.}\ ratio = .3790$	$\gamma_m = 20.7591$	$G.P.E._2{}' = .3480$
3).	$\theta_m = 60$	$R.E._3 = 18.2586$	$\frac{K.E.}{R.E.}\ ratio = 1.2731$	$\gamma_m = 51.8509$	$G.P.E._3{}' = .0446$
4).	$\theta_m = 30$	$R.E._4 = 9.7674$	$\frac{K.E.}{R.E.}\ ratio = 2.3890$	$\gamma_m = 67.2866$	$G.P.E._4{}' = .0132$
5).	$\theta_m = 15$	$R.E._5 = 4.3089$	$\frac{K.E.}{R.E.}\ ratio = 5.3950$	$\gamma_m = 79.4990$	$G.P.E._5{}' = .0047$
6).	$\theta_m = 0$	$R.E._6 = 0.0000$	$\frac{K.E.}{R.E.}\ ratio = \infty$	$\gamma_m = 90$	$G.P.E._6{}' = 0$

Table B.

1).	$\theta_m = 49.2935$	$R.E. = 20.0000$	$\frac{K.E.}{R.E.}\ ratio = 1.16233$	$\gamma_m = 49.2935$	$\gamma_c = 49.2935$
2).	$\theta_m = 30.9953$	$R.E. = 15$	$\frac{K.E.}{R.E.}\ ratio = 1.5497$	$\gamma_m = 57.1664$	$\gamma_c = 32.8335$
3).	$\theta_m = 16.3724$	$R.E. = 5$	$\frac{K.E.}{R.E.}\ ratio = 4.6493$	$\gamma_m = 77.8614$	$\gamma_c = 12.1385$
4).	$\theta_m = 8.9670$	$R.E. = 2.5$	$\frac{K.E.}{R.E.}\ ratio = 9.2986$	$\gamma_m = 83.8618$	$\gamma_c = 6.1381$
5).	$\theta_m = 0$	$R.E. = 0$	$\frac{K.E.}{R.E.}\ ratio = \infty$	$\gamma_m = 90$	$\gamma_c = 0$

In table B, some sample values are computed and presented. These values conform with Eq. 16. From the table, the minimax for each process is identical; the values however differ, as theory would dictate. The minimum K.E. from the hyperbola-parabola generator, is zero, and this occurs at $R.E. = 0$ which makes $\theta = 0$ also. The parabolicity of the xy slices of this function, (figure 11), becomes clearer analytically when the minimax is taken as an origin, for this equation. Using a transpose or conversion matrix would serve as a solution to this orientation problem. Hyperbolic double sheets occur with the zx slices to fig. 11. Interestingly, at the minimax abscissa angle the tangent reaches a minimum at $\gamma = 49.2934$, then recedes; this is reassuringly the minimum K.E./R.E. ratio of 1.16233. The numbers can change, but the minimax and obelus ratios presented and highlighted will always remain the same for this formula.

As in fig. 6, the offset is governed by the formula: $\lambda_{offset} = \frac{\pi}{n}$, where n is the number of sides of a regular polygon design, and $2\lambda_{offset}$ is exactly the angular offset between any two adjacent sides. Spacing is dependent upon angular offset and the R.E., as in appendix V.

In summary, six new geometric formulae fully describe the tri-modal relationship in the geometry of a previously unexamined total energy model. The solution generated a parabola and hyperbola generating cone. the parabolic operator is an child object from the parent hyperbolic function. The new cone reviewed generates the same curves as the traditional cone, with the exception of the circle and the ellipse.

Appendix A:

Axioms and Identities:

$$A1.\ \ \theta + \gamma \leq \pi$$

$$A2.\ \ \frac{\cos(\theta)}{\cos(\gamma)} = \frac{\gamma}{\theta} = \frac{z + K.E.}{T.P.E.}$$

$$A3.\ \ \left(z + K.E.\right)^2 = K.E.^2 + R.E.^2$$

$$A4.\ \ \delta^2 = \left(4K.E.^2 \sin^2\left(\frac{\frac{\pi}{2} - \gamma}{2}\right) - R.E.^2 \sin^2(\gamma)\right)$$

$$A5.\ \ T.P.E. \cos(\theta) = R.E.$$

$$A6.\ \ \delta + \sigma = K.E.$$

$$A7.\ \ z + K.E. = T.I.E.$$

Appendix B:

$$B1.\quad \left(z+K.E.\right)^2 = K.E.^2 + R.E.^2$$

$$B2.\; z\left(z+2K.E.\right) = R.E.^2 = T.P.E.^2\cos^2(\theta)$$

$$B3.\; T.P.E.\gamma = \theta\left(z+K.E.\right)$$

$$B4.\; z = \frac{T.P.E.\gamma - K.E.\,\theta}{\theta}$$

$$B5.\quad \left(\frac{T.P.E.\gamma - K.E.\,\theta}{\theta}\right)\left(\frac{T.P.E.\gamma - K.E.\,\theta}{\theta} + 2K.E.\right) = R.E.^2$$

$$B6.\quad \left(h\gamma - K.E.\,\theta\right)\left(h\gamma + K.E.\,\theta\right) = \theta^2 R.E.^2$$

$$B7.\; T.P.E. = \frac{R.E.}{\cos(\theta)} \rightarrow \left(\frac{R.E.\,\gamma}{\cos(\theta)} - K.E.\,\theta\right)\left(\frac{R.E.\,\gamma}{\cos(\theta)} + K.E.\,\theta\right) = \theta^2 R.E.^2$$

$$B8.\; \frac{R.E.^2\gamma^2}{\cos^2(\theta)} - K.E.^2\theta^2 = R.E.^2\theta^2$$

$$B9.\; R.E.^2\gamma^2 - K.E.^2\theta^2\cos^2(\theta) = R.E.^2\theta^2\cos^2(\theta)$$

$$B10.\; \frac{R.E.^2\gamma^2}{R.E.^2} = \frac{R.E.^2\theta^2\cos^2(\theta)}{R.E.^2} + \frac{K.E.^2}{R.E.^2}\theta^2\cos^2(\theta)$$

$$B11.\; \frac{\gamma^2}{\theta^2} = \cos^2(\theta) + \frac{K.E.^2}{R.E.^2}\cos^2(\theta)$$

$$B12.\; \frac{\gamma^2}{\theta^2\cos^2(\theta)} - \frac{K.E.^2}{R.E.^2} = 1$$

Hyperbolic Cosine Energy Formula

$$B13.\; \frac{\theta^2}{R.E.^2} - \frac{\gamma^2}{\cos^2(\theta)\left(K.E.^2 + R.E.^2\right)} = 0$$

Hyperbolic Cosine Energy Formula Cone

Appendix C:

$$C1.\quad \frac{\gamma^2}{\theta^2\cos^2(\theta)} = 1 + \frac{K.E.^2}{R.E.^2}$$

$$C2.\quad \frac{\gamma^2}{\theta^2} = \cos^2(\theta) + \frac{K.E.^2\cos^2(\theta)}{R.E.^2}$$

$$C3.\quad \frac{K.E.^2}{R.E.^2} + \frac{R.E.^2}{R.E.^2} = \frac{T.I.E.^2}{R.E.^2} \rightarrow \frac{K.E.^2}{R.E.^2} = \frac{T.I.E.^2}{R.E.^2} - 1$$

$$C4.\quad \frac{\gamma^2}{\theta^2} = \cos^2(\theta) + \cos^2(\theta)\left(\frac{T.I.E.^2}{R.E.^2} - 1\right)$$

$$C5.\quad \frac{R.E.^2\gamma^2}{\theta^2} = R.E.^2\cos^2(\theta) + T.I.E.^2\cos^2(\theta) - R.E.^2\cos^2(\theta)$$

$$C6.\quad \frac{R.E.^2\gamma^2}{\theta^2} = T.I.E.^2\cos^2(\theta)$$

$$C7.\quad \frac{\gamma^2}{\theta^2} = \frac{T.I.E.^2}{R.E.^2\cos^2(\theta)} \qquad \frac{T.I.E.}{R.E.} = \frac{1}{\cos(\gamma)}$$

$$C8.\quad \frac{\gamma^2}{\theta^2} = \frac{\cos^2(\theta)}{\cos^2(\gamma)}$$

Hyperbolic Paraboloid Cosine Energy Formula

Appendix D:

Axioms and Identities:

$$D1.\ \ T.I.E.\ \sin(\gamma) = K.E. + G.P.E.$$

$$D2.\ \ T.I.E. = z + K.E.$$

$$D3.\ \ \frac{z + K.E.}{T.P.E.} = \frac{\gamma}{\theta} = \frac{\cos(\theta)}{\cos(\gamma)}$$

$$D4.\ \ z = \frac{T.P.E.\ \gamma - K.E.\ \theta}{\theta}$$

Appendix E:

$$E1.\quad T.I.E.^{2} = \left(K.E. + G.P.E.\right)^{2} + R.E.^{2}$$

$$E2.\quad \left(z + K.E.\right)^{2} = K.E.^{2} + 2\,G.P.E.\,K.E. + G.P.E.^{2} + R.E.^{2}$$

$$E3.\quad z\left(z + 2K.E.\right) = G.P.E.\left(G.P.E. + 2K.E.\right) + R.E.^{2}$$

$$E4.\quad z\left(z + 2K.E.\right) = G.P.E.\left(T.I.E.\sin(\gamma) + K.E.\right) + R.E.^{2}$$

$$E5.\quad \left(\frac{T.P.E.\,\gamma - K.E.\,\theta}{\theta}\right)\left(\frac{T.P.E.\,\gamma + K.E.\,\theta}{\theta}\right) = \left(T.I.E.\sin(\gamma) - K.E.\right)\left(T.I.E.\sin(\gamma) + K.E.\right) + R.E.^{2}$$

$$E6.\quad \left(\frac{T.P.E.^{2}\gamma^{2} - K.E.^{2}\theta^{2}}{\theta^{2}}\right) = T.I.E.^{2}\sin^{2}(\gamma) - K.E.^{2} + R.E.^{2}$$

$$E7.\quad \frac{T.P.E.^{2}\gamma^{2}}{\theta^{2}} = T.I.E.^{2}\sin^{2}(\gamma) + R.E.^{2}$$

$$E8.\quad \frac{T.P.E.^{2}\gamma^{2}}{\theta^{2}} = \left(z + K.E.\right)^{2}\sin^{2}(\gamma) + R.E.^{2}$$

$$E9.\quad \frac{T.P.E.^{2}\gamma^{2}}{\theta^{2}} = \frac{T.P.E.^{2}\gamma^{2}}{\theta^{2}}\sin^{2}(\gamma) + R.E.^{2}$$

$$E10.\quad \frac{R.E.^{2}}{T.I.E.^{2}} = 1 - \sin^{2}(\gamma)$$

$$E11.\quad \frac{R.E.^{2}}{T.I.E.^{2}} = \cos^{2}(\gamma)$$

Cosine Square Energy Formula

Appendix F:

Axioms and Identities:

$$F1.\quad \frac{\sin(\alpha)}{\sin(\beta)} = \frac{\alpha}{\beta} = \frac{T.P.E.}{z + K.E.}$$

$$F2.\quad \frac{R.E.}{T.I.E.} = \sin(\alpha)$$

$$F3.\quad \frac{R.E.}{T.P.E.} = \sin(\beta)$$

Appendix G:

$$G1.\quad T.I.E.^2 = R.E.^2 + K.E.^2$$

$$G2.\quad z\left(z + 2K.E.\right) = R.E.^2 = T.P.E.^2 \sin^{2(}(\beta)$$

$$G3.\quad \left(\frac{T.P.E.\,\beta - K.E.\,\alpha}{\alpha}\right)\left(\frac{T.P.E.\,\beta - K.E.\,\alpha + 2K.E.\,\alpha}{\alpha}\right) = R.E.^2$$

$$G4.\quad T.P.E.^2\,\beta^2 - K.E.^2\,\alpha^2 = R.E.^2\,\alpha^2$$

$$G5.\quad \frac{R.E.^2\beta^2}{\sin^2(\beta)} - K.E.^2\,\alpha^2 = R.E.^2\,\alpha^2$$

$$G6.\quad \frac{\beta^2}{\sin^2(\beta)} - \frac{K.E.^2\,\alpha^2}{R.E.^2} = \alpha^2$$

$$G7.\quad \frac{\beta^2}{\alpha^2\sin^2(\beta)} - \frac{K.E.^2}{R.E.^2} = 1$$

Hyperbolic Sine Energy Formula:

Rearrangement yields the ratio form:

$$G8.\quad \frac{\alpha^2}{\beta^2} - \frac{\left(R.E.^2 + K.E.^2\right)}{K.E.^2\sin^2(\beta)} = 0$$

Then also:

$$G9.\quad \frac{\beta^2}{\alpha^2} - \frac{K.E.^2\sin^2(\beta)}{R.E.^2} = \sin^2(\beta)$$

$$G10.\quad \frac{\beta^2}{\alpha^2} - \sin^2(\beta)\left(\frac{T.I.E.^2}{R.E.^2} - 1\right) = \sin^2(\beta)$$

$$G11.\quad \frac{R.E.^2\beta^2}{\alpha^2} - T.I.E.^2\sin^2(\beta) + R.E.^2\sin^2(\beta) = R.E.^2\sin^2(\beta)$$

$$G12.\quad \frac{R.E.^2\beta^2}{\alpha^2} = T.I.E.^2\sin^2(\beta)$$

$$G\,13.\quad \frac{\beta^2}{\alpha^2} = \frac{T.I.E.^{\,2}}{R.E.^{\,2}} \sin^2(\beta)$$

$$G\,14.\quad \frac{T.I.E.}{R.E.} = \frac{1}{\sin(\alpha)}$$

$$G\,15.\quad \frac{\beta^2}{\alpha^2} = \frac{\sin^2(\beta)}{\sin^2(\alpha)}$$

<u>Hemi-Hyperbolic Paraboloid Sine Energy Formula</u>

Appendix H:

Axioms and Identities

$$H1.\;\; T.I.E.\cos(\alpha) = K.E. + G.P.E.$$

$$H2.\;\; \frac{\alpha}{\beta} = \frac{T.P.E.}{T.I.E.} = \frac{T.P.E.}{z + K.E.} = \frac{\sin(\alpha)}{\sin(\beta)}$$

$$H3.\;\; z + K.E. = \frac{T.P.E.\beta}{\alpha} = T.I.E.$$

Appendix I:

$$I1.\;\; T.I.E.^2 = \left(K.E. + G.P.E.\right)^2 + R.E.^2$$

$$I2.\;\; z\left(z + 2K.E.\right) = G.P.E.\left(T.I.E.\cos(\alpha) + K.E.\right) + R.E.^2$$

$$I3.\;\; \left(\frac{T.P.E.\beta - K.E.\alpha}{\alpha}\right)\left(\frac{T.P.E.\beta + K.E.\alpha}{\alpha}\right) = \left(T.I.E.\cos(\alpha) - K.E.\right)\left(T.I.E.\cos(\alpha) + K.E.\right) + R.E.^2$$

$$I4.\;\; \frac{T.P.E.^2\beta^2 - K.E.^2\alpha^2}{\alpha^2} = T.I.E.^2\cos^2(\alpha) - K.E.^2 + R.E.^2$$

$$I5.\;\; \frac{T.P.E.^2\beta^2 - K.E.^2\alpha^2 + K.E.^2\alpha^2}{\alpha^2} = \left(z + K.E.\right)^2\cos^2(\alpha) + R.E.^2$$

$$I6.\;\; \frac{T.P.E.^2\beta^2}{\alpha^2} = \frac{T.P.E.^2\beta^2}{\alpha^2}\cos^2(\alpha) + R.E.^2$$

$$I7.\;\; 1 - \cos^2(\alpha) = \frac{R.E.^2}{T.I.E.^2}$$

$$I8.\;\; \frac{R.E.^2}{T.I.E.^2} = \sin^2(\alpha)$$

Sine Square Energy Formula:

Appendix J:

Multi-Thruster Layout

$$J1.\quad \delta = l\cos(\lambda) - 2r$$

$$J2.\quad l = \frac{r + \sigma}{\sin(\frac{\pi}{n})}$$

Within the mathematical treatment to follow, is developed a tri-obelus hyperbolic equation. Naturally, this equation has a quadric surface associated with it, which generates both hyperbolae as well as parabolic curves which compose the hyperbolic paraboloid cone for time-warp. Described within is the symbolic development of a new total time-warp model now with known results. The fundamental surface involved is discovered and the isolation of the hybrid axes is performed. The cone of parabolas and hyperbolas is also evaluated and illustrated. This geometric cone manifests as a hyperbolic function of three variables. As is often the case, when two or more variables are combined and squared,a quadric surface often ensues. The hyperbolic paraboloidal time-warp cone is isolated and the curves generated are both sets of the parabolic, mixed with the hyperbolic; the former being different in cross section geometrical than the latter, upon the same conic. Although the results from cross sectioning are similar, the cone is deficient of circles or ellipses in the cut, atypical to those commonly generated.

The features of this model have principally to do with the incorporation of the general symbolic geometric solution to the typical two right triangle with perpendicular drawn to base problem should have caught the attention of early geometry mathematicians, and are reproduced here. Within this document six new laws governing the dynamics of the double triangle with base drawn problem are listed. The solution to the geometry yielded six new geometric laws; isolating the correct graph rewarded the promised hyperbolic paraboloid. Isolated was a function that generated contours of a trapped parabolic operator which opened and closed with variation in the other two terms. Within the daughter formula is a related quadric, was another quadric cone that acted as a generator to both parabolics and hyperbolics, as predicted. (7)

Summary of the Problem:

A general relation should involve variables of G.P.W., I.W., and R.W., As angles of incidence and exit angle attainable through common means of reduction, result in the double right triangle model of fig. 7a. Holding *G.P.W.* constant, the two tangents composed of *G.P.W.* and *R.W.* are complimentary Pythagorean components of the time-warp triangle. In the bottom triangle the I.W. is subtracted from the G.P.W. As such $\gamma_c = \frac{\pi}{2} - \gamma_m$. The hypotenuses compile to Total Kinetic Time-warp (T.I.W.), and Total Gravitational Potential Time-warp (T.G.W.) segments.

In obtaining the difference of squares relation equal to one, That operation yields a two-dimensional segment of a hyperbola of one sheet, shown here as equation L12 of appendix L., (fig. 14) and its fundamental hyperbolic paraboloid quadric is in this case, M8, of appendix M, or (figs. 14, 15, 16, 17). The proofs, (appendices K-T), show the derivation of a hyperbolic formula governing the reticulation of two adjacent right triangles and the quadric functions associated with this R^2 geometric model. The saddle-point of the quadric of figs. 15, 16, 17. (fig. 16 is the root plot of fig. 15), and lies at (.8603, .8603) radians, representing a point in the cross section of the midsection of a hyperbola of one sheet, with the minimax shifted along the hybrid linear axis, i.e. the $\theta = \gamma$ axis of fig. 16. The two roots correspond to two solution lines, which make diagonals across the original quadric surface. The trigonometric square cosine factor of equation L12, produces one of the two independent root lines seen in fig. 16. Through symbolic rearrangement and functional analysis the root-lines are separated and the results are displayed in equation Eq. 16, (figs. 8, 9, 10, and 10a). The units cancel in all cases. The figures are presented in radians, although degrees may be used with equal success. Cartesian coordinates are preferred in this case over polar ones (due to the obelus triploidy).

Description of the Geometric Time-Warp Model:

Theoretically, a geometric solution in the tri-modal reticulation of similar right triangles can be derived from the model. The general solution, is without constraint; applies for any value of the three variables, θ, *R.W.*, and fixed *G.P.W.* Initially, as the bottom angle θ increases and the top angle γ varies directly or inversely with θ, respectively. Secondarily, γ, is a dependent variable, in *K.E* and *R.W.* are the two sides. These first two movements are depicted in fig. 15, and 16, and are axial solution sets to the original equation's (M8) hyperbolic paraboloid. Tertiarily movement is where the R.W. line moves along the y-axis as per fig. 7a, reducing to two minor formulas, (O11, S8). The useful contour is generated by the secondary, inverse variation in the adjacent angles of the triangle model, and is a function of θ, *G.P.W.*, and *R.W.*

As review, triangle < G.P.W.,T.G.W.,R.W. > and triangle e < I.W.,T.I.W.,R.W. >, are similar but not congruent, with the R.W. and perpendicular angles being common. From proportionality, the three-way angle equality K2 can be formulated, which leads to L3 and L4 being substituted into L5; which is the Pythagorean triple used in the subsequent derivation of the two formulae. Notably axiom K2 is revisited as M8. (appendices K, L, and M).

In expression K6, and of fig. 7a, the δ is composed of the segment difference between one G.P.W. along the length *T.G.W.*, and σ. That small segment is δ, which varies with *G.P.W.* and γ directly. σ is the remainder such that $\delta + \sigma = G.P.W.$ Subtract *G.P.W.* from *T.G.W.* to obtain the *z* that is double substituted for, in the Pythagorean right triangle L1, L3, and L4, which once completed, leads to L6; (see appendix L, and fig. 7a). No condition is made on the *z*, which varies directly with the angle γ, which in turn varies with θ any of two ways, as stated. A more important key lies in the extra *G.P.W.* in expression L2, which leads to a perfect square relation in expression L6, and L8. Rearranged the perfect square leads to the Hyperbolic Cosine Time-Warp Formula, a difference of squares relation equal to one; which is an expression of an already reduced number of independent variables: *G.P.W.*, and *R.W.*, and θ; displayed in expression L12, The graph of L12 is fig. 14, is constrained by the square cosine factor in the denominator; and is factored out, yields the backbone function to the parent equation to L12, Eq. 24; (figs. 17, and 18). The Pythagorean triple is used in equation L3; and then the trigonometric L7 is employed to finalize the proof yielding the predicted quadric M8, (1).

Analysis and Discussion:

The hybrid solution axes or roots to the equation, the hyperbolic cosine formula function are simple to comprehend. The linear root corresponds to the angle pair in direct variance, the other is a function of a trapped parabolic variable in an hyperbolic equation. Since this is a function of an angle and two sides it would be wise to convert the angle to linear rectangular coordinates through the conversion: $(k\,\theta_m)^2 = 4\,p\,R.W.$ If theta is an incident angle, the angle of reflection would equal the incident angle, and the sum would equal θ*model*. That is one way the two angles vary, and yields the linear root. If by fixing the cosine remnant of B12 to be equal to 1 at all times, the result is equation 24; the child is process to the parent function L12. Also the point values differ for the child process than for the parent equation B12; although the saddle-point remains the same. Regarding the dynamic analysis pertaining to the geometry of the triangle with base model; these six new laws contained here add to that known regarding the former. Thus in equation 24, that isolated cone generates both the parabolas and the hyperbolas (fig. 18), and the planar harmonics of such are similar to that generated by the general quadratic equation, the cone differs in shape from those normally seen as the cross section results are deficient in generating circles and ellipses.

With G.P.W. fixed the R.W. varies up to the minimum G.P.W./R.W. ratio of 1.16233, leaving θ to vary bi-linearly with the two sides, in the double obelus construction. The partial derivative of Eq. 24 is completely linear with respect to θ, as one would suspect, and the two first order partial differentials vary according to fig. 18. As already noted, the quadric in question has implicit a periodic and re-iterations of the other two variables. If one obelus actually degenerates, the result will be the parabola. If one is dependent or is chained formulated, the result is the hybrid axes conglomerate displayed in figs. 14, 15, and 16. The general form of a hyperboloid of one sheet is as follows in Eq. 17.

$$Eq.17 \quad \frac{x^2}{a^2}+\frac{y^2}{b^2}-\frac{z^2}{c^2}=1$$

Equation 17, breaks down into three component combinations of two-dimensional parts, namely Eqs. 18, 19, and 20:

$$Eq.18 \quad \frac{x^2}{a^2}+\frac{y^2}{b^2}=1$$

$$Eq.19 \quad \frac{x^2}{a^2}-\frac{z^2}{c^2}=1$$

$$Eq.20 \quad \frac{y^2}{b^2}-\frac{z^2}{c^2}=1$$

Equation 18, is an ellipse, or circle. Equations 19, and 20, are both two dimensional, two sheet, hyperbolic components. Together they compose the whole, or three-dimensional hyperbola of one sheet. Since the Hyperbolic Cosine Time-Warp Formula equation is also two termed, by contrast, produces figs. 16, 17, 18, and 19; the application of quadric tests can be performed as well. In the general quadric equation Eq. 22, the quadric discriminant, Eq. 23 could be useful in determining the minimax of M8, of figs. 14, and 15. The isolated hybrid axes displayed in figs. 16, and 17, are generated by Eq. 24; the cone associated with this equation could later prove valuable to astronomy buffs, but this quadric law that generates both and only hyperbolas and parabolas which stem from a the slices to this cone in the xy and xz axes. This is a new cone and the cross-sections are easier to generate than in the traditional "hour-glass" conic. This hyperbolic equation generates a refreshing solution to an age old problem; namely that of the reticulation and reciprocation of the components to two similar right triangles associated with the geometric model.

In table A, some common values are presented from the parent equation B12. For a point to be a minimax, the quadric must obey the above condition; where $G.P.W._{xx} = \frac{\partial^2(G.P.W.)}{\partial(x)^2}$. When the symbolic quadric test is performed to Eq. M8 and the minimax, (.8603, .8603), (see fig. 15, 16, and 17, the result is -5.4335; thus confirming that that point, (.8603, .8603), is the true minimax. For the hyperbolic paraboloid of figs. 15, 16, and 17, shows a relative minimum occurs at $\theta = 0$, and at the maximum R.W. of 20. This was determined from the discriminant after the partials were generated; this same conic however, has no saddle-point.

$$Eq.21 \;\; Ax^2 + Bxy + Cy^2 + Dx + Ey + F = 0$$

$$Eq.22 \;\; G.P.W._{xx}\, G.P.W._{yy} - G.P.W._{xy}^{\,2} = \begin{vmatrix} G.P.W._{xx} & G.P.W._{yx} \\ G.P.W._{xy} & G.P.W._{yy} \end{vmatrix}$$

$$Eq.23 \;\; G.P.W._{xx} G.P.W._{yy} - G.P.W._{xy}^{\,2} < 0$$

$$Eq.24 \;\; \frac{\gamma^2}{\theta^2} - \frac{G.P.W.^{\,2}}{R.W.^{\,2}} = 1$$

From the drawings and throughout the discussion, it is clear that the cosine factor of B12 is responsible for the double root. Through functional analysis, setting θ equal to zero, such that $\cos^2(\theta) = 1$, the net result is a decoupled fundamental equation whose eccentricity and discriminant show parabolic and hyperbolic features depending on the view or slice, without participation from the linear component. Accordingly, the partial derivative is linear for θ, confirming potential bi-linearity, as predictable from the form. As was stated earlier a constant would be valuable to convert the principle angle, θ to linear coordinate values. A linear coordinate transpose matrix could further un-tangle the analytical knot.

The linear coordinate translation for the theta, or x- axis, of fig. 16, is such that: $R.W.' = (k \times \theta)$. For this graph $k = 14.79924...$, in respective length units per radian. After transposing the minimax the parabolic latus rectum can be computed. For review the latus rectum is $lr = 4p$, where $p = 11.6233$, and $G.P.W. = 2p$; and plugging into yields: $(k\theta)^2 = 2G.P.W.\ R.W.$

Geometrical Results:

Table C.

1).	$\theta_m = 90$	$R.W._1 = \infty$	$\frac{G.P.W.}{R.W.}$ $ratio = 0$	$\gamma_m = 0$	$I.W._1' = \infty$
2).	$\theta_m = 75$	$R.W._2 = 61.3288$	$\frac{G.P.W.}{R.W.}$ $ratio = .3790$	$\gamma_m = 20.7591$	$I.W._2' = .3480$
3).	$\theta_m = 60$	$R.W._3 = 18.2586$	$\frac{G.P.W.}{R.W.}$ $ratio = 1.2731$	$\gamma_m = 51.8509$	$I.W._3' = .0446$
4).	$\theta_m = 30$	$R.W._4 = 9.7674$	$\frac{G.P.W.}{R.W.}$ $ratio = 2.3890$	$\gamma_m = 67.2866$	$I.W._4' = .0132$
5).	$\theta_m = 15$	$R.W._5 = 4.3089$	$\frac{G.P.W.}{R.W.}$ $ratio = 5.3950$	$\gamma_m = 79.4990$	$I.W._5' = .0047$
6).	$\theta_m = 0$	$R.W._6 = 0.0000$	$\frac{G.P.W.}{R.W.}$ $ratio = \infty$	$\gamma_m = 90$	$I.W._6' = 0$

Table D.

1).	$\theta_m = 49.2935$	$R.W. = 20.0000$	$\frac{G.P.W.}{R.W.}$ $ratio = 1.16233$	$\gamma_m = 49.2935$	$\gamma_c = 49.2935$
2).	$\theta_m = 30.9953$	$R.W. = 15$	$\frac{G.P.W.}{R.W.}$ $ratio = 1.5497$	$\gamma_m = 57.1664$	$\gamma_c = 32.8335$
3).	$\theta_m = 16.3724$	$R.W. = 5$	$\frac{G.P.W.}{R.W.}$ $ratio = 4.6493$	$\gamma_m = 77.8614$	$\gamma_c = 12.1385$
4).	$\theta_m = 8.9670$	$R.W. = 2.5$	$\frac{G.P.W.}{R.W.}$ $ratio = 9.2986$	$\gamma_m = 83.8618$	$\gamma_c = 6.1381$
5).	$\theta_m = 0$	$R.W. = 0$	$\frac{G.P.W.}{R.W.}$ $ratio = \infty$	$\gamma_m = 90$	$\gamma_c = 0$

Analysis and Discussion:

In table C, some sample values are computed and presented. These values conform with Eq. 24. From the table, the minimax for each process is identical; the values however differ, as theory would dictate. The minimum G.P.W. from the hyperbola-parabola generator, is zero, and this occurs at $R.W. = 0$ which makes $\theta = 0$ also. The parabolicity of the xy slices of this function, (figure 17), becomes clearer analytically when the minimax is taken as an origin, for this equation. Using a transpose or conversion matrix would serve as a solution to this orientation problem. Hyperbolic double sheets occur with the zx slices to fig. 17. Interestingly, at the minimax abscissa angle the tangent reaches a minimum at $\gamma = 49.2934$, then recedes; this is reassuringly the minimum G.P.W./R.W. ratio of 1.16233. The numbers can change, but the minimax and obelus ratios presented and highlighted will always remain the same for this formula.

As in fig. 10, the offset is governed by the formula: $\lambda_{offset} = \frac{\pi}{n}$, where n is the number of sides of a regular polygon design, and $2\lambda_{offset}$ is exactly the angular offset between any two adjacent sides. Spacing is dependent upon angular offset and the R.W., as in appendix T; differentially as appendix U, and fig. 7c.

In summary, six new geometric formulae fully describe the tri-modal relationship in the geometry of a previously unexamined total time-warp model. The solution generated a parabola and hyperbola generating cone. the parabolic operator is an child object from the parent hyperbolic function. The new cone reviewed generates the same curves as the traditional cone, with the exception of the circle and the ellipse.

Appendix K:

Axioms and Identities of Time-Warp Triangle, (Fig. 7a):

$$K1.\ \ \theta + \gamma \leq \pi$$

$$K2.\ \ \frac{\cos(\theta)}{\cos(\gamma)} = \frac{\gamma}{\theta} = \frac{z+G.P.W.}{T.I.W.}$$

$$K3.\ \ \left(z+G.P.W.\right)^2 = G.P.W.^2 + R.W.^2$$

$$K4.\ \ \delta^2 = \left(4\,G.P.W.^2 \sin^2\left(\frac{\frac{\pi}{2} - \gamma}{2}\right) - R.W.^2 \sin^2(\gamma)\right)$$

$$K5.\ \ T.I.W. \cos(\theta) = R.W.$$

$$K6.\ \ \delta + \sigma = G.P.W.$$

$$K7.\ \ z+G.P.W. = T.G.W.$$

Appendix L:

$$L1.\quad \left(z + G.P.W.\right)^2 = G.P.W.^2 + R.W.^2$$

$$L2.\quad z\left(z + 2G.P.W.\right) = R.W.^2 = T.I.W.^2\cos^2(\theta)$$

$$L3.\quad T.I.W.\gamma = \theta\left(z + G.P.W.\right)$$

$$L4.\quad z = \frac{T.I.W.\gamma - G.P.W.\,\theta}{\theta}$$

$$L5.\quad \left(\frac{T.I.W.\gamma - G.P.W.\,\theta}{\theta}\right)\left(\frac{T.I.W.\gamma - G.P.W.\,\theta}{\theta} + 2G.P.W.\right) = R.W.^2$$

$$L6.\quad \left(h\gamma - G.P.W.\,\theta\right)\left(h\gamma + G.P.W.\,\theta\right) = \theta^2 R.W.^2$$

$$L7.\quad T.I.W. = \frac{R.W.}{\cos(\theta)} \rightarrow \left(\frac{R.W.\,\gamma}{\cos(\theta)} - G.P.W.\,\theta\right)\left(\frac{R.W.\,\gamma}{\cos(\theta)} + G.P.W.\,\theta\right) = \theta^2 R.W.^2$$

$$L8.\quad \frac{R.W.^2\gamma^2}{\cos^2(\theta)} - G.P.W.^2\theta^2 = R.W.^2\theta^2$$

$$L9.\quad R.W.^2\gamma^2 - G.P.W.^2\theta^2\cos^2(\theta) = R.W.^2\theta^2\cos^2(\theta)$$

$$L10.\quad \frac{R.W.^2\gamma^2}{R.W.^2} = \frac{R.W.^2\theta^2\cos^2(\theta)}{R.W.^2} + \frac{G.P.W.^2}{R.W.^2}\theta^2\cos^2(\theta)$$

$$L11.\quad \frac{\gamma^2}{\theta^2} = \cos^2(\theta) + \frac{G.P.W.^2}{R.W.^2}\cos^2(\theta)$$

$$L12.\quad \frac{\gamma^2}{\theta^2\cos^2(\theta)} - \frac{G.P.W.^2}{R.W.^2} = 1$$

Hyperbolic Cosine Time-Warp Formula

$$L13.\quad \frac{\theta^2}{R.W.^2} - \frac{\gamma^2}{\cos^2(\theta)\left(G.P.W.^2 + R.W.^2\right)} = 0$$

Hyperbolic Cosine Time-Warp Formula Cone

Appendix M:

$$M1.\quad \frac{\gamma^2}{\theta^2\cos^2(\theta)} = 1 + \frac{G.P.W.^2}{R.W.^2}$$

$$M2.\quad \frac{\gamma^2}{\theta^2} = \cos^2(\theta) + \frac{G.P.W.^2\cos^2(\theta)}{R.W.^2}$$

$$M3.\quad \frac{G.P.W.^2}{R.W.^2} + \frac{R.W.^2}{R.W.^2} = \frac{T.G.W.^2}{R.W.^2} \rightarrow \frac{G.P.W.^2}{R.W.^2} = \frac{T.G.W.^2}{R.W.^2} - 1$$

$$M4.\quad \frac{\gamma^2}{\theta^2} = \cos^2(\theta) + \cos^2(\theta)\left(\frac{T.G.W.^2}{R.W.^2} - 1\right)$$

$$M5.\quad \frac{R.W.^2\gamma^2}{\theta^2} = R.W.^2\cos^2(\theta) + T.G.W.^2\cos^2(\theta) - R.W.^2\cos^2(\theta)$$

$$M6.\quad \frac{R.W.^2\gamma^2}{\theta^2} = T.G.W.^2\cos^2(\theta)$$

$$M7.\quad \frac{\gamma^2}{\theta^2} = \frac{T.G.W.^2}{R.W.^2\cos^2(\theta)} \qquad \frac{T.G.W.}{R.W.} = \frac{1}{\cos(\gamma)}$$

$$M8.\quad \frac{\gamma^2}{\theta^2} = \frac{\cos^2(\theta)}{\cos^2(\gamma)}$$

Hyperbolic Paraboloid Cosine Time-Warp Formula

Appendix N:

Axioms and Identities:

$$N1.\quad T.G.W.\ \sin(\gamma) = G.P.W. + I.W.$$

$$N2.\quad T.G.W. = z + G.P.W.$$

$$N3.\quad \frac{z + G.P.W.}{T.I.W.} = \frac{\gamma}{\theta} = \frac{\cos(\theta)}{\cos(\gamma)}$$

$$N4.\quad z = \frac{T.I.W.\ \gamma - G.P.W.\ \theta}{\theta}$$

Appendix O:

$$O1.\quad T.G.W.^2 = \left(G.P.W. + I.W.\right)^2 + R.W.^2$$

$$O2.\quad \left(z + G.P.W.\right)^2 = G.P.W.^2 + 2\,I.W.\;G.P.W. + I.W.^2 + R.W.^2$$

$$O3.\quad z\left(z + 2G.P.W.\right) = I.W.\left(I.W. + 2G.P.W.\right) + R.W.^2$$

$$O4.\quad z\left(z + 2G.P.W.\right) = I.W.\left(T.G.W.\sin(\gamma) + G.P.W.\right) + R.W.^2$$

$$O5.\quad \left(\frac{T.I.W.\,\gamma - G.P.W.\,\theta}{\theta}\right)\left(\frac{T.I.W.\,\gamma + G.P.W.\,\theta}{\theta}\right) = \left(T.G.W.\sin(\gamma) - G.P.W.\right)\left(T.G.W.\sin(\gamma) + G.P.W.\right) + R.W.^2$$

$$O6.\quad \left(\frac{T.I.W.^2\gamma^2 - G.P.W.^2\theta^2}{\theta^2}\right) = T.G.W.^2\sin^2(\gamma) - G.P.W.^2 + R.W.^2$$

$$O7.\quad \frac{T.I.W.^2\gamma^2}{\theta^2} = T.G.W.^2\sin^2(\gamma) + R.W.^2$$

$$O8.\quad \frac{T.I.W.^2\gamma^2}{\theta^2} = \left(z + G.P.W.\right)^2\sin^2(\gamma) + R.W.^2$$

$$O9.\quad \frac{T.I.W.^2\gamma^2}{\theta^2} = \frac{T.I.W.^2\gamma^2}{\theta^2}\sin^2(\gamma) + R.W.^2$$

$$O10.\quad \frac{R.W.^2}{T.G.W.^2} = 1 - \sin^2(\gamma)$$

$$O11.\quad \frac{R.W.^2}{T.G.W.^2} = \cos^2(\gamma)$$

Cosine Square Time-Warp Formula

Appendix P:

Axioms and Identities:

$$P\,1.\quad \frac{\sin(\alpha)}{\sin(\beta)} = \frac{\alpha}{\beta} = \frac{T.I.W.}{z + G.P.W.}$$

$$P\,2.\quad \frac{R.W.}{T.G.W.} = \sin(\alpha)$$

$$P\,3.\quad \frac{R.W.}{T.I.W.} = \sin(\beta)$$

Appendix Q:

$$Q1.\;\; T.G.W.^{2} = R.W.^{2} + G.P.W.^{2}$$

$$Q2.\;\; z\left(z+2G.P.W.\right) = R.W.^{2} = T.I.W.^{2}\sin^{2(}(\beta)$$

$$Q3.\;\; \left(\frac{T.I.W.\,\beta - G.P.W.\,\alpha}{\alpha}\right)\left(\frac{T.I.W.\,\beta - G.P.W.\,\alpha + 2\,G.P.W.\,\alpha}{\alpha}\right) = R.W.^{2}$$

$$Q4.\;\; T.I.W.^{2}\,\beta^{2} - G.P.W.^{2}\,\alpha^{2} = R.W.^{2}\,\alpha^{2}$$

$$Q5.\;\; \frac{R.W.^{2}\beta^{2}}{\sin^{2}(\beta)} - G.P.W.^{2}\,\alpha^{2} = R.W.^{2}\,\alpha^{2}$$

$$Q6.\;\; \frac{\beta^{2}}{\sin^{2}(\beta)} - \frac{G.P.W.^{2}\,\alpha^{2}}{R.W.^{2}} = \alpha^{2}$$

$$Q7.\;\; \frac{\beta^{2}}{\alpha^{2}\sin^{2}(\beta)} - \frac{G.P.W.^{2}}{R.W.^{2}} = 1$$

Hyperbolic Sine Time-Warp Formula:

Rearrangement yields the ratio form:

$$Q8.\;\; \frac{\alpha^{2}}{\beta^{2}} - \frac{\left(R.W.^{2} + G.P.W.^{2}\right)}{G.P.W.^{2}\sin^{2}(\beta)} = 0$$

Then also:

$$Q9.\;\; \frac{\beta^{2}}{\alpha^{2}} - \frac{G.P.W.^{2}\sin^{2}(\beta)}{R.W.^{2}} = \sin^{2}(\beta)$$

$$Q10.\;\; \frac{\beta^{2}}{\alpha^{2}} - \sin^{2}(\beta)\left(\frac{T.G.W.^{2}}{R.W.^{2}} - 1\right) = \sin^{2}(\beta)$$

$$Q11.\;\; \frac{R.W.^{2}\beta^{2}}{\alpha^{2}} - T.G.W.^{2}\sin^{2}(\beta) + R.W.^{2}\sin^{2}(\beta) = R.W.^{2}\sin^{2}(\beta)$$

$$Q12.\;\; \frac{R.W.^{2}\beta^{2}}{\alpha^{2}} = T.G.W.^{2}\sin^{2}(\beta)$$

$$Q\,13.\quad \frac{\beta^2}{\alpha^2} = \frac{T.G.W.^{\,2}}{R.W.^{\,2}} \sin^2(\beta)$$

$$Q\,14.\quad \frac{T.G.W.}{R.W.} = \frac{1}{\sin(\alpha)}$$

$$Q\,15.\quad \frac{\beta^2}{\alpha^2} = \frac{\sin^2(\beta)}{\sin^2(\alpha)}$$

<u>Hemi-Hyperbolic Paraboloid Sine Time-Warp Formula</u>

Appendix R:

Axioms and Identities

$$R1.\ \ T.G.W. \cos(\alpha) = G.P.W. + I.W.$$

$$R2.\ \ \frac{\alpha}{\beta} = \frac{T.I.W.}{T.G.W.} = \frac{T.I.W.}{z + G.P.W.} = \frac{\sin(\alpha)}{\sin(\beta)}$$

$$R3.\ \ z + G.P.W. = \frac{T.I.W. \beta}{\alpha} = T.G.W.$$

Appendix S:

$$S1.\ \ T.G.W.^{\,2} = \left(G.P.W. + I.W.\right)^2 + R.W.^{\,2}$$

$$S2.\ \ z\left(z + 2\,G.P.W.\right) = I.W.\left(T.G.W. \cos(\alpha) + G.P.W.\right) + R.W.^{\,2}$$

$$S3.\ \ \left(\frac{T.I.W.\, \beta - G.P.W.\, \alpha}{\alpha}\right)\left(\frac{T.I.W.\, \beta + G.P.W.\, \alpha}{\alpha}\right) = \left(T.G.W. \cos(\alpha) - G.P.W.\right)\left(T.G.W. \cos(\alpha) + G.P.W.\right) + R.W.^{\,2}$$

$$S4.\ \ \frac{T.I.W.^{\,2}\beta^2 - G.P.W.^{\,2}\alpha^2}{\alpha^2} = T.G.W.^{\,2}\cos^2(\alpha) - G.P.W.^{\,2} + R.W.^{\,2}$$

$$S5.\ \ \frac{T.I.W.^{\,2}\beta^2 - G.P.W.^{\,2}\alpha^2 + G.P.W.^{\,2}\alpha^2}{\alpha^2} = \left(z + G.P.W.\right)^2\cos^2(\alpha) + R.W.^{\,2}$$

$$S6.\ \ \frac{T.I.W.^{\,2}\beta^2}{\alpha^2} = \frac{T.I.W.^{\,2}\beta^2}{\alpha^2}\cos^2(\alpha) + R.W.^{\,2}$$

$$S7.\ \ 1 - \cos^2(\alpha) = \frac{R.W.^{\,2}}{T.G.W.^{\,2}}$$

$$S8.\ \ \frac{R.W.^{\,2}}{T.G.W.^{\,2}} = \sin^2(\alpha)$$

Sine Square Time-Warp Formula:

Appendix T:

$$T1.\ \frac{\gamma^2}{\theta^2\cos^2(\theta)} - \frac{\Delta(K.E.)^2}{\Delta(R.E.)^2} = \frac{\gamma^2}{\theta^2\cos^2(\theta)} - \frac{\Delta(I.W.)^2}{\Delta(R.W.)^2} = 1$$

Hyperbolic Cosine Energy Time-Warp Formula

$$T2.\ \frac{\theta^2}{\Delta(R.E.)^2} - \frac{\gamma^2}{\cos^2(\theta)\left[\Delta(K.E.)^2 + \Delta(R.E.)^2\right]} = \frac{\theta^2}{\Delta(R.W.)^2} - \frac{\gamma^2}{\cos^2(\theta)\left[\Delta(I.W.)^2 + \Delta(R.W.)^2\right]} = 0$$

Hyperbolic Cosine Energy Time-Warp Formula Cone

$$T3.\ \frac{\gamma^2}{\theta^2} = \frac{\cos^2(\theta)}{\cos^2(\gamma)} = \frac{\gamma^2}{\theta^2} = \cos^2(\theta)$$

Hyperbolic Paraboloid Cosine Energy Time-Warp Formula

$$T4.\ \frac{\Delta(R.E.)^2}{\Delta(T.I.E.)^2} = \cos^2(\gamma) = \frac{\Delta(R.W.)^2}{\Delta(T.I.W.)^2} = \cos^2(\gamma)$$

Cosine Square Energy Time-Warp Formula

$$T5.\ \frac{\beta^2}{\alpha^2\sin^2(\beta)} - \frac{\Delta(K.E.)^2}{\Delta(R.E.)^2} = \frac{\beta^2}{\alpha^2\sin^2(\beta)} - \frac{\Delta(I.W.)^2}{\Delta(R.W.)^2} = 1$$

Hyperbolic Sine Energy Time-Warp Formula:

$$T6.\ \frac{\alpha^2}{\beta^2} - \frac{\left[\Delta(R.E.)^2 + \Delta(K.E.)^2\right]}{\Delta(K.E.)^2\sin^2(\beta)} = \frac{\alpha^2}{\beta^2} - \frac{\left[\Delta(R.W.)^2 + \Delta(I.W.)^2\right]}{\Delta(I.W.)^2\sin^2(\beta)}$$

Hyperbolic Sine Energy Time-Warp Formula:

Rearrangement yields the ratio form:

$$T7.\ \frac{\Delta(R.E.)^2}{\Delta(T.I.E.)^2} = \sin^2(\alpha) = \frac{\Delta(R.W.)^2}{\Delta(T.I.W.)^2}$$

The Time-Warp Theorem - General Form:

$$T8.\ \left[\Delta(K.E.) - \Delta(G.P.E.)\right]^2 + \Delta(R.E.)^2 = \Delta(T.E.)^2 = \left[\Delta(I.W.) - \Delta(G.P.W.)\right]^2 + \Delta(R.W.)^2 = \Delta(T.W)^2$$

Appendix U:

$$U1.\ \ \frac{\gamma^2}{\theta^2\cos^2(\theta)} - \frac{d(K.E.)^2}{d(R.E.)^2} = \frac{\gamma^2}{\theta^2\cos^2(\theta)} - \frac{d(G.P.W.)^2}{d(R.W.)^2} = 1$$

Hyperbolic Cosine Differential Energy Time-Warp Formula

$$U2.\ \ \frac{\theta^2}{d(R.E.)^2} - \frac{\gamma^2}{\cos^2(\theta)\left(d(K.E.)^2 + d(R.E.)^2\right)} = \frac{\theta^2}{d(R.W.)^2} - \frac{\gamma^2}{\cos^2(\theta)\left(d(G.P.W.)^2 + d(R.W.)^2\right)} = 0$$

Hyperbolic Cosine Differential Energy Time-Warp Formula Cone

$$U3.\ \ \frac{\gamma^2}{\theta^2} = \frac{\cos^2(\theta)}{\cos^2(\gamma)} = \frac{\gamma^2}{\theta^2} = \cos^2(\theta)$$

Hyperbolic Paraboloid Cosine Differential Energy Time-Warp Formula

$$U4.\ \ \frac{d(R.E.)^2}{d(T.I.E.)^2} = \cos^2(\gamma) = \frac{d(R.W.)^2}{d(T.G.W.)^2} = \cos^2(\gamma)$$

Cosine Square Differential Energy Time-Warp Formula

$$U5.\ \ \frac{\beta^2}{\alpha^2\sin^2(\beta)} - \frac{d(K.E.)^2}{d(R.E.)^2} = \frac{\beta^2}{\alpha^2\sin^2(\beta)} - \frac{d(G.P.W.)^2}{d(R.W.)^2} = 1$$

Hyperbolic Sine Differential Energy Time-Warp Formula:

$$U6.\ \ \frac{\alpha^2}{\beta^2} - \frac{\left(d(R.E.)^2 + d(K.E.)^2\right)}{d(K.E.)^2\sin^2(\beta)} = \frac{\alpha^2}{\beta^2} - \frac{\left(d(R.W.)^2 + d(G.P.W.)^2\right)}{d(G.P.W.)^2\sin^2(\beta)}$$

Hyperbolic Sine Differential Energy Time-Warp Formula:

Rearrangement yields the ratio form:

$$U7.\ \ \frac{d(R.E.)^2}{d(T.I.E.)^2} = \sin^2(\alpha) = \frac{d(R.W.)^2}{d(T.G.W.)^2}$$

The Time-Warp Theorem - General Differential Form:

$$U8.\ \ (d(K.E.) - d(G.P.E.))^2 + (d(R.E.))^2 = (d(T.I.E.))^2 = (d(G.P.W.) - d(I.W.))^2 + (d(R.W.))^2 = (d(T.W.))^2$$

Appendix V:

Carbo-Myte Device Layout Key

$$V1.\ \ \delta = l\cos(\lambda) - 2r$$

$$V2.\ \ l = \frac{r+\sigma}{\sin(\frac{\pi}{n})}$$

Further Geometrical Derivations:

To begin with, regarding the geometric laws presented; the lengths of the terms are all positive, but the values of the terms can be negative, i.e. meta-normal terms. By virtue of the similarity in models, relativistic momentum vs. space-warp; one is not independent of the other but the actual relationship between these two is clarified in this manuscript. and why this occurs. This pertains also to the Fubrini developed as Eq. 9a. With regard to the line sums and their multiplication, Eq. 9a solves this. As such, and within the mathematical treatment to follow, developed are two sets of quadra-obelus space-momentum hyperbolic equations. The equation which has a quadric surface associated with it, is discerned and generates both hyperbolae as well as parabolic curves composing the hyperbolic paraboloid cone for momentum, and one for space-warp. The latter is completely dependent upon the former. Described within is the symbolic development of a new total momentum space-warp model with reproducible results.

The fundamental surface involved is discovered and the isolation of the hybrid axes is performed. The cone of parabolas and hyperbolas is also evaluated and illustrated. This geometric cone manifests as a hyperbolic function of three variables. As is often the case, when two or more variables are combined and squared, a quadric surface often ensues.

The hyperbolic paraboloidal momentum cone is isolated and the curves generated are both sets of the parabolic, mixed with the hyperbolic; the former being different in cross section geometrical than the latter, upon the same conic. Although the results from cross sectioning are similar, the cone is deficient of circles or ellipses in the cut, atypical to those commonly generated.

The features of this model have principally to do with the incorporation of the general symbolic geometric solution to the typical two right triangle with perpendicular drawn to base problem should have caught the attention of early geometry mathematicians, and are reproduced here. Within this document six new laws governing the dynamics of the double triangle with base drawn problem are listed. The solution to the geometry yielded six new geometric laws; isolating the correct graph rewarded the promised hyperbolic paraboloid. Isolated was a function that generated contours of a trapped parabolic operator which opened and closed with variation in the other two terms. Within the daughter formula is a related quadric, was another quadric cone that acted as a generator to both parabolics and hyperbolics, as predicted. (7)

Summary of the Problem:

A general relation should involve variables of I.P., R.P., and T.I.P, As angles of incidence and exit angle attainable through common means of reduction, result in the double right triangle model of fig. 7d. Holding *I.P.* constant, the two tangents composed of *I.P.* and *R.P.* are complimentary Pythagorean components of the momentum triangle. In the bottom triangle the G.P.E. is subtracted from the I.P., but as for the geometry, all the lengths must be positive. Afterwards, the sign substitution may be applied. As such $\gamma_c = \frac{\pi}{2} - \gamma_m$. The hypotenuses compile to Total Kinetic Momentum (T.I.P), and Total Gravitational Potential Energy (T.P.E.) segments.

In obtaining the difference of squares relation equal to one, That operation yields a two-dimensional segment of a hyperbola of one sheet, shown here as equation Bi12 of appendix Bi., (fig. 8i) and its fundamental hyperbolic paraboloid quadric is in this case, Ci8, of appendix Ci, or (figs. 8i, 9i, 10i, 10ai). The proofs, (appendices Ai-Ji), show the derivation of a hyperbolic formula governing the reticulation of two adjacent right triangles and the quadric functions associated with this R^2 geometric model. The saddle-point of the quadric of figs. 9i, 10i, 10ai. (fig. 10i is the root plot of fig. 9i), and lies at (.8603, .8603) radians, representing a point in the cross section of the midsection of a hyperbola of one sheet, with the minimax shifted along the hybrid linear axis, i.e. the $\theta = \gamma$ axis of fig. 10ai. The two roots correspond to two solution lines, which make diagonals across the original quadric surface. The trigonometric square cosine factor of equation Bi12, produces one of the two independent root lines seen in fig. 10i. Through symbolic rearrangement and functional analysis the root-lines are separated and the results are displayed in equation Eq. 16, (figs. 8i, 9i, 10i, and 10ai). The units cancel in all cases. The figures are presented in radians, although degrees may be used with equal success. Cartesian coordinates are preferred in this case over polar ones (due to the obelus triploidy).

Description of the Geometric Model:

Theoretically, a geometric solution in the tri-modal reticulation of similar right triangles can be derived from the model. The general solution, is without constraint; applies for any value of the three variables, θ, *R.P.*, and fixed *I.P.* Initially, as the bottom angle θ increases and the top angle γ varies directly or inversely with θ, respectively. Secondarily, γ, is a dependent variable, in *K.E* and *R.P.* are the two sides. These first two movements are depicted in fig. 9i, and 10, and are axial solution sets to the original equation’s (Ci8) hyperbolic paraboloid. Tertiarily movement is where the R.P. line moves along the y-axis as per fig. 7d, reducing to two minor formulas, (Ei11, Ii8). The useful contour is generated by the secondary, inverse variation in the adjacent angles of the triangle model, and is a function of θ, *I.P.*, and *R.P.*

As review, triangle < I.P.,T.I.P,R.P. > and triangle e < G.P.E.,T.P.E.,R.P. >, are similar but not congruent, with the R.P. and perpendicular angles being common. From proportionality, the three-way angle equality Ai2 can be formulated, which leads to Bi3 and Bi4 being substituted into Bi5; which is the Pythagorean triple used in the subsequent derivation of the two formulae. Notably axiom Ai2 is revisited as Ci8. (appendices Ai, Bi, and Ci).

In expression Ai6, and of fig. 7d, the δ is composed of the segment difference between one I.P. along the length *T.I.P*, and σ. That small segment is δ, which varies with *I.P.* and γ directly. σ is the remainder such that $\delta + \sigma = I.P.$ Subtract *I.P.* from *T.I.P* to obtain the *z* that is double substituted for, in the Pythagorean right triangle Bi1, Bi3, and Bi4, which once completed, leads to Bi6; (see appendix Bi, and fig. 7d). No condition is made on the *z*, which varies directly with the angle γ, which in turn varies with θ any of two ways, as stated. A more important key lies in the extra *I.P.* in expression Bi2, which leads to a perfect square relation in expression Bi6, and Bi8. Re-arranged the perfect square leads to the Hyperbolic Cosine Momentum Formula, a difference of squares relation equal to one; which is an expression of an already reduced number of independent variables: *I.P.*, and *R.P.*, and θ; displayed in expression Bi12, The graph of Bi12 is fig. 8i, is constrained by the square cosine factor in the denominator; and is factored out, yields the backbone function to the parent equation to Bi12, Eq. 24; (figs. 17i, and 18i). The Pythagorean triple is used in equation Ci3; and then the trigonometric Ci7 is employed to finalize the proof yielding the predicted quadric Ci8, (1).

Geometrical Analysis and Discussion:

The hybrid solution axes or roots to the equation, the hyperbolic cosine formula function are simple to comprehend. The linear root corresponds to the angle pair in direct variance, the other is a function of a trapped parabolic variable in an hyperbolic equation. Since this is a function of an angle and two sides it would be wise to convert the angle to linear rectangular coordinates through the conversion: $(k\,\theta_m)^2 = 4\,p\,R.P.$ If theta is an incident angle, the angle of reflection would equal the incident angle, and the sum would equal θ*model*. That is one way the two angles vary, and yields the linear root. If by fixing the cosine remnant of Bi12 to be equal to 1 at all spaces, the result is equation 16; the child is process to the parent function Bi12. Also the point values differ for the child process than for the parent equation Bi12; although the saddle-point remains the same. Regarding the dynamic analysis pertaining to the geometry of the triangle with base model; these six new laws contained here add to that known regarding the former. Thus in equation 16, that isolated cone generates both the parabolas and the hyperbolas (fig. 11i), and the planar harmonics of such are similar to that generated by the general quadratic equation, the cone differs in shape from those normally seen as the cross section results are deficient in generating circles and ellipses.

With I.P. fixed the R.P. varies up to the minimum I.P./R.P. ratio of 1.16233, leaving θ to vary bi-linearly with the two sides, in the double obelus construction. The partial derivative of Eq. 16 is completely linear with respect to θ, as one would suspect, and the two first order partial differentials vary according to fig. 2c, 2d. As already noted, the quadric in question has implicit a periodic and re-iterations of the other two variables. If one obelus actually degenerates, the result will be the parabola. If one is dependent or is chained formulated, the result is the hybrid axes conglomerate displayed in figs. 2a 3, and 4. The general form of a hyperboloid of one sheet is as follows in Eq. 10.

$$Eq. 10 \quad \frac{x^2}{a^2} + \frac{y^2}{b^2} - \frac{z^2}{c^2} = 1$$

Equation 10, breaks down into three component combinations of two-dimensional parts, namely Eqs. 11, 12, and 13:

$$Eq.11 \quad \frac{x^2}{a^2} + \frac{y^2}{b^2} = 1$$

$$Eq.12 \quad \frac{x^2}{a^2} - \frac{z^2}{c^2} = 1$$

$$Eq.13 \quad \frac{y^2}{b^2} - \frac{z^2}{c^2} = 1$$

Equation 2, is an ellipse, or circle. Equations 3, and 4, are both two dimensional, two sheet, hyperbolic components. Together they compose the whole, or three-dimensional hyperbola of one sheet. Since the Hyperbolic Cosine Momentum Formula equation is also two termed, by contrast, produces figs. 8i, 9i, 10i, and 10ai; the application of quadric tests can be performed as well. In the general quadric equation Eq. 5, the quadric discriminant, Eq. 15 could be useful in determining the minimax of Ci8, of figs. 8i, and 9i. The isolated hybrid axes displayed in figs. 10i, and 10ai, are generated by Eq. 7d; the cone associated with this equation could later prove valuable to astronomy buffs, but this quadric law that generates both and only hyperbolas and parabolas which stem from a the slices to this cone in the xy and xz axes. This is a new cone and the cross-sections are easier to generate than in the traditional "hour-glass" conic. This hyperbolic equation generates a refreshing solution to an age old problem; namely that of the reticulation and reciprocation of the components to two similar right triangles associated with the geometric model.

In table E, some common values are presented from the parent equation Bi12. For a point to be a minimax, the quadric must obey the above condition; where $I.P._{xx} = \frac{\partial^2 (I.P.)}{\partial (x)^2}$. When the symbolic quadric test is applied to the Eq. Ci8; the minimax,

(.8603, .8603), of fig. 9i, 10i, and 10ai, the result is -5.4335; thus confirming that that point, (.8603, .8603), is the true minimax. For the hyperbolic paraboloid of figs. 9i, 10i, and 10ai, shows a relative minimum occurs at $\theta = 0$, and at the maximum R.P. of 20. This was determined from the discriminant after the partials were generated; this same conic however, has no saddle-point.

$$Eq.14 \;\; Ax^2 + Bxy + Cy^2 + Dx + Ey + F = 0$$

$$Eq.15 \;\; I.P._{xx}\, I.P._{yy} - I.P.\,^2_{xy} = \begin{vmatrix} I.P._{xx} & I.P._{yx} \\ I.P._{xy} & I.P._{yy} \end{vmatrix}$$

$$Eq.15a \;\; I.P._{xx} I.P._{yy} - I.P.\,^2_{xy} < 0$$

$$Eq.16 \;\; \frac{\gamma^2}{\theta^2} - \frac{I.P.\,^2}{R.P.\,^2} = 1$$

From the drawings and throughout the discussion, it is clear that the cosine factor of Bi12 is responsible for the double root. Through functional analysis, setting θ equal to zero, such that $\cos^2(\theta) = 1$, the net result is a decoupled fundamental equation whose eccentricity and discriminant show parabolic and hyperbolic features depending on the view or slice, without participation from the linear component. Accordingly, the partial derivative is linear for θ, confirming potential bi-linearity, as predictable from the form. As was stated earlier a constant would be valuable to convert the principle angle, θ to linear coordinate values. A linear coordinate transpose matrix could further untangle the analytical knot.

In accordance with Snell’s law, when parallel light from a star or distant light source is collected by a concave surface and the angle of the displacement of that ray is equal to twice the tangent angle at the surface. The linear coordinate translation for the theta, or x-axis, of fig. 10i, is such that: $R.P.' = (k \;\; spaces \;\; \theta)$. For this graph

$k = 14.79924...$, in respective length units per radian. After transposing the minimax the parabolic latus rectum can be computed. For review the latus rectum is $lr = 4p$, where $p = 11.6233$, and $I.P. = 2p$; and plugging into yields: $(k\theta)^2 = 2I.P.\ R.P.$

Geometrical Results:

Table E.

1).	$\theta_m = 90$	$R.P._1 = \infty$	$\dfrac{I.P.}{R.P.}\ ratio = 0$	$\gamma_m = 0$	$G.P.E._1{}' = \infty$
2).	$\theta_m = 75$	$R.P._2 = 61.3288$	$\dfrac{I.P.}{R.P.}\ ratio = .3790$	$\gamma_m = 20.7591$	$G.P.E._2{}' = .3480$
3).	$\theta_m = 60$	$R.P._3 = 18.2586$	$\dfrac{I.P.}{R.P.}\ ratio = 1.2731$	$\gamma_m = 51.8509$	$G.P.E._3{}' = .0446$
4).	$\theta_m = 30$	$R.P._4 = 9.7674$	$\dfrac{I.P.}{R.P.}\ ratio = 2.3890$	$\gamma_m = 67.2866$	$G.P.E._4{}' = .0132$
5).	$\theta_m = 15$	$R.P._5 = 4.3089$	$\dfrac{I.P.}{R.P.}\ ratio = 5.3950$	$\gamma_m = 79.4990$	$G.P.E._5{}' = .0047$
6).	$\theta_m = 0$	$R.P._6 = 0.0000$	$\dfrac{I.P.}{R.P.}\ ratio = \infty$	$\gamma_m = 90$	$G.P.E._6{}' = 0$

Table F.

1).	$\theta_m = 49.2935$	$R.P. = 20.0000$	$\dfrac{I.P.}{R.P.}\ ratio = 1.16233$	$\gamma_m = 49.2935$	$\gamma_c = 49.2935$
2).	$\theta_m = 30.9953$	$R.P. = 15$	$\dfrac{I.P.}{R.P.}\ ratio = 1.5497$	$\gamma_m = 57.1664$	$\gamma_c = 32.8335$
3).	$\theta_m = 16.3724$	$R.P. = 5$	$\dfrac{I.P.}{R.P.}\ ratio = 4.6493$	$\gamma_m = 77.8614$	$\gamma_c = 12.1385$
4).	$\theta_m = 8.9670$	$R.P. = 2.5$	$\dfrac{I.P.}{R.P.}\ ratio = 9.2986$	$\gamma_m = 83.8618$	$\gamma_c = 6.1381$
5).	$\theta_m = 0$	$R.P. = 0$	$\dfrac{I.P.}{R.P.}\ ratio = \infty$	$\gamma_m = 90$	$\gamma_c = 0$

In table F, some sample values are computed and presented. These values conform with Eq. 16. From the table, the minimax for each process is identical; the values however differ, as theory would dictate. The minimum I.P. from the hyperbola-parabola generator, is zero, and this occurs at $R.P. = 0$ which makes $\theta = 0$ also. The parabolicity of the xy slices of this function, (figure 11i), becomes clearer analytically when the minimax is taken as an origin, for this equation. Using a transpose or conversion matrix would serve as a solution to this orientation problem. Hyperbolic double sheets occur with the zx slices to fig. 11i. Interestingly, at the minimax abscissa angle the tangent reaches a minimum at $\gamma = 49.2934$, then recedes; this is reassuringly the minimum I.P./R.P. ratio of 1.16233. The numbers can change, but the minimax and obelus ratios presented and highlighted will always remain the same for this formula.

As in fig. 6, the offset is governed by the formula: $\lambda_{offset} = \frac{\pi}{n}$, where n is the number of sides of a regular polygon design, and $2\lambda_{offset}$ is exactly the angular offset between any two adjacent sides. Spacing is dependent upon angular offset and the R.P., as in appendix Vi.

In summary, six new geometric formulae fully describe the tri-modal relationship in the geometry of a previously unexamined total momentum model. The solution generated a parabola and hyperbola generating cone. the parabolic operator is an child object from the parent hyperbolic function. The new cone reviewed generates the same curves as the traditional cone, with the exception of the circle and the ellipse.

Appendix Ai:

Axioms and Identities:

$$Ai\,1.\quad \theta + \gamma \le \pi$$

$$Ai\,2.\quad \frac{\cos(\theta)}{\cos(\gamma)} = \frac{\gamma}{\theta} = \frac{z + I.P.}{T.P.E.}$$

$$Ai\,3.\quad \left(z + I.P.\right)^2 = I.P.^2 + R.P.^2$$

$$Ai\,4.\quad \delta^2 = \left(4\,I.P.^2 \sin^2\left(\frac{\frac{\pi}{2} - \gamma}{2}\right) - R.P.^2 \sin^2(\gamma)\right)$$

$$Ai\,5.\quad T.P.E.\cos(\theta) = R.P.$$

$$Ai\,6.\quad \delta + \sigma = I.P.$$

$$Ai\,7.\quad z + I.P. = T.I.P$$

Appendix Bi:

$$Bi\,1.\quad \left(z + I.P.\right)^2 = I.P.^{\,2} + R.P.^{\,2}$$

$$Bi\,2.\quad z\left(z + 2I.P.\right) = R.P.^{\,2} = T.P.E.^{\,2}\cos^2(\theta)$$

$$Bi\,3.\quad T.P.E.\gamma = \theta\left(z + I.P.\right)$$

$$Bi\,4.\quad z = \frac{T.P.E.\gamma - I.P.\,\theta}{\theta}$$

$$Bi\,5.\quad \left(\frac{T.P.E.\gamma - I.P.\,\theta}{\theta}\right)\left(\frac{T.P.E.\gamma - I.P.\,\theta}{\theta} + 2I.P.\right) = R.P.^{\,2}$$

$$Bi\,6.\quad \left(h\gamma - I.P.\,\theta\right)\left(h\gamma + I.P.\,\theta\right) = \theta^2 R.P.^{\,2}$$

$$Bi\,7.\quad T.P.E. = \frac{R.P.}{\cos(\theta)} \rightarrow \left(\frac{R.P.\,\gamma}{\cos(\theta)} - I.P.\,\theta\right)\left(\frac{R.P.\,\gamma}{\cos(\theta)} + I.P.\,\theta\right) = \theta^2 R.P.^{\,2}$$

$$Bi\,8.\quad \frac{R.P.^{\,2}\gamma^2}{\cos^2(\theta)} - I.P.^{\,2}\theta^2 = R.P.^{\,2}\theta^2$$

$$Bi\,9.\quad R.P.^{\,2}\gamma^2 - I.P.^{\,2}\theta^2\cos^2(\theta) = R.P.^{\,2}\theta^2\cos^2(\theta)$$

$$Bi\,10.\quad \frac{R.P.^{\,2}\gamma^2}{R.P.^{\,2}} = \frac{R.P.^{\,2}\theta^2\cos^2(\theta)}{R.P.^{\,2}} + \frac{I.P.^{\,2}}{R.P.^{\,2}}\theta^2\cos^2(\theta)$$

$$Bi\,11.\quad \frac{\gamma^2}{\theta^2} = \cos^2(\theta) + \frac{I.P.^{\,2}}{R.P.^{\,2}}\cos^2(\theta)$$

$$Bi\,12.\quad \frac{\gamma^2}{\theta^2\cos^2(\theta)} - \frac{I.P.^{\,2}}{R.P.^{\,2}} = 1$$

Hyperbolic Cosine Momentum Formula

$$Bi\,13.\quad \frac{\theta^2}{R.P.^{\,2}} - \frac{\gamma^2}{\cos^2(\theta)\left(I.P.^{\,2} + R.P.^{\,2}\right)} = 0$$

Hyperbolic Cosine Momentum Formula Cone

Appendix Ci:

$$Ci\,1.\quad \frac{\gamma^2}{\theta^2\cos^2(\theta)} = 1 + \frac{I.P.^2}{R.P.^2}$$

$$Ci\,2.\quad \frac{\gamma^2}{\theta^2} = \cos^2(\theta) + \frac{I.P.^2\cos^2(\theta)}{R.P.^2}$$

$$Ci\,3.\quad \frac{I.P.^2}{R.P.^2} + \frac{R.P.^2}{R.P.^2} = \frac{T.I.P^2}{R.P.^2} \rightarrow \frac{I.P.^2}{R.P.^2} = \frac{T.I.P^2}{R.P.^2} - 1$$

$$Ci\,4.\quad \frac{\gamma^2}{\theta^2} = \cos^2(\theta) + \cos^2(\theta)\left(\frac{T.I.P^2}{R.P.^2} - 1\right)$$

$$Ci\,5.\quad \frac{R.P.^2\,\gamma^2}{\theta^2} = R.P.^2\cos^2(\theta) + T.I.P^2\cos^2(\theta) - R.P.^2\cos^2(\theta)$$

$$Ci\,6.\quad \frac{R.P.^2\gamma^2}{\theta^2} = T.I.P^2\cos^2(\theta)$$

$$Ci\,7.\quad \frac{\gamma^2}{\theta^2} = \frac{T.I.P^2}{R.P.^2\cos^2(\theta)} \qquad \frac{T.I.P}{R.P.} = \frac{1}{\cos(\gamma)}$$

$$Ci\,8.\quad \frac{\gamma^2}{\theta^2} = \frac{\cos^2(\theta)}{\cos^2(\gamma)}$$

Hyperbolic Paraboloid Cosine Momentum Formula

Appendix Di:

Axioms and Identities:

$$Di\,1.\;\; T.I.P\,\sin(\gamma) = I.P. + G.P.E.$$

$$Di\,2.\;\; T.I.P = z + I.P.$$

$$Di\,3.\;\; \frac{z + I.P.}{T.P.E.} = \frac{\gamma}{\theta} = \frac{\cos(\theta)}{\cos(\gamma)}$$

$$Di\,4.\;\; z = \frac{T.P.E.\,\gamma - I.P.\,\theta}{\theta}$$

Appendix Ei:

$$Ei\,1.\ \ T.I.P^{\,2} = \left(I.P. + G.P.E.\right)^{2} + R.P.^{\,2}$$

$$Ei\,2.\ \ \left(z + I.P.\right)^{2} = I.P.^{\,2} + 2\,G.P.E.\ I.P. + G.P.E.^{\,2} + R.P.^{\,2}$$

$$Ei\,3.\ \ z\left(z + 2I.P.\right) = G.P.E.\left(G.P.E. + 2I.P.\right) + R.P.^{\,2}$$

$$Ei\,4.\ \ z\left(z + 2I.P.\right) = G.P.E.\left(T.I.P\sin(\gamma) + I.P.\right) + R.P.^{\,2}$$

$$Ei\,5.\ \ \left(\frac{T.P.E.\ \gamma - I.P.\ \theta}{\theta}\right)\left(\frac{T.P.E.\ \gamma + I.P.\ \theta}{\theta}\right) = \left(T.I.P\sin(\gamma) - I.P.\right)\left(T.I.P\sin(\gamma) + I.P.\right) + R.P.^{\,2}$$

$$Ei\,6.\ \ \left(\frac{T.P.E.^{\,2}\gamma^{2} - I.P.^{\,2}\theta^{2}}{\theta^{2}}\right) = T.I.P^{\,2}\sin^{2}(\gamma) - I.P.^{\,2} + R.P.^{\,2}$$

$$Ei\,7.\ \ \frac{T.P.E.^{\,2}\gamma^{2}}{\theta^{2}} = T.I.P^{\,2}\sin^{2}(\gamma) + R.P.^{\,2}$$

$$Ei\,8.\ \ \frac{T.P.E.^{\,2}\gamma^{2}}{\theta^{2}} = \left(z + I.P.\right)^{2}\sin^{2}(\gamma) + R.P.^{\,2}$$

$$Ei\,9.\ \ \frac{T.P.E.^{\,2}\gamma^{2}}{\theta^{2}} = \frac{T.P.E.^{\,2}\gamma^{2}}{\theta^{2}}\sin^{2}(\gamma) + R.P.^{\,2}$$

$$Ei\,10.\ \ \frac{R.P.^{\,2}}{T.I.P^{\,2}} = 1 - \sin^{2}(\gamma)$$

$$Ei\,11.\ \ \frac{R.P.^{\,2}}{T.I.P^{\,2}} = \cos^{2}(\gamma)$$

Cosine Square Momentum Formula

Appendix Fi:

Axioms and Identities:

$$Fi\,1.\quad \frac{\sin(\alpha)}{\sin(\beta)} = \frac{\alpha}{\beta} = \frac{T.P.E.}{z + I.P.}$$

$$Fi\,2.\quad \frac{R.P.}{T.I.P} = \sin(\alpha)$$

$$Fi\,3.\quad \frac{R.P.}{T.P.E.} = \sin(\beta)$$

Appendix Gi:

$$Gi\,1.\ \ T.I.P^{\,2} = R.P.^{\,2} + I.P.^{\,2}$$

$$Gi\,2.\ \ z\left(z + 2I.P.\right) = R.P.^{\,2} = T.P.E.^{\,2}\sin^{2}(\beta)$$

$$Gi\,3.\ \ \left(\frac{T.P.E.\ \beta - I.P.\ \alpha}{\alpha}\right)\left(\frac{T.P.E.\ \beta - I.P.\ \alpha + 2\,I.P.\ \alpha}{\alpha}\right) = R.P.^{\,2}$$

$$Gi\,4.\ \ T.P.E.^{\,2}\,\beta^{2} - I.P.^{\,2}\,\alpha^{2} = R.P.^{\,2}\,\alpha^{2}$$

$$Gi\,5.\ \ \frac{R.P.^{\,2}\beta^{2}}{\sin^{2}(\beta)} - I.P.^{\,2}\,\alpha^{2} = R.P.^{\,2}\,\alpha^{2}$$

$$Gi\,6.\ \ \frac{\beta^{2}}{\sin^{2}(\beta)} - \frac{I.P.^{\,2}\,\alpha^{2}}{R.P.^{\,2}} = \alpha^{2}$$

$$Gi\,7.\ \ \frac{\beta^{2}}{\alpha^{2}\sin^{2}(\beta)} - \frac{I.P.^{\,2}}{R.P.^{\,2}} = 1$$

Hyperbolic Sine Momentum Formula:

Rearrangement yields the ratio form:

$$Gi\,8.\ \ \frac{\alpha^{2}}{\beta^{2}} - \frac{\left(R.P.^{\,2} + I.P.^{\,2}\right)}{I.P.^{\,2}\sin^{2}(\beta)} = 0$$

Then also:

$$Gi\,9.\ \ \frac{\beta^{2}}{\alpha^{2}} - \frac{I.P.^{\,2}\sin^{2}(\beta)}{R.P.^{\,2}} = \sin^{2}(\beta)$$

$$Gi\,10.\ \ \frac{\beta^{2}}{\alpha^{2}} - \sin^{2}(\beta)\left(\frac{T.I.P^{\,2}}{R.P.^{\,2}} - 1\right) = \sin^{2}(\beta)$$

$$Gi\,11.\ \ \frac{R.P.^{\,2}\beta^{2}}{\alpha^{2}} - T.I.P^{\,2}\sin^{2}(\beta) + R.P.^{\,2}\sin^{2}(\beta) = R.P.^{\,2}\sin^{2}(\beta)$$

$$Gi\,12.\ \ \frac{R.P.^{\,2}\beta^{2}}{\alpha^{2}} = T.I.P^{\,2}\sin^{2}(\beta)$$

$$Gi\,13.\quad \frac{\beta^2}{\alpha^2} = \frac{T.I.P^{\,2}}{R.P.^{\,2}}\sin^2(\beta)$$

$$Gi\,14.\quad \frac{T.I.P}{R.P.} = \frac{1}{\sin(\alpha)}$$

$$Gi\,15.\quad \frac{\beta^2}{\alpha^2} = \frac{\sin^2(\beta)}{\sin^2(\alpha)}$$

<u>Hemi-Hyperbolic Paraboloid Sine Momentum Formula</u>

Appendix Hi:

Axioms and Identities

$$Hi\,1.\ \ T.I.P\cos(\alpha) = I.P. + G.P.E.$$

$$Hi\,2.\ \ \frac{\alpha}{\beta} = \frac{T.P.E.}{T.I.P} = \frac{T.P.E.}{z + I.P.} = \frac{\sin(\alpha)}{\sin(\beta)}$$

$$Hi\,3.\ \ z + I.P. = \frac{T.P.E.\beta}{\alpha} = T.I.P$$

Appendix Ii:

$$Ii\,1.\ \ T.I.P^{\,2} = \left(I.P. + G.P.E.\right)^2 + R.P.^{\,2}$$

$$Ii\,2.\ \ z\left(z + 2\,I.P.\right) = G.P.E.\left(T.I.P\cos(\alpha) + I.P.\right) + R.P.^{\,2}$$

$$Ii\,3.\ \ \left(\frac{T.P.E.\,\beta - I.P.\,\alpha}{\alpha}\right)\left(\frac{T.P.E.\,\beta + I.P.\,\alpha}{\alpha}\right) = \left(T.I.P\cos(\alpha) - I.P.\right)\left(T.I.P\cos(\alpha) + I.P.\right) + R.P.^{\,2}$$

$$Ii\,4.\ \ \frac{T.P.E.^{\,2}\beta^2 - I.P.^{\,2}\alpha^2}{\alpha^2} = T.I.P^{\,2}\cos^2(\alpha) - I.P.^{\,2} + R.P.^{\,2}$$

$$Ii\,5.\ \ \frac{T.P.E.^{\,2}\beta^2 - I.P.^{\,2}\alpha^2 + I.P.^{\,2}\alpha^2}{\alpha^2} = \left(z + I.P.\right)^2\cos^2(\alpha) + R.P.^{\,2}$$

$$Ii\,6.\ \ \frac{T.P.E.^{\,2}\beta^2}{\alpha^2} = \frac{T.P.E.^{\,2}\beta^2}{\alpha^2}\cos^2(\alpha) + R.P.^{\,2}$$

$$Ii\,7.\ \ 1 - \cos^2(\alpha) = \frac{R.P.^{\,2}}{T.I.P^{\,2}}$$

$$Ii\,8.\ \ \frac{R.P.^{\,2}}{T.I.P^{\,2}} = \sin^2(\alpha)$$

Sine Square Momentum Formula:

Appendix Ji:

Multi-Thruster Layout

$$Ji\,1.\quad \delta = l\cos(\lambda) - 2r$$

$$Ji\,2.\quad l = \frac{r + \sigma}{\sin(\frac{\pi}{n})}$$

Within the mathematical treatment to follow, is developed a tri-obelus hyperbolic equation. Naturally, this equation has a quadric surface associated with it, which generates both hyperbolae as well as parabolic curves which compose the hyperbolic paraboloid cone for space-warp. Described within is the symbolic development of a new total space-warp model now with known results. The fundamental surface involved is discovered and the isolation of the hybrid axes is performed. The cone of parabolas and hyperbolas is also evaluated and illustrated. This geometric cone manifests as a hyperbolic function of three variables. As is often the case, when two or more variables are combined and squared,a quadric surface often ensues. The hyperbolic paraboloidal space-warp cone is isolated and the curves generated are both sets of the parabolic, mixed with the hyperbolic; the former being different in cross section geometrical than the latter, upon the same conic. Although the results from cross sectioning are similar, the cone is deficient of circles or ellipses in the cut, atypical to those commonly generated.

The features of this model have principally to do with the incorporation of the general symbolic geometric solution to the typical two right triangle with perpendicular drawn to base problem should have caught the attention of early geometry mathematicians, and are reproduced here. Within this document six new laws governing the dynamics of the double triangle with base drawn problem are listed. The solution to the geometry yielded six new geometric laws; isolating the correct graph rewarded the promised hyperbolic paraboloid. Isolated was a function that generated contours of a trapped parabolic operator which opened and closed with variation in the other two terms. Within the daughter formula is a related quadric, was another quadric cone that acted as a generator to both parabolics and hyperbolics, as predicted. (7)

<u>Summary of the Problem:</u>

A general relation should involve variables of G.P.W., I.X., and R.X., As angles of incidence and exit angle attainable through common means of reduction, result in the double right triangle model of fig. 7e. Holding *G.P.W.* constant, the two tangents composed of *G.P.W.* and *R.X.* are complimentary Pythagorean components of the space-warp triangle. In the bottom triangle the I.X. is subtracted from the G.P.W. As such $\gamma_c = \frac{\pi}{2} - \gamma_m$. The hypotenuses compile to Total Kinetic Space-warp (T.I.X.), and Total Gravitational Potential Space-warp (T.G.W.) segments.

In obtaining the difference of squares relation equal to one, That operation yields a two-dimensional segment of a hyperbola of one sheet, shown here as equation Li12 of appendix Li., (fig. 14i) and its fundamental hyperbolic paraboloid quadric is in this case, Mi8, of appendix Mi, or (figs. 14i, 15i, 16i, 17i). The proofs, (appendices Ki-Ti), show the derivation of a hyperbolic formula governing the reticulation of two adjacent right triangles and the quadric functions associated with this R^2 geometric model. The saddle-point of the quadric of figs. 15i, 16i, 17i. (fig. 16i is the root plot of fig. 15i), and lies at (.8603, .8603) radians, representing a point in the cross section of the midsection of a hyperbola of one sheet, with the minimax shifted along the hybrid linear axis, i.e. the $\theta = \gamma$ axis of fig. 16i. The two roots correspond to two solution lines, which make diagonals across the original quadric surface. The trigonometric square cosine factor of equation Li12, produces one of the two independent root lines seen in fig. 16i. Through symbolic rearrangement and functional analysis the root-lines are separated and the results are displayed in equation Eq. 24, (figs. 14i, 15i, 16i, and 17i). The units cancel in all cases. The figures are presented in radians, although degrees may be used with equal success. Cartesian coordinates are preferred in this case over polar ones (due to the obelus triploidy).

Description of the Geometric Space-Warp Model:

Theoretically, a geometric solution in the tri-modal reticulation of similar right triangles can be derived from the model. The general solution, is without constraint; applies for any value of the three variables, θ, *R.X.*, and fixed *G.P.W.* Initially, as the bottom angle θ increases and the top angle γ varies directly or inversely with θ, respectively. Secondarily, γ, is a dependent variable, in *I.P.* and *R.X.* are the two sides. These first two movements are depicted in fig. 15i, and 16, and are axial solution sets to the original equation's (Mi8) hyperbolic paraboloid. Tertiarily movement is where the R.X. line moves along the y-axis as per fig. 7e, reducing to two minor formulas, (Oi11, Si8). The useful contour is generated by the secondary, inverse variation in the adjacent angles of the triangle model, and is a function of θ, *G.P.W.*, and *R.X.*

As review, triangle < G.P.W.,T.G.W.,R.X. > and triangle e < I.X.,T.I.X.,R.X. >, are similar but not congruent, with the R.X. and perpendicular angles being common. From proportionality, the three-way angle equality Ki2 can be formulated, which leads to Li3 and Li4 being substituted into Li5; which is the Pythagorean triple used in the subsequent derivation of the two formulae. Notably axiom Ki2 is revisited as Mi8. (appendices Ki, Li, and Mi).

In expression Ki6, and of fig. 7e, the δ is composed of the segment difference between one G.P.W. along the length *T.G.W.*, and σ. That small segment is δ, which varies with *G.P.W.* and γ directly. σ is the remainder such that $\delta + \sigma = G.P.W.$ Subtract *G.P.W.* from *T.G.W.* to obtain the *z* that is double substituted for, in the Pythagorean right triangle Li1, Li3, and Li4, which once completed, leads to Li6; (see appendix Li, and fig. 7e). No condition is made on the *z*, which varies directly with the angle γ, which in turn varies with θ any of two ways, as stated. A more important key lies in the extra *G.P.W.* in expression Li2, which leads to a perfect square relation in expression Li6, and Li8. Re-arranged the perfect square leads to the Hyperbolic Cosine Space-Warp Formula, a difference of squares relation equal to one; which is an expression of an already reduced number of independent variables: *G.P.W.*, and *R.X.*, and θ; displayed in expression Li12, The graph of Li12 is fig. 14i, is constrained by the square cosine factor in the denominator; and is factored out, yields the backbone function to the parent equation to Li12, Eq. 24; (figs. 17i, and 18i). The Pythagorean triple is used in equation Li3; and then the trigonometric Li7 is employed to finalize the proof yielding the predicted quadric Mi8, (1).

Analysis and Discussion:

The hybrid solution axes or roots to the equation, the hyperbolic cosine formula function are simple to comprehend. The linear root corresponds to the angle pair in direct variance, the other is a function of a trapped parabolic variable in an hyperbolic equation. Since this is a function of an angle and two sides it would be wise to convert the angle to linear rectangular coordinates through the conversion: $(k\,\theta_m)^2 = 4\,p\,R.X.$ If theta is an incident angle, the angle of reflection would equal the incident angle, and the sum would equal θ*model*. That is one way the two angles vary, and yields the linear root. If by fixing the cosine remnant of Bi12 to be equal to 1 at all times, the result is equation 24; the child is process to the parent function Li12. Also the point values differ for the child process than for the parent equation Bi12; although the saddle-point remains the same. Regarding the dynamic analysis pertaining to the geometry of the triangle with base model; these six new laws contained here add to that known regarding the former. Thus in equation 24, that isolated cone generates both the parabolas and the hyperbolas (fig. 18i), and the planar harmonics of such are similar to that generated by the general quadratic equation, the cone differs in shape from those normally seen as the cross section results are deficient in generating circles and ellipses.

With G.P.W. fixed the R.X. varies up to the minimum G.P.W./R.X. ratio of 1.16233, leaving θ to vary bi-linearly with the two sides, in the double obelus construction. The partial derivative of Eq. 24 is completely linear with respect to θ, as one would suspect, and the two first order partial differentials vary according to fig. 18i. As already noted, the quadric in question has implicit a periodic and re-iterations of the other two variables. If one obelus actually degenerates, the result will be the parabola. If one is dependent or is chained formulated, the result is the hybrid axes conglomerate displayed in figs. 14i, 15i, and 16i. The general form of a hyperboloid of one sheet is as follows in Eq. 17.

$$Eq.17 \quad \frac{x^2}{a^2} + \frac{y^2}{b^2} - \frac{z^2}{c^2} = 1$$

Equation 17, breaks down into three component combinations of two-dimensional parts, namely Eqs. 18, 19, and 20:

$$Eq.18 \quad \frac{x^2}{a^2} + \frac{y^2}{b^2} = 1$$

$$Eq.19 \quad \frac{x^2}{a^2} - \frac{z^2}{c^2} = 1$$

$$Eq.20 \quad \frac{y^2}{b^2} - \frac{z^2}{c^2} = 1$$

Equation 18, is an ellipse, or circle. Equations 19, and 20, are both two dimensional, two sheet, hyperbolic components. Together they compose the whole, or three-dimensional hyperbola of one sheet. Since the Hyperbolic Cosine Space-Warp Formula equation is also two termed, by contrast, produces figs. 16i, 17i, 18i, and 19i; the application of quadric tests can be performed as well. In the general quadric equation Eq. 22, the quadric discriminant, Eq. 23 could be useful in determining the minimax of Mi8, of figs. 14i, and 15i. The isolated hybrid axes displayed in figs. 16i, and 17i, are generated by Eq. 24; the cone associated with this equation could later prove valuable to astronomy buffs, but this quadric law that generates both and only hyperbolas and parabolas which stem from a the slices to this cone in the xy and xz axes. This is a new cone and the cross-sections are easier to generate than in the traditional "hour-glass" conic. This hyperbolic equation generates a refreshing solution to an age old problem; namely that of the reticulation and reciprocation of the components to two similar right triangles associated with the geometric model.

In table E, some common values are presented from the parent equation Bi12. For a point to be a minimax, the quadric must obey the above condition; where $G.P.W._{xx} = \dfrac{\partial^2(G.P.W.)}{\partial(x)^2}$. When the symbolic quadric test is performed to Eq. Mi8 and the minimax, (.8603, .8603), (see fig. 15i, 16i, and 17i, the result is -5.4335; thus confirming that that point, (.8603, .8603), is the true minimax. For the hyperbolic paraboloid of figs. 15i, 16i, and 17i, shows a relative minimum occurs at $\theta = 0$, and at the maximum R.X. of 20. This was determined from the discriminant after the partials were generated; this same conic however, has no saddle-point.

$$Eq.21 \;\; Ax^2 + Bxy + Cy^2 + Dx + Ey + F = 0$$

$$Eq.22 \;\; G.P.W._{xx}\, G.P.W._{yy} - G.P.W._{xy}^{\,2} = \begin{vmatrix} G.P.W._{xx} & G.P.W._{yx} \\ G.P.W._{xy} & G.P.W._{yy} \end{vmatrix}$$

$$Eq.23 \;\; G.P.W._{xx} G.P.W._{yy} - G.P.W._{xy}^{\,2} < 0$$

$$Eq.24 \;\; \frac{\gamma^2}{\theta^2} - \frac{G.P.W.^{\,2}}{R.X.^{\,2}} = 1$$

From the drawings and throughout the discussion, it is clear that the cosine factor of Bi12 is responsible for the double root. Through functional analysis, setting θ equal to zero, such that $\cos^2(\theta) = 1$, the net result is a decoupled fundamental equation whose eccentricity and discriminant show parabolic and hyperbolic features depending on the view or slice, without participation from the linear component. Accordingly, the partial derivative is linear for θ, confirming potential bi-linearity, as predictable from the form. As was stated earlier a constant would be valuable to convert the principle angle, θ to linear coordinate values. A linear coordinate transpose matrix could further untangle the analytical knot.

The linear coordinate translation for the theta, or x- axis, of fig. 16i, is such that: $R.X.' = (k \times \theta)$. For this graph $k = 14.79924...$, in respective length units per radian. After transposing the minimax the parabolic latus rectum can be computed. For review the latus rectum is $lr = 4p$, where $p = 11.6233$, and $G.P.W. = 2p$; and plugging into yields: $(k\theta)^2 = 2G.P.W.\ R.X.$

Geometrical Results:

Table G.

1).	$\theta_m = 90$	$R.X._1 = \infty$	$\frac{G.P.W.}{R.X.}\ ratio = 0$	$\gamma_m = 0$	$I.X._1' = \infty$
2).	$\theta_m = 75$	$R.X._2 = 61.3288$	$\frac{G.P.W.}{R.X.}\ ratio = .3790$	$\gamma_m = 20.7591$	$I.X._2' = .3480$
3).	$\theta_m = 60$	$R.X._3 = 18.2586$	$\frac{G.P.W.}{R.X.}\ ratio = 1.2731$	$\gamma_m = 51.8509$	$I.X._3' = .0446$
4).	$\theta_m = 30$	$R.X._4 = 9.7674$	$\frac{G.P.W.}{R.X.}\ ratio = 2.3890$	$\gamma_m = 67.2866$	$I.X._4' = .0132$
5).	$\theta_m = 15$	$R.X._5 = 4.3089$	$\frac{G.P.W.}{R.X.}\ ratio = 5.3950$	$\gamma_m = 79.4990$	$I.X._5' = .0047$
6).	$\theta_m = 0$	$R.X._6 = 0.0000$	$\frac{G.P.W.}{R.X.}\ ratio = \infty$	$\gamma_m = 90$	$I.X._6' = 0$

Table H.

1).	$\theta_m = 49.2935$	$R.X. = 20.0000$	$\frac{G.P.W.}{R.X.}\ ratio = 1.16233$	$\gamma_m = 49.2935$	$\gamma_c = 49.2935$
2).	$\theta_m = 30.9953$	$R.X. = 15$	$\frac{G.P.W.}{R.X.}\ ratio = 1.5497$	$\gamma_m = 57.1664$	$\gamma_c = 32.8335$
3).	$\theta_m = 16.3724$	$R.X. = 5$	$\frac{G.P.W.}{R.X.}\ ratio = 4.6493$	$\gamma_m = 77.8614$	$\gamma_c = 12.1385$
4).	$\theta_m = 8.9670$	$R.X. = 2.5$	$\frac{G.P.W.}{R.X.}\ ratio = 9.2986$	$\gamma_m = 83.8618$	$\gamma_c = 6.1381$
5).	$\theta_m = 0$	$R.X. = 0$	$\frac{G.P.W.}{R.X.}\ ratio = \infty$	$\gamma_m = 90$	$\gamma_c = 0$

Analysis and Discussion:

In table G, some sample values are computed and presented. These values conform with Eq. 24. From the table, the minimax for each process is identical; the values however differ, as theory would dictate. The minimum G.P.W. from the hyperbola-parabola generator, is zero, and this occurs at $R.X. = 0$ which makes $\theta = 0$ also. The parabolicity of the xy slices of this function, (figure 17i), becomes clearer analytically when the minimax is taken as an origin, for this equation. Using a transpose or conversion matrix would serve as a solution to this orientation problem. Hyperbolic double sheets occur with the zx slices to fig. 17i. Interestingly, at the minimax abscissa angle the tangent reaches a minimum at $\gamma = 49.2934$, then recedes; this is reassuringly the minimum G.P.W./R.X. ratio of 1.16233. The numbers can change, but the minimax and obelus ratios presented and highlighted will always remain the same for this formula.

As in fig. 10i, the offset is governed by the formula: $\lambda_{offset} = \frac{\pi}{n}$, where n is the number of sides of a regular polygon design, and $2\lambda_{offset}$ is exactly the angular offset between any two adjacent sides. Spacing is dependent upon angular offset and the R.X., as in appendix Ti; differentially as appendix Ui, and fig. 7g.

In summary, six new geometric formulae fully describe the tri-modal relationship in the geometry of a previously unexamined total space-warp model. The solution generated a parabola and hyperbola generating cone. the parabolic operator is an child object from the parent hyperbolic function. The new cone reviewed generates the same curves as the traditional cone, with the exception of the circle and the ellipse.

Appendix Ki:

Axioms and Identities of Space-Warp Triangle, (Fig. 7e):

$$Ki\,1.\ \ \theta + \gamma \leq \pi$$

$$Ki\,2.\ \ \frac{\cos(\theta)}{\cos(\gamma)} = \frac{\gamma}{\theta} = \frac{z+G.P.W.}{T.I.X.}$$

$$Ki\,3.\ \ \left(z+G.P.W.\right)^{2} = G.P.W.^{\,2} + R.X.^{\,2}$$

$$Ki\,4.\ \ \delta^{2} = \left(4\,G.P.W.^{\,2}\sin^{2}\left(\frac{\frac{\pi}{2}-\gamma}{2}\right) - R.X.^{\,2}\sin^{2}(\gamma)\right)$$

$$Ki\,5.\ \ T.I.X.\cos(\theta) = R.X.$$

$$Ki\,6.\ \ \delta+\sigma = G.P.W.$$

$$Ki\,7.\ \ z+G.P.W. = T.G.W.$$

Appendix Li:

$$Li\,1.\quad \left(z+G.P.W.\right)^2 = G.P.W.^2 + R.X.^2$$

$$Li\,2.\quad z\left(z+2G.P.W.\right) = R.X.^2 = T.I.X.^2\cos^2(\theta)$$

$$Li\,3.\quad T.I.X.\gamma = \theta\left(z+G.P.W.\right)$$

$$Li\,4.\quad z = \frac{T.I.X.\gamma - G.P.W.\,\theta}{\theta}$$

$$Li\,5.\quad \left(\frac{T.I.X.\gamma - G.P.W.\,\theta}{\theta}\right)\left(\frac{T.I.X.\gamma - G.P.W.\,\theta}{\theta} + 2G.P.W.\right) = R.X.^2$$

$$Li\,6.\quad \left(h\gamma - G.P.W.\,\theta\right)\left(h\gamma + G.P.W.\,\theta\right) = \theta^2 R.X.^2$$

$$Li\,7.\quad T.I.X. = \frac{R.X.}{\cos(\theta)} \rightarrow \left(\frac{R.X.\,\gamma}{\cos(\theta)} - G.P.W.\,\theta\right)\left(\frac{R.X.\,\gamma}{\cos(\theta)} + G.P.W.\,\theta\right) = \theta^2 R.X.^2$$

$$Li\,8.\quad \frac{R.X.^2\gamma^2}{\cos^2(\theta)} - G.P.W.^2\theta^2 = R.X.^2\theta^2$$

$$Li\,9.\quad R.X.^2\gamma^2 - G.P.W.^2\theta^2\cos^2(\theta) = R.X.^2\theta^2\cos^2(\theta)$$

$$Li\,10.\quad \frac{R.X.^2\gamma^2}{R.X.^2} = \frac{R.X.^2\theta^2\cos^2(\theta)}{R.X.^2} + \frac{G.P.W.^2}{R.X.^2}\theta^2\cos^2(\theta)$$

$$Li\,11.\quad \frac{\gamma^2}{\theta^2} = \cos^2(\theta) + \frac{G.P.W.^2}{R.X.^2}\cos^2(\theta)$$

$$Li\,12.\quad \frac{\gamma^2}{\theta^2\cos^2(\theta)} - \frac{G.P.W.^2}{R.X.^2} = 1$$

Hyperbolic Cosine Space-Warp Formula

$$Li\,13.\quad \frac{\theta^2}{R.X.^2} - \frac{\gamma^2}{\cos^2(\theta)\left(G.P.W.^2 + R.X.^2\right)} = 0$$

Hyperbolic Cosine Space-Warp Formula Cone

Appendix Mi:

$$Mi\,1.\quad \frac{\gamma^2}{\theta^2\cos^2(\theta)} = 1 + \frac{G.P.W.^2}{R.X.^2}$$

$$Mi\,2.\quad \frac{\gamma^2}{\theta^2} = \cos^2(\theta) + \frac{G.P.W.^2\cos^2(\theta)}{R.X.^2}$$

$$Mi\,3.\quad \frac{G.P.W.^2}{R.X.^2} + \frac{R.X.^2}{R.X.^2} = \frac{T.G.W.^2}{R.X.^2} \rightarrow \frac{G.P.W.^2}{R.X.^2} = \frac{T.G.W.^2}{R.X.^2} - 1$$

$$Mi\,4.\quad \frac{\gamma^2}{\theta^2} = \cos^2(\theta) + \cos^2(\theta)\left(\frac{T.G.W.^2}{R.X.^2} - 1\right)$$

$$Mi\,5.\quad \frac{R.X.^2\,\gamma^2}{\theta^2} = R.X.^2\cos^2(\theta) + T.G.W.^2\cos^2(\theta) - R.X.^2\cos^2(\theta)$$

$$Mi\,6.\quad \frac{R.X.^2\gamma^2}{\theta^2} = T.G.W.^2\cos^2(\theta)$$

$$Mi\,7.\quad \frac{\gamma^2}{\theta^2} = \frac{T.G.W.^2}{R.X.^2\cos^2(\theta)} \qquad \frac{T.G.W.}{R.X.} = \frac{1}{\cos(\gamma)}$$

$$Mi\,8.\quad \frac{\gamma^2}{\theta^2} = \frac{\cos^2(\theta)}{\cos^2(\gamma)}$$

Hyperbolic Paraboloid Cosine Space-Warp Formula

Appendix Ni:

Axioms and Identities:

$$Ni\,1.\quad T.G.W.\ \sin(\gamma) = G.P.W. + I.X.$$

$$Ni\,2.\quad T.G.W. = z + G.P.W.$$

$$Ni\,3.\quad \frac{z + G.P.W.}{T.I.X.} = \frac{\gamma}{\theta} = \frac{\cos(\theta)}{\cos(\gamma)}$$

$$Ni\,4.\quad z = \frac{T.I.X.\ \gamma - G.P.W.\ \theta}{\theta}$$

Appendix Oi:

$$Oi\,1.\quad T.G.W.^{\,2} = \left(G.P.W. + I.X.\right)^{2} + R.X.^{\,2}$$

$$Oi\,2.\quad \left(z + G.P.W.\right)^{2} = G.P.W.^{\,2} + 2\,I.X.\;G.P.W. + I.X.^{\,2} + R.X.^{\,2}$$

$$Oi\,3.\quad z\left(z + 2G.P.W.\right) = I.X.\left(I.X. + 2G.P.W.\right) + R.X.^{\,2}$$

$$Oi\,4.\quad z\left(z + 2G.P.W.\right) = I.X.\left(T.G.W.\,\sin(\gamma) + G.P.W.\right) + R.X.^{\,2}$$

$$Oi\,5.\quad \left(\frac{T.I.X.\,\gamma - G.P.W.\,\theta}{\theta}\right)\left(\frac{T.I.X.\,\gamma + G.P.W.\,\theta}{\theta}\right) = \left(T.G.W.\,\sin(\gamma) - G.P.W.\right)\left(T.G.W.\,\sin(\gamma) + G.P.W.\right) + R.X.^{\,2}$$

$$Oi\,6.\quad \left(\frac{T.I.X.^{\,2}\gamma^{2} - G.P.W.^{\,2}\theta^{2}}{\theta^{2}}\right) = T.G.W.^{\,2}\sin^{2}(\gamma) - G.P.W.^{\,2} + R.X.^{\,2}$$

$$Oi\,7.\quad \frac{T.I.X.^{\,2}\gamma^{2}}{\theta^{2}} = T.G.W.^{\,2}\sin^{2}(\gamma) + R.X.^{\,2}$$

$$Oi\,8.\quad \frac{T.I.X.^{\,2}\gamma^{2}}{\theta^{2}} = \left(z + G.P.W.\right)^{2}\sin^{2}(\gamma) + R.X.^{\,2}$$

$$Oi\,9.\quad \frac{T.I.X.^{\,2}\gamma^{2}}{\theta^{2}} = \frac{T.I.X.^{\,2}\gamma^{2}}{\theta^{2}}\sin^{2}(\gamma) + R.X.^{\,2}$$

$$Oi\,10.\quad \frac{R.X.^{\,2}}{T.G.W.^{\,2}} = 1 - \sin^{2}(\gamma)$$

$$Oi\,11.\quad \frac{R.X.^{\,2}}{T.G.W.^{\,2}} = \cos^{2}(\gamma)$$

Cosine Square Space-Warp Formula

Appendix Pi:

Axioms and Identities:

$$Pi\,1.\quad \frac{\sin(\alpha)}{\sin(\beta)} = \frac{\alpha}{\beta} = \frac{T.I.X.}{z + G.P.W.}$$

$$Pi\,2.\quad \frac{R.X.}{T.G.W.} = \sin(\alpha)$$

$$Pi\,3.\quad \frac{R.X.}{T.I.X.} = \sin(\beta)$$

Appendix Qi:

$$Qi\,1.\;\; T.G.W.^{\,2} = R.X.^{\,2} + G.P.W.^{\,2}$$

$$Qi\,2.\;\; z\left(z + 2G.P.W.\right) = R.X.^{\,2} = T.I.X.^{\,2}\sin^{2(}(\beta)$$

$$Qi\,3.\;\; \left(\frac{T.I.X.\,\beta - G.P.W.\,\alpha}{\alpha}\right)\left(\frac{T.I.X.\,\beta - G.P.W.\,\alpha + 2\,G.P.W.\,\alpha}{\alpha}\right) = R.X.^{\,2}$$

$$Qi\,4.\;\; T.I.X.^{\,2}\,\beta^2 - G.P.W.^{\,2}\,\alpha^2 = R.X.^{\,2}\,\alpha^2$$

$$Qi\,5.\;\; \frac{R.X.^{\,2}\beta^2}{\sin^2(\beta)} - G.P.W.^{\,2}\,\alpha^2 = R.X.^{\,2}\,\alpha^2$$

$$Qi\,6.\;\; \frac{\beta^2}{\sin^2(\beta)} - \frac{G.P.W.^{\,2}\,\alpha^2}{R.X.^{\,2}} = \alpha^2$$

$$Qi\,7.\;\; \frac{\beta^2}{\alpha^2\sin^2(\beta)} - \frac{G.P.W.^{\,2}}{R.X.^{\,2}} = 1$$

Hyperbolic Sine Space-Warp Formula:

Rearrangement yields the ratio form:

$$Qi\,8.\;\; \frac{\alpha^2}{\beta^2} - \frac{\left(R.X.^{\,2} + G.P.W.^{\,2}\right)}{G.P.W.^{\,2}\sin^2(\beta)} = 0$$

Then also:

$$Qi\,9.\;\; \frac{\beta^2}{\alpha^2} - \frac{G.P.W.^{\,2}\sin^2(\beta)}{R.X.^{\,2}} = \sin^2(\beta)$$

$$Qi\,10.\;\; \frac{\beta^2}{\alpha^2} - \sin^2(\beta)\left(\frac{T.G.W.^{\,2}}{R.X.^{\,2}} - 1\right) = \sin^2(\beta)$$

$$Qi\,11.\;\; \frac{R.X.^{\,2}\beta^2}{\alpha^2} - T.G.W.^{\,2}\sin^2(\beta) + R.X.^{\,2}\sin^2(\beta) = R.X.^{\,2}\sin^2(\beta)$$

$$Qi\,12.\;\; \frac{R.X.^{\,2}\beta^2}{\alpha^2} = T.G.W.^{\,2}\sin^2(\beta)$$

$$Qi\ 13.\quad \frac{\beta^2}{\alpha^2} = \frac{T.G.W.^2}{R.X.^2}\sin^2(\beta)$$

$$Qi\ 14.\quad \frac{T.G.W.}{R.X.} = \frac{1}{\sin(\alpha)}$$

$$Qi\ 15.\quad \frac{\beta^2}{\alpha^2} = \frac{\sin^2(\beta)}{\sin^2(\alpha)}$$

<u>Hemi-Hyperbolic Paraboloid Sine Space-Warp Formula</u>

Appendix Ri:

Axioms and Identities

$$Ri\,1.\quad T.G.W.\cos(\alpha) = G.P.W. + I.X.$$

$$Ri\,2.\quad \frac{\alpha}{\beta} = \frac{T.I.X.}{T.G.W.} = \frac{T.I.X.}{z + G.P.W.} = \frac{\sin(\alpha)}{\sin(\beta)}$$

$$Ri\,3.\quad z + G.P.W. = \frac{T.I.X.\,\beta}{\alpha} = T.G.W.$$

Appendix Si:

$$Si\,1.\quad T.G.W.^{\,2} = \left(G.P.W. + I.X.\right)^2 + R.X.^{\,2}$$

$$Si\,2.\quad z\left(z + 2\,G.P.W.\right) = I.X.\left(T.G.W.\cos(\alpha) + G.P.W.\right) + R.X.^{\,2}$$

$$Si\,3.\quad \left(\frac{T.I.X.\,\beta - G.P.W.\,\alpha}{\alpha}\right)\left(\frac{T.I.X.\,\beta + G.P.W.\,\alpha}{\alpha}\right) = \left(T.G.W.\cos(\alpha) - G.P.W.\right)\left(T.G.W.\cos(\alpha) + G.P.W.\right) + R.X.^{\,2}$$

$$Si\,4.\quad \frac{T.I.X.^{\,2}\beta^2 - G.P.W.^{\,2}\alpha^2}{\alpha^2} = T.G.W.^{\,2}\cos^2(\alpha) - G.P.W.^{\,2} + R.X.^{\,2}$$

$$Si\,5.\quad \frac{T.I.X.^{\,2}\beta^2 - G.P.W.^{\,2}\alpha^2 + G.P.W.^{\,2}\alpha^2}{\alpha^2} = \left(z + G.P.W.\right)^2\cos^2(\alpha) + R.X.^{\,2}$$

$$Si\,6.\quad \frac{T.I.X.^{\,2}\beta^2}{\alpha^2} = \frac{T.I.X.^{\,2}\beta^2}{\alpha^2}\cos^2(\alpha) + R.X.^{\,2}$$

$$Si\,7.\quad 1 - \cos^2(\alpha) = \frac{R.X.^{\,2}}{T.G.W.^{\,2}}$$

$$Si\,8.\quad \frac{R.X.^{\,2}}{T.G.W.^{\,2}} = \sin^2(\alpha)$$

Sine Square Space-Warp Formula:

Appendix Ti:

$$Ti\,1.\quad \frac{\gamma^2}{\theta^2\cos^2(\theta)} - \frac{\Delta(I.P.)^2}{\Delta(R.P.)^2} = \frac{\gamma^2}{\theta^2\cos^2(\theta)} - \frac{\Delta(I.X.)^2}{\Delta(R.X.)^2} = 1$$

Hyperbolic Cosine Momentum Space-Warp Formula

$$Ti\,2.\quad \frac{\theta^2}{\Delta(R.P.)^2} - \frac{\gamma^2}{\cos^2(\theta)\left(\Delta(I.P.)^2 + \Delta(R.P.)^2\right)} = \frac{\theta^2}{\Delta(R.X.)^2} - \frac{\gamma^2}{\cos^2(\theta)\left(\Delta(I.X.)^2 + \Delta(R.X.)^2\right)} = 0$$

Hyperbolic Cosine Momentum Space-Warp Formula Cone

$$Ti\,3.\quad \frac{\gamma^2}{\theta^2} = \frac{\cos^2(\theta)}{\cos^2(\gamma)} = \frac{\gamma^2}{\theta^2} = \cos^2(\theta)$$

Hyperbolic Paraboloid Cosine Momentum Space-Warp Formula

$$Ti\,4.\quad \frac{\Delta(R.P.)^2}{\Delta(T.I.P)^2} = \cos^2(\gamma) = \frac{\Delta(R.X.)^2}{\Delta(T.I.X.)^2} = \cos^2(\gamma)$$

Cosine Square Momentum Space-Warp Formula

$$Ti\,5.\quad \frac{\beta^2}{\alpha^2\sin^2(\beta)} - \frac{\Delta(I.P.)^2}{\Delta(R.P.)^2} = \frac{\beta^2}{\alpha^2\sin^2(\beta)} - \frac{\Delta(I.X.)^2}{\Delta(R.X.)^2} = 1$$

Hyperbolic Sine Momentum Space-Warp Formula:

$$Ti\,6.\quad \frac{\alpha^2}{\beta^2} - \frac{\left(\Delta(R.P.)^2 + \Delta(I.P.)^2\right)}{\Delta(I.P.)^2\sin^2(\beta)} = \frac{\alpha^2}{\beta^2} - \frac{\left(\Delta(R.X.)^2 + \Delta(I.X.)^2\right)}{\Delta(I.X.)^2\sin^2(\beta)}$$

Hyperbolic Sine Momentum Space-Warp Formula:

Rearrangement yields the ratio form:

$$Ti\,7.\quad \frac{\Delta(R.P.)^2}{\Delta(T.I.P)^2} = \sin^2(\alpha) = \frac{\Delta(R.X.)^2}{\Delta(T.I.X.)^2}$$

The Space-Warp Theorem - General Form:

$$Ti\,8.\quad \left(\Delta(I.P.) - \Delta(G.P.E.)\right)^2 + \Delta(R.P.)^2 = \Delta(T.I.P)^2 = \left(\Delta(I.X.) - \Delta(G.P.W.)\right)^2 + \Delta(R.X.)^2 = \Delta(T.W)^2$$

Appendix Ui:

$$Ui\,1.\quad \frac{\gamma^2}{\theta^2\cos^2(\theta)} - \frac{d(I.P.)^2}{d(R.P.)^2} = \frac{\gamma^2}{\theta^2\cos^2(\theta)} - \frac{d(G.P.W.)^2}{d(R.X.)^2} = 1$$

Hyperbolic Cosine Differential Momentum Space-Warp Formula

$$Ui\,2.\quad \frac{\theta^2}{d(R.P.)^2} - \frac{\gamma^2}{\cos^2(\theta)\left[d(I.P.)^2 + d(R.P.)^2\right]} = \frac{\theta^2}{d(R.X.)^2} - \frac{\gamma^2}{\cos^2(\theta)\left[d(G.P.W.)^2 + d(R.X.)^2\right]} = 0$$

Hyperbolic Cosine Differential Momentum Space-Warp Formula Cone

$$Ui\,3.\quad \frac{\gamma^2}{\theta^2} = \frac{\cos^2(\theta)}{\cos^2(\gamma)} = \frac{\gamma^2}{\theta^2} = \cos^2(\theta)$$

Hyperbolic Paraboloid Cosine Differential Momentum Space-Warp Formula

$$Ui\,4.\quad \frac{d(R.P.)^2}{d(T.I.P)^2} = \cos^2(\gamma) = \frac{d(R.X.)^2}{d(T.G.W.)^2} = \cos^2(\gamma)$$

Cosine Square Differential Momentum Space-Warp Formula

$$Ui\,5.\quad \frac{\beta^2}{\alpha^2\sin^2(\beta)} - \frac{d(I.P.)^2}{d(R.P.)^2} = \frac{\beta^2}{\alpha^2\sin^2(\beta)} - \frac{d(G.P.W.)^2}{d(R.X.)^2} = 1$$

Hyperbolic Sine Differential Momentum Space-Warp Formula:

$$Ui\,6.\quad \frac{\alpha^2}{\beta^2} - \frac{\left[d(R.P.)^2 + d(I.P.)^2\right]}{d(I.P.)^2\sin^2(\beta)} = \frac{\alpha^2}{\beta^2} - \frac{\left[d(R.X.)^2 + d(G.P.W.)^2\right]}{d(G.P.W.)^2\sin^2(\beta)}$$

Hyperbolic Sine Differential Momentum Space-Warp Formula:

Rearrangement yields the ratio form:

$$Ui\,7.\quad \frac{d(R.P.)^2}{d(T.I.P)^2} = \sin^2(\alpha) = \frac{d(R.X.)^2}{d(T.G.W.)^2}$$

The Space-Warp Theorem - General Differential Form:

$$Ui\,8.\quad (d(I.P.) - d(G.P.E.))^2 + (d(R.P.))^2 = (d(T.I.P))^2 = (d(G.P.W.) - d(I.X.))^2 + (d(R.X.))^2 = (d(T.W.))^2$$

Bibliography:

1. Schaum’s Outline. "Physics for Engineering and Science". 1998
Michael Browne.

2. The Gemological Institute of America. "Gems made by Man."
1980.

3. Bantam Books. "In Search of Schrödinger’s Cat".
1984.

4. The Viking Press. "The Coffee Table Book of Astrology"
1967.

5. S. Hawking and R. Penrose "The Nature of Space and Warp"
1996.

6. "MacGraw Hill Science and Technology Encyclopedia".
1998

7. John Caldwell. "Calculus: A Linear Algebra Approach." Addison-Wesley; 1979;
Volumes I & II, Pgs. 665-667.

8. McGraw-Hill. "Encyclopedia of Science and Technology". 5th edition.
1982; Volume 6, Pgs. 787-788.

9. Thomas and Finney; "Calculus and Analytical Geometry". 6th edition.
Narosa Pub. House. New Delhi, India. 1984. Pgs. 530-550.

10. Ibid. Pgs. 517-521.

Captions:

Figure 1*a*: The Lorentz Transform Viewed from Earth.

Figure 1*b*: The Lorentz Transform Viewed from Earth - Joined.

Figure 2: The Inertial & Gravitational (Causal - Super-Causal)
Time-Warp Graph.

Figure 2*a*: The Super-Causal Temproal Function - Sine.

Figure 2*b*: The Temporal (Crab) Causal - Super-Causal Overlay .

Figure 2*c*: Inertial Frame Derivative Time-Warp.

Figure 2*ci*: Type I Crossover - Inertial Time-Warp Derivative.

Figure 2*d*: Gravitational Time-Warp.

Figure 2*di*: Type II Crossover - Gravitational Time-Warp Derivative.

Figure 2*cii*: Type III Crossover - Inertial Time-Warp Derivative.

Figure 2*dii*: Type IV Crossover - Gravitational Time-Warp.

Figure 2*cii* and *dii*: Composite Overlay All-Crossover Time-Warp Derivative.

Figure 2*e*: Super-Imposed Inertial-Gravitational Time-Warps.

Figure 2*f*: Inertial-Gravitational Singly Energy Star.

Figure 2*g*: Derivative of Singly Inertial Energy Calculation.

Figure 2*h*: Derivative of Inertial Singly Energy Curve

Figure 2*i*: Derivative of Gravitational Singly Energy Curve.

Figure 2*j*: Overlay of Derivatives of Inertial and Gravitatioinal Singly Energy Curves.

Figure 2*k*: Overlay of ET Inertial and Gravitational Singly Energy - and Singly Time Warp Star.

Figure 2*ki*: SuperOrigin Graph of Derivatives of Inertial and Gravitational Energy Curves.

Figure 2*l*: Inertial Energy Curve - Inertial Time Warp Composite.

Figure 2*m*: Gravitational Energy Curve - Gravitational Time Warp Composite.

Figure 2*n*: Doubly Warp Factor - Singly Warp Factor Complex.

Figure 2*o*: Singly Gravitational Warp Factor with Doubly Warp Complex.

Captions:

Figure 8*i*: Parent Hyperbolic Cosine Equation Plot -
Highlighting hybrid roots.

Figure 9*i*: Hyperbolic Paraboloid Quadric (C8).

Figure 10*i*: Fundamental Quadric of the Cosine Momentum Formula (C8).

Figure 11*i*: Cone of Central Parabololoid of the Child Equation Momentum Formula Derivative

Figure 12*i*: The Daughter Hyperbolic Momentum Formula Eq. 7. -
The Isolated Derivative.

Figure 13*i*: Contourplot of the Hemi-Hyperbolic Paraboloid (G15)

Figure 14*i*: Parent Hyperbolic Cosine Space-Warp Equation Plot -
Highlighting hybrid roots.

Figure 15*i*: Hyperbolic Paraboloid Quadric (C8).

Figure 16*i*: Fundamental Quadric of the Cosine Space-Warp Formula (M8).

Figure 17*i*: Cone of Central Space-Warp Parabololoid of the
Child Equation Momentum Formula Derivative

Figure 18*i*: The Daughter Hyperbolic Space-Warp Formula Eq. 7. -
The Isolated Derivative.

Figure 19*i*: Contourplot of the Hemi-Hyperbolic Paraboloid (G15)

```
"Expanded Lorentz Relativity Factor - Time Dilation"

Z=2.998*10^8
Plot[{(1/(Sqrt[1-X^2/Z^2])),Im[(1/(Sqrt[1-X^2/Z^2]))]},
{X,-2Z,2Z},Axes->True,PlotPoints->2000,
PlotRange->{{-2Z,2Z},{-10,10}},AxesLabel->
{"x","t"}]
```

Expanded Lorentz Relativity Factor - Time Dilation

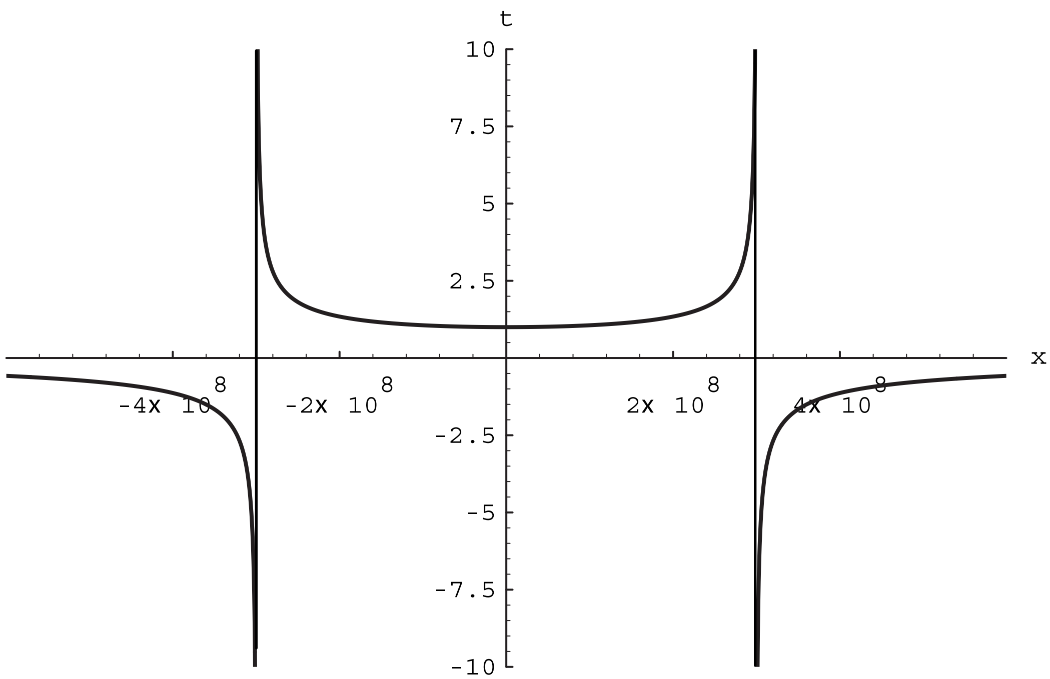

```
"Expanded Lorentz Relativity Factor - Time Dilation"

Z=2.998*10^8
Plot[{(1/(Sqrt[1-X^2/Z^2])),Im[(1/(Sqrt[1-X^2/Z^2]))]},
{X,-2Z,2Z},Axes->True,PlotPoints->2000,
PlotRange->{{-2Z,2Z},{-60,60}},AxesLabel->
{"x","t"}]
```

Expanded Lorentz Relativity Factor - Time Dilation

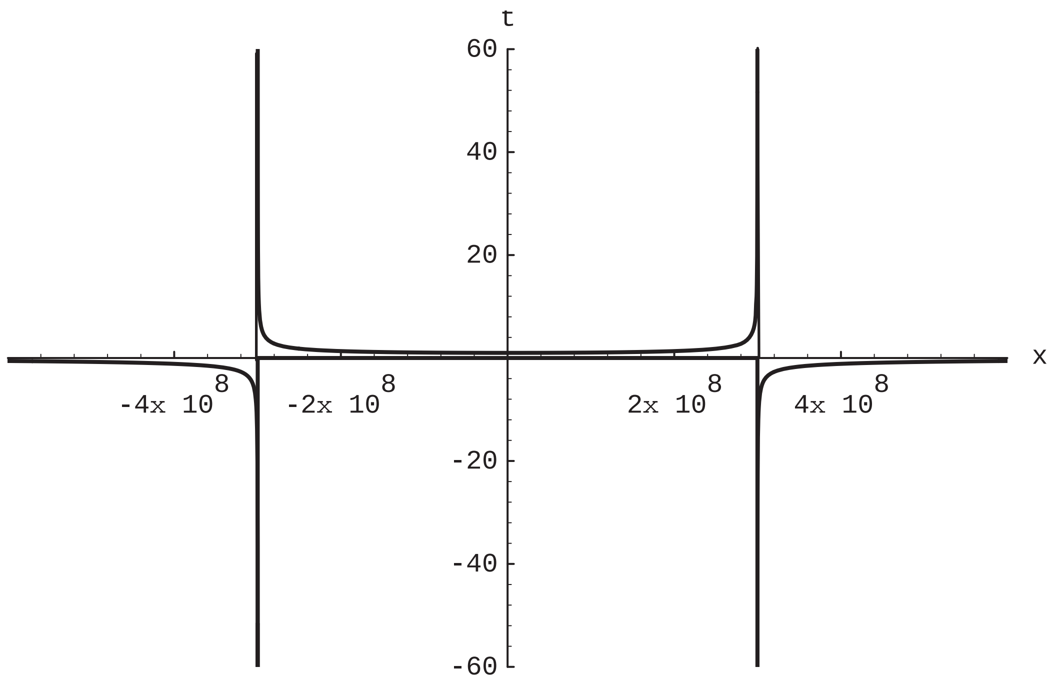

```
"Figure 2
Causal Universe & SuperCausal
Universe Moving Frame Numerical
Time-Warp Curve"
```

```
Z=2.998*10^8
Plot[{((Sqrt[1-X^2/Z^2])),Im[((Sqrt[1-X^2/Z^2]))],
((-Sqrt[1-X^2/Z^2])),Im[-((Sqrt[1-X^2/Z^2]))]},
{X,-5Z,5Z},Axes->True,PlotPoints->1000,
PlotRange->{{-7Z,7Z},{-4.0,4.0}},
AxesLabel->{"dx","dt'"}]
```

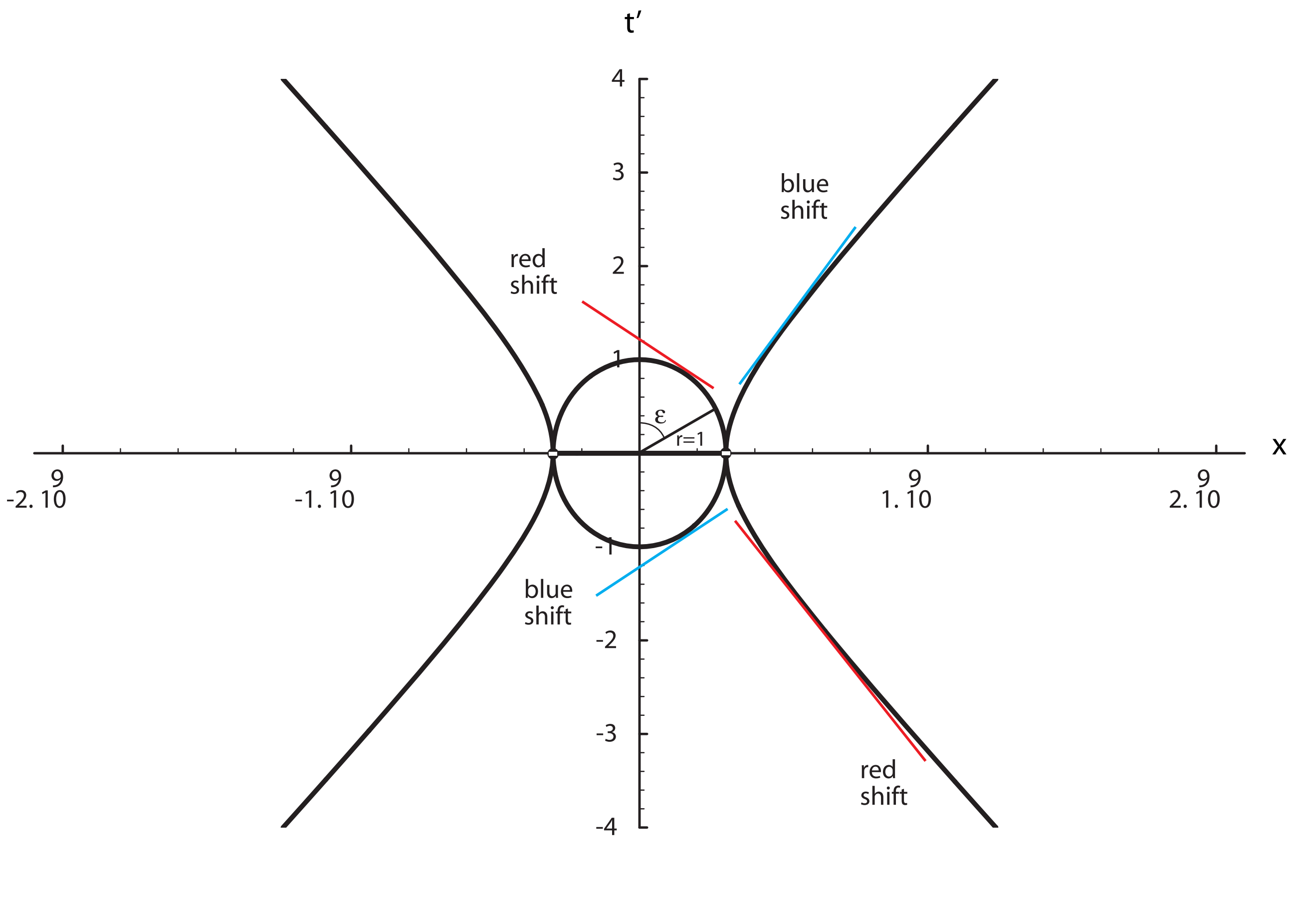

Figure 2a. Relativistic Velocity Causal
and Supercausal - Unity.

```
Z=2.998*10^8
Plot[{((Sqrt[1-X^2/Z^2])),Im[((Sqrt[1-X^2/Z^2]))],
((-Sqrt[1-X^2/Z^2])),Im[-((Sqrt[1-X^2/Z^2]))]},
{X,-5Z,5Z},Axes->True,PlotPoints->1000,
PlotRange->{{-7Z,7Z},{-4.0,4.0}},
AxesLabel->{"dx","dt'"}]
```

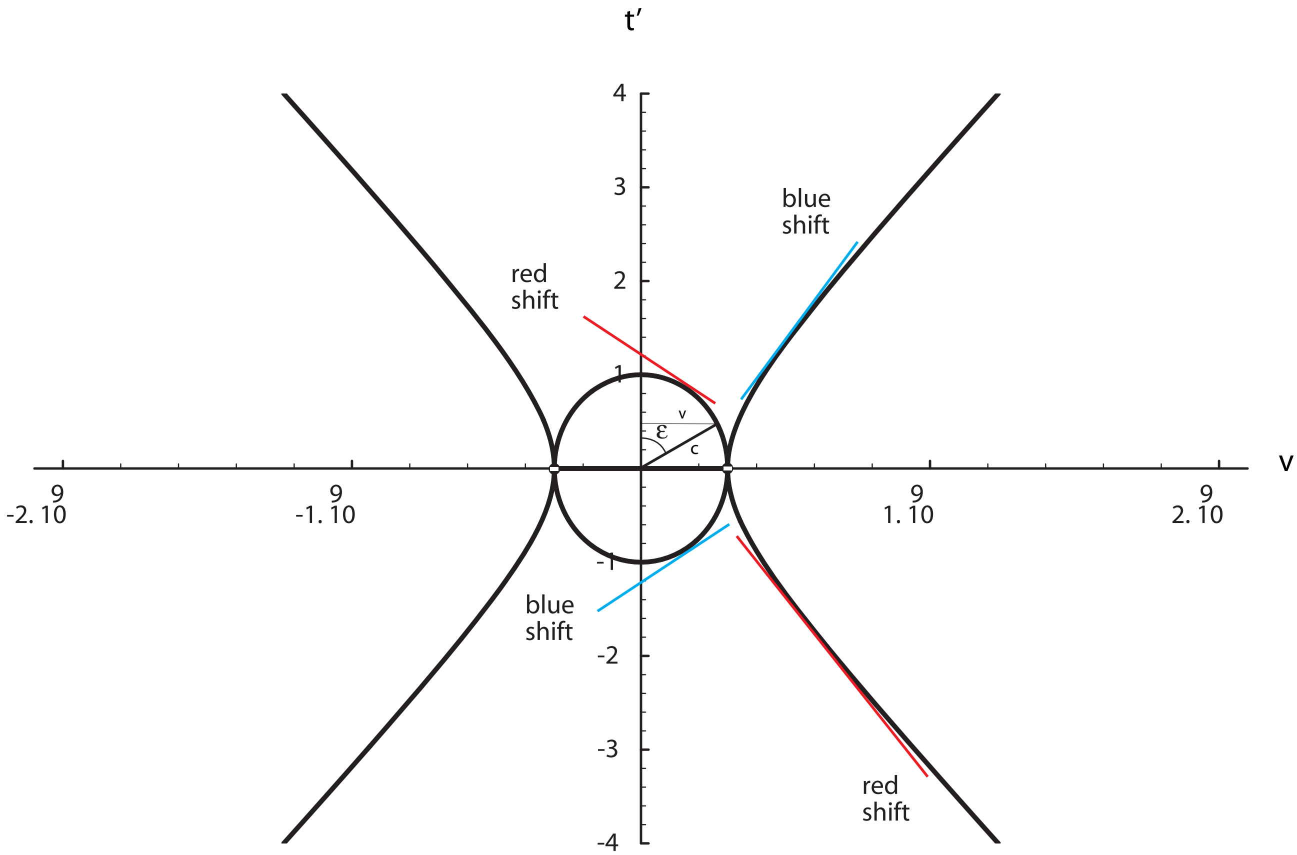

"Figure 2b - Inertial/Gravitational Causal/SuperCausal Warp-Conservation Graph"

```
Z=2.998*10^8
Plot[{((Sqrt[1-X^2/Z^2])),Im[((Sqrt[1-X^2/Z^2]))],
(-(Sqrt[1-X^2/Z^2])),Im[((Sqrt[1-X^2/Z^2]))],
(1-(Sqrt[1-X^2/Z^2])),Im[(1-(Sqrt[1-X^2/Z^2]))],
(-(1-(Sqrt[1-X^2/Z^2]))),Im[(-(1-(Sqrt[1-X^2/Z^2])))]},
{X,-2Z,2Z},Axes->True,AxesLabel->{"x","t'"}]
```

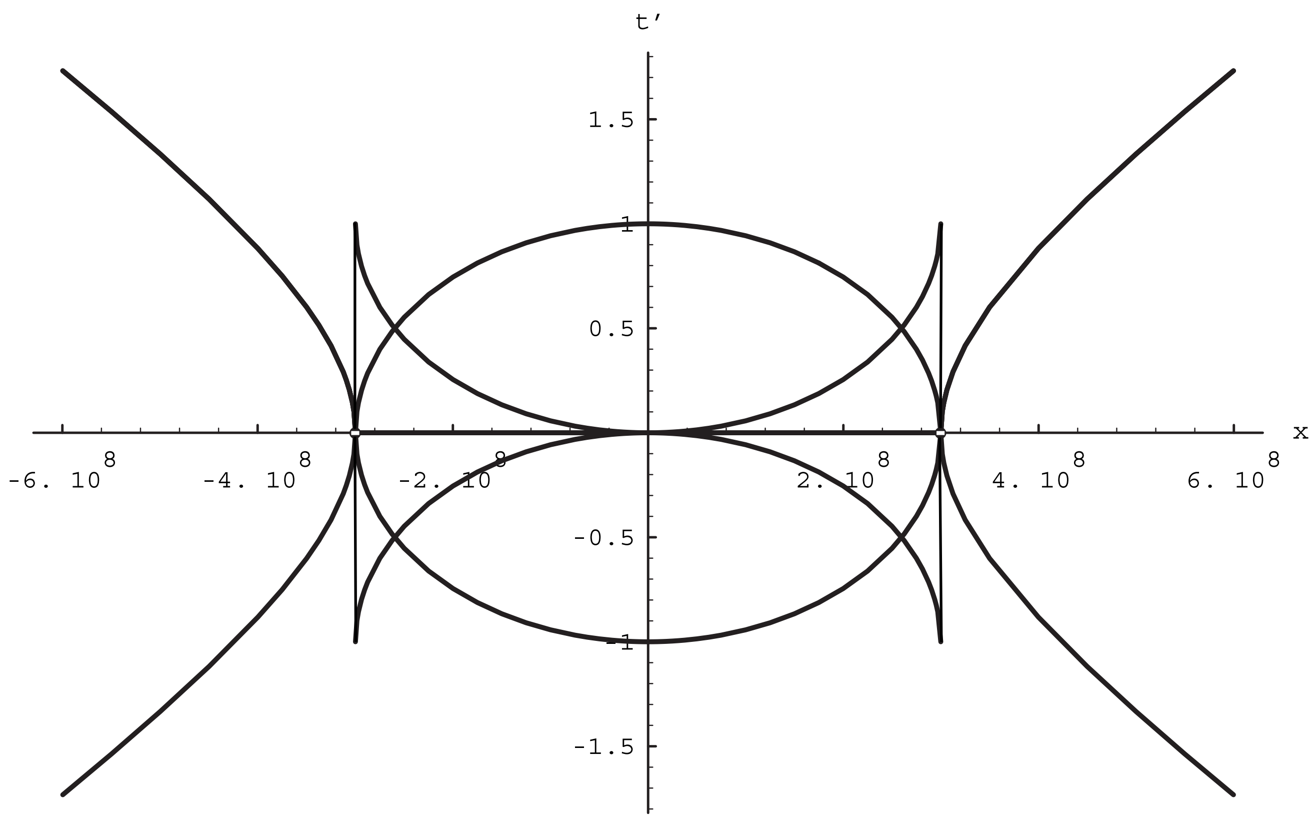

-Graphics-

"Figure 2c"
"Inertial Frame Derivative Time-Warp"

```
Z=2.998*10^8
Plot[{-X/((Sqrt[1-X^2/Z^2])*Z^2),Im[-X/((Sqrt
[1-X^2/Z^2])*Z^2)]},{X,-2Z,2Z},Axes->
True,PlotPoints->1000,
PlotRange->{{-2Z,2Z},
{-.00000005,.00000005}},
AxesLabel->{"dx","dt'"}]
```

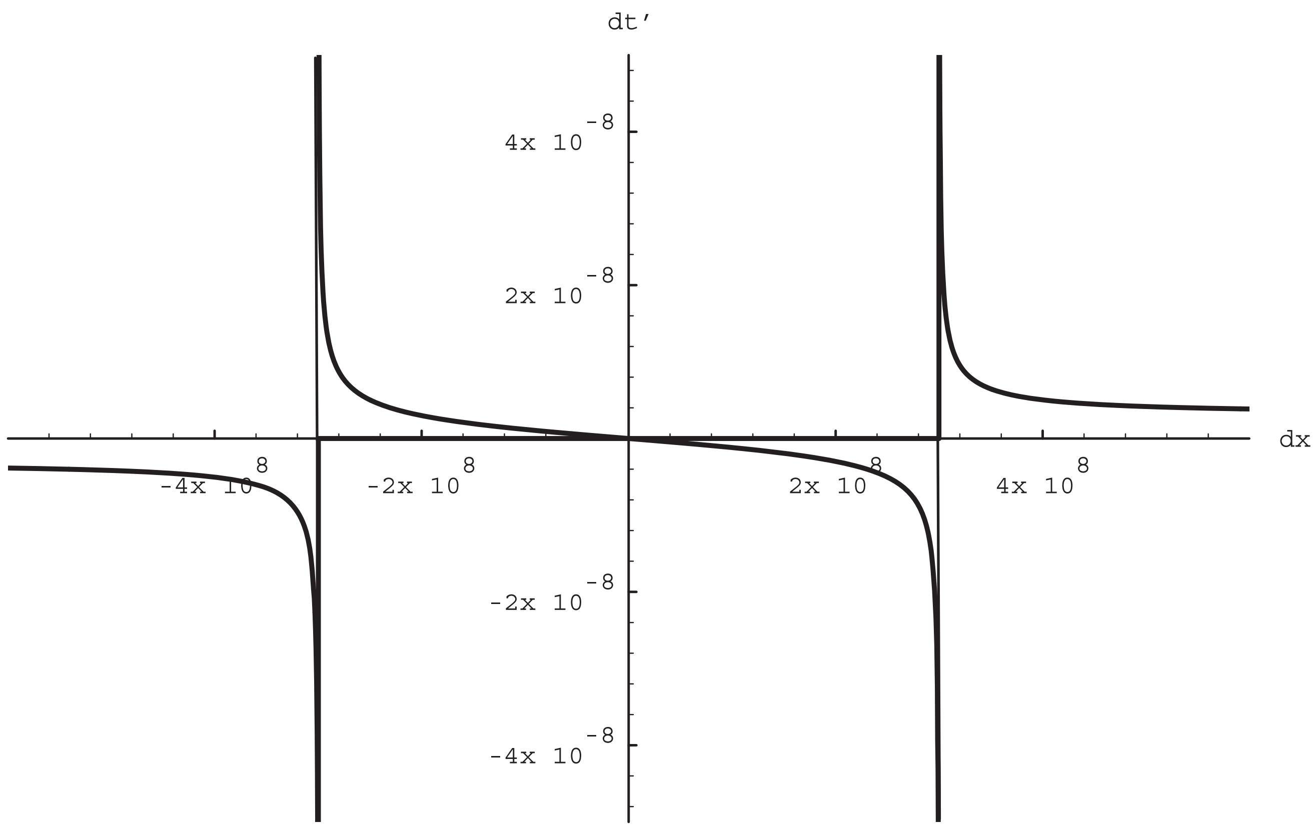

```
"Figure 2cii"
"Type I Crossover - Inertial Time-Warp Derivative"

Z=2.998*10^8
Plot[{-X/((Sqrt[1-X^2/Z^2])*Z^2),Im[-X/((Sqrt
[1-X^2/Z^2])*Z^2)]},{X,-2Z,2Z},Axes->
True,PlotPoints->1000,
PlotRange->{{-2Z,2Z},
{-.00000005,.00000005}},
AxesLabel->{"dx","dt'"}]
```

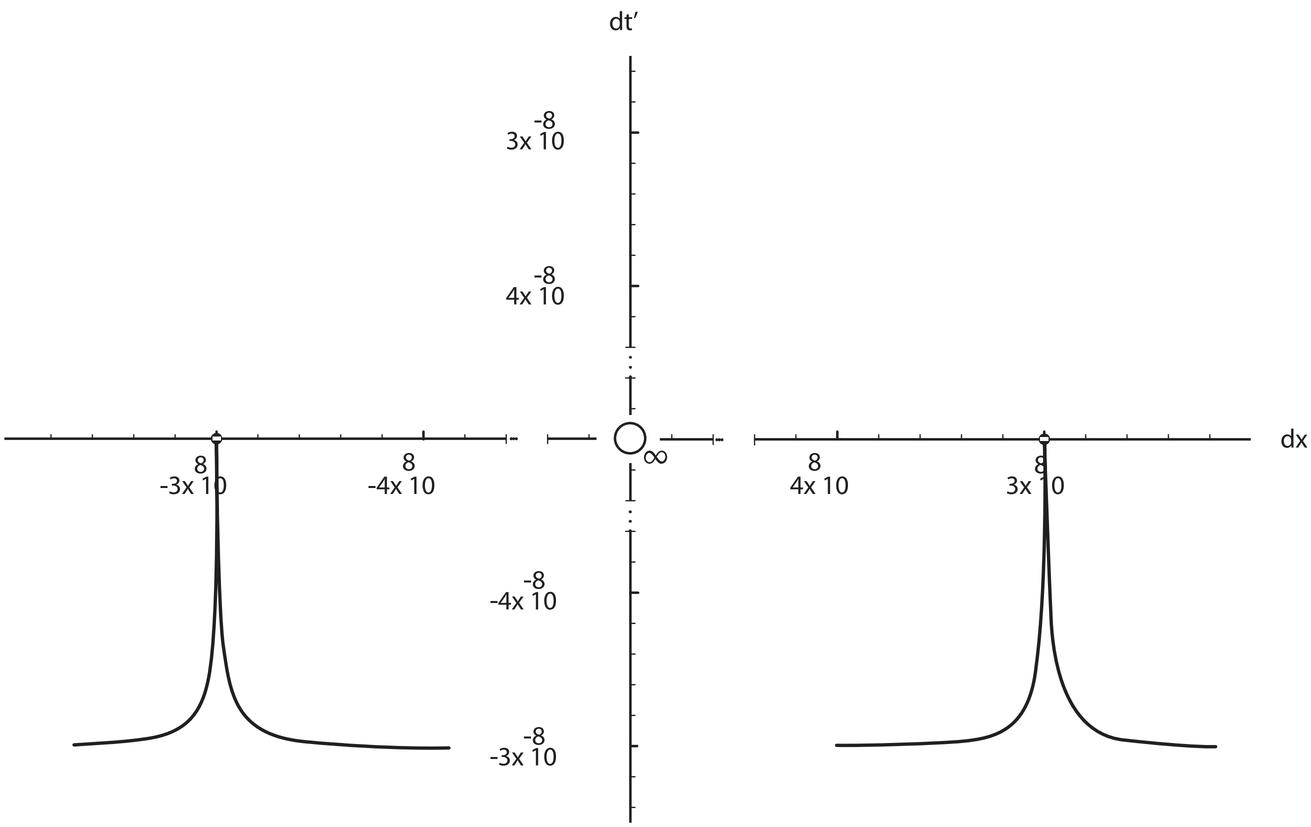

```
"Figure 2d"
"Gravitational Time-Warp"

Z=2.998*10^8
Plot[{X/((Sqrt[1-X^2/Z^2])*Z^2),Im[X/
((Sqrt[1-X^2/Z^2])*Z^2)]},{X,-2Z,2Z},
Axes->True,PlotPoints->1000,
PlotRange->{{-2Z,2Z},
{-.00000005,.00000005}},
AxesLabel->{"dx","dt'"}]
```

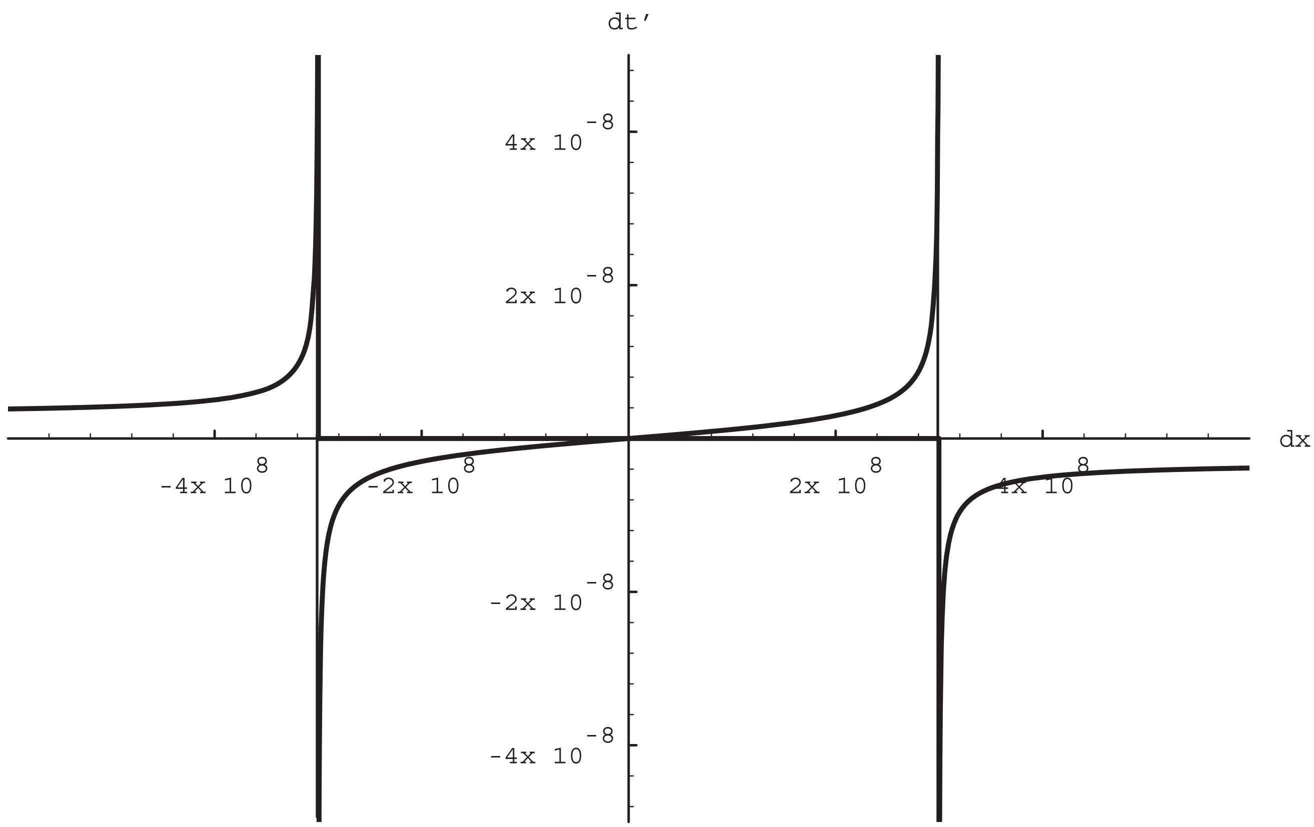

"Figure 2dii"
"Type II Crossover - Gravitational Time-Warp Derivative"

```
Z=2.998*10^8
Plot[{X/((Sqrt[1-X^2/Z^2])*Z^2),Im[X/
((Sqrt[1-X^2/Z^2])*Z^2)]},{X,-2Z,2Z},
Axes->True,PlotPoints->1000,
PlotRange->{{-2Z,2Z},
{-.00000005,.00000005}},
AxesLabel->{"dx","dt'"}]
```

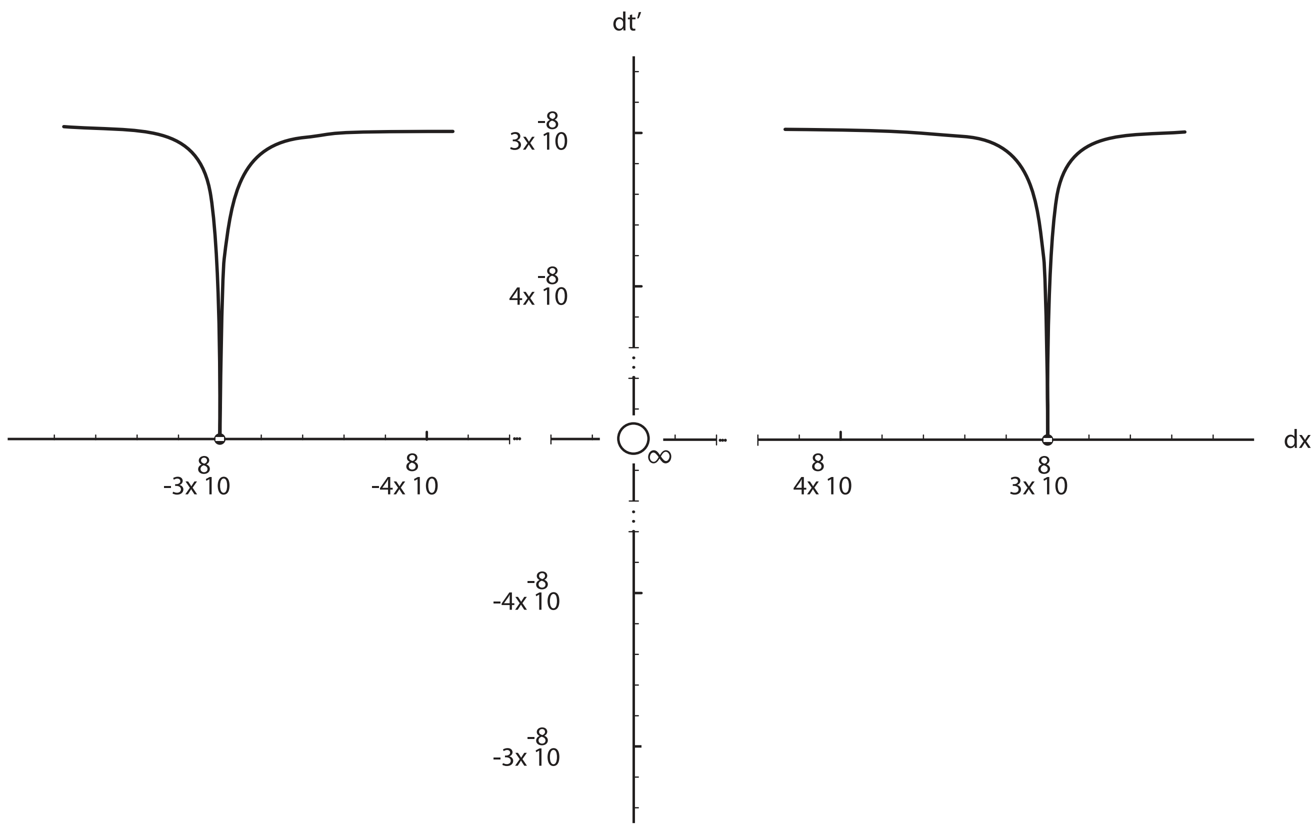

"Figure 2ci"
"Type III Crossover Inertial Time-Warp Derivative"

```
Z=2.998*10^8
Plot[{-X/((Sqrt[1-X^2/Z^2])*Z^2),Im[-X/((Sqrt
[1-X^2/Z^2])*Z^2)]},{X,-2Z,2Z},Axes->
True,PlotPoints->1000,
PlotRange->{{-2Z,2Z},
{-.00000005,.00000005}},
AxesLabel->{"dx","dt'"}]
```

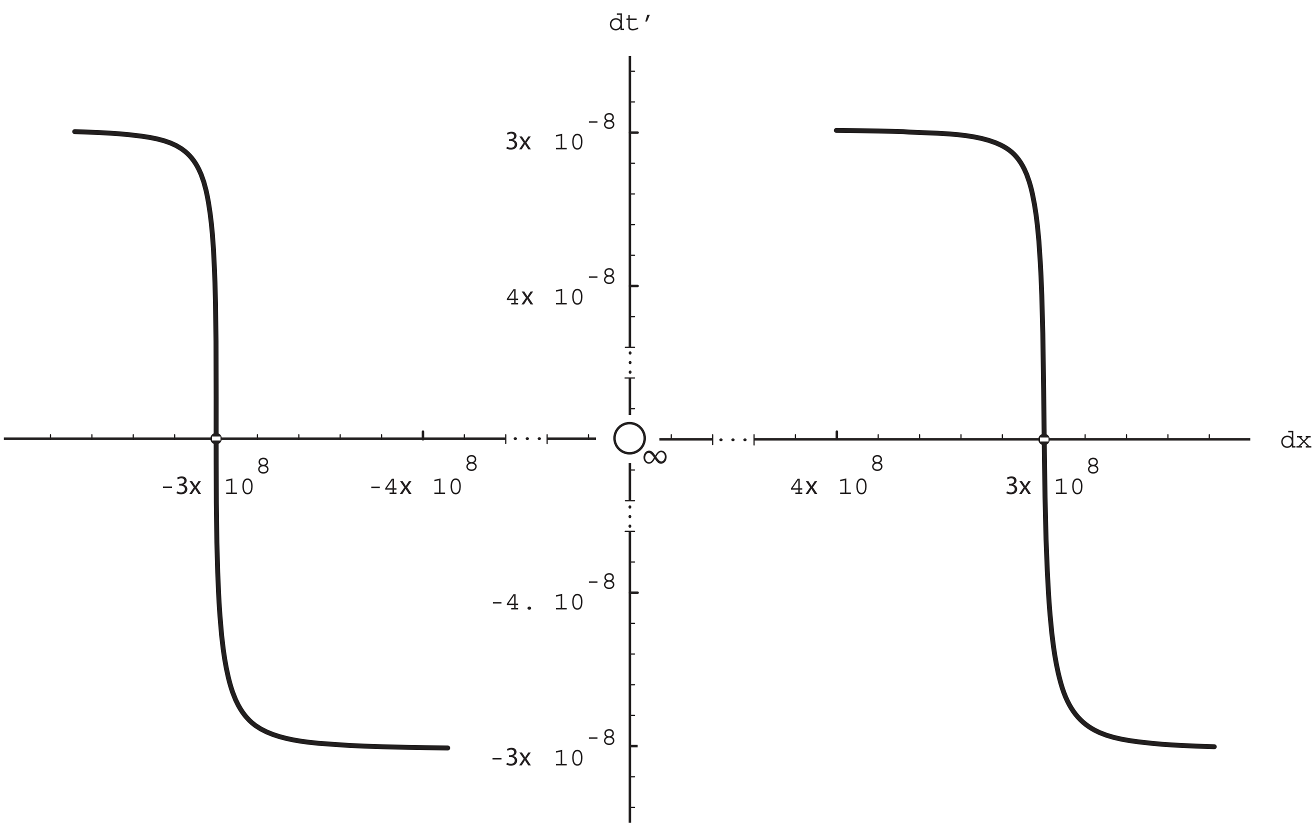

"Figure 2di"
"Type IV Crossover - Gravitational Time-Warp Dervative"

```
Z=2.998*10^8
Plot[{X/((Sqrt[1-X^2/Z^2])*Z^2),Im[X/
((Sqrt[1-X^2/Z^2])*Z^2)]},{X,-2Z,2Z},
Axes->True,PlotPoints->1000,
PlotRange->{{-2Z,2Z},
{-.00000005,.00000005}},
AxesLabel->{"dx","dt'"}]
```

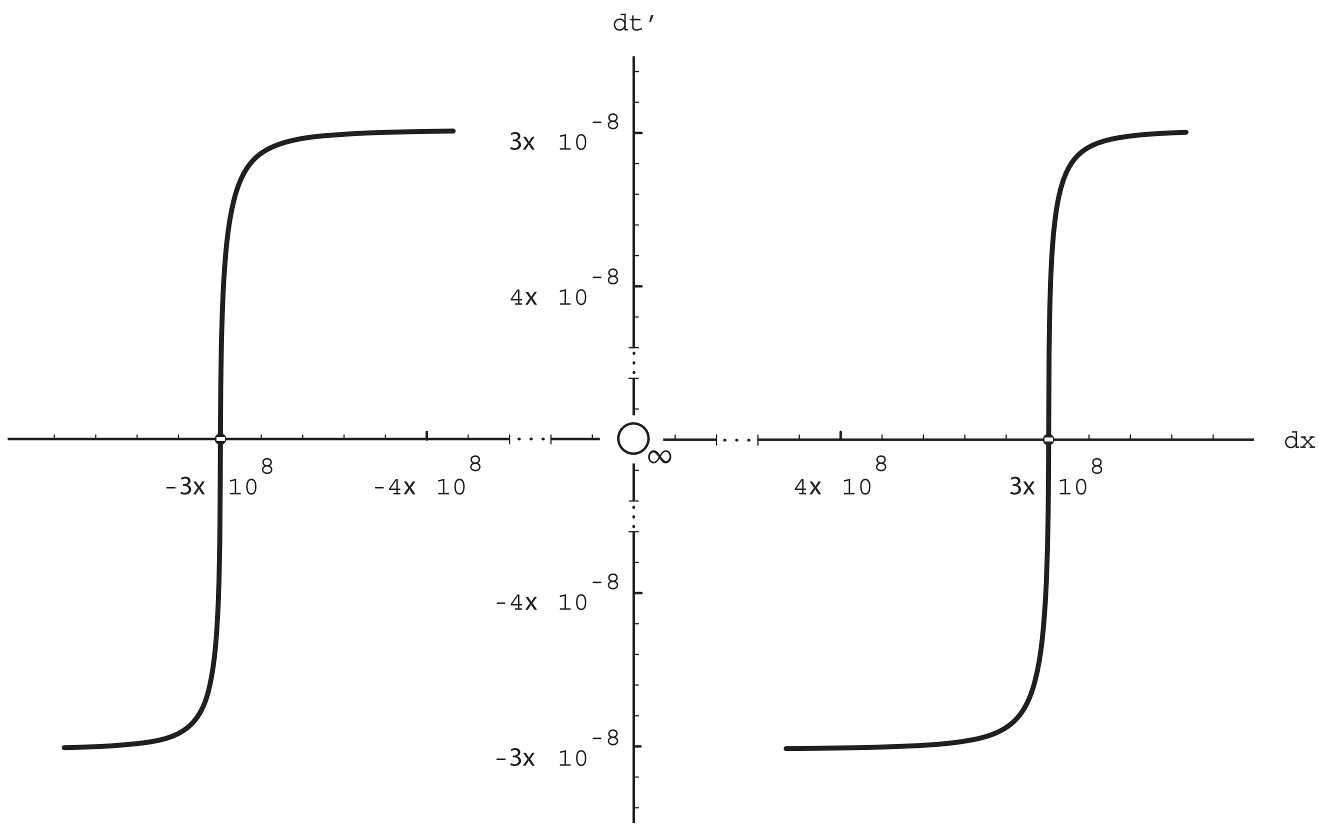

```
"Figure 2ci and 2di Composite OverLay"
"All Crossover - Time-Warp Derivative"

Z=2.998*10^8
Plot[{-X/((Sqrt[1-X^2/Z^2])*Z^2),Im[-X/((Sqrt
[1-X^2/Z^2])*Z^2)]},{X,-2Z,2Z},Axes->
True,PlotPoints->1000,
PlotRange->{{-2Z,2Z},
{-.00000005,.00000005}},
AxesLabel->{"dx","dt'"}]
```

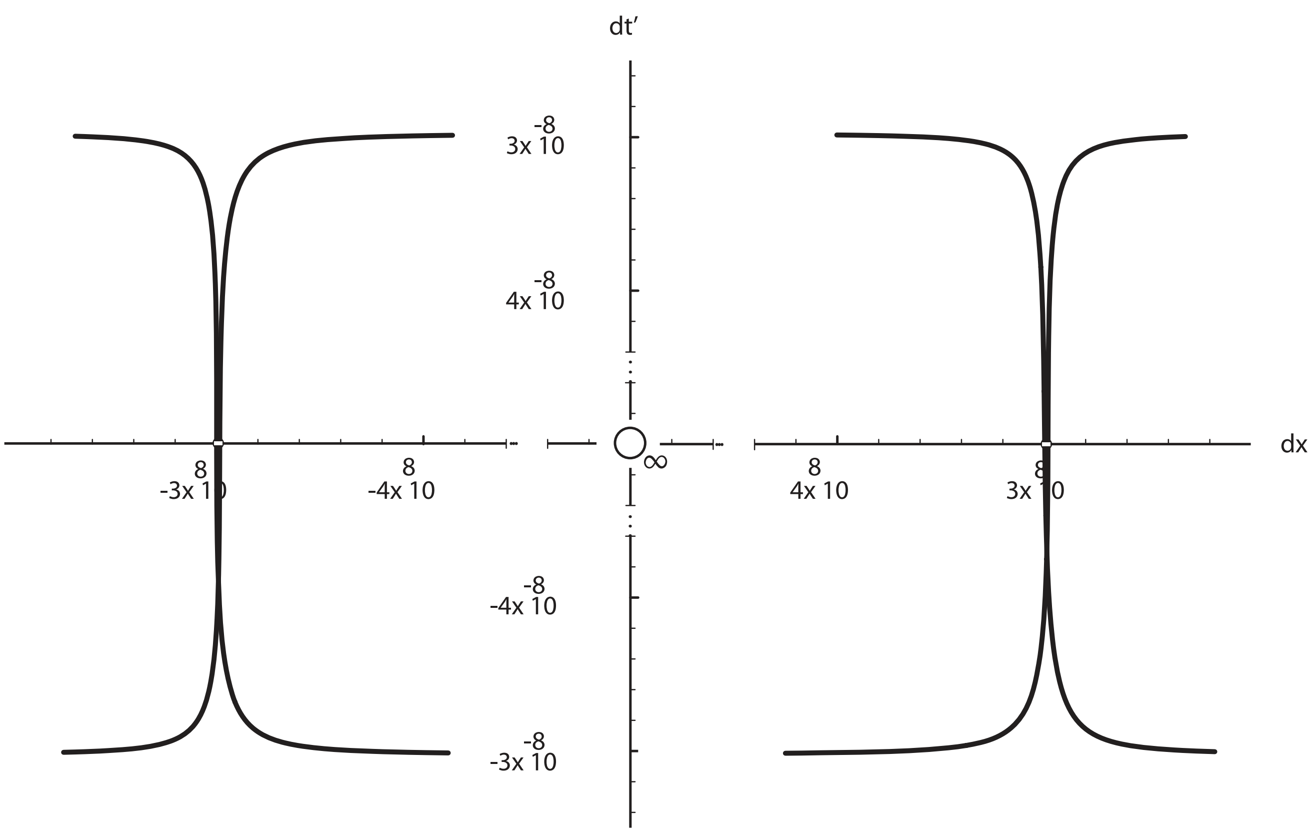

"Figure 2e"
"Super-Imposed Inertial-Gravitational Time-Warps"

```
Z=2.998*10^8
Plot[{-X/((Sqrt[1-X^2/Z^2])*Z^2),Im[-X/
((Sqrt[1-X^2/Z^2])*Z^2)],X/((Sqrt[1-X^2/Z^2])
*Z^2),Im[X/((Sqrt[1-X^2/Z^2])*Z^2)]},{X,-2Z,2Z},
Axes->True,PlotPoints->1000,PlotRange->
{{-2Z,2Z},{-.00000005,.00000005}},
AxesLabel->{"dx","dt'"}]
```

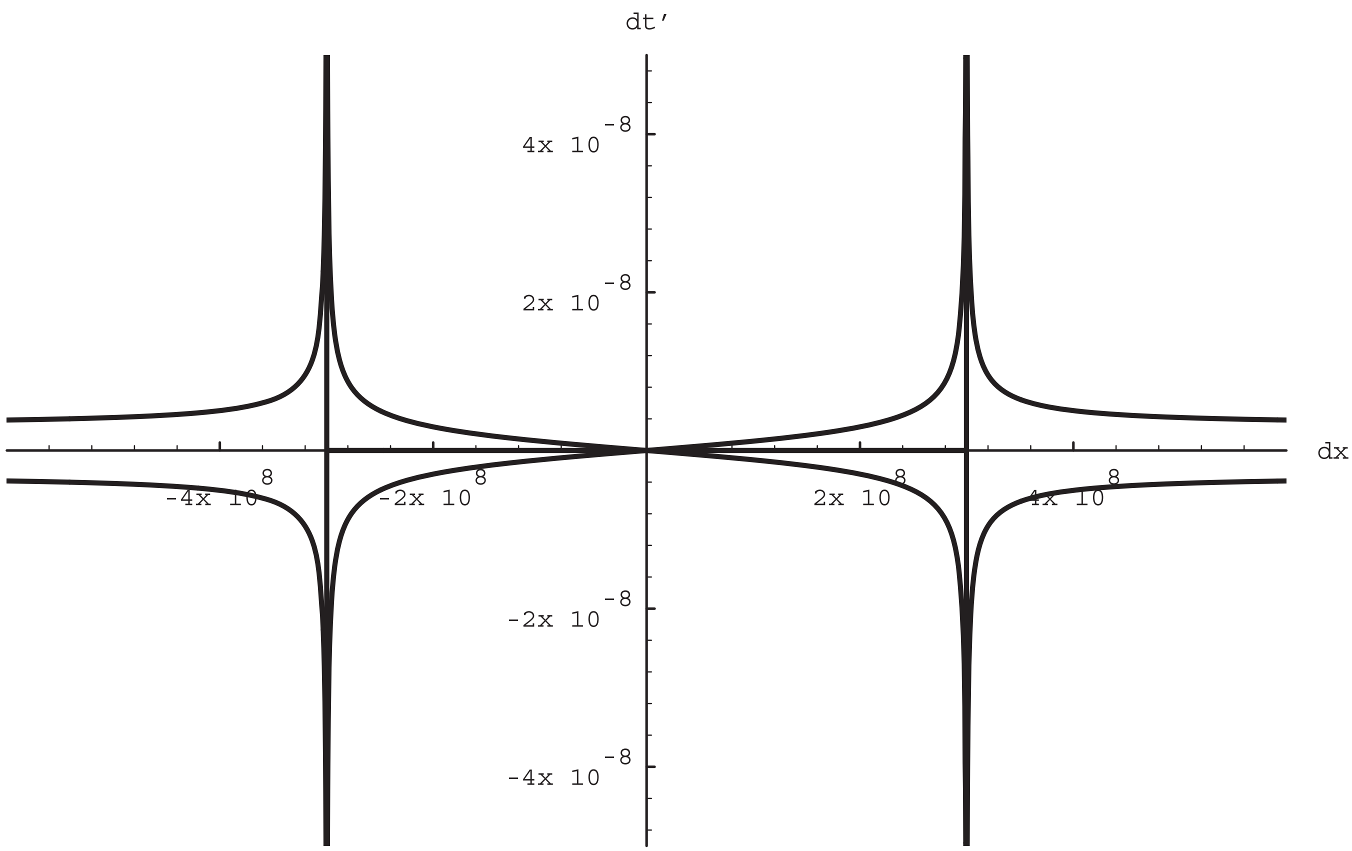

"Inertial-Gravitational Singly Energy Star Fig. 2f"

```
Z=2.998*10^8
Plot[{-X/((Sqrt[1-X^2/Z^2])*Z^2),Im[-X/
((Sqrt[1-X^2/Z^2])*Z^2)],X/((Sqrt[1-X^2/Z^2])
*Z^2),Im[X/((Sqrt[1-X^2/Z^2])*Z^2)]},
{X,-2Z,2Z},Axes->True,PlotPoints->1000,
PlotRange->{{-2Z,2Z},{-.0000001,.0000001}},
AxesLabel->{"dx","dt'"}]
```

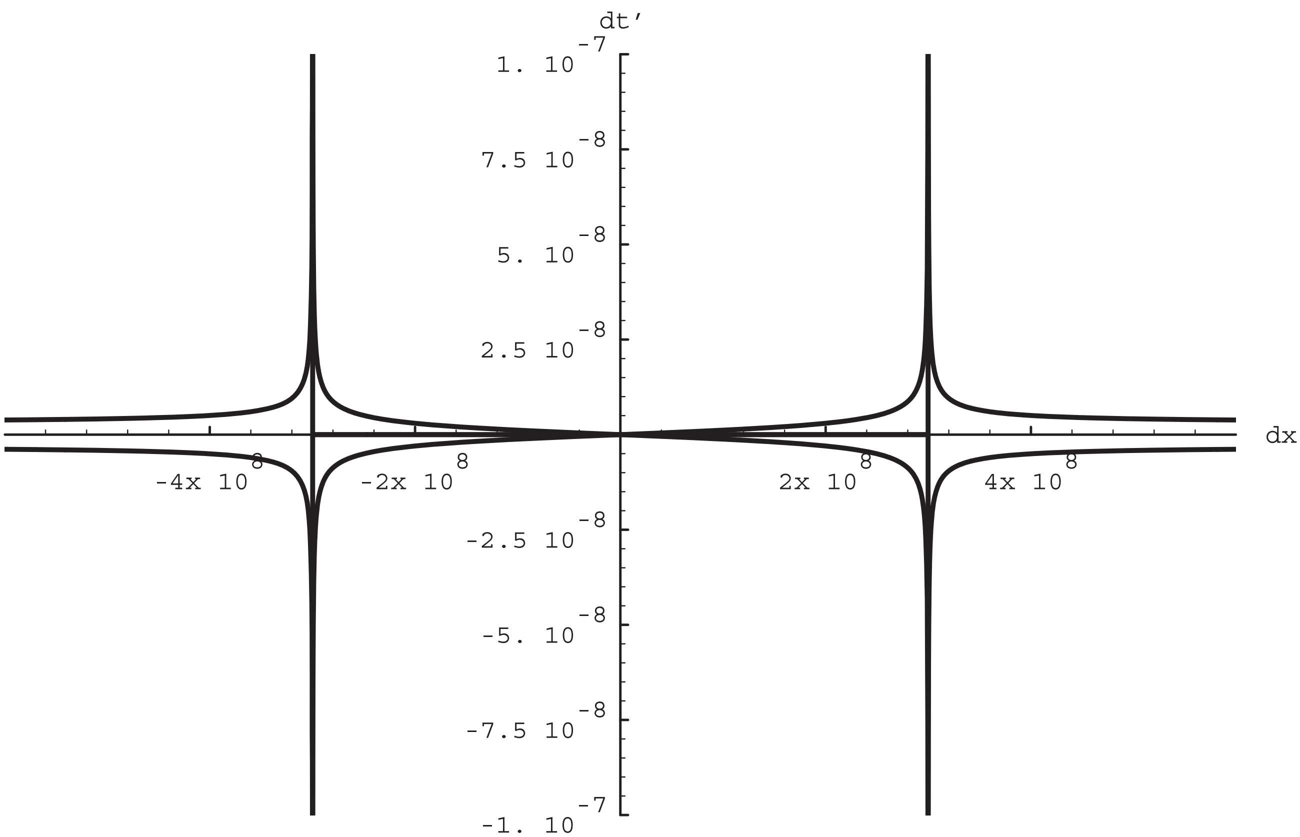

"Derivative of Singly Inertial Energy - Calculation Fig. 2g."

```
D[Sqrt[1/(1-((X^2)/(Z^2)))],X]
```

$$\frac{X}{\mathrm{Sqrt}\left[\frac{1}{1-\frac{X^2}{Z^2}}\right]\left(1-\frac{X^2}{Z^2}\right)^2 Z^2}$$

```
"Derivative of Inertial Singly Energy Curve
 Fig. 2h"


Z=2.998*10^8
Plot[{(X)/(((1 - X^2/Z^2)^(-1))^(1/2)*
(1 - X^2/Z^2)^2*Z^2),Im[(X)/(((1 - X^2/Z^2)^
(-1))^(1/2)*(1 - X^2/Z^2)^2*Z^2)]},{X,-2Z,2Z},
Axes->True,PlotPoints->1000,PlotRange->{{-2Z,2Z},
{-.0000004,.0000004}},AxesLabel->{"dx","dt'"}]
```

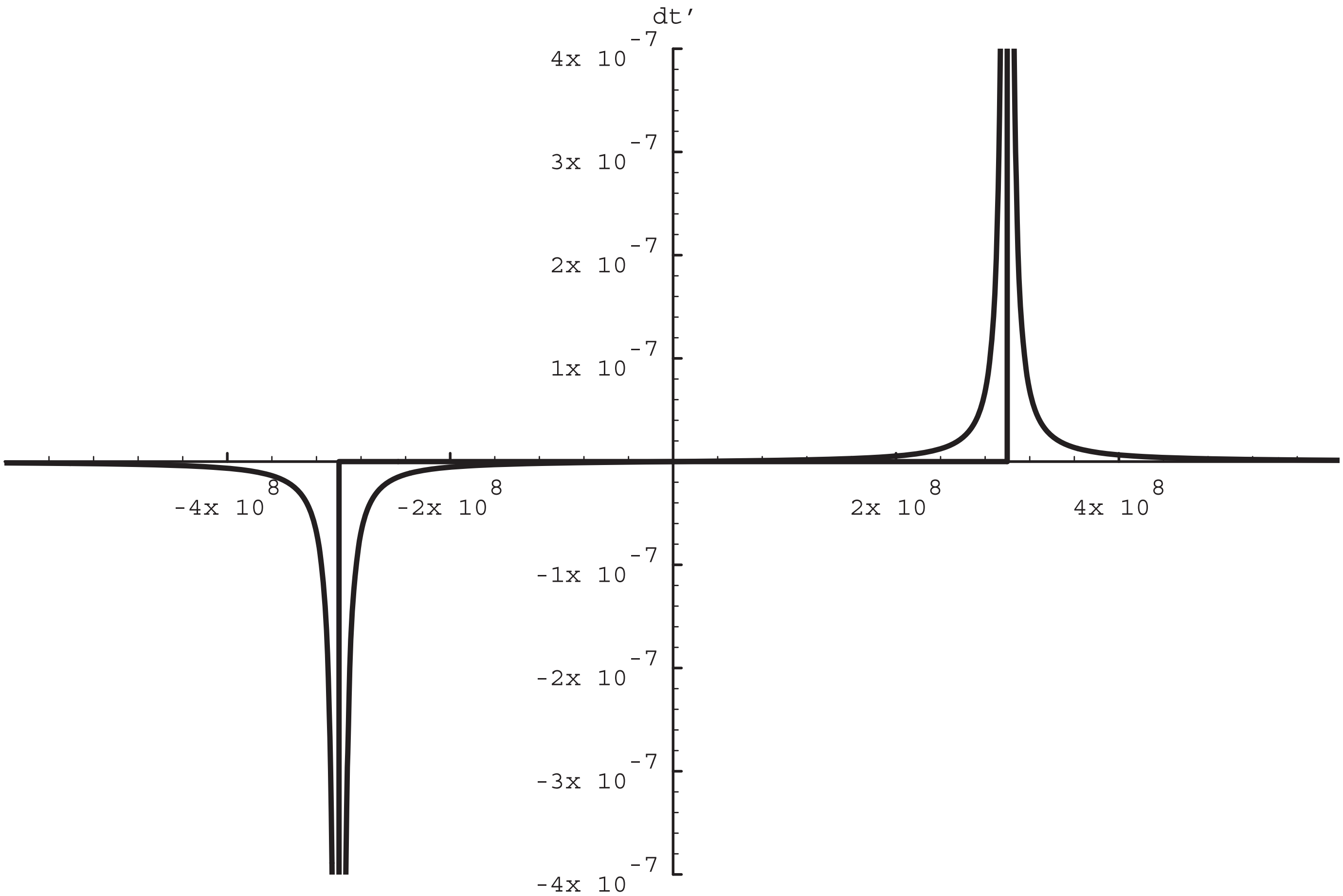

```
"Derivative of Gravitational Singly Energy Curve - Fig.2i"

Z=2.998*10^8
Plot[{(-X)/(((1 - X^2/Z^2)^(-1))^(1/2)*
(1 - X^2/Z^2)^2*Z^2),Im[(-X)/(((1 - X^2/Z^2)^
(-1))^(1/2)*(1 - X^2/Z^2)^2*Z^2)]},{X,-2Z,2Z},
Axes->True,PlotPoints->1000,PlotRange->{{-2Z,2Z},
{-.0000004,.0000004}},AxesLabel->{"dx","dt'"}]
```

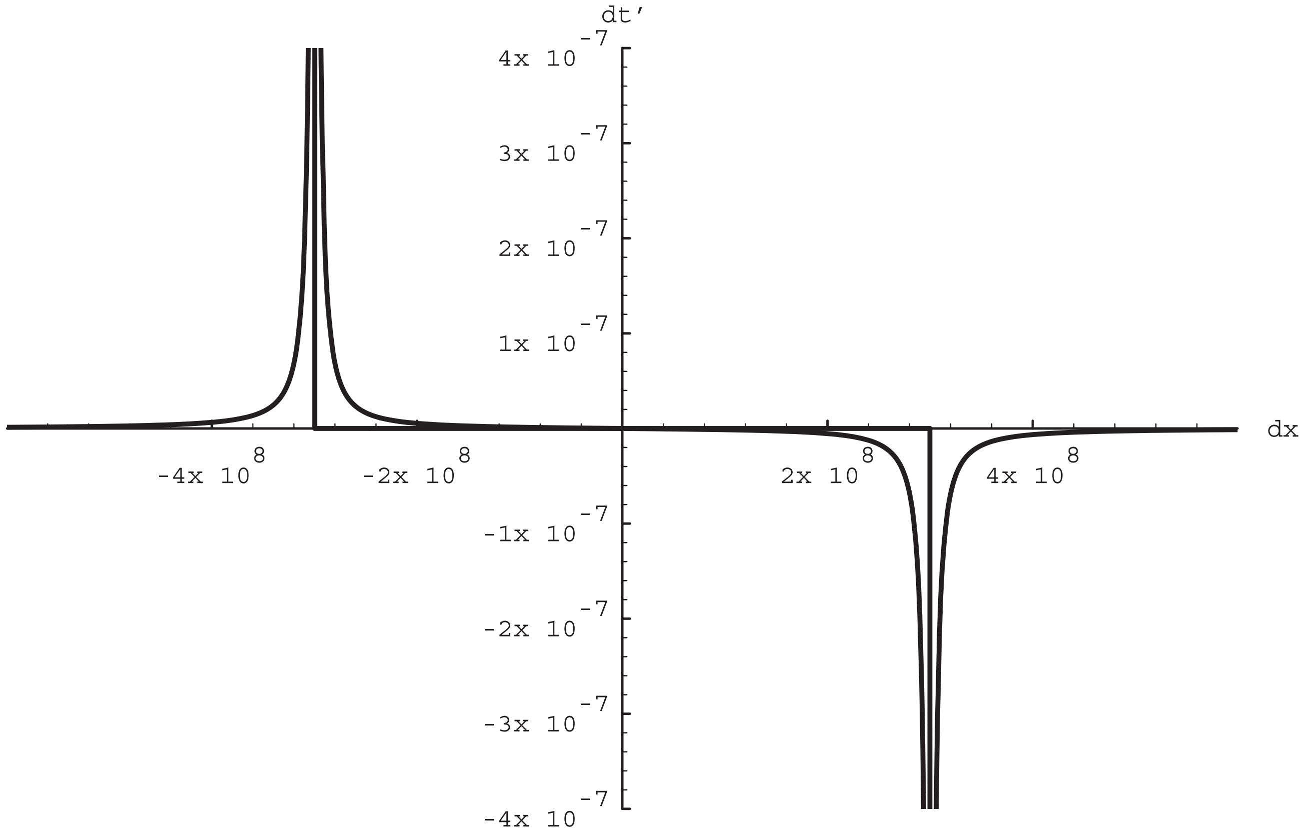

```
"Overlay of Derivatives of Inertial and
Gravitatioinal Singly Energy Curves - Fig. 2j"


Z=2.998*10^8
Plot[{(X)/(((1 - X^2/Z^2)^(-1))^(1/2)*
(1 - X^2/Z^2)^2*Z^2),Im[(X)/(((1 - X^2/Z^2)^
(-1))^(1/2)*(1 - X^2/Z^2)^2*Z^2)],(-X)/
(((1 - X^2/Z^2)^(-1))^(1/2)*(1 - X^2/Z^2)^2*
Z^2),Im[(-X)/(((1 - X^2/Z^2)^(-1))^(1/2)*
(1 - X^2/Z^2)^2*Z^2)]},{X,-2Z,2Z},Axes->True,
PlotPoints->1000,PlotRange->{{-2Z,2Z},
{-.0000001,.0000001}},AxesLabel->{"dx","dt'"}]
```

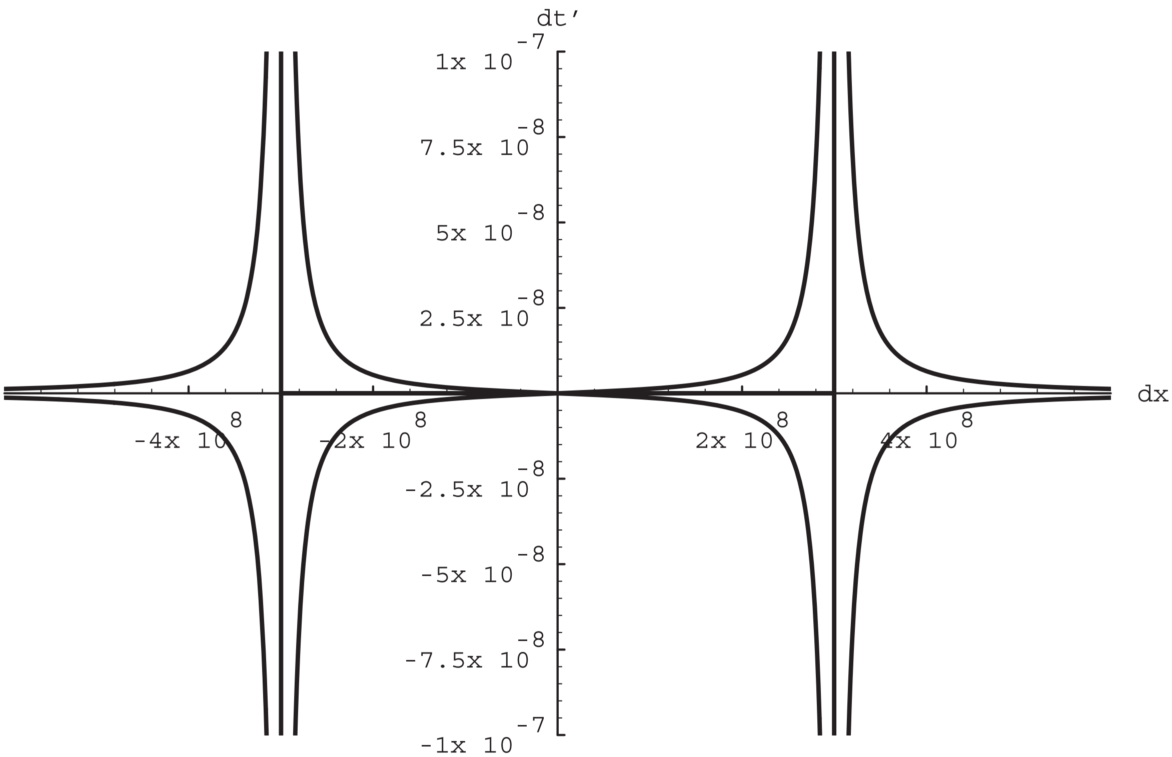

```
"Overlay of ET Inertial and Gravitational Singly Energy -
and Singly Time Warp Star - Fig. 2k"


Z=2.998*10^8
Plot[{-X/((Sqrt[1-X^2/Z^2])*Z^2),Im[-X/
((Sqrt[1-X^2/Z^2])*Z^2)],X/((Sqrt[1-X^2/Z^2])
*Z^2),Im[X/((Sqrt[1-X^2/Z^2])*Z^2)],
(X)/(((1 - X^2/Z^2)^(-1))^(1/2)*
(1 - X^2/Z^2)^2*Z^2),Im[(X)/(((1 - X^2/Z^2)^
(-1))^(1/2)*(1 - X^2/Z^2)^2*Z^2)],(-X)/
(((1 - X^2/Z^2)^(-1))^(1/2)*(1 - X^2/Z^2)^2*
Z^2),Im[(-X)/(((1 - X^2/Z^2)^(-1))^(1/2)*
(1 - X^2/Z^2)^2*Z^2)]},{X,-2Z,2Z},Axes->True,
PlotPoints->1000,PlotRange->{{-2Z,2Z},
{-.0000001,.0000001}},AxesLabel->{"dx","dt'"}]
```

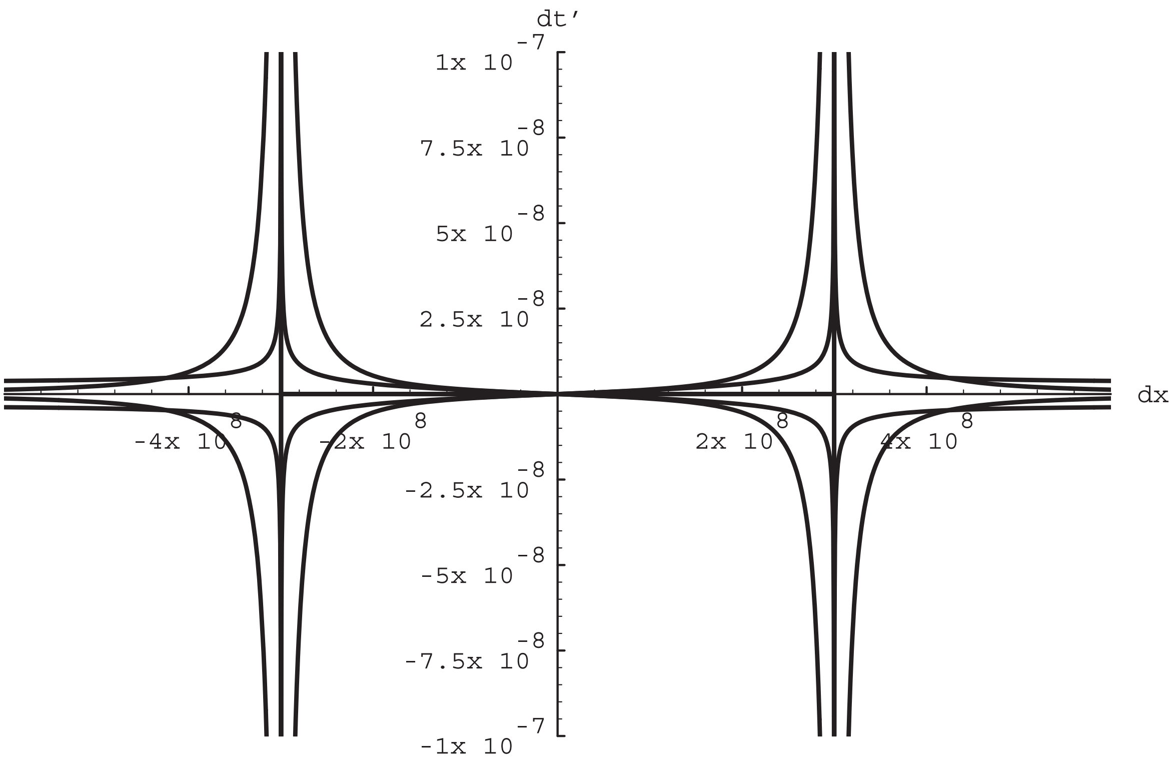

"SuperOrigin Graph of Derivatives of Inertial and Gravitatioinal Energy Curves - Fig. 2ki"

```
Z=2.998*10^8
Plot[{(X)/(((1 - X^2/Z^2)^(-1))^(1/2)*
(1 - X^2/Z^2)^2*Z^2),Im[(X)/(((1 - X^2/Z^2)^
(-1))^(1/2)*(1 - X^2/Z^2)^2*Z^2)],(-X)/
(((1 - X^2/Z^2)^(-1))^(1/2)*(1 - X^2/Z^2)^2*
Z^2),Im[(-X)/(((1 - X^2/Z^2)^(-1))^(1/2)*
(1 - X^2/Z^2)^2*Z^2)]},{X,-2Z,2Z},Axes->True,
PlotPoints->1000,PlotRange->{{-2Z,2Z},
{-.00000066,.00000066}},AxesLabel->{"dx","dt'"}]
```

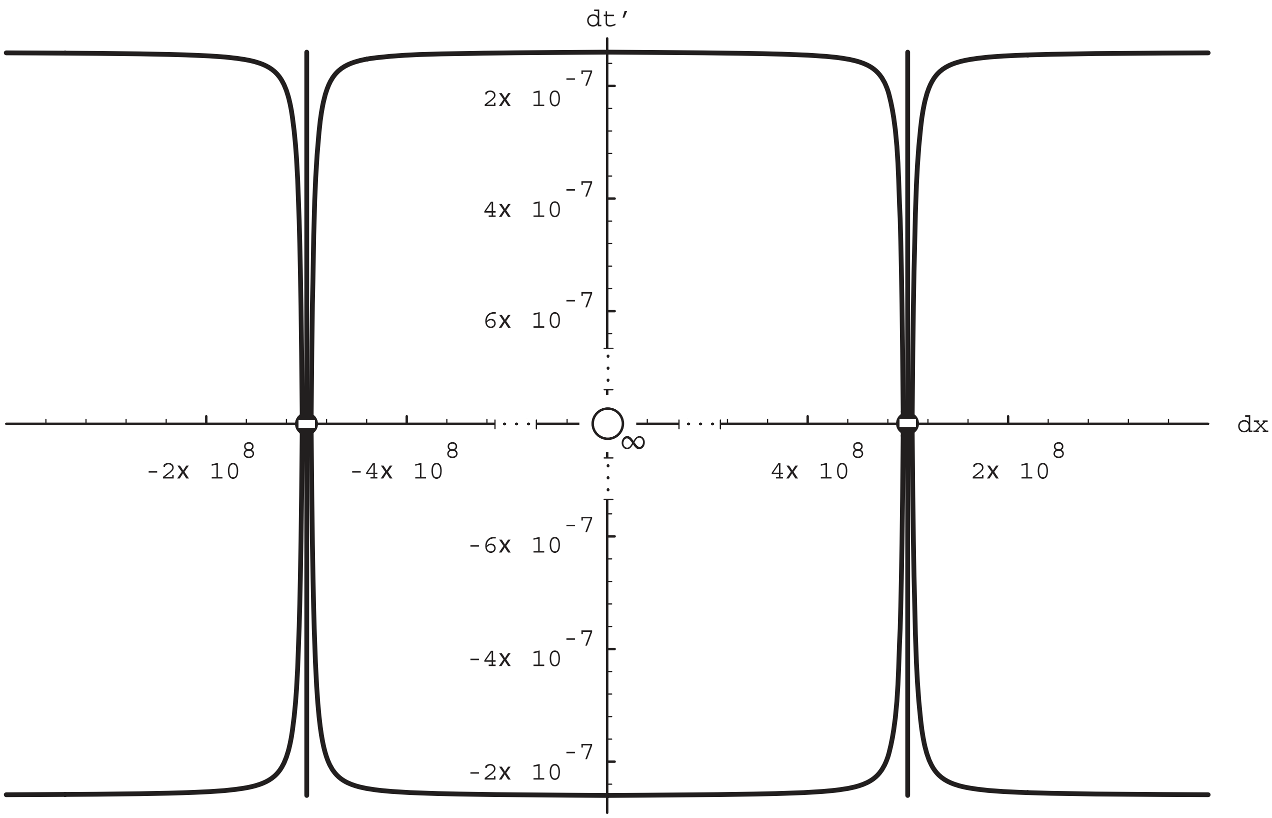

```
"Inertial Energy Curve - Inertial Time Warp
 Composite Fig.2l"

Z=2.998*10^8
Plot[{(-X)/(((1 - X^2/Z^2)^(-1))^(1/2)*
(1 - X^2/Z^2)^2*Z^2),Im[(-X)/(((1 - X^2/Z^2)^
(-1))^(1/2)*(1 - x^2/z^2)^2*z^2)],
X/((Sqrt[1-X^2/Z^2])*Z^2),
Im[X/((Sqrt[1-X^2/Z^2])*Z^2)]},
{X,-2Z,2Z},Axes->True,PlotPoints->
1000,PlotRange->{{-2Z,2Z},
{-.0000001,.0000001}},AxesLabel->
{"dx","dt'"}]
```

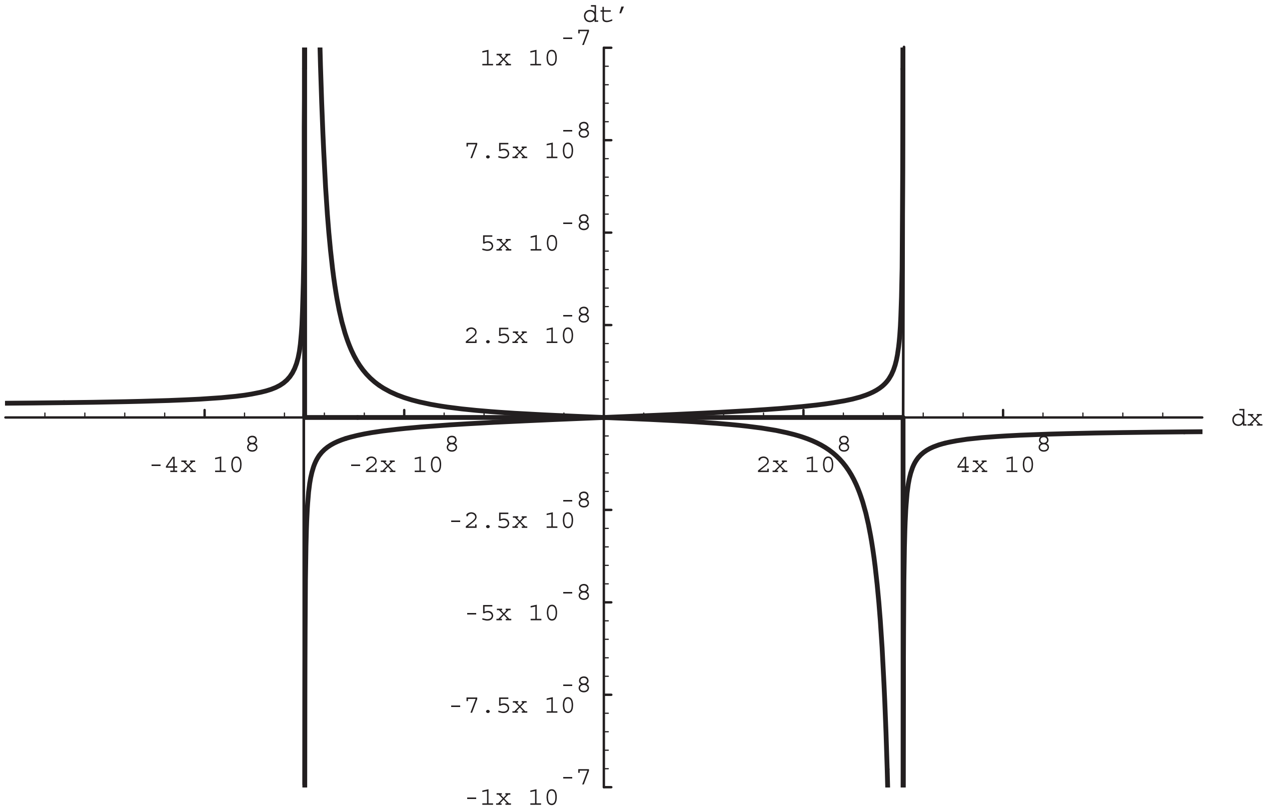

```
"Fig. 2m - Gravitational Energy Curve - Gravitational
Time Warp Composite"

Z=2.998*10^8
Plot[{-X/((Sqrt[1-X^2/Z^2])*Z^2),Im[-X/((Sqrt
[1-X^2/Z^2])*Z^2)],(X)/(((1 - X^2/Z^2)^(-1))^(1/2)*
(1 - X^2/Z^2)^2*Z^2),Im[(X)/(((1 - X^2/Z^2)^
(-1))^(1/2)*(1 - X^2/Z^2)^2*Z^2)]},{X,-2Z,2Z},
Axes->True,PlotPoints->1000,PlotRange->{{-2Z,2Z},
{-.0000001,.0000001}},AxesLabel->{"dx","dt'"}]
```

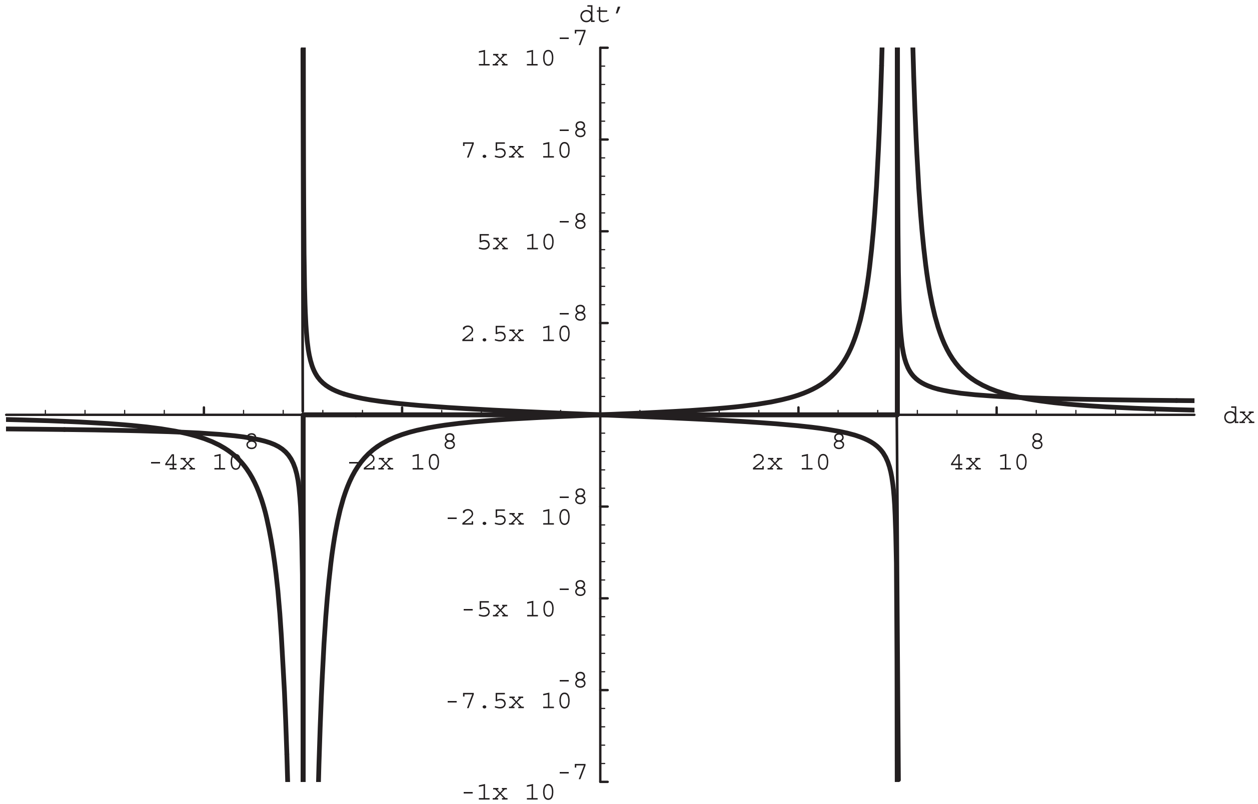

```
"Fig. 2n. Doubly Warp Factor - Singly Warp Factor Complex"

Z=2.9985*10^8
Plot[{1/(1-X^2/Z^2),Im[1/(1-X^2/Z^2)],
Sqrt[(1-X^2/Z^2)],Im[Sqrt[(1-X^2/Z^2)]]},
{X,-7Z,7Z},Axes->True,PlotPoints->1000,
PlotRange->{{-7Z,7Z},{-4.0,4.0}},
AxesLabel->{"dx","dt'"}]
```

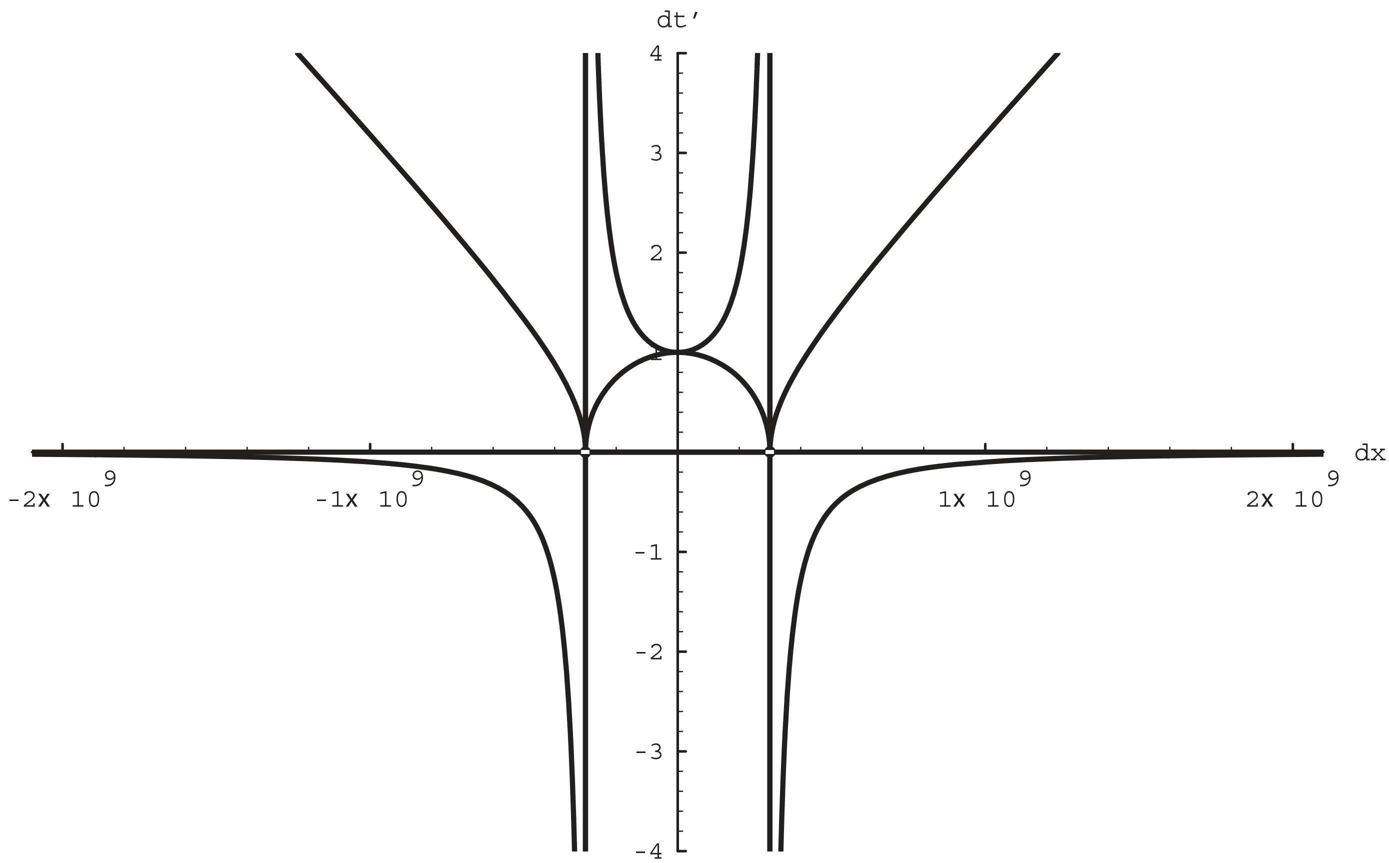

"Fig. 2o. Singly Gravity Warp Factor with Doubly Warp Factor Complex"

```
Z=2.9985*10^8
Plot[{-1/(1-X^2/Z^2),Im[-1/(1-X^2/Z^2)],
-Sqrt[(1-X^2/Z^2)],Im[-Sqrt[(1-X^2/Z^2)]]},
{X,-7Z,7Z},Axes->True,PlotPoints->1000,
PlotRange->{{-7Z,7Z},{-4.0,4.0}},
AxesLabel->{"dx","dt'"}]
```

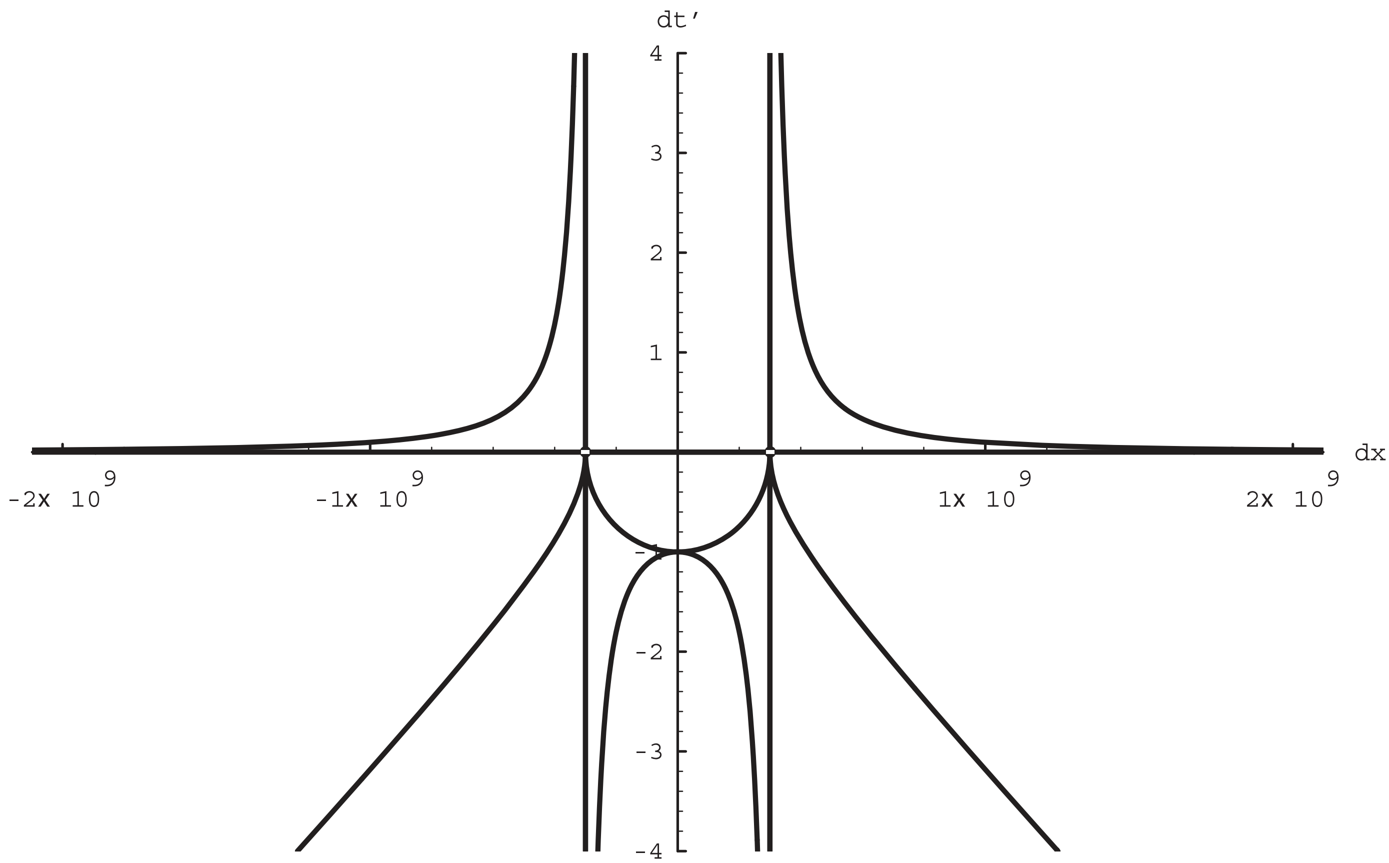

```
"Fig. 2p. Doubly Gravitational Energy Factor
          with Singly Energy Factor Complex"

Z=2.9985*10^8
Plot[{1/(1-X^2/Z^2),Im[1/(1-X^2/Z^2)],
Sqrt[(1-X^2/Z^2)],Im[Sqrt[(1-X^2/Z^2)]],
-1/(1-X^2/Z^2),Im[-1/(1-X^2/Z^2)],
-Sqrt[(1-X^2/Z^2)],Im[-Sqrt[(1-X^2/Z^2)]]},
{X,-7Z,7Z},Axes->True,PlotPoints->1000,
PlotRange->{{-7Z,7Z},{-4.0,4.0}},
AxesLabel->{"dx","dt'"}]
```

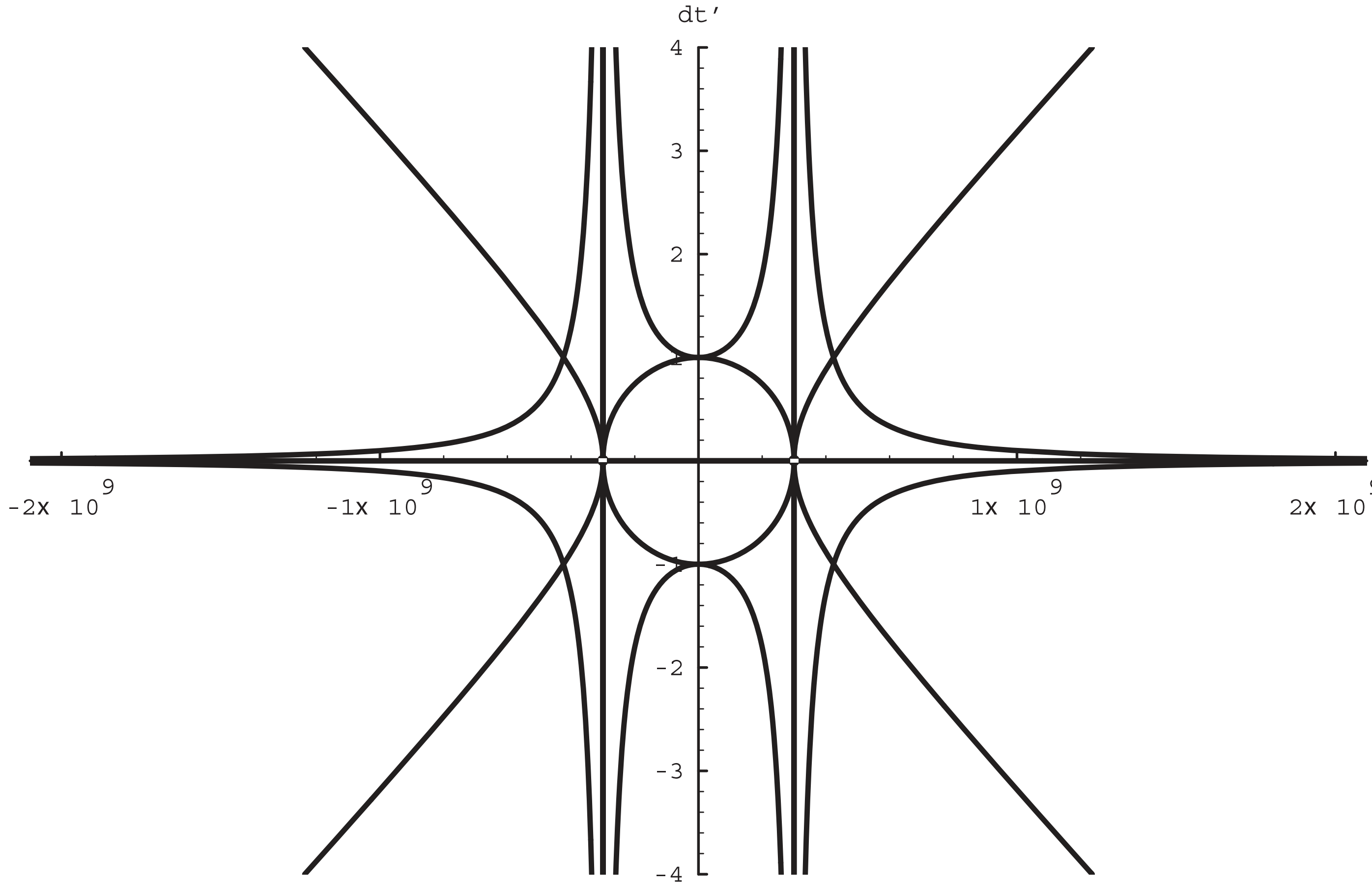

```
"Fig. 2q. Rest Energy Warp Factor"

Z=2.9985*10^8
Plot[{(1-X^2/Z^2)/(1-X^2/Z^2),Im[(1-X^2/Z^2)/(1-X^2/Z^2)],
(1-X^2/Z^2)/(1-X^2/Z^2),Im[(1-X^2/Z^2)/(1-X^2/Z^2)]},
{X,-7Z,7Z},Axes->True,PlotPoints->1000,
PlotRange->{{-7Z,7Z},{-4.0,4.0}},
AxesLabel->{"dx","dt'"}]
```

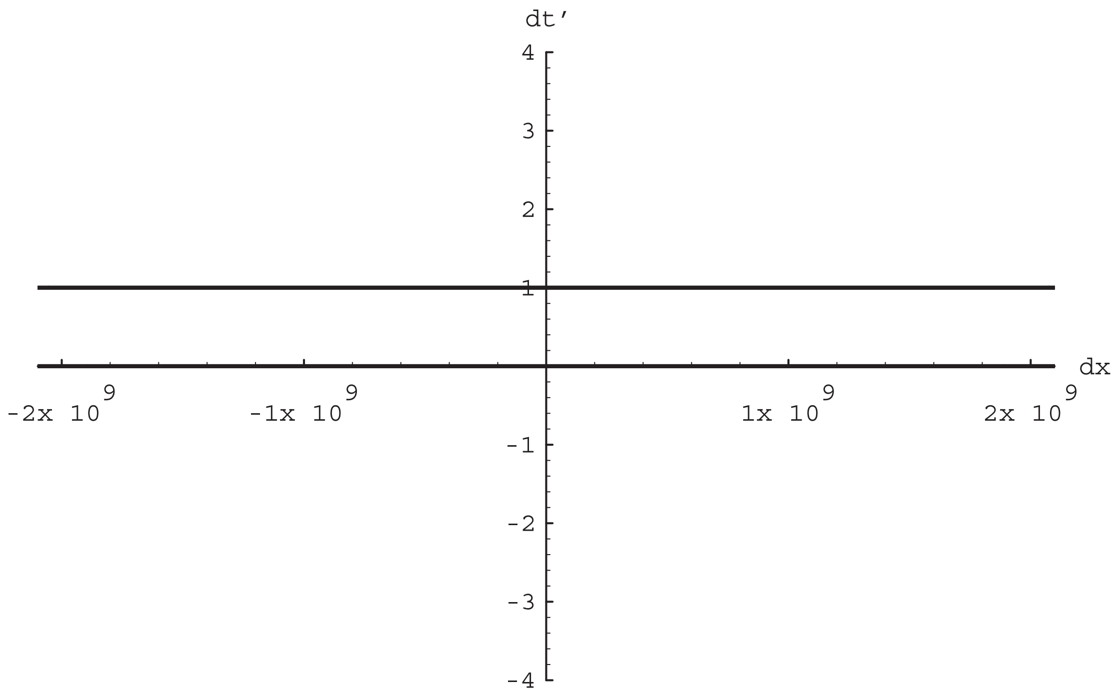

```
"Fig. 2r. Remainder Gravitational P.E. Singly &
          Doubly Lambda Factor Complex Overlay"

Z=2.9985*10^8
Plot[{-1/2*(1-X^2/Z^2),Im[-1/2*(1-X^2/Z^2)],
-1/2*Sqrt[(1-X^2/Z^2)],Im[-1/2*Sqrt[(1-X^2/Z^2)]]},
{X,-7Z,7Z},Axes->True,PlotPoints->1000,
PlotRange->{{-7Z,7Z},{-4.0,4.0}},
AxesLabel->{"dx","dt'"}]
```

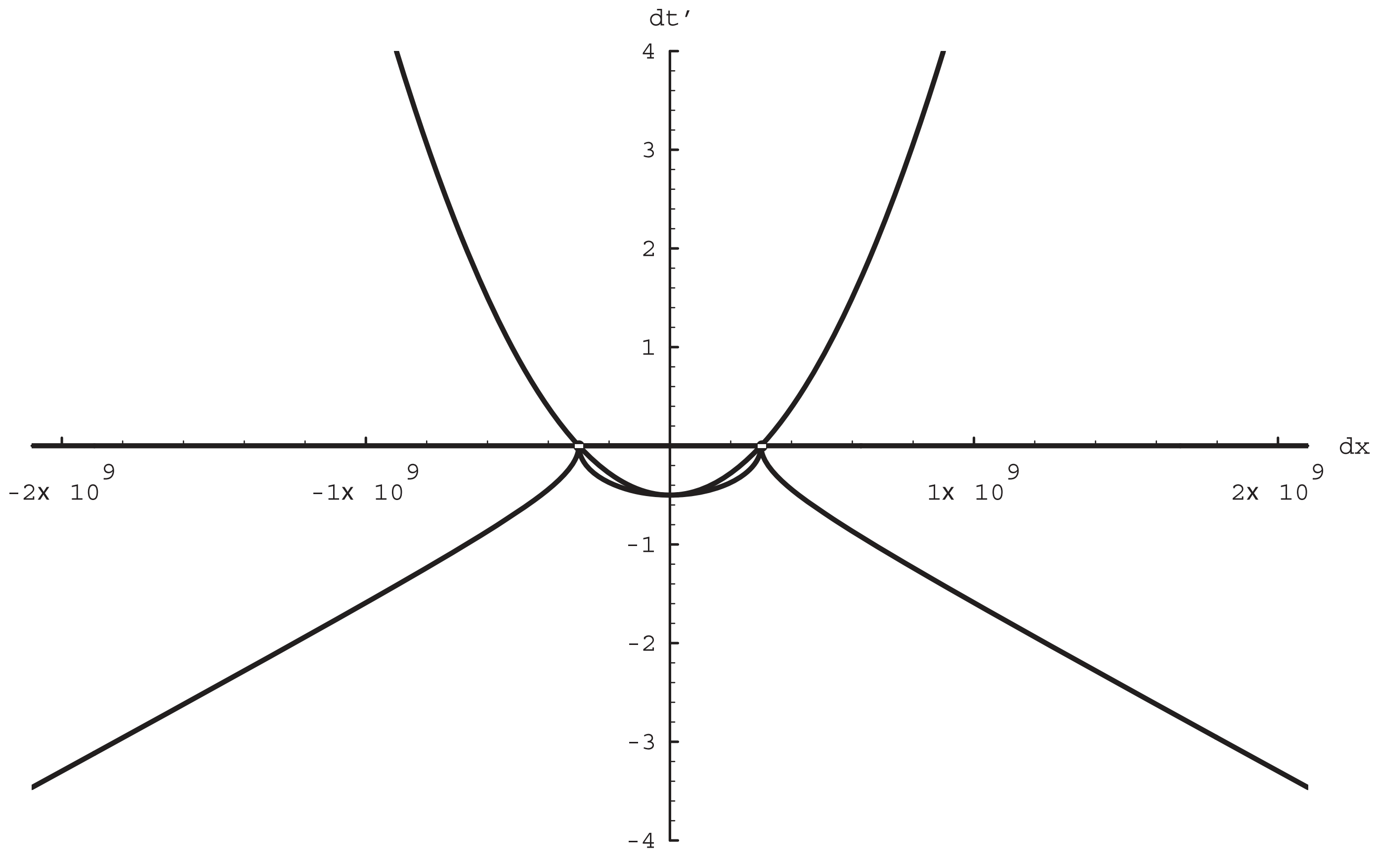

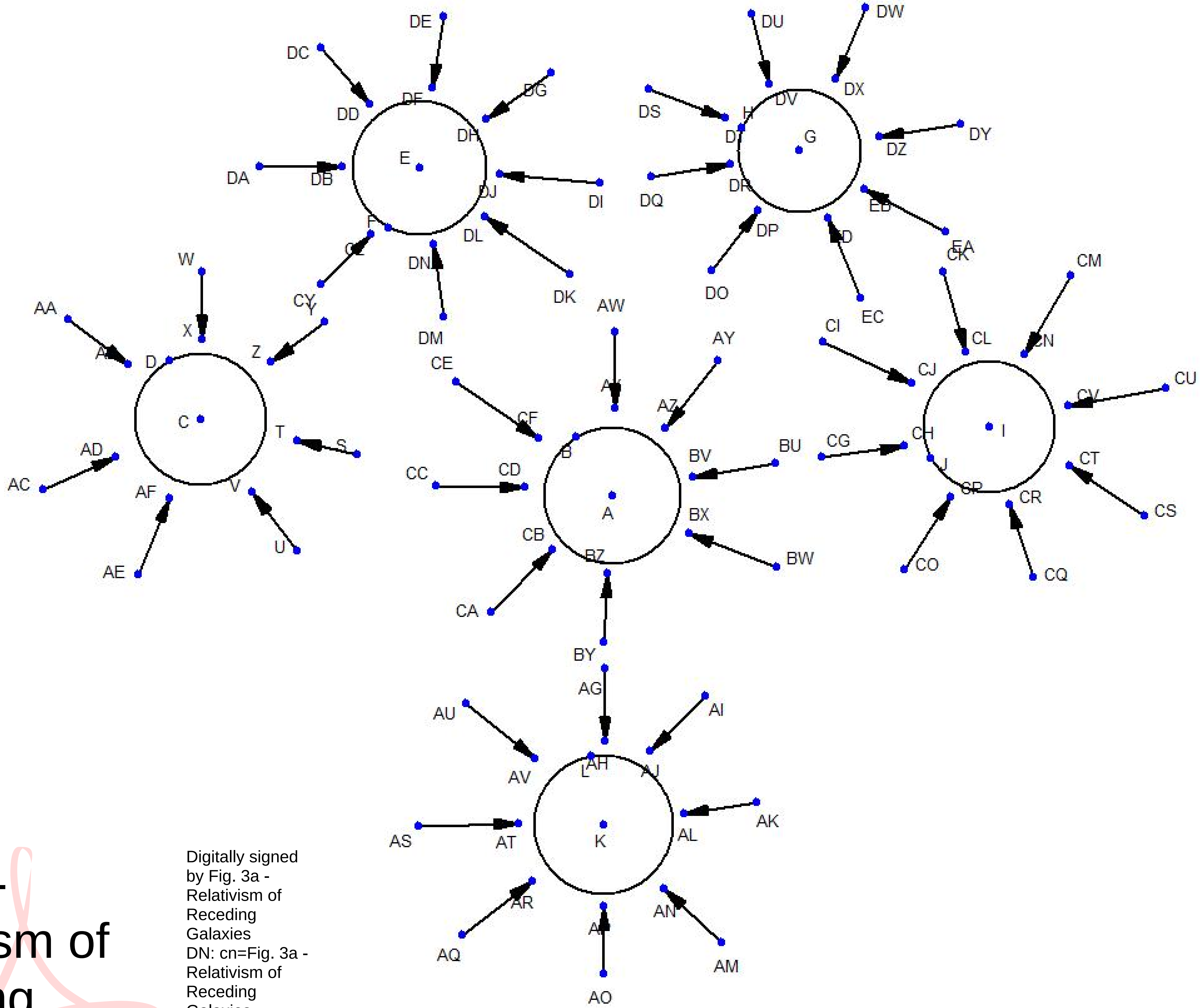

Fig. 3a - Relativism of Receding Galaxies

Signature Valid

Digitally signed by Fig. 3a - Relativism of Receding Galaxies
DN: cn=Fig. 3a - Relativism of Receding Galaxies, o=UCSD, c=US
Date: 2009.05.07 17:04:32 -07'00'

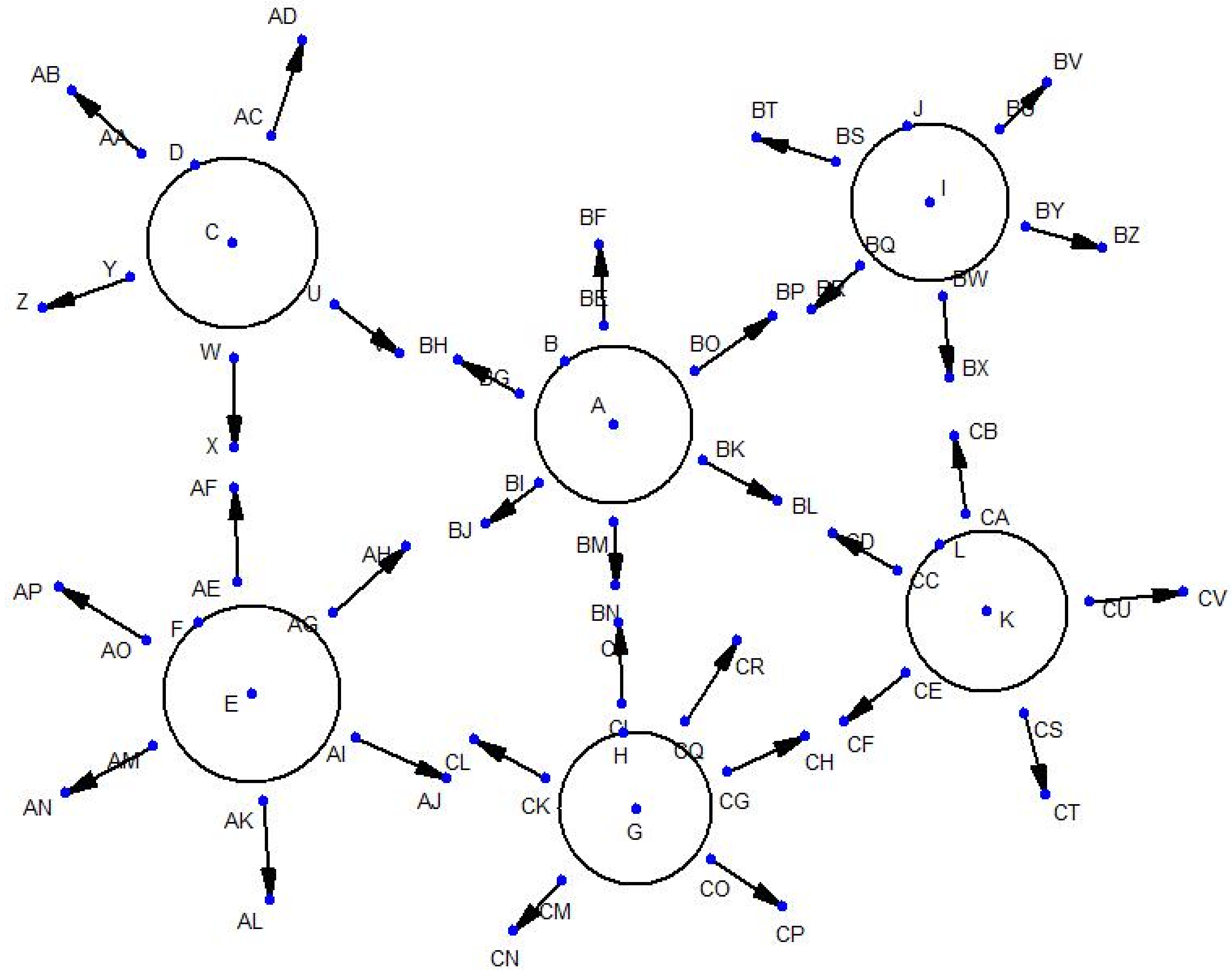
A B C D E F G H I J K L
AA AB AC AD AE AF AG AH AI AJ AK AL AM AN AO AP
BE BF BG BH BI BJ BK BL BM BN BO BP BQ BS BT BU BV BW BX BY BZ
CA CB CC CD CE CF CG CH CI CK CL CM CN CO CP CQ CR CS CT CU CV
U W X Y Z

Figure 4. - Temporal Conservation - Time

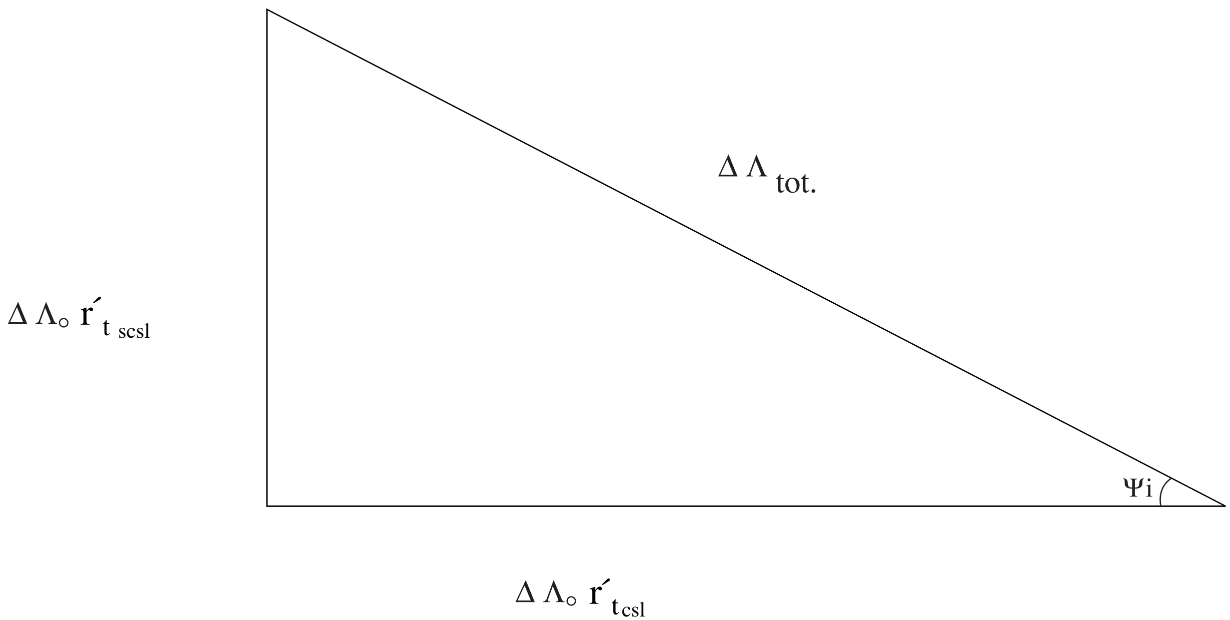

Figure 4a. - Temporal Conservation - Span.

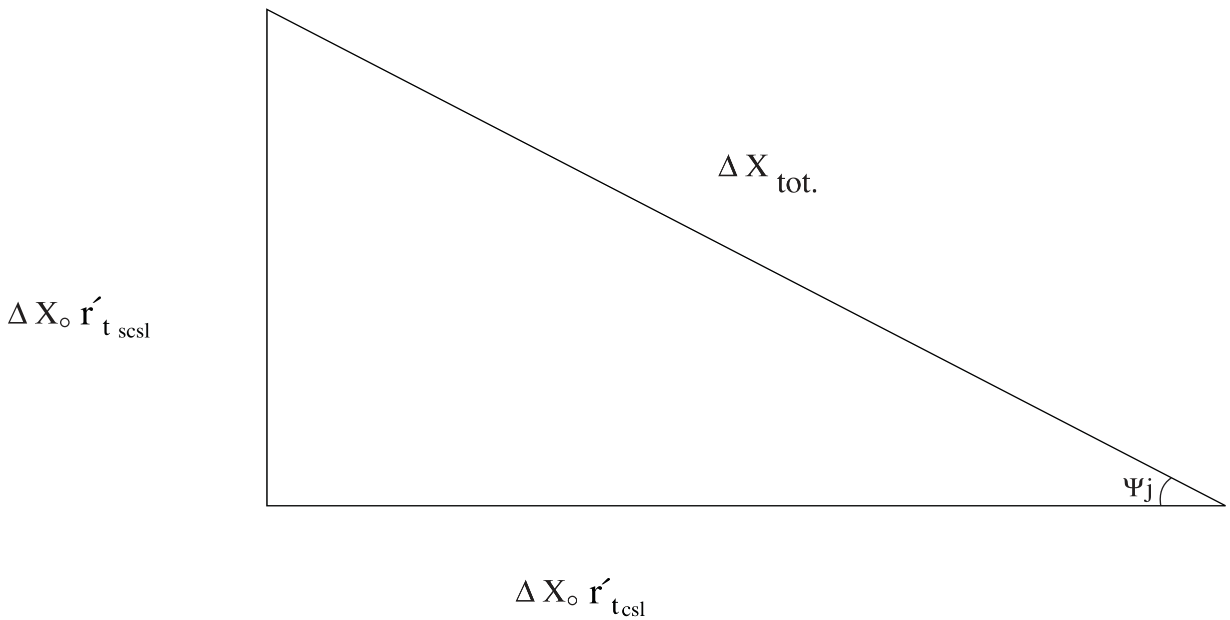

Figure 4b. - Total Temporally Relativised Energy

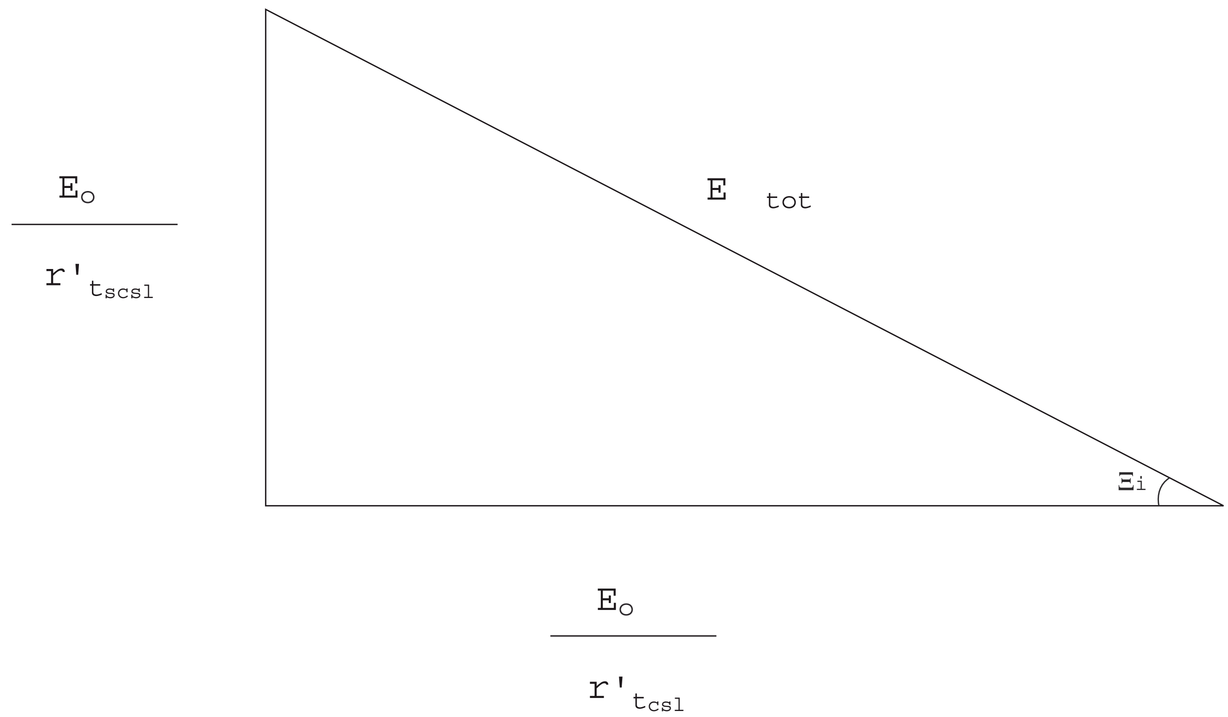

Figure 4c. - Total Temporally Relativised Momentum

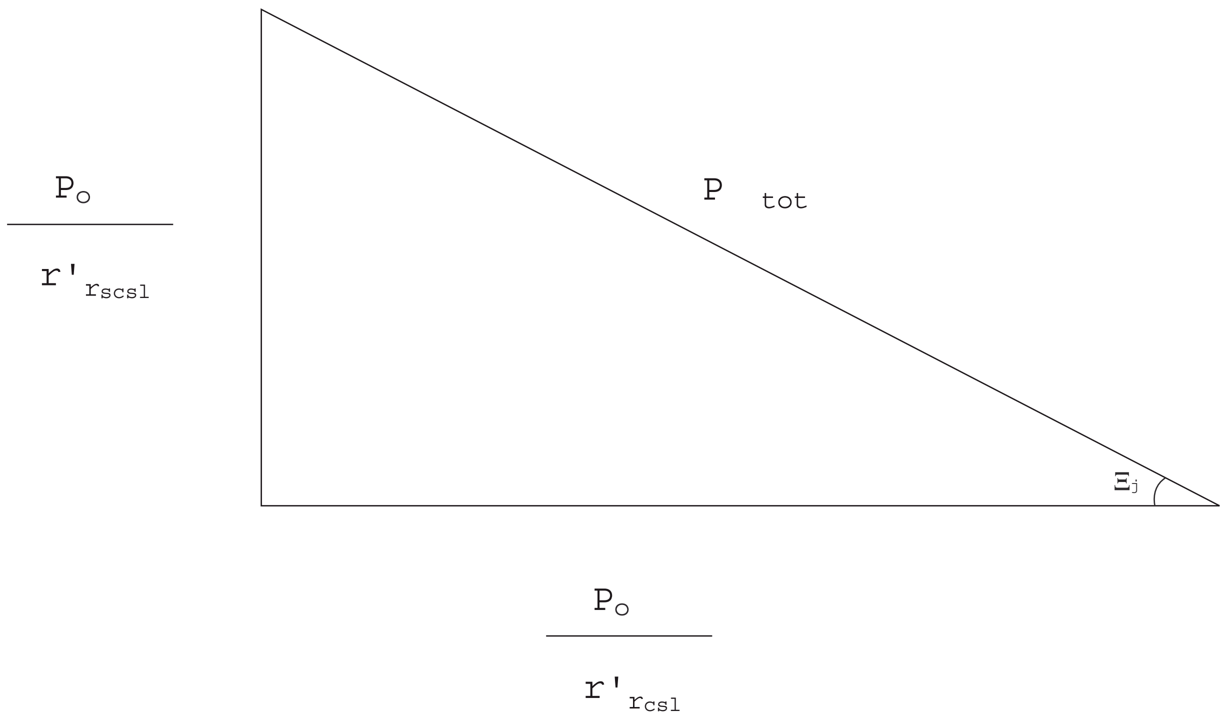

Signature Valid

Fig. 5a. Time-Warp Engine (Side Pull)

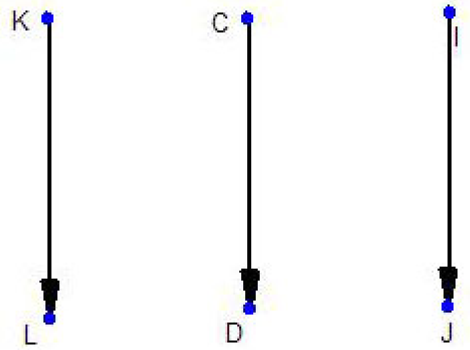

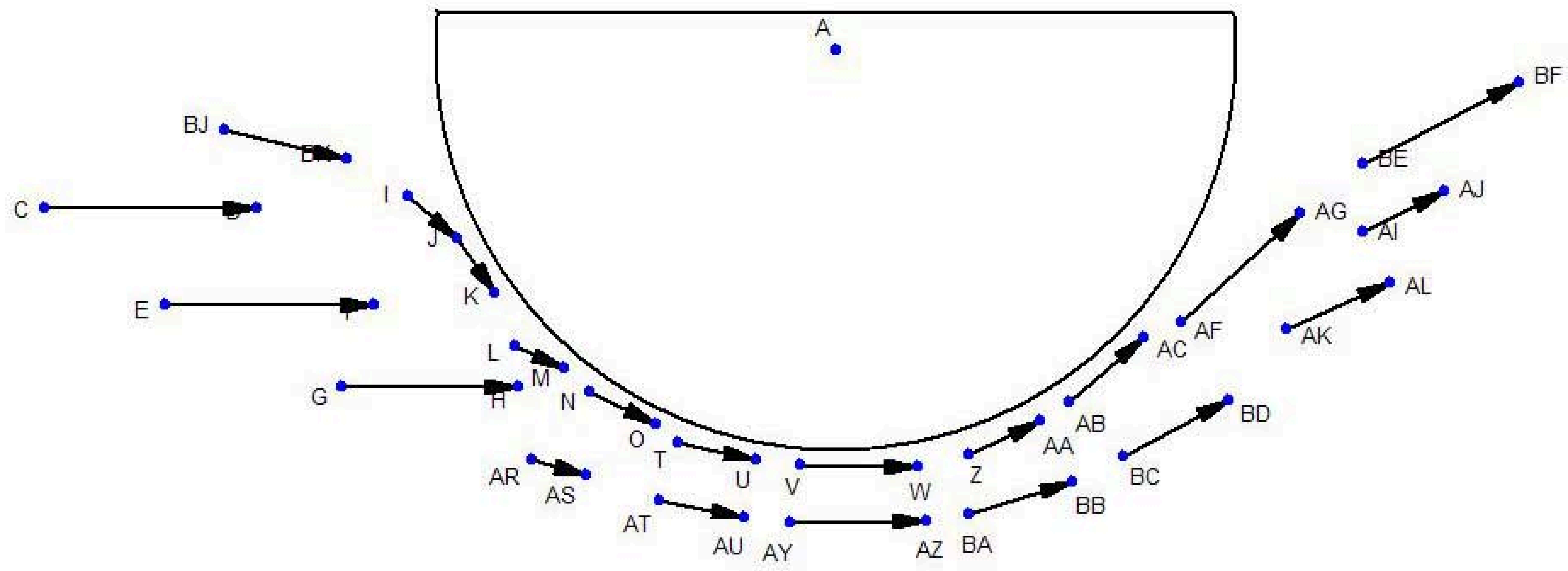
A
BJ
BK
C
D
I
J
K
E
F
L
M
G
H
N
O
T
U
V
W
AR
AS
AT
AU
AY
AZ
BA
BB
Z
AA
AB
AC
AF
AG
AI
AJ
AK
AL
BC
BD
BE
BF

Fig. 5b - Direct Push Time-Warp Foil

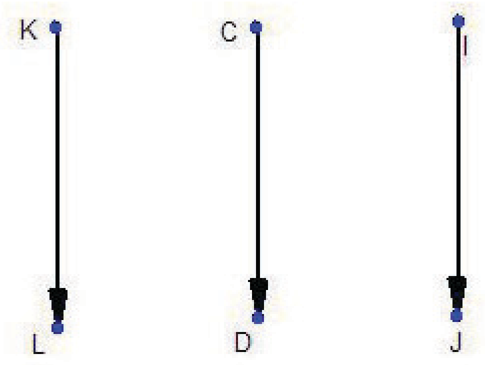

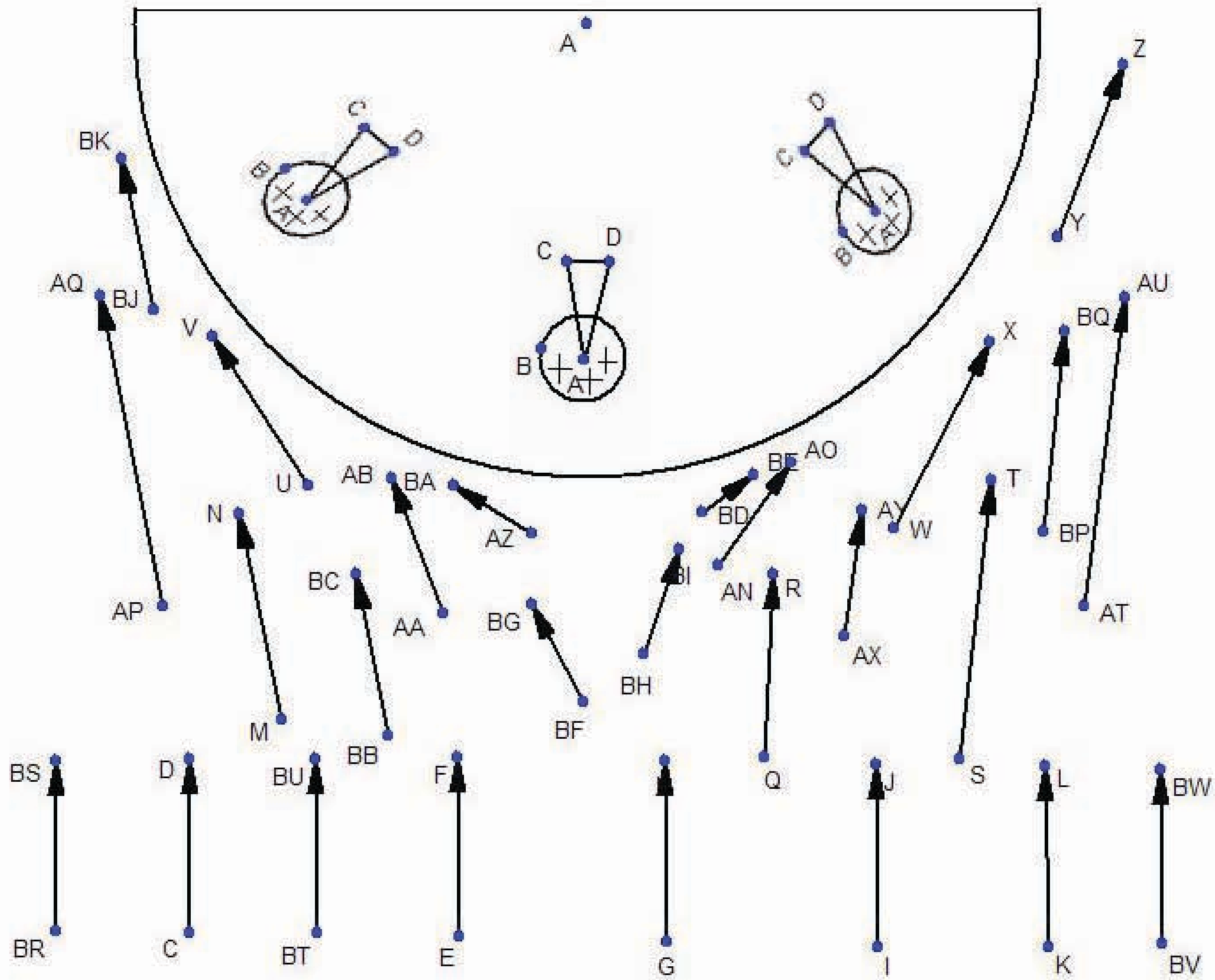

A
Z
BK
C
D
B
A
D
C
B
A
C
D
B
A
Y
AQ
BJ
V
AU
BQ
X
U
AB
BA
BE
AO
BD
N
AZ
AY
W
T
BP
BC
BI
AN
R
AP
AA
BG
AT
AX
BH
M
BB
BF
BS
D
BU
F
Q
J
S
L
BW
BR
C
BT
E
G
I
K
BV

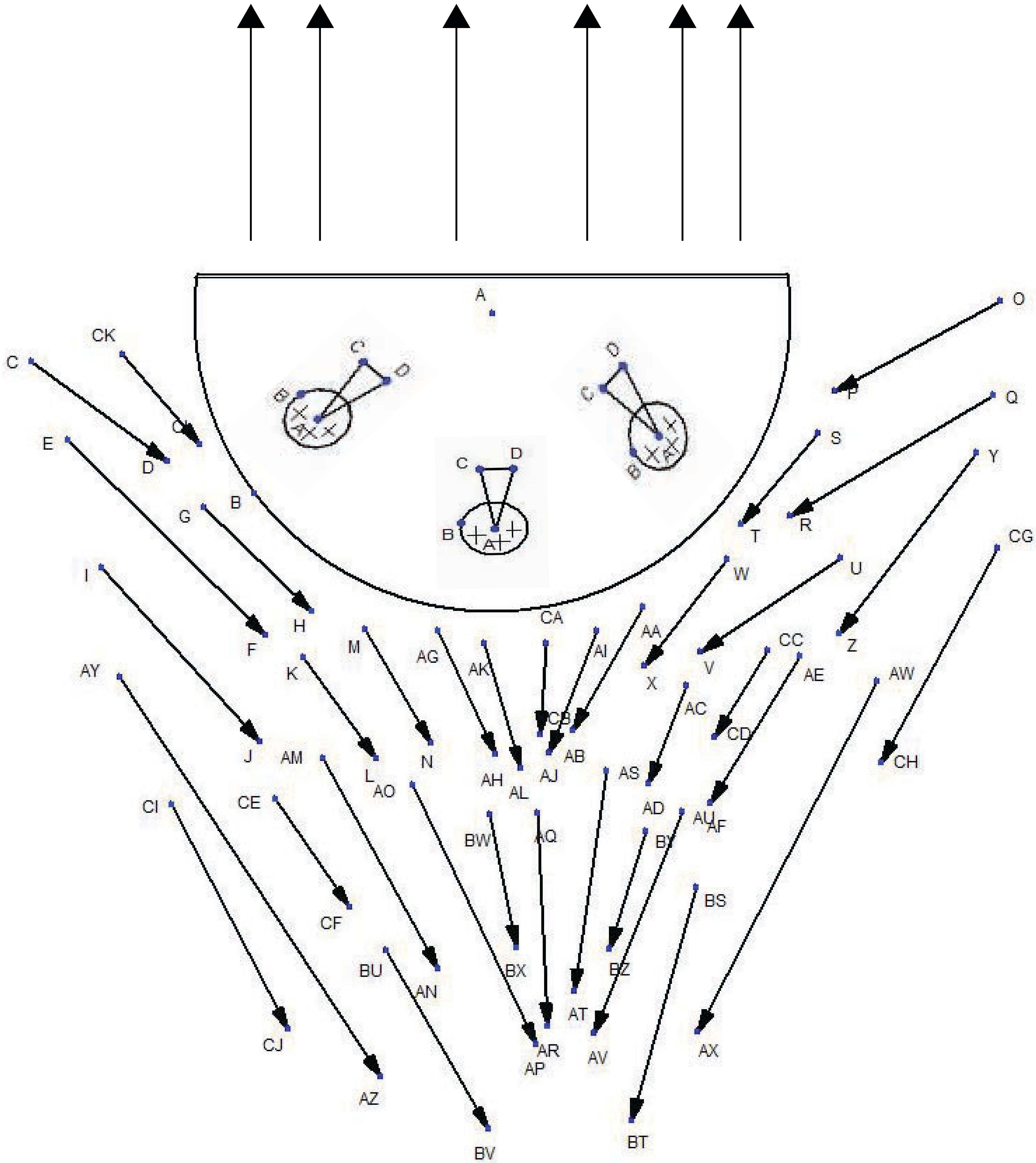

Fig. 5c - Direct Pull Time-Warp Foil

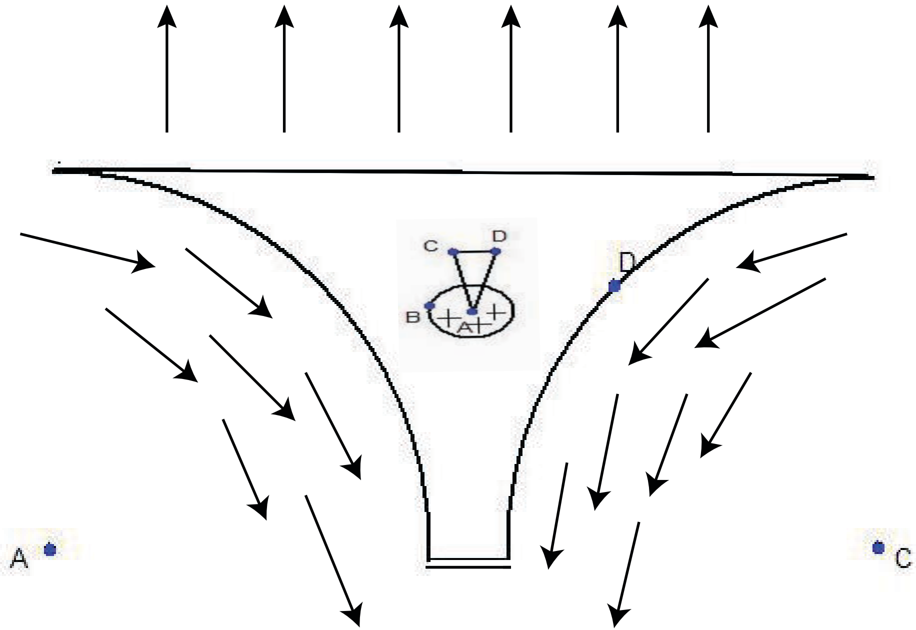

Fig. 5d. Time-Warp Engine (Direct- Pull)

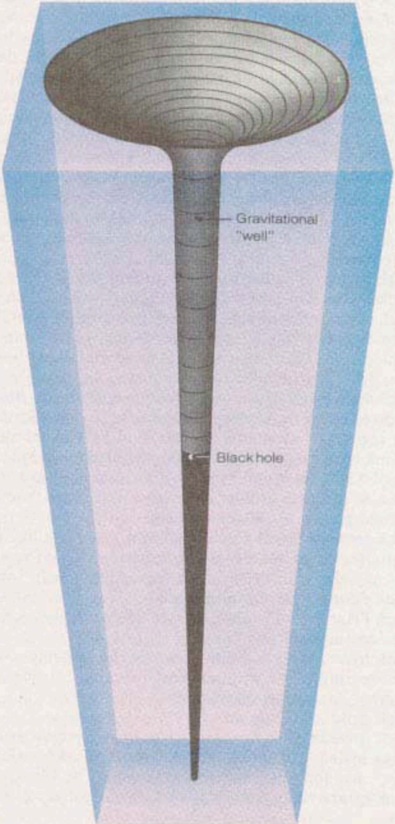
Gravitational "well"
Black hole

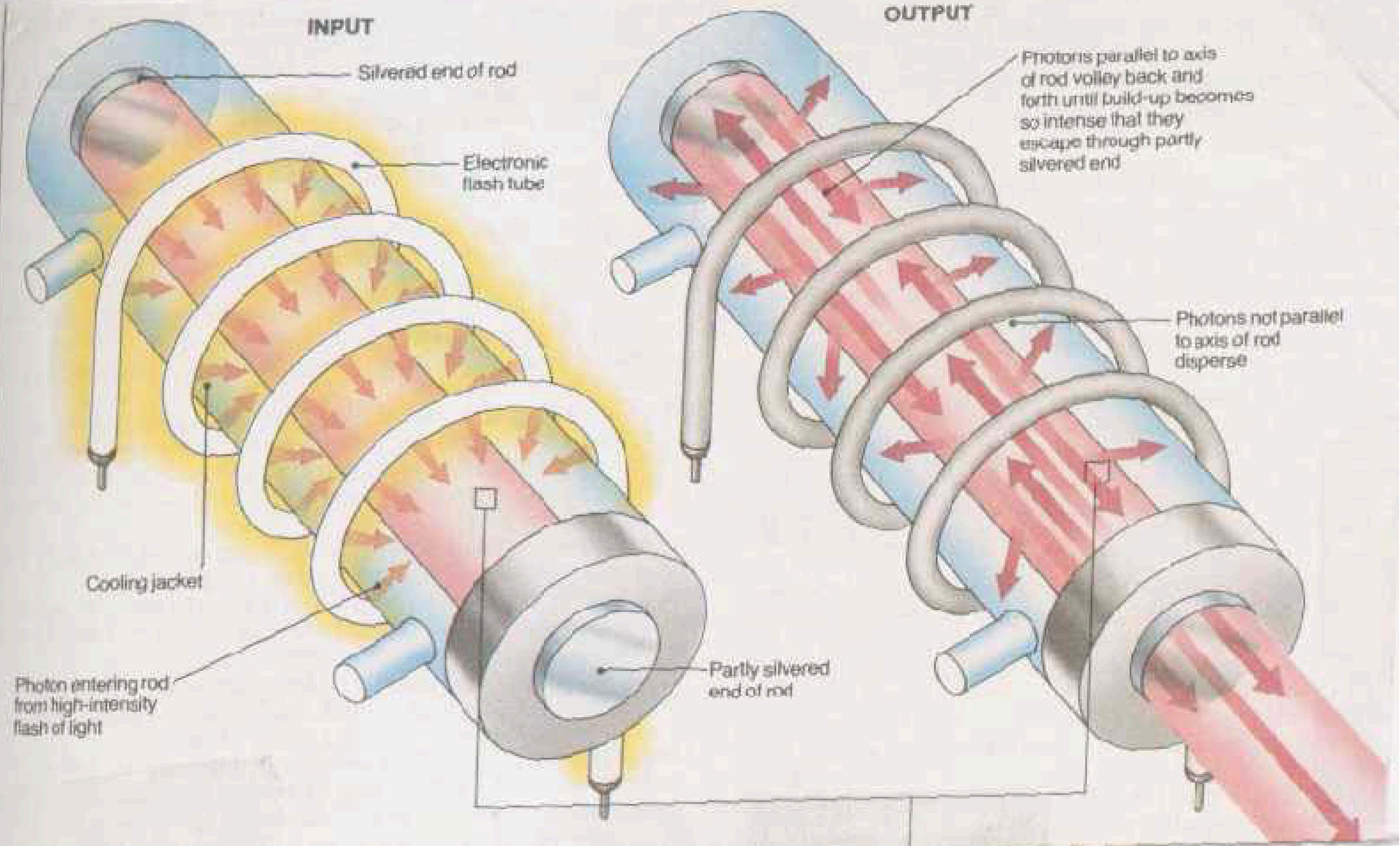
INPUT
OUTPUT
Silvered end of rod
Electronic flash tube
Cooling jacket
Photon entering rod from high-intensity flash of light
Partly silvered end of rod
Photons parallel to axis of rod volley back and forth until build-up becomes so intense that they escape through partly silvered end
Photons not parallel to axis of rod disperse

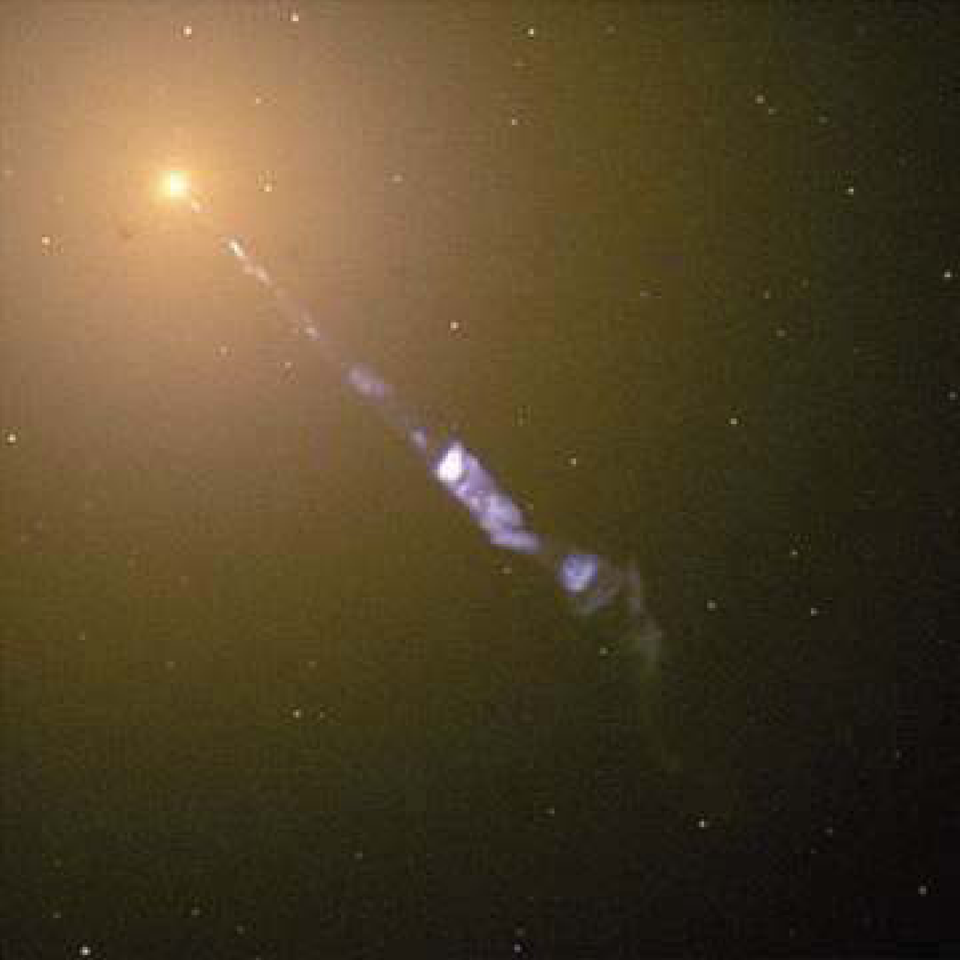


X-RAY / OPTICAL
EVOLUTION OF THE UNIVERSE (ILLUSTRATION)

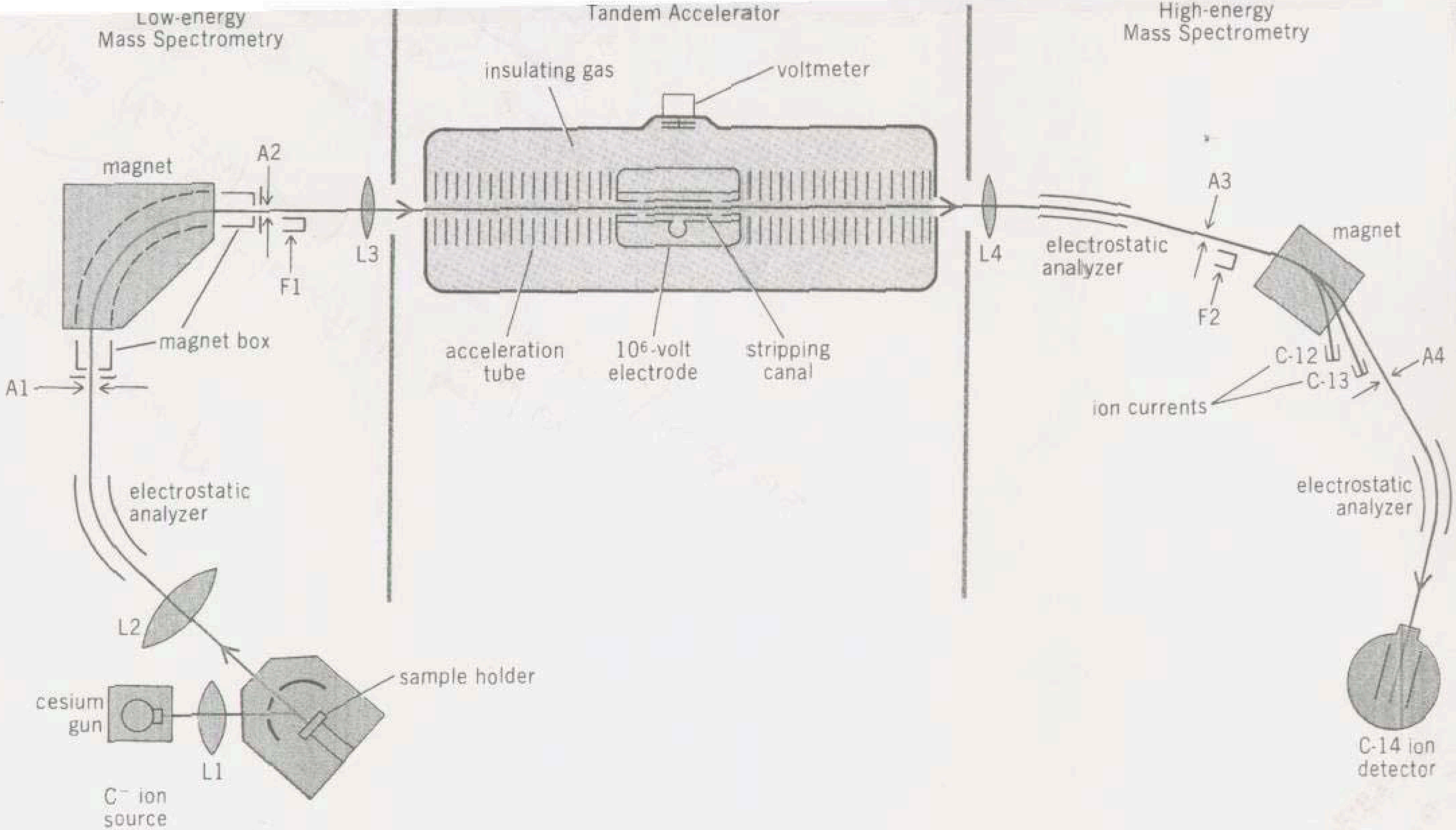

Simplified diagram of an accelerator mass spectrometer used for radiocarbon dating. The equipment is divided into three sections. Electric lenses L1–L4 are used to focus the ion beams. Apertures A1–A4 and charge collection cups F1 and F2 are used for setting up the equipment. The cesium ions from the gun create the negative ions of carbon at the surface of the sample.

Dies diei eructat uerb
Numerus
Mensura
Pondus
nocti indicat scientiam
Videbo Cælos tuos, opera digitor. tuor.
Non Inclinabitur in Sæculum Sæculi
Ponderibus librata suis
Erigor dum Corrigor
Cl. Ptolem.

Figure 6. Enneaspheral Multi-Thruster Array

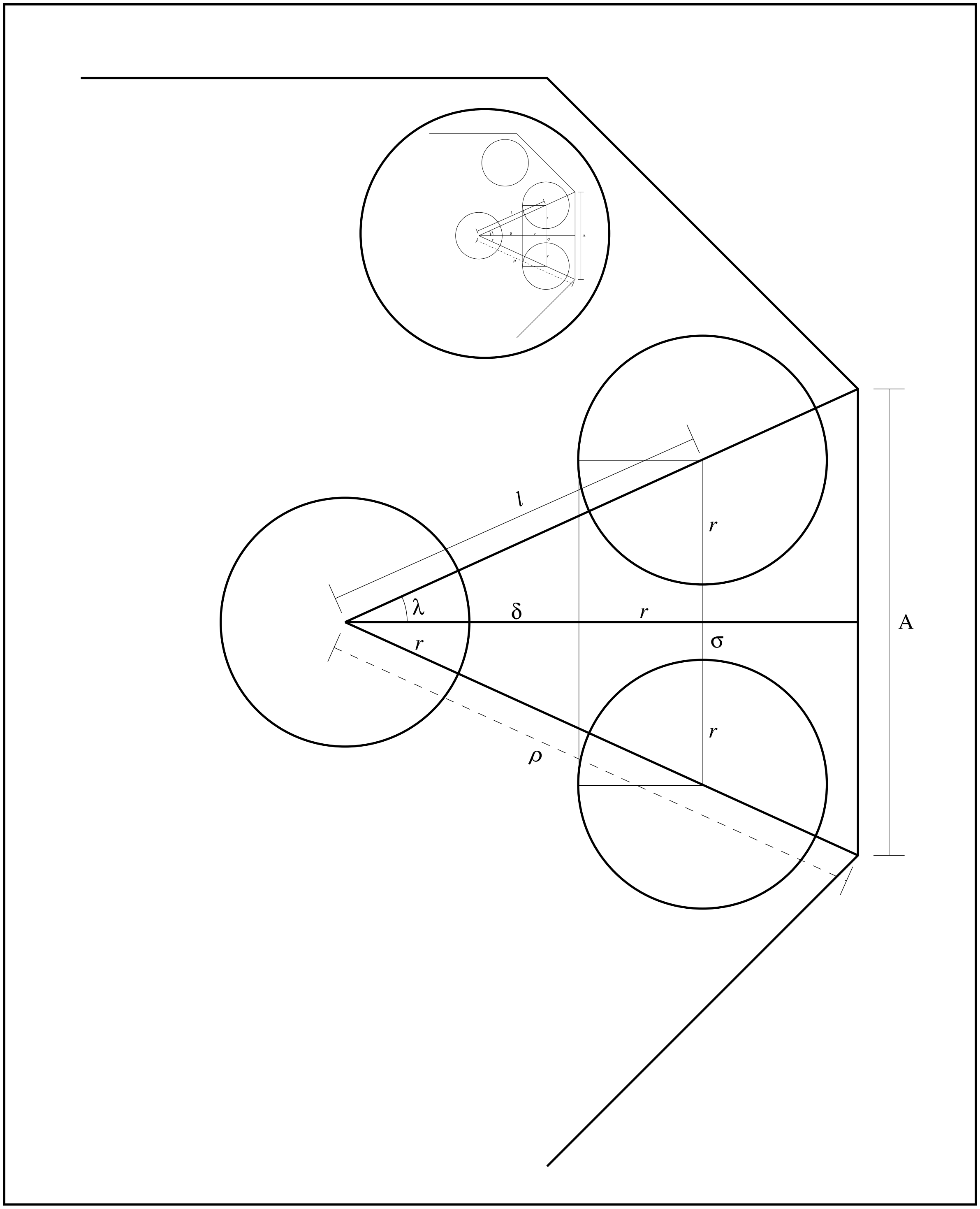

Figure 6a. Carbo-Myte Device-Array.

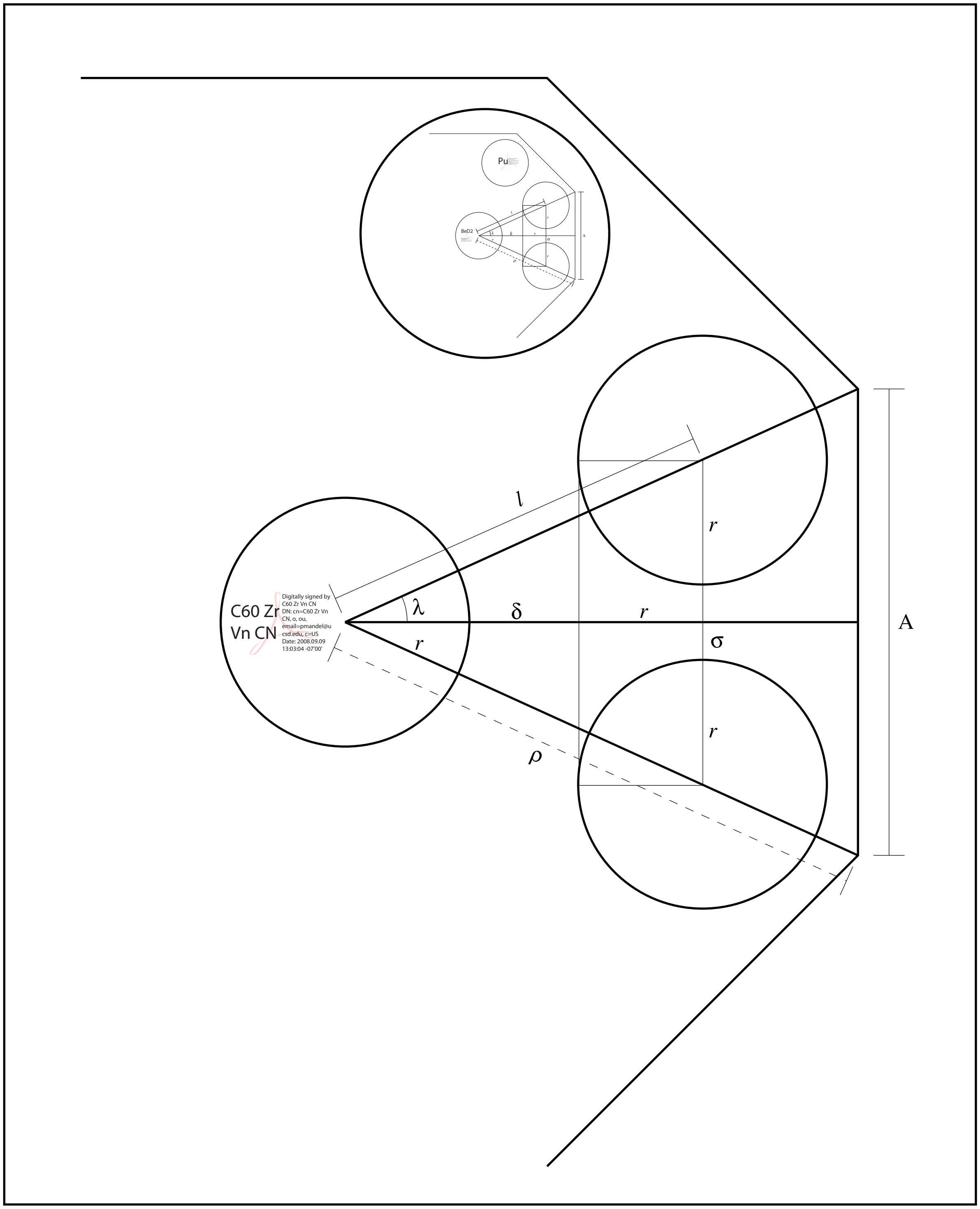

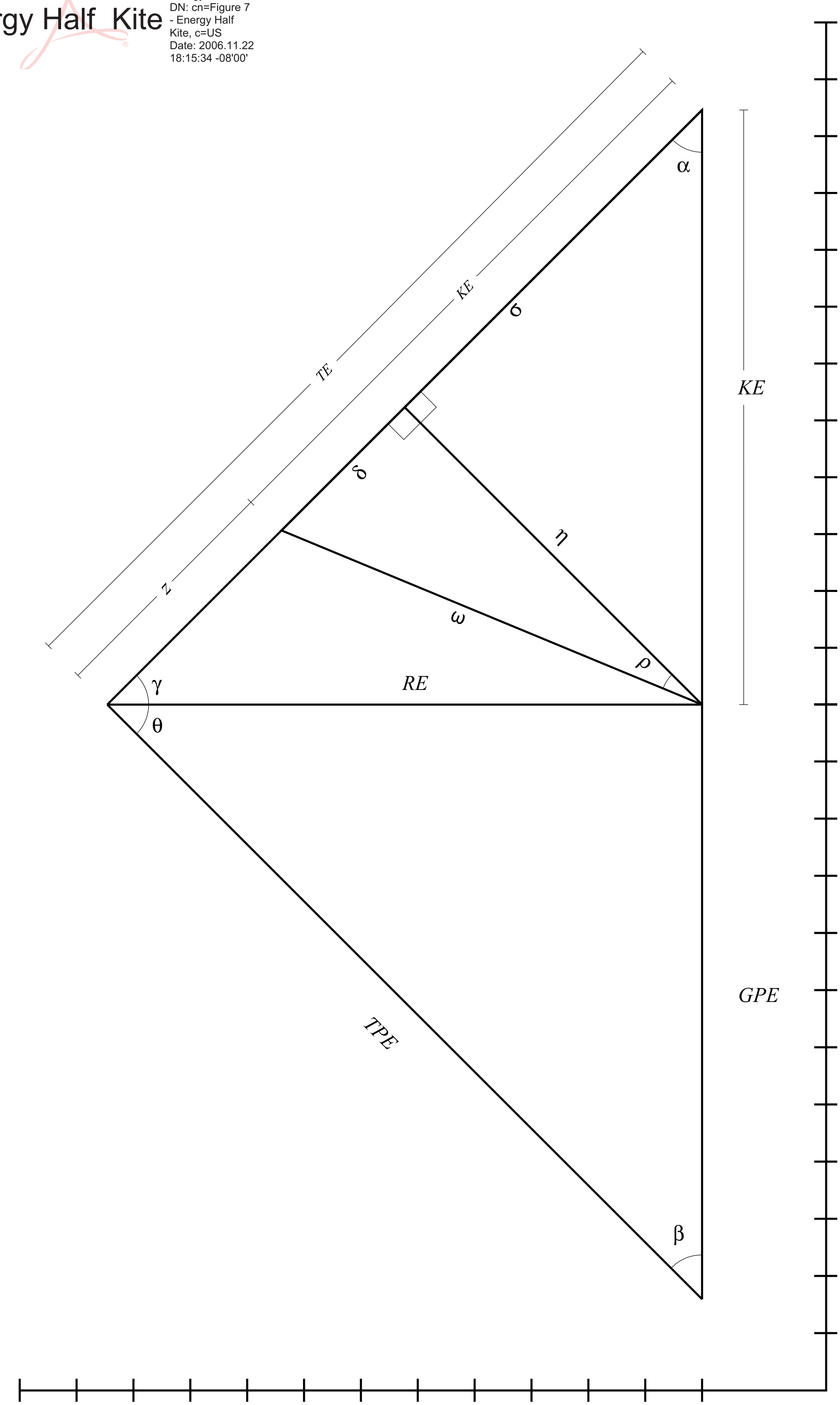
TE
KE
σ
δ
z
η
ω
ρ
α
γ
θ
RE
KE
GPE
TPE
β

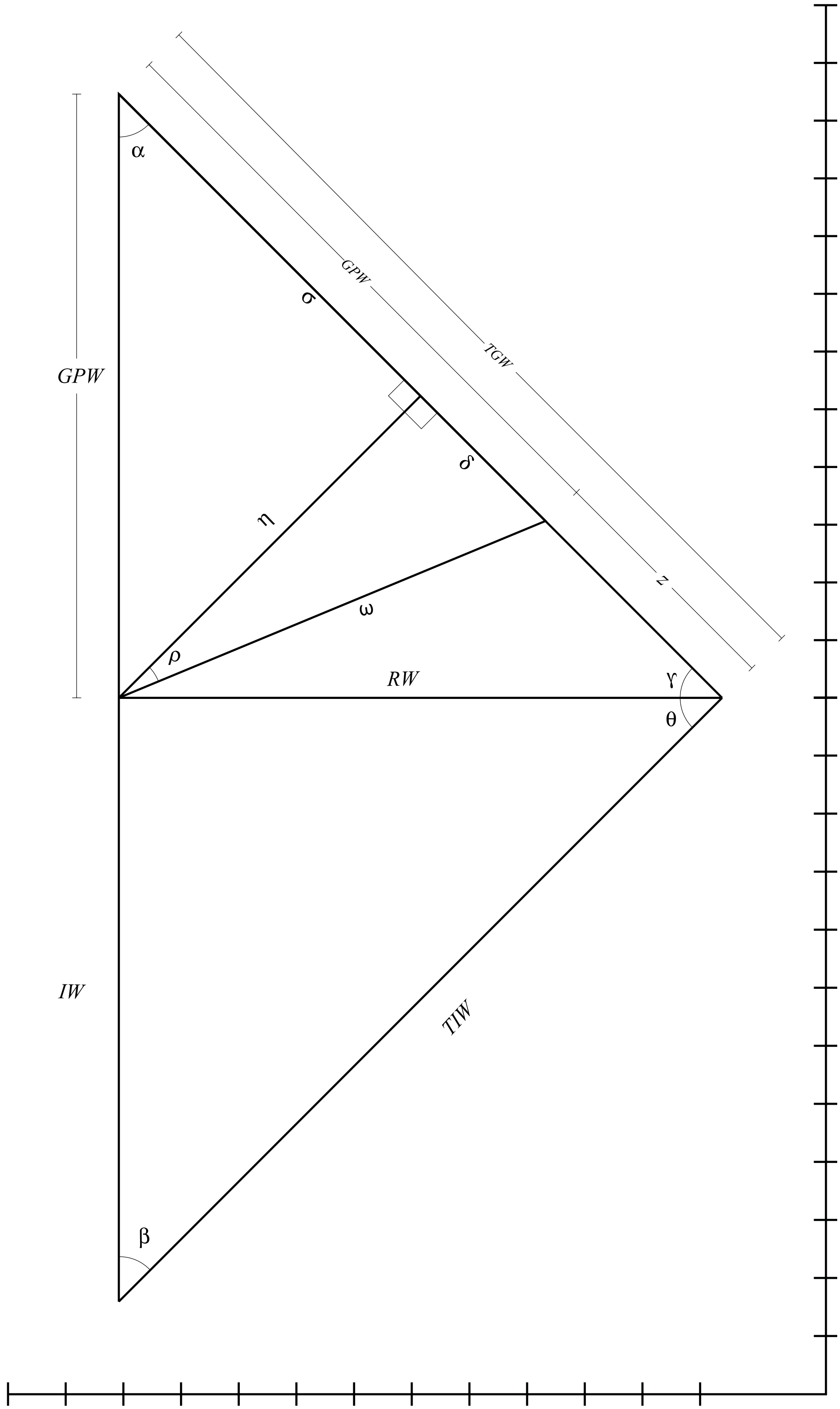
α
GPW
TGW
GPW
σ
δ
η
z
ω
ρ
RW
γ
θ
IW
TIW
β

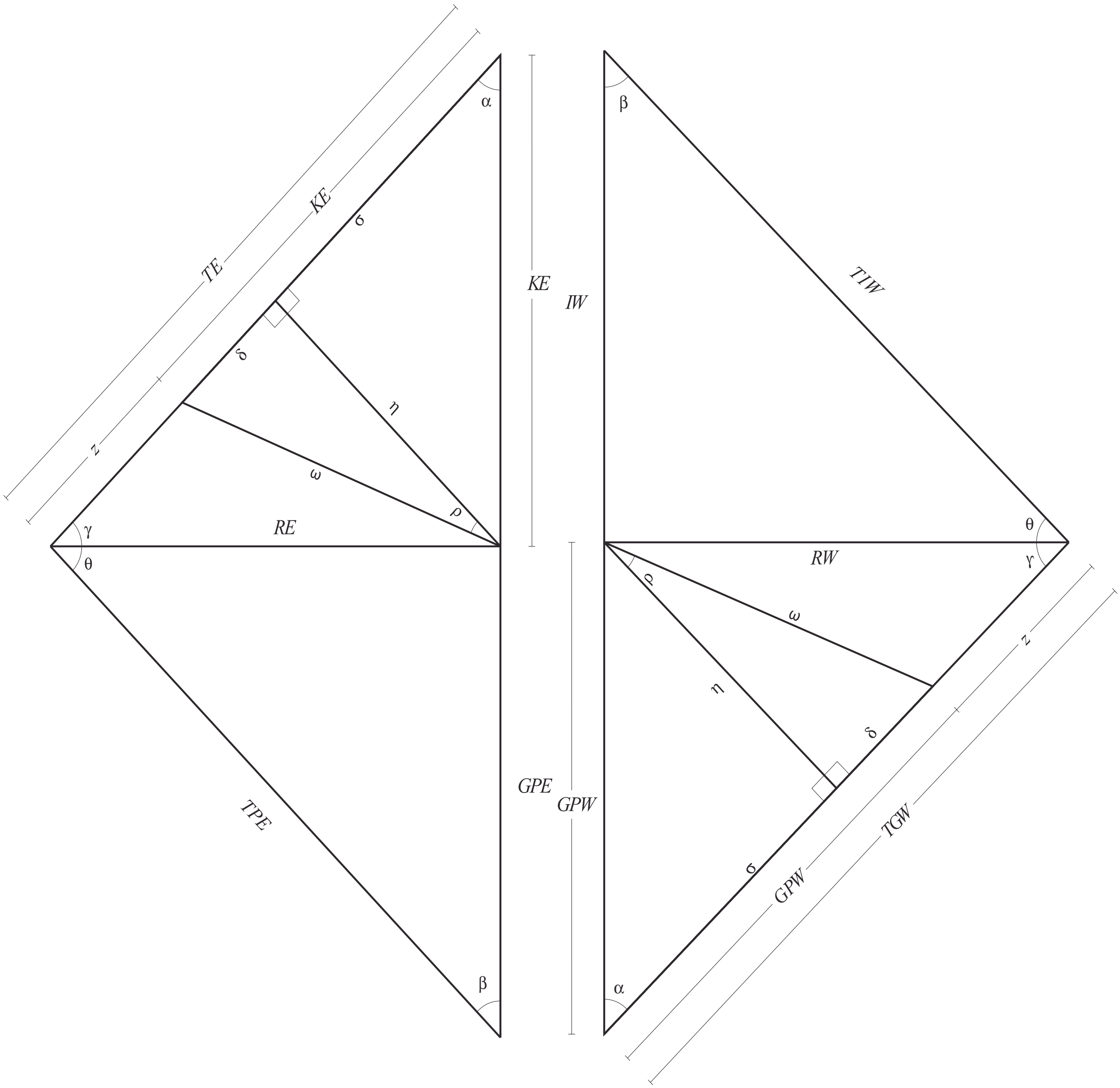
TE
KE
z
σ
δ
η
ω
ρ
α
γ
θ
RE
KE
IW
β
TIW
θ
RW
γ
ρ
ω
η
δ
z
TPE
β
GPE
GPW
σ
GPW
TGW
α

Signature Valid

Figure 7c - dEnergy - Time Warp Full Kite

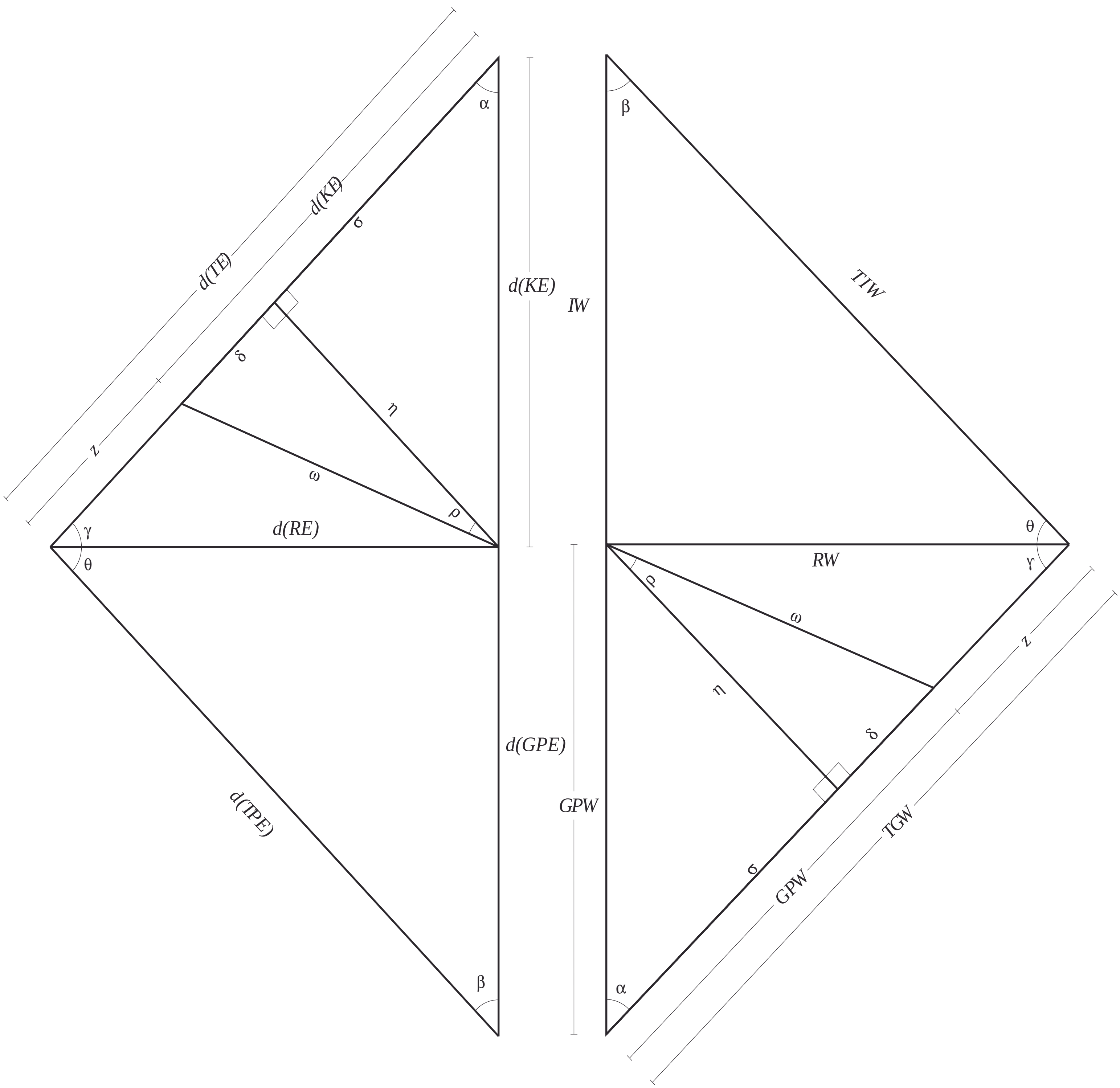

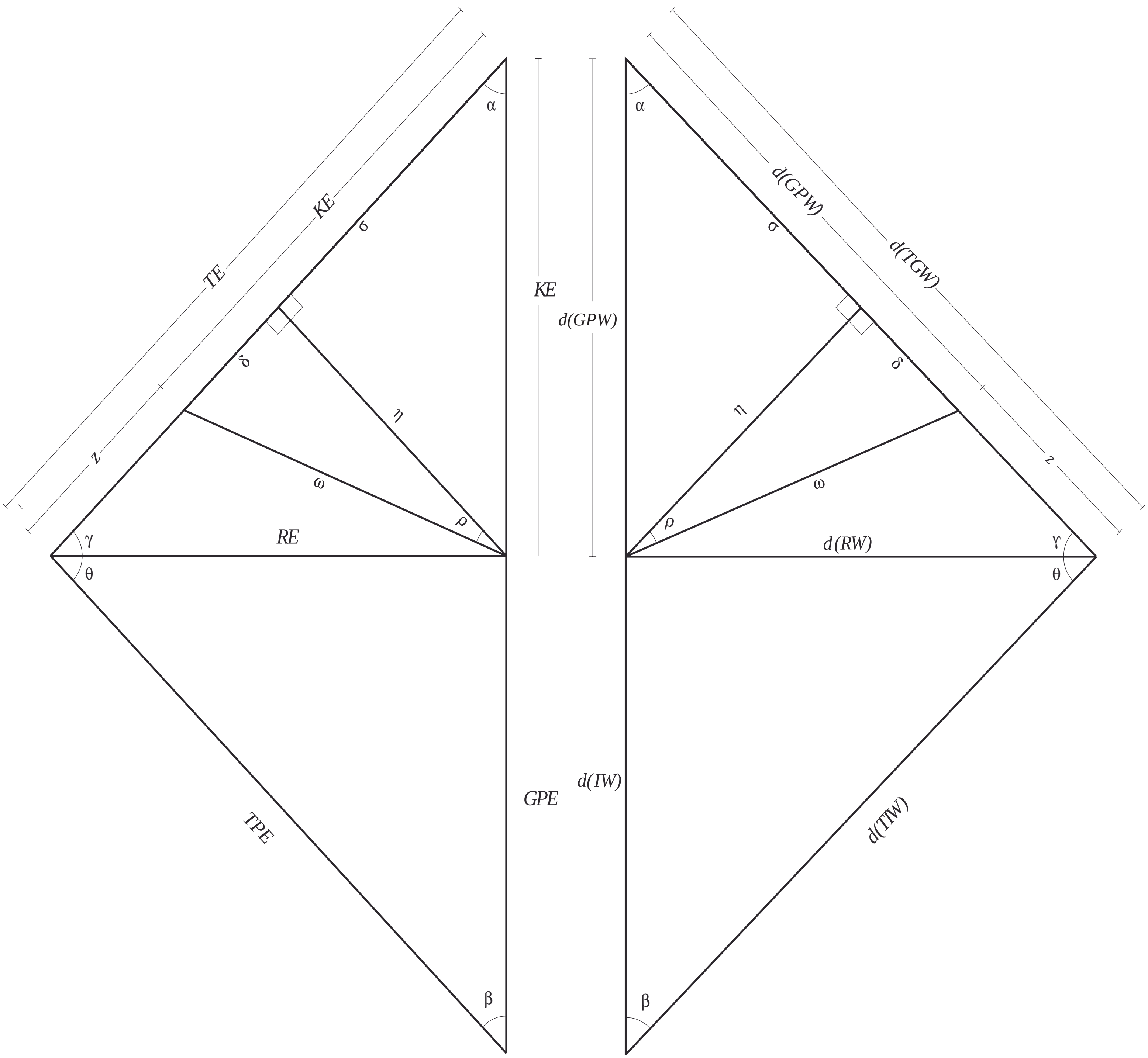
TE
KE
σ
δ
z
η
ω
ρ
RE
γ
θ
α
KE
d(GPW)
GPE
d(IW)
TPE
β
d(GPW)
d(TGW)
σ
δ
η
ω
z
ρ
d(RW)
γ
θ
d(TIW)
β
α

Figure 7e - dEnergy - dTime Warp Full Kite

Signature Valid

Digitally signed by Figure 7b - Energy - Time Warp Full Kite
DN: cn=Figure 7b - Energy - Time Warp Full Kite, c=US
Date: 2006.11.22 18:19:06 -08'00'

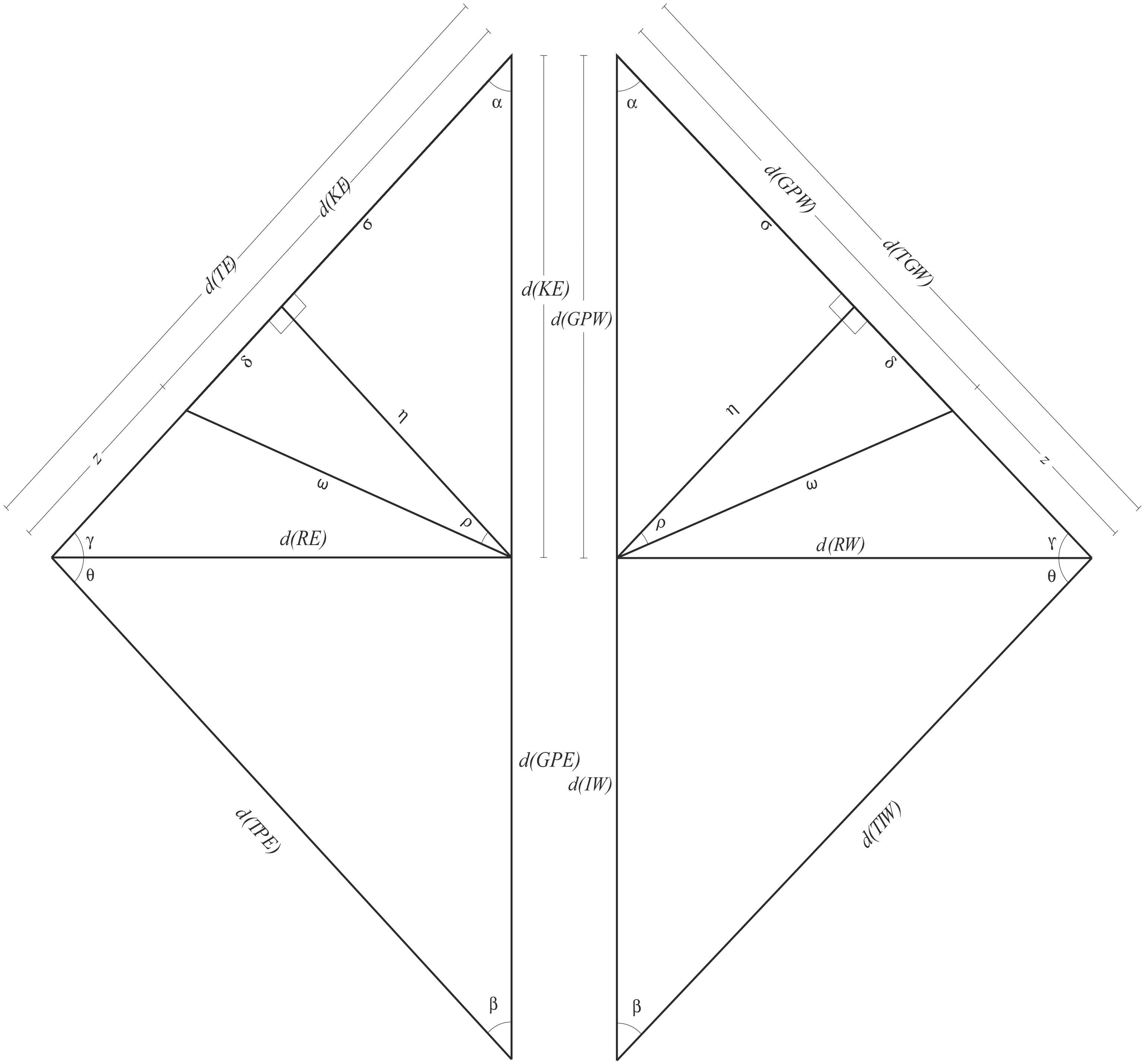

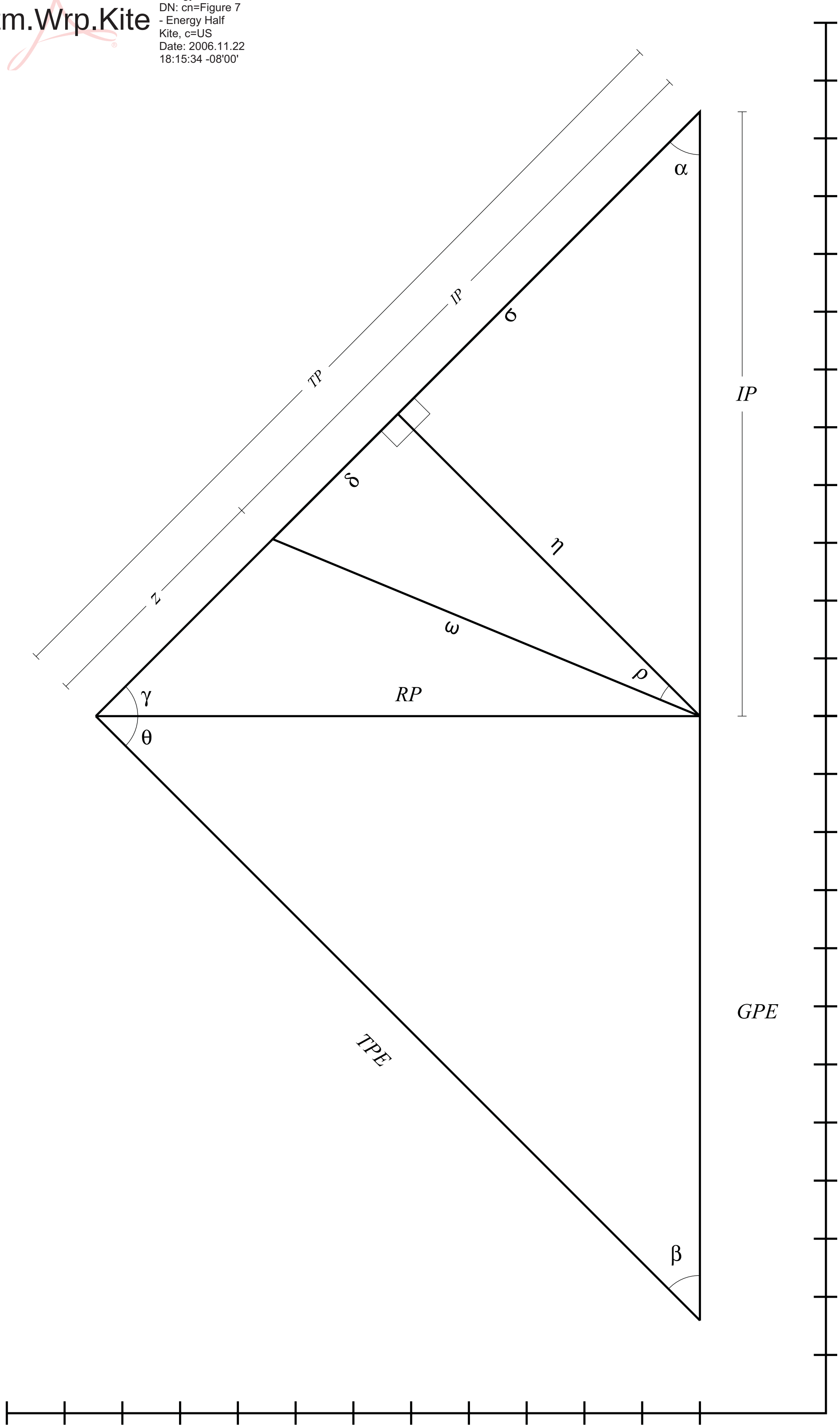
α
TP
IP
σ
IP
δ
η
z
ω
ρ
γ
RP
θ
TPE
GPE
β

Signature Valid

Figure 7g -Grav. Dist.-Warp Kite

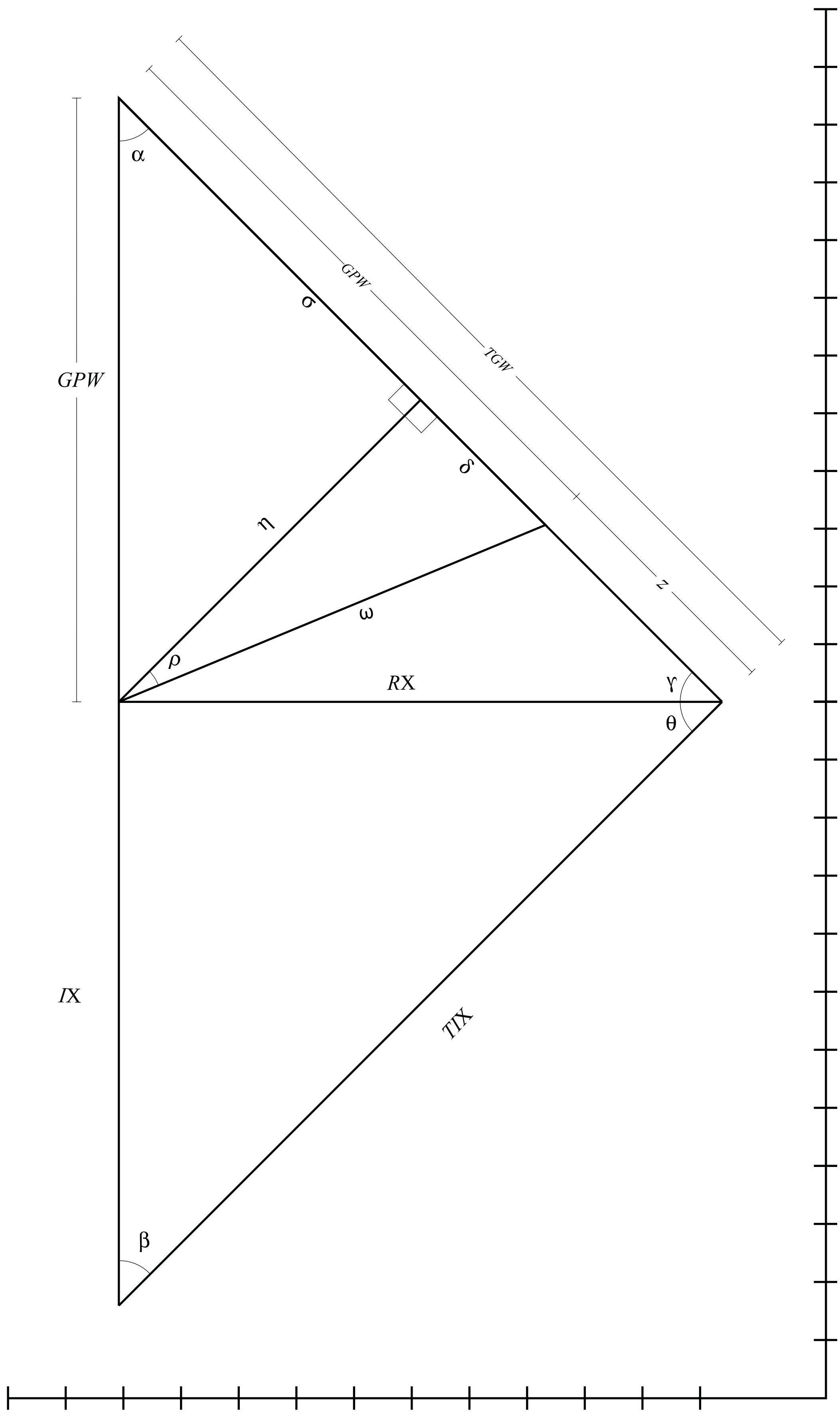

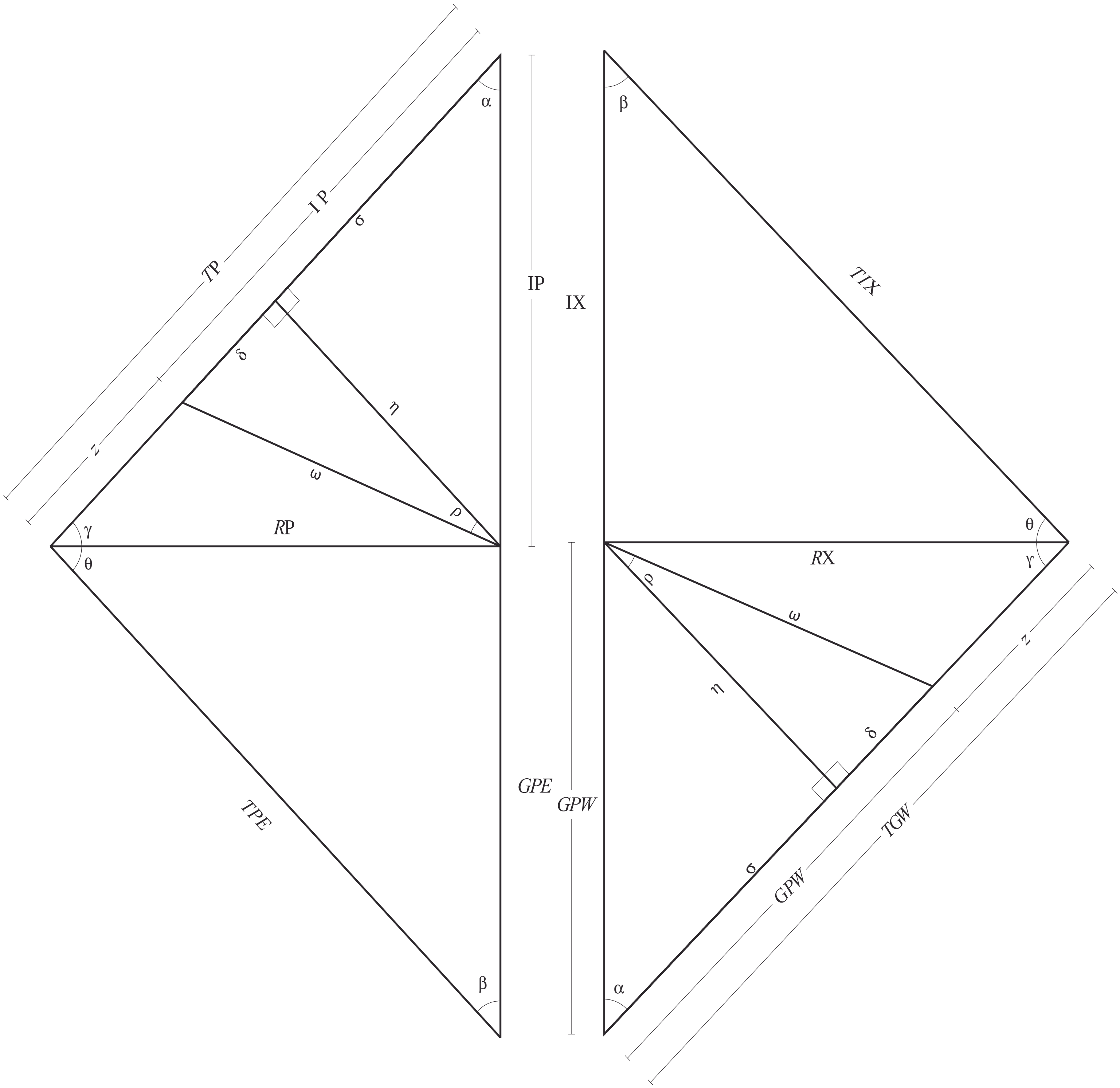
TP
I P
α
σ
IP
IX
β
TIX
δ
η
z
ω
ρ
γ
RP
θ
RX
γ
θ
ρ
ω
η
z
δ
GPE
GPW
TPE
TGW
σ
GPW
β
α

Signatur
e Valid

Figure 7i -
Momntm-dTime
Warp Full Kite

Digitally signed by
Figure 7b -
Energy - Time
Warp Full Kite
DN: cn=Figure 7b
- Energy - Time
Warp Full Kite,
c=US
Date: 2006.11.22
18:19:06 -08'00'

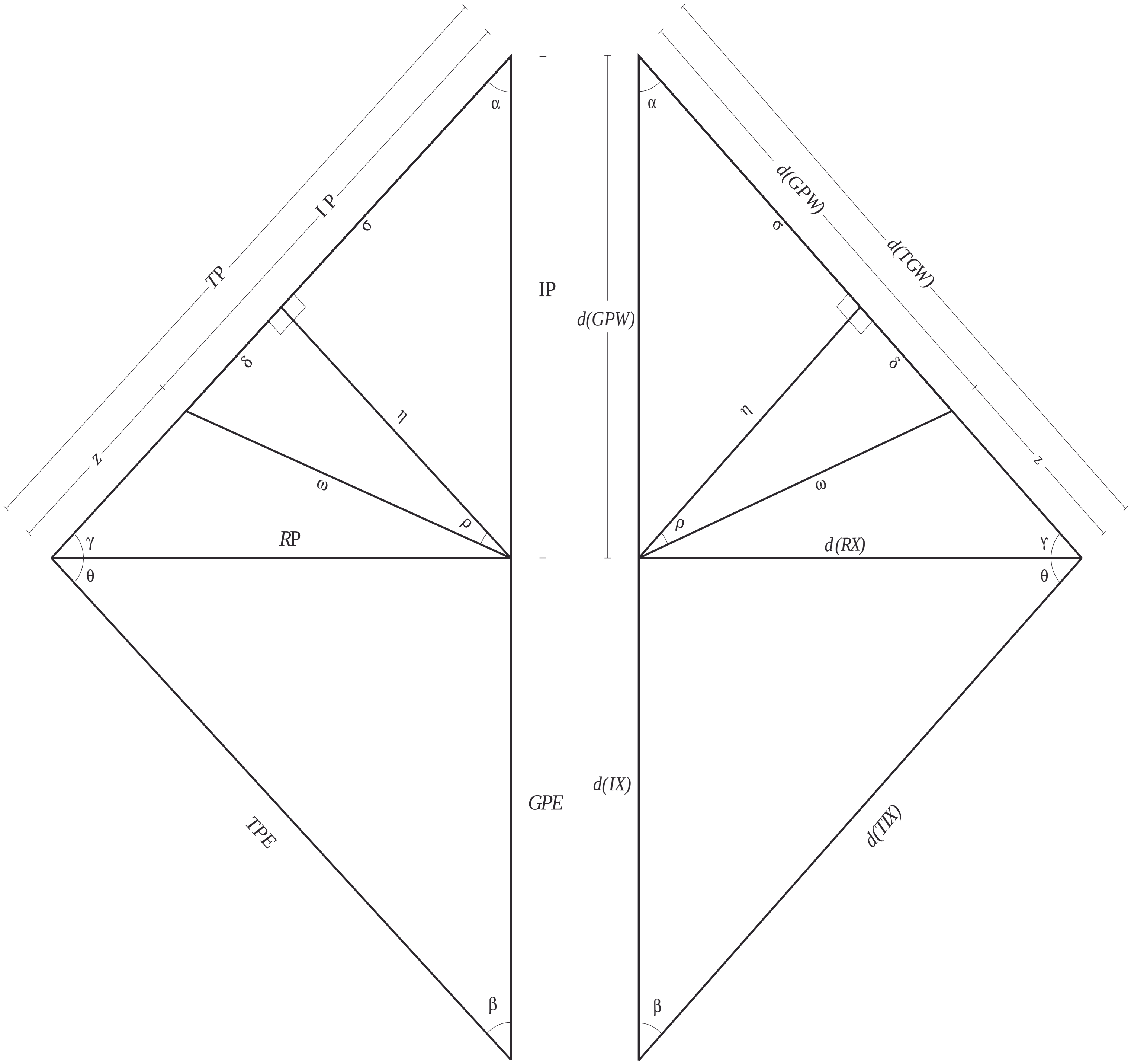

Figure 7j - dMomntm.-Dist. Warp Full Kite

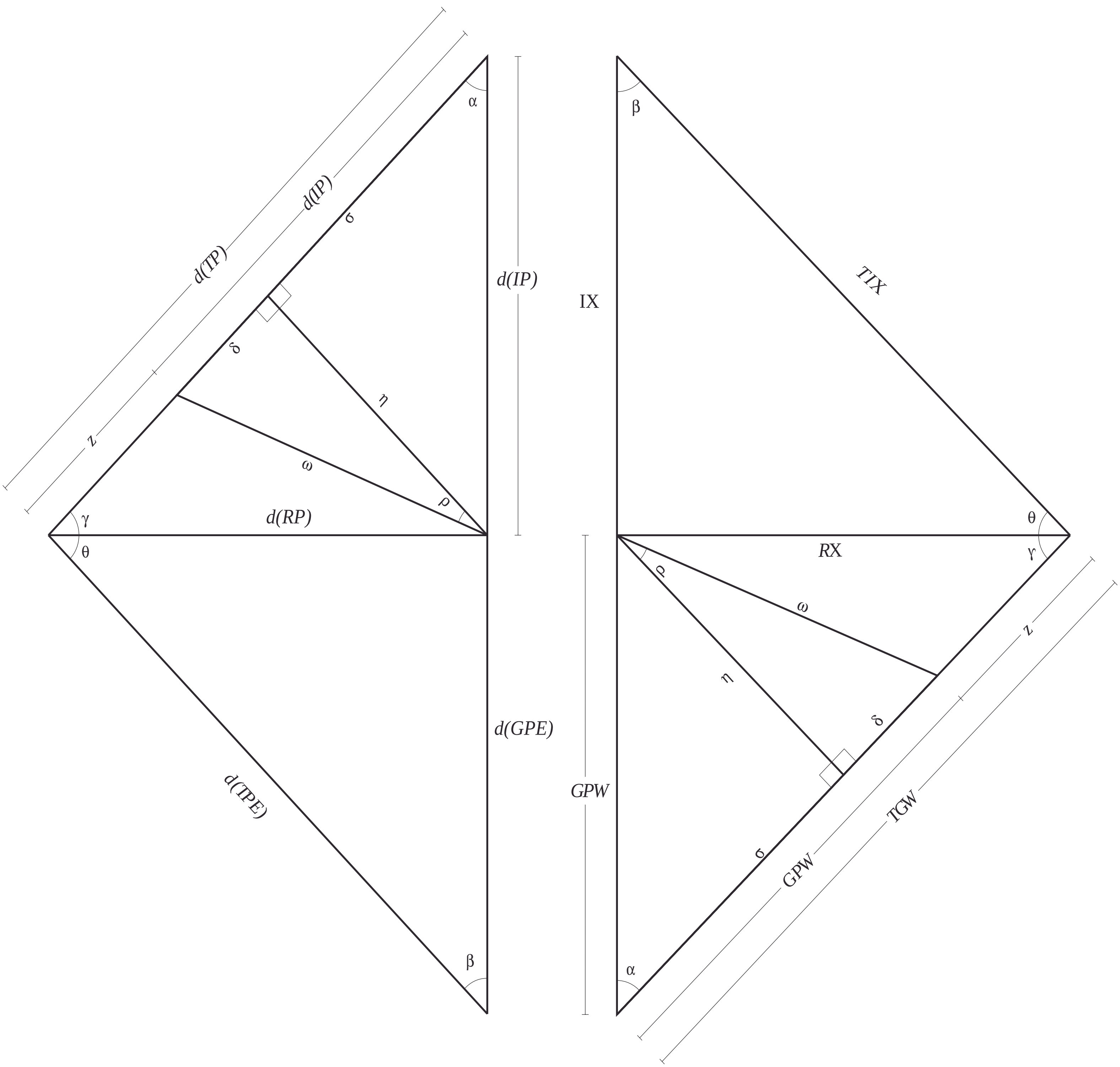

Figure 7k - dMomtm-dTime Warp Full Kite

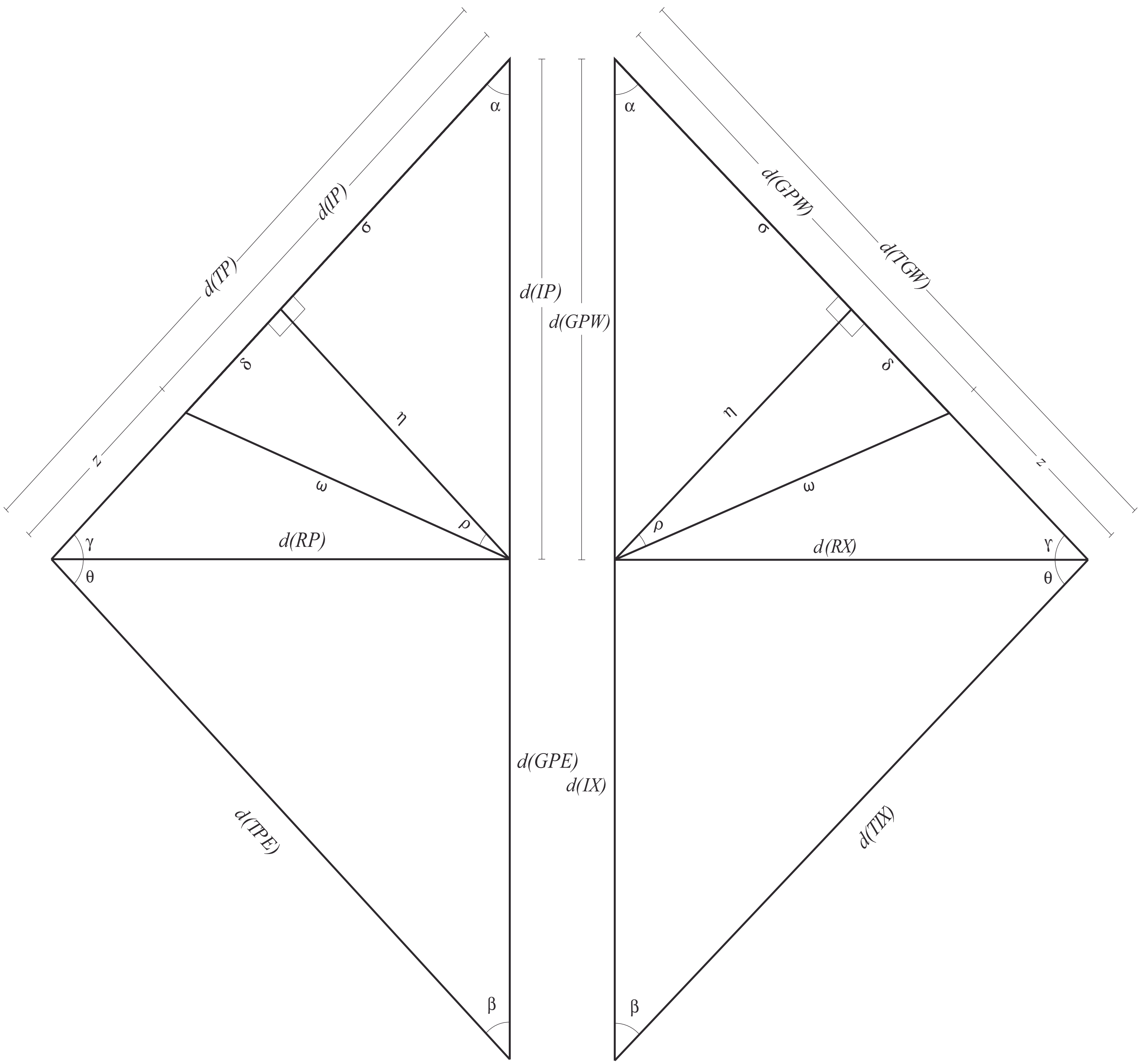

```
"Figure - 8 Hyperbolic Cosine Law"

(KE)=23.2466
Plot3D[((ArcTan[(KE)/(RE)]^2)/(X^2)*(Cos[X]^2))-
((KE)^2/(RE)^2)-1,{X,-Pi/2,Pi/2},{(RE),-50,50},
PlotPoints->{50,50},PlotRange->{{-Pi/2,Pi/2},
{-50,50},{-1000,3000}},ViewPoint->{5,-2.4,2},
AxesLabel->{"Theta","Rest Energy",""}]
```

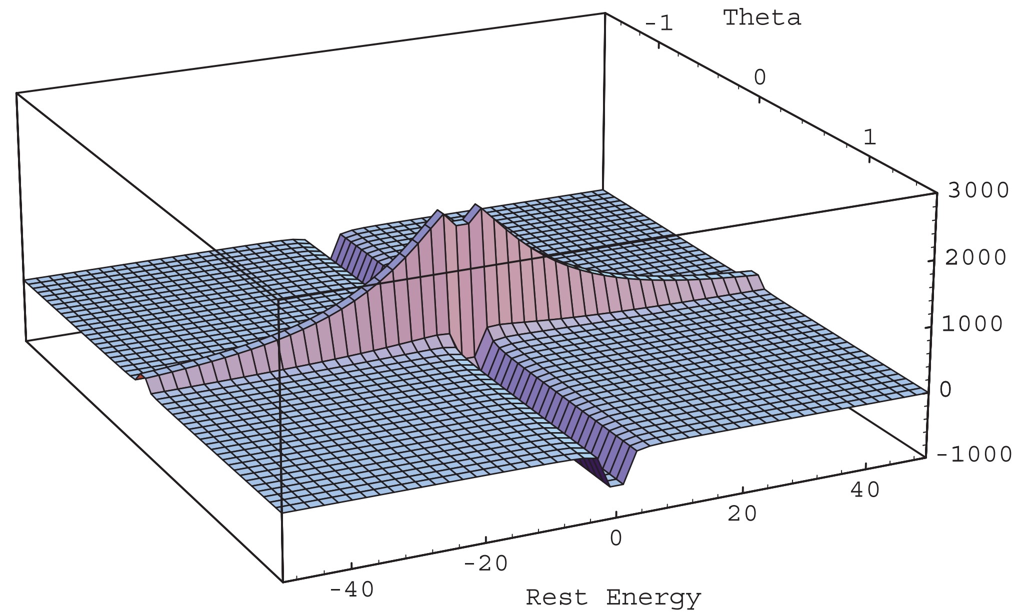

"Figure 9 - Quadric Surface - C8"

```
Plot3D[(X^2)*Cos[X]^2-(Y^2)*Cos[Y]^2,
{X,0,Pi/2},{Y,0,Pi/2},PlotRange->{{0,Pi/2},
{0,Pi/2},{-.31489,.31489}},AxesLabel->
{"Theta","Gamma",""}]
```

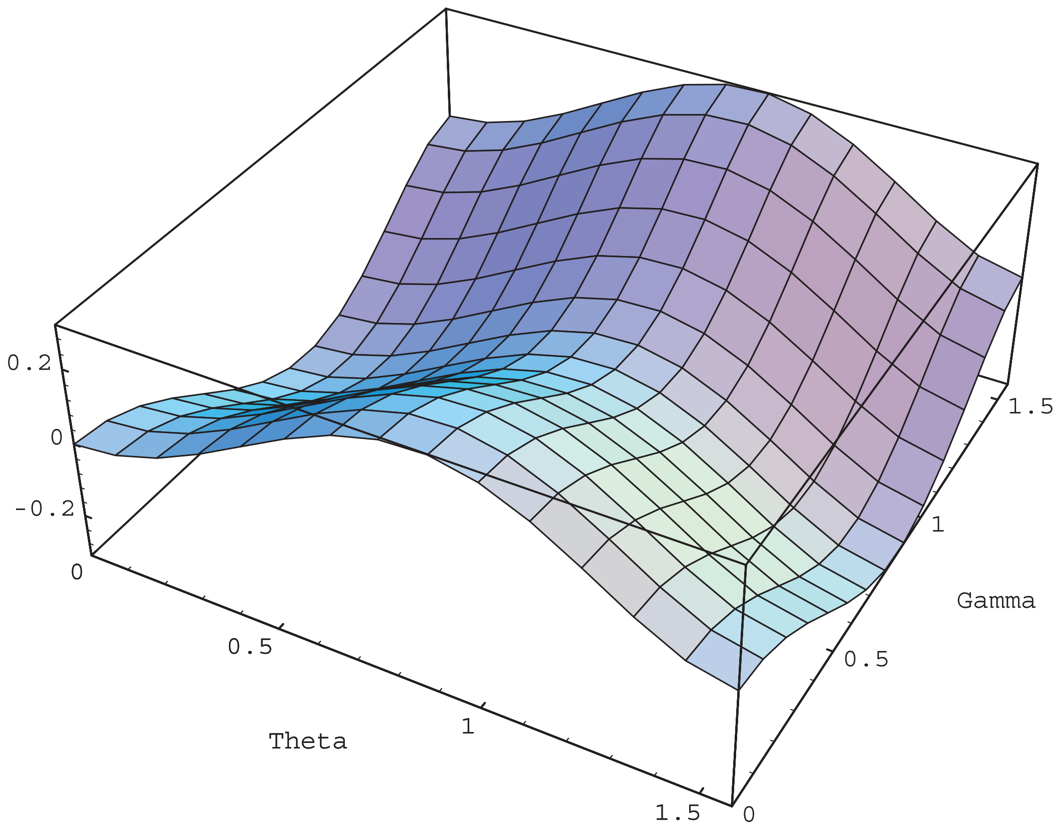

```
"Figure 10 - Fundamental Quadric Surface - C8"

Plot3D[(X*Cos[X]-Y*Cos[Y]),{X,0,Pi/2},{Y,0,Pi/2},
PlotRange->{{0,Pi/2},{0,Pi/2},
{-.56109,.56109}},Axes->True,AxesLabel->
{"Theta","Gamma",""}]
```

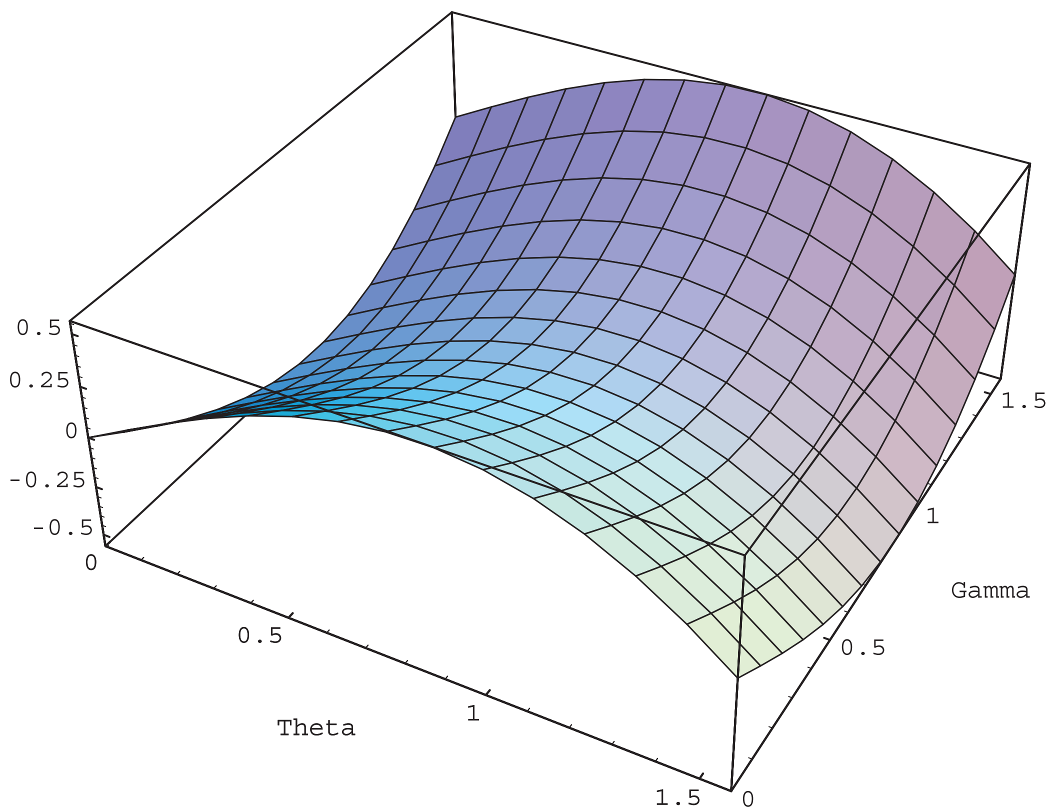

```
"Figure - 10a.
ContourPlot of Hyper-Paraboloid Fundamental"

ContourPlot[X*Cos[X]-Y*Cos[Y],{X,0,Pi/2},{Y,0,Pi/2},
Axes->True,AxesLabel -> {"Theta","Gamma"}]
```

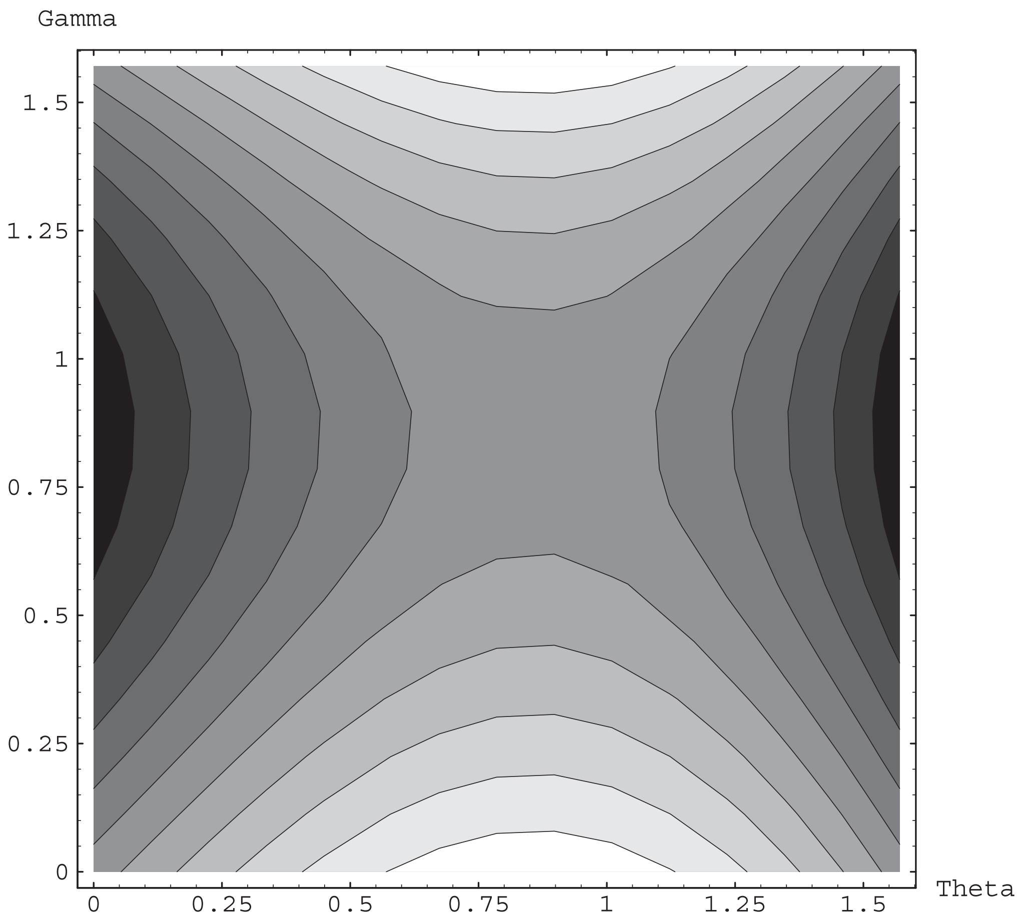

-ContourGraphics-

```
"Hyperbolic Paraboloid Cone"

(RE)=23.2466
Plot3D[(((14.7992*X)^2)/(ArcTan[(KE)/(RE)]^2))-
((RE)^2)/(((RE)^2+(KE)^2)),{X,-Pi/10.30,Pi/10.30},
{(KE),-30,30},PlotPoints->{70,70},PlotRange->
{{-Pi/10.30,Pi/10.30},{-30,30},{-23.2466,23.2466}},
AxesLabel->{"Theta","Kinetic-Energy",""}]
```

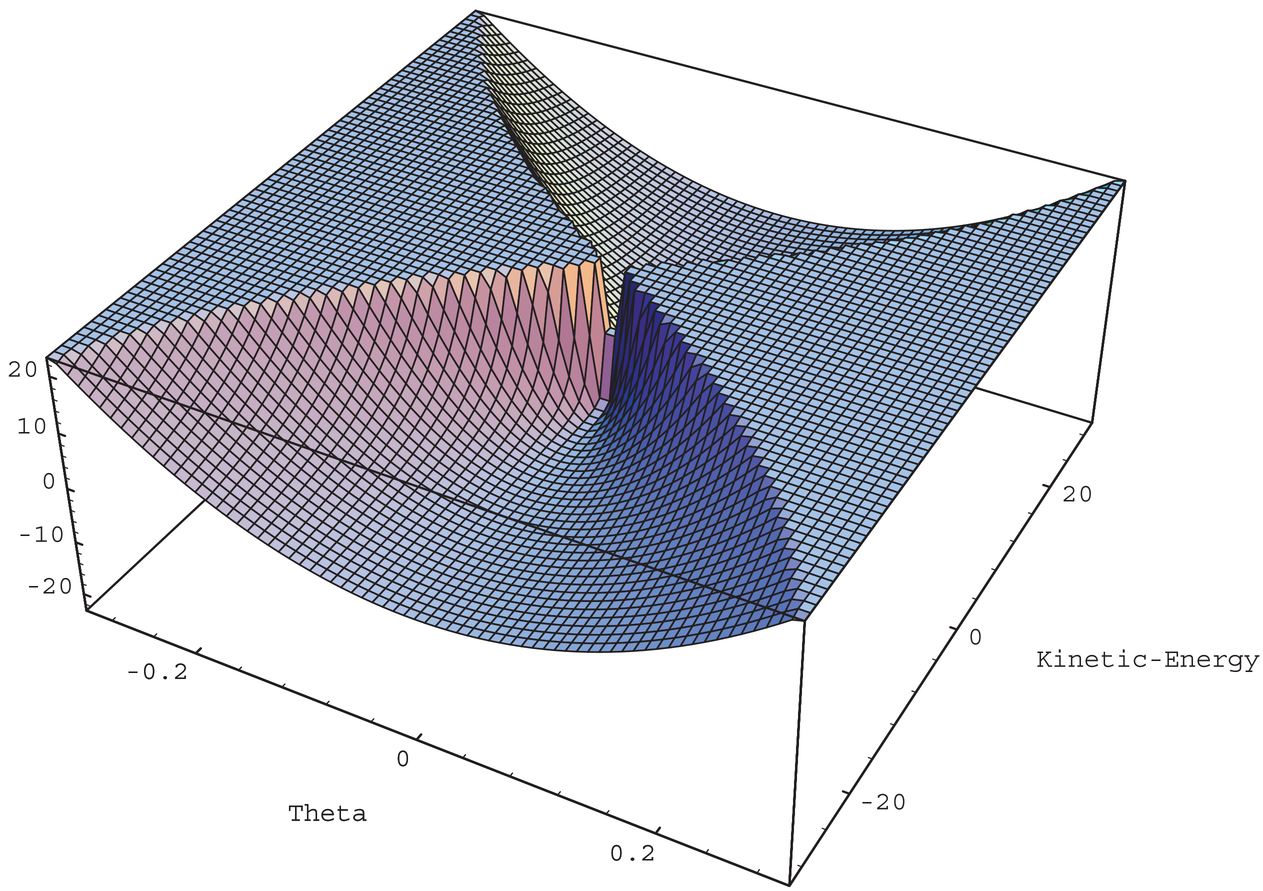

```
"Daughter Equation Parabola"

(KE)=23.2466
Plot3D[((X^2)/((RE)^2))-((ArcTan[(KE)/(RE)]^2)/
((KE)^2+(RE)^2)),{X,-Pi/2,Pi/2},
{(RE),-23.2466,23.2466},
PlotPoints->{72,72},PlotRange->
{{-Pi/2,Pi/2},{-23.2466,23.2466},
{-2,23.2466}},AxesLabel->
{"Theta","Rest Energy",""}]
```

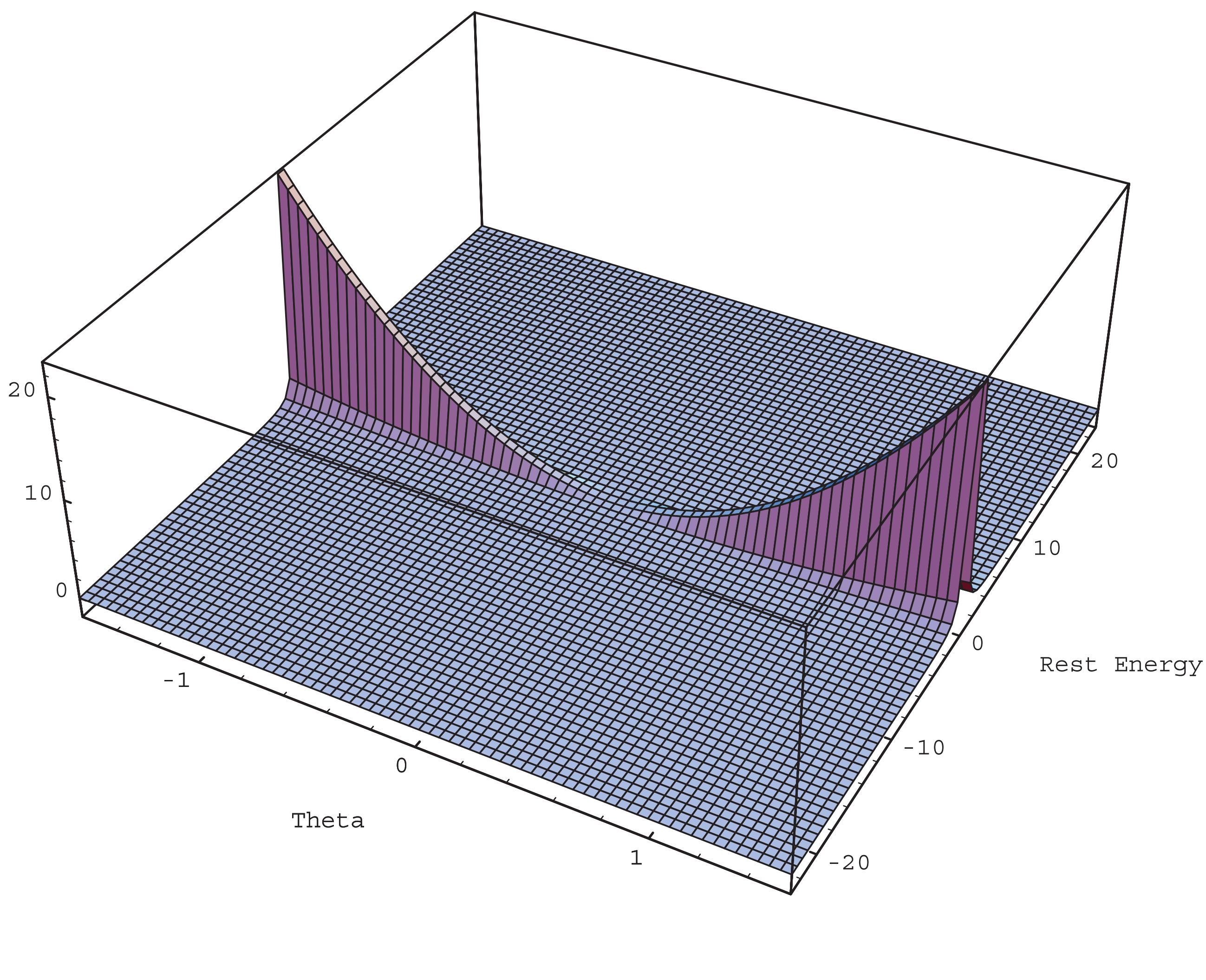

```
"Figure 12a - 1st Order Partial Differential"

KE=11.6233
Plot3D[2*X/ArcTan[KE/RE]^2,{X,-Pi/2,Pi/2},
{RE,-23.2466,23.2466},PlotPoints->{20,20},
PlotRange->{{-Pi/2,Pi/2},{-23.2466,23.2466},
{-14.6123,14.6123}},Axes->True,AxesLabel->
{"Theta","Rest Energy","df/d(theta)"}]
```

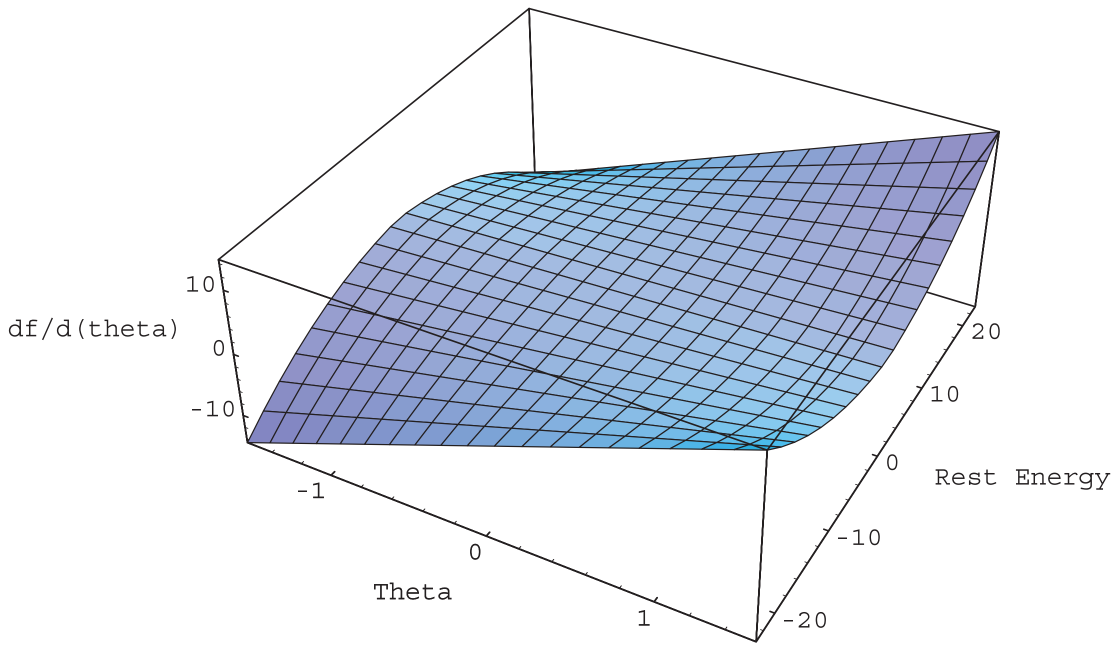

```
"HemiQuadric Surface - G15"

Plot3D[(B^2)*Sin[A]^2-(A^2)*Sin[B]^2,{A,0,Pi/2},
{B,0,Pi/2},PlotRange->{{0,Pi/2},{0,Pi/2},
{-.7580,.7580}},AxesLabel->{"Alpha","Beta",""}]
```

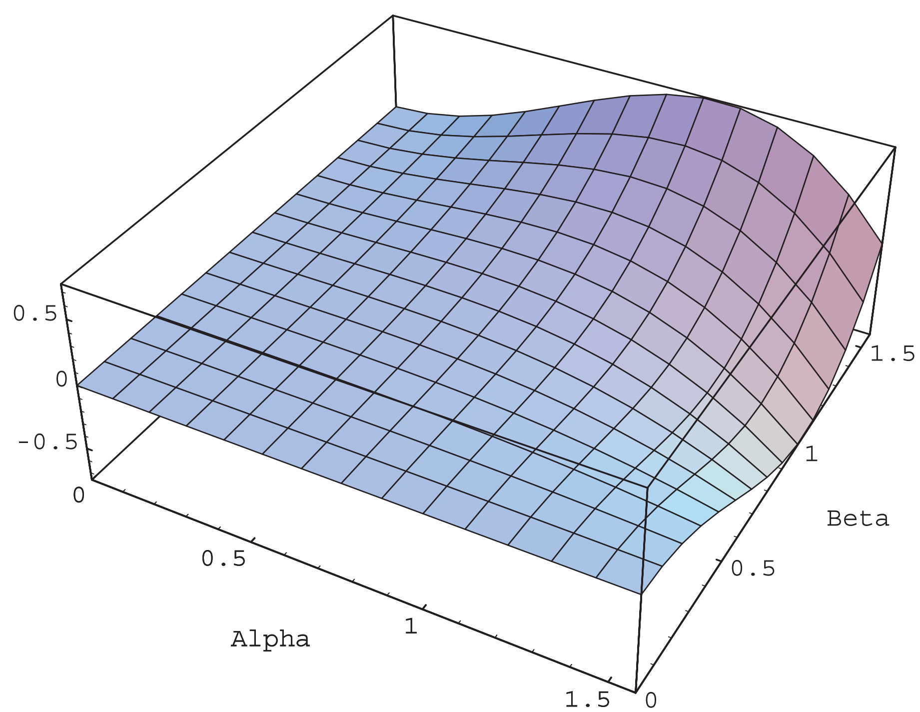

```
"Figure - 14 Hyperbolic Cosine Law of Time Warp"

(TGW)=23.2466
Plot3D[((ArcTan[(TGW)/(RW)]^2)/(X^2)*(Cos[X]^2))-
((TGW)^2/(RW)^2)-1,{X,-Pi/2,Pi/2},{(RW),-50,50},
PlotPoints->{50,50},PlotRange->{{-Pi/2,Pi/2},
{-50,50},{-1000,3000}},ViewPoint->{5,-2.4,2},
AxesLabel->{"Theta","Rest Warp",""}]
```

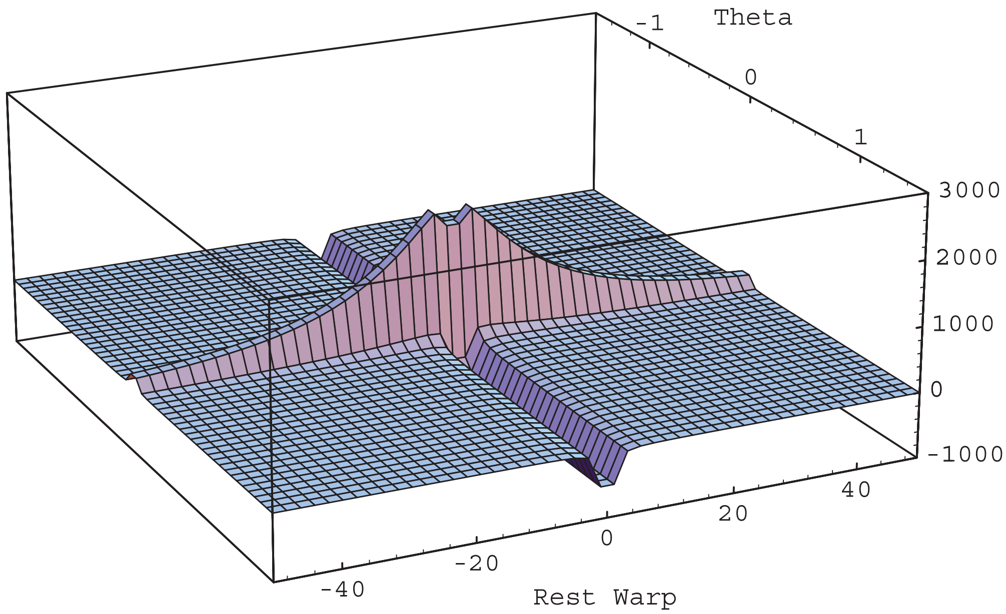

```
"Figure 15 - Quadric Surface - C8"

Plot3D[(X^2)*Cos[X]^2-(Y^2)*Cos[Y]^2,
{X,0,Pi/2},{Y,0,Pi/2},PlotRange->{{0,Pi/2},
{0,Pi/2},{-.31489,.31489}},AxesLabel->
{"Theta","Gamma",""}]
```

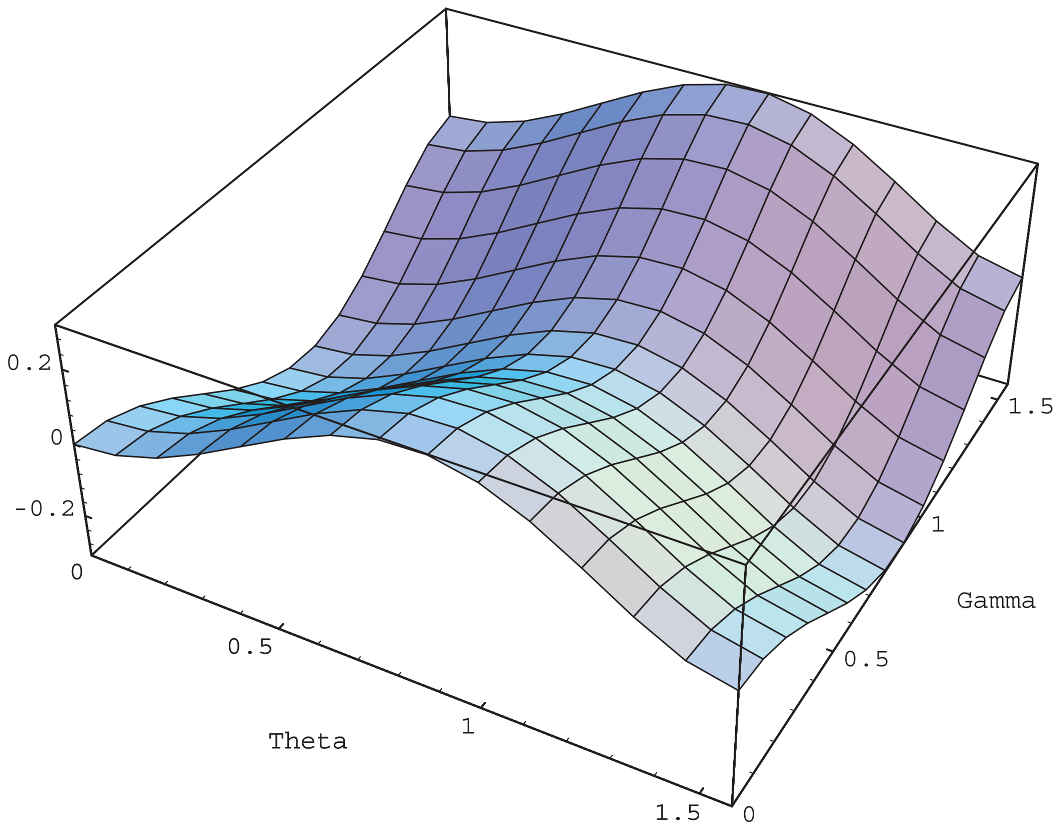

```
"Hyperbolic Paraboloid Time-Warp Cone"

(RW)=23.2466
Plot3D[(((14.7992*X)^2)/(ArcTan[(TGW)/(RW)]^2))-
((RW)^2)/(((RW)^2+(TGW)^2)),{X,-Pi/10.30,Pi/10.30},
{(TGW),-30,30},PlotPoints->{70,70},PlotRange->
{{-Pi/10.30,Pi/10.30},{-30,30},{-23.2466,23.2466}},
AxesLabel->{"Theta","Total Grav-Time-Warp",""}]
```

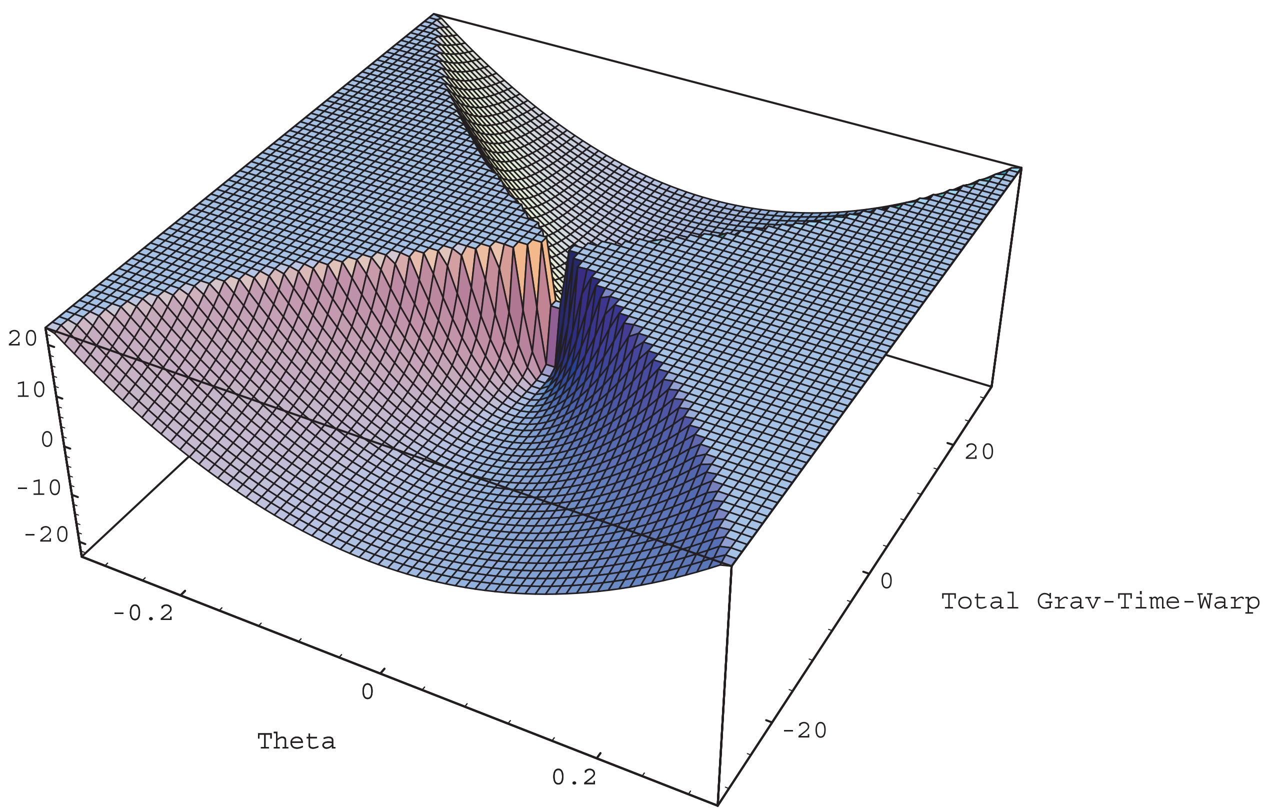

```
"Daughter Time Warp Equation Parabola"

(TGW)=23.2466
Plot3D[((X^2)/((RW)^2))-((ArcTan[(TGW)/(RW)]^2)/
((TGW)^2+(RW)^2)),{X,-Pi/2,Pi/2},
{(RW),-23.2466,23.2466},
PlotPoints->{72,72},PlotRange->
{{-Pi/2,Pi/2},{-23.2466,23.2466},
{-2,23.2466}},AxesLabel->
{"Theta","Rest Warp",""}]
```

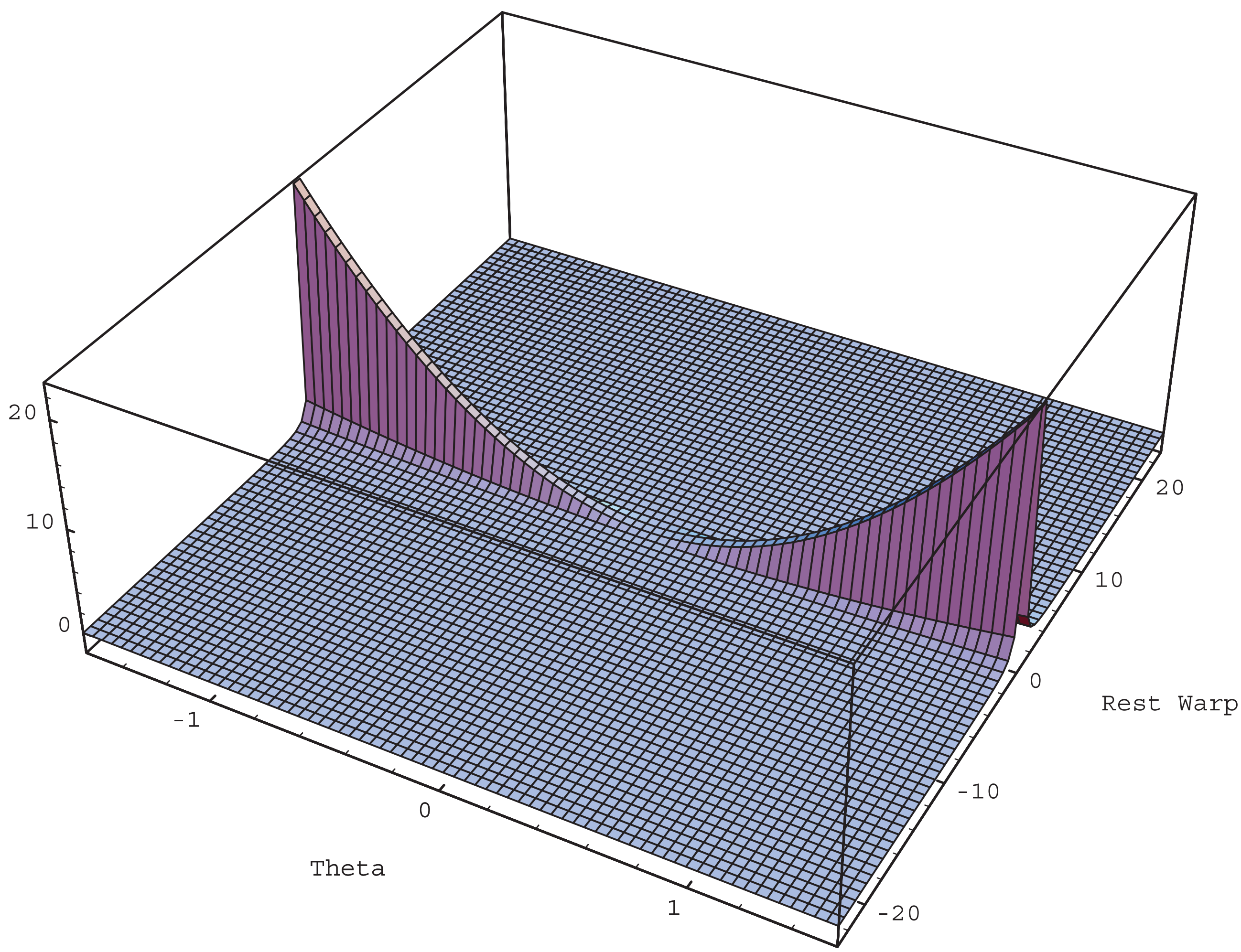

```
"Figure 18 - 1st Order Partial Differential"

TGW=11.6233
Plot3D[2*X/ArcTan[TGW/RW]^2,{X,-Pi/2,Pi/2},
{RW,-23.2466,23.2466},PlotPoints->{20,20},
PlotRange->{{-Pi/2,Pi/2},{-23.2466,23.2466},
{-14.6123,14.6123}},Axes->True,AxesLabel->
{"Theta","Rest Warp","df/d(theta)"}]
```

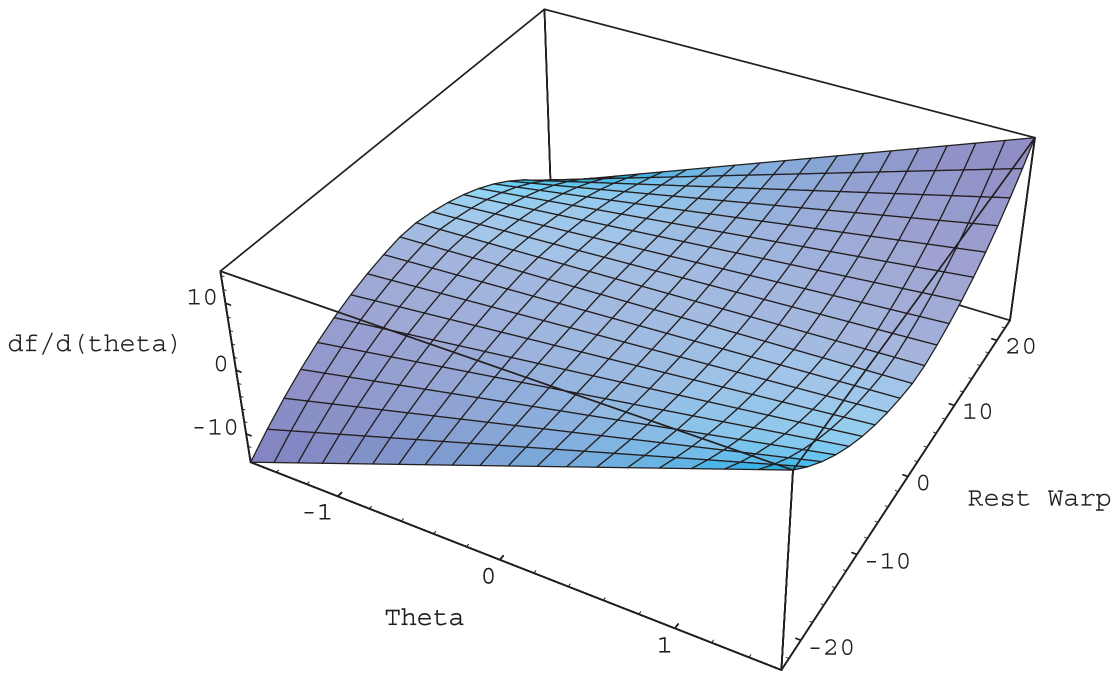

```
"HemiQuadric Surface - G15"

Plot3D[(B^2)*Sin[A]^2-(A^2)*Sin[B]^2,{A,0,Pi/2},
{B,0,Pi/2},PlotRange->{{0,Pi/2},{0,Pi/2},
{-.7580,.7580}},AxesLabel->{"Alpha","Beta",""}]
```

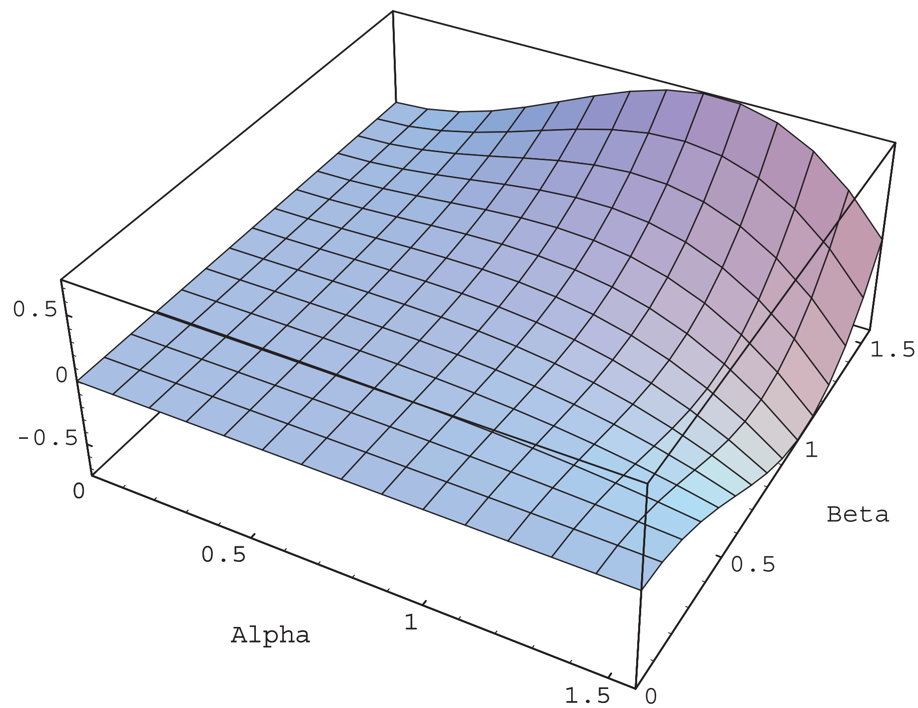

```
"Figure - 8i. Hyperbolic Cosine Momentum Law"

(IP)=23.2466
Plot3D[((ArcTan[(IP)/(RP)]^2)/(X^2)*(Cos[X]^2))-
((IP)^2/(RP)^2)-1,{X,-Pi/2,Pi/2},{(RP),-50,50},
PlotPoints->{50,50},PlotRange->{{-Pi/2,Pi/2},
{-50,50},{-1000,3000}},ViewPoint->{5,-2.4,2},
AxesLabel->{"Theta","Rest Momentum",""}]
```

Figure - 8i. Hyperbolic Cosine Momentum Law

23.2466

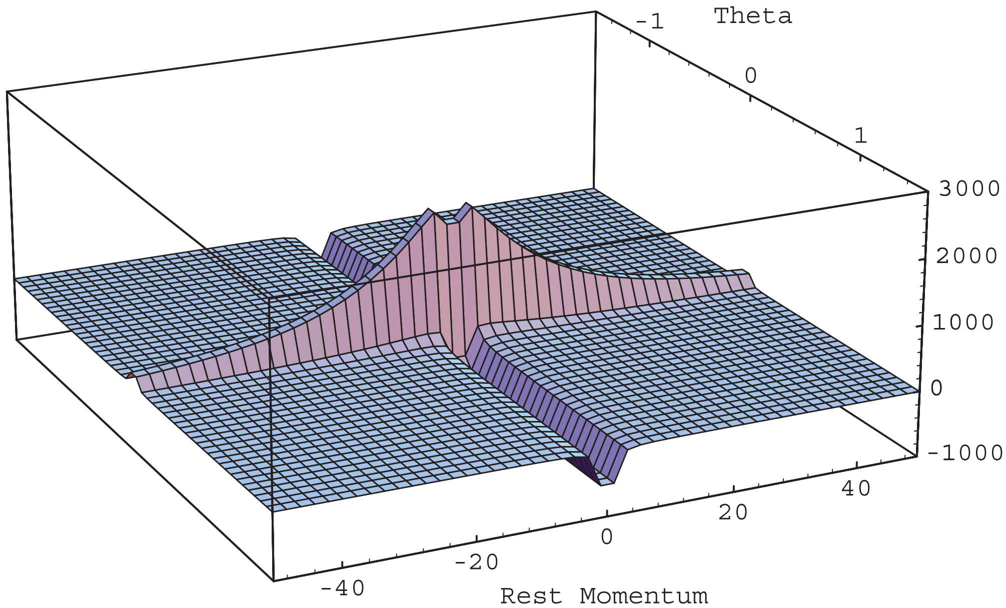

-SurfaceGraphics-

```
"Figure 9i. - Quadric Surface - C8"

Plot3D[(X^2)*Cos[X]^2-(Y^2)*Cos[Y]^2,
{X,0,Pi/2},{Y,0,Pi/2},PlotRange->{{0,Pi/2},
{0,Pi/2},{-.31489,.31489}},AxesLabel->
{"Theta","Gamma",""}]
```

```
Figure 9i. - Quadric Surface - C8
```

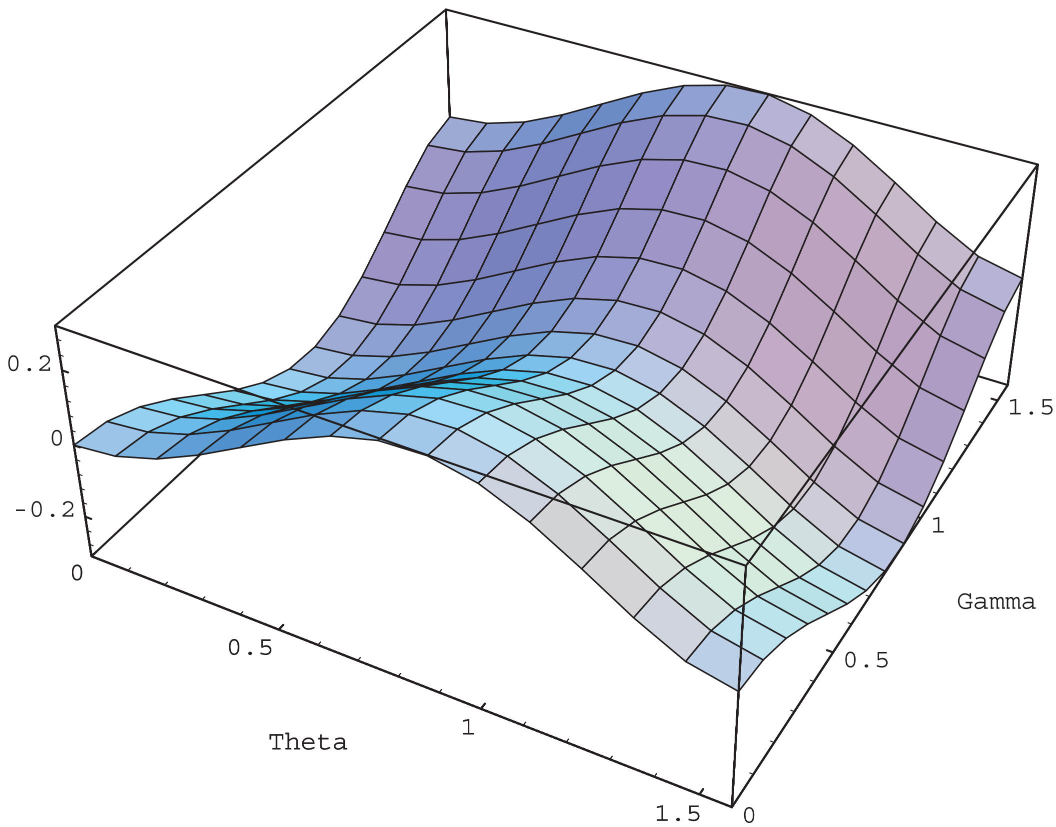


```
-SurfaceGraphics-
```

"Figure 10i - Fundamental Quadric Surface - C8"

```
Plot3D[(X*Cos[X]-Y*Cos[Y]),{X,0,Pi/2},{Y,0,Pi/2},
PlotRange->{{0,Pi/2},{0,Pi/2},
{-.56109,.56109}},Axes->True,AxesLabel->
{"Theta","Gamma",""}]
```

Figure 10i - Fundamental Quadric Surface - C8

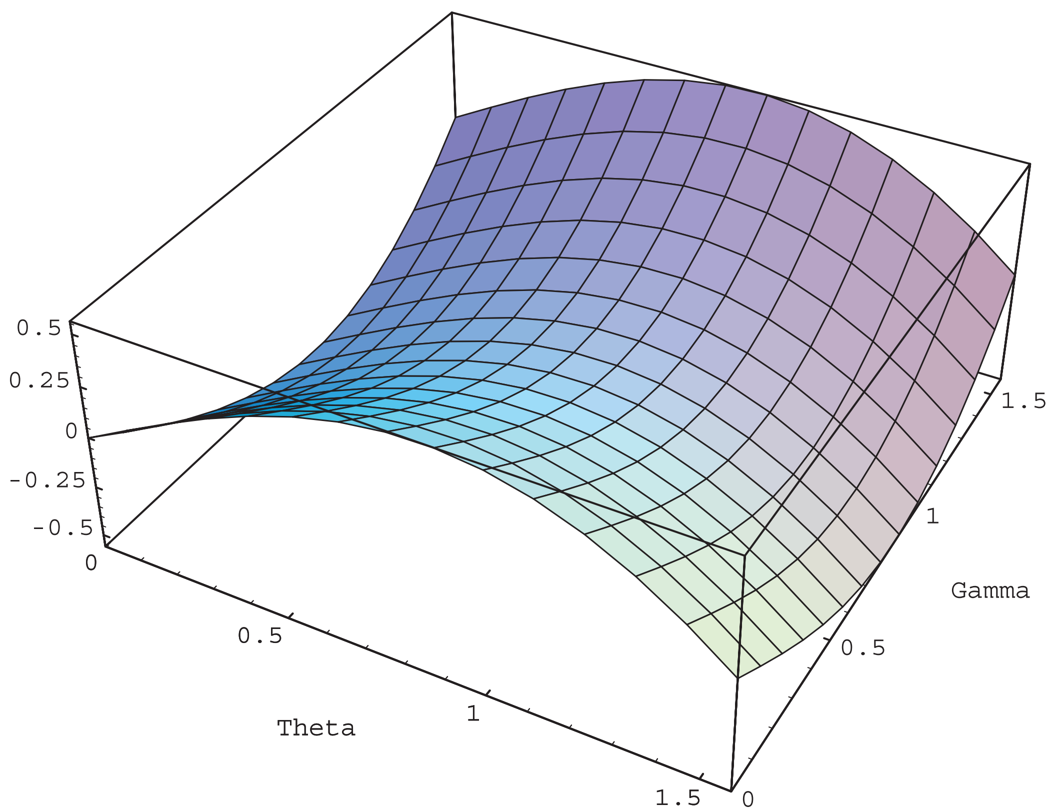

-SurfaceGraphics-

"Figure - 10ai.
ContourPlot of Hyper-Paraboloid Fundamental"

```
ContourPlot[X*Cos[X]-Y*Cos[Y],{X,0,Pi/2},{Y,0,Pi/2},
Axes->True,AxesLabel -> {"Theta","Gamma"}]
```

Figure - 10ai. ContourPlot of Hyper-Paraboloid Fundamental

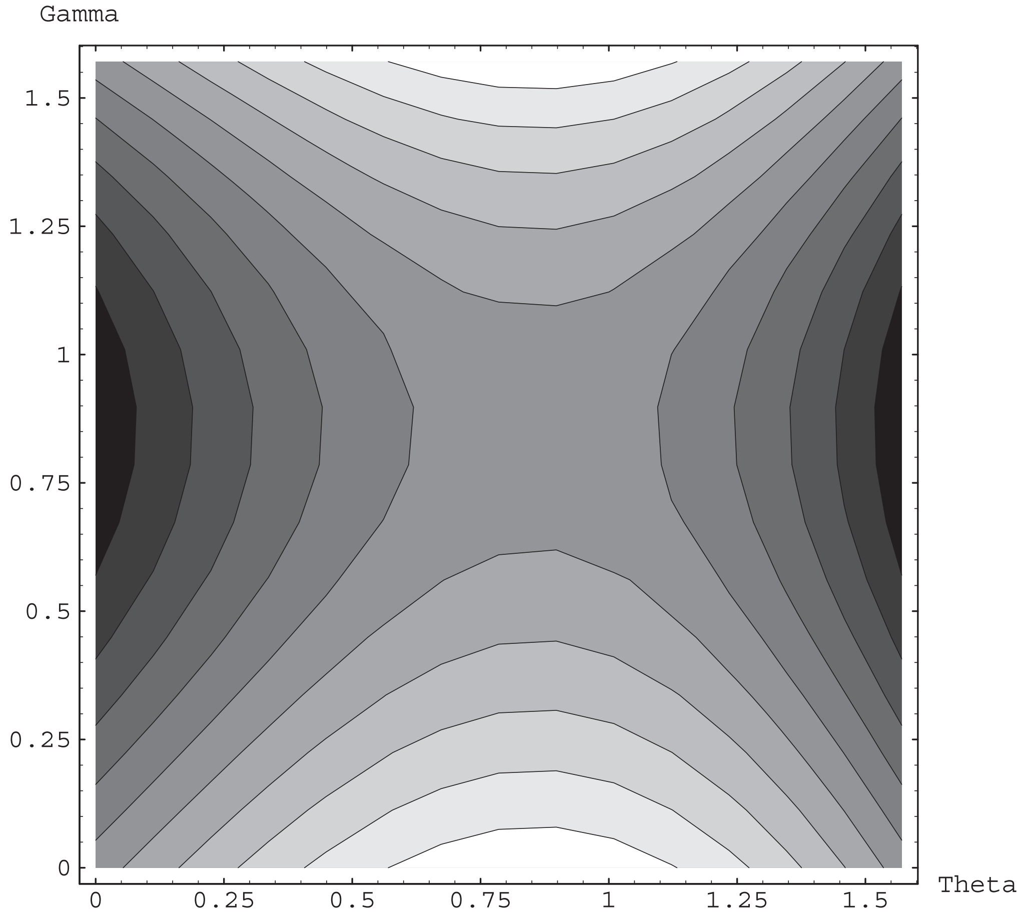

-ContourGraphics-

"Hyperbolic Paraboloid Momentum Cone"

```
(RP)=23.2466
Plot3D[(((14.7992*X)^2)/(ArcTan[(IP)/(RP)]^2))-
((RP)^2)/(((RP)^2+(IP)^2)),{X,-Pi/10.30,Pi/10.30},
{(IP),-30,30},PlotPoints->{70,70},PlotRange->
{{-Pi/10.30,Pi/10.30},{-30,30},{-23.2466,23.2466}},
AxesLabel->{"Theta","Inertial-Momentum",""}]
```

Hyperbolic Paraboloid Momentum Cone

23.2466

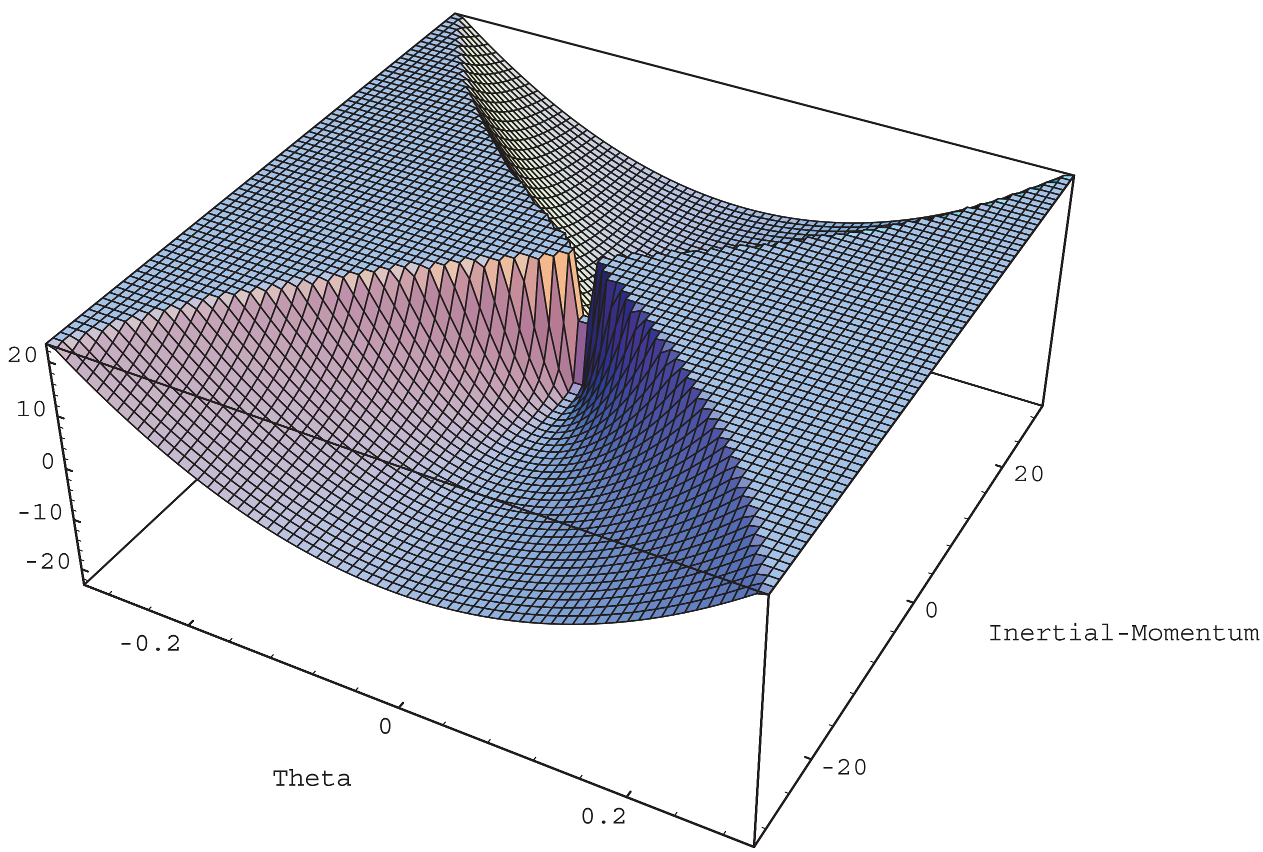

-SurfaceGraphics-

```
"Daughter Equation Momentum Parabola"

(IP)=23.2466
Plot3D[((X^2)/((RP)^2))-((ArcTan[(IP)/(RP)]^2)/
((IP)^2+(RP)^2)),{X,-Pi/2,Pi/2},
{(RP),-23.2466,23.2466},
PlotPoints->{72,72},PlotRange->
{{-Pi/2,Pi/2},{-23.2466,23.2466},
{-2,23.2466}},AxesLabel->
{"Theta","Rest Momentum",""}]
```

```
Daughter Equation Momentum Parabola

23.2466
```

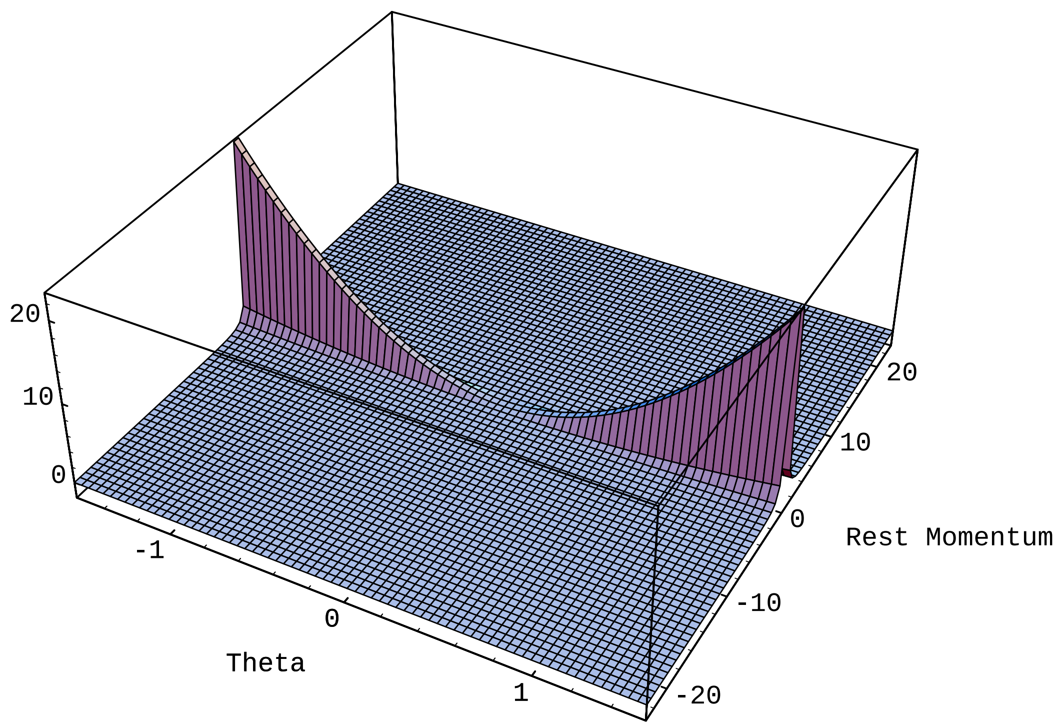


```
-SurfaceGraphics-
```

```
"Figure 12ai - 1st Order Partial Differential"

IP=11.6233
Plot3D[2*X/ArcTan[IP/RP]^2,{X,-Pi/2,Pi/2},
{RP,-23.2466,23.2466},PlotPoints->{20,20},
PlotRange->{{-Pi/2,Pi/2},{-23.2466,23.2466},
{-14.6123,14.6123}},Axes->True,AxesLabel->
{"Theta","Rest Momentum","df/d(theta)"}]
```

```
Figure 12ai - 1st Order Partial Differential

11.6233
```

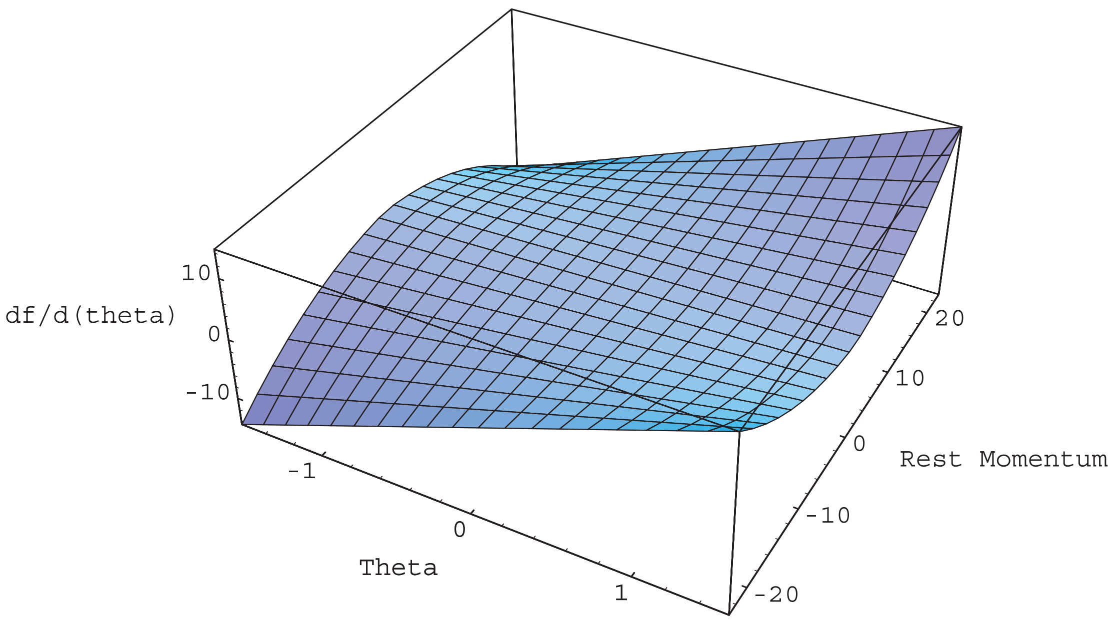


```
-SurfaceGraphics-
```

```
"HemiQuadric Surface - Q15"

Plot3D[(B^2)*Sin[A]^2-(A^2)*Sin[B]^2,{A,0,Pi/2},
{B,0,Pi/2},PlotRange->{{0,Pi/2},{0,Pi/2},
{-.7580,.7580}},AxesLabel->{"Alpha","Beta",""}]

HemiQuadric Surface - Q15
```

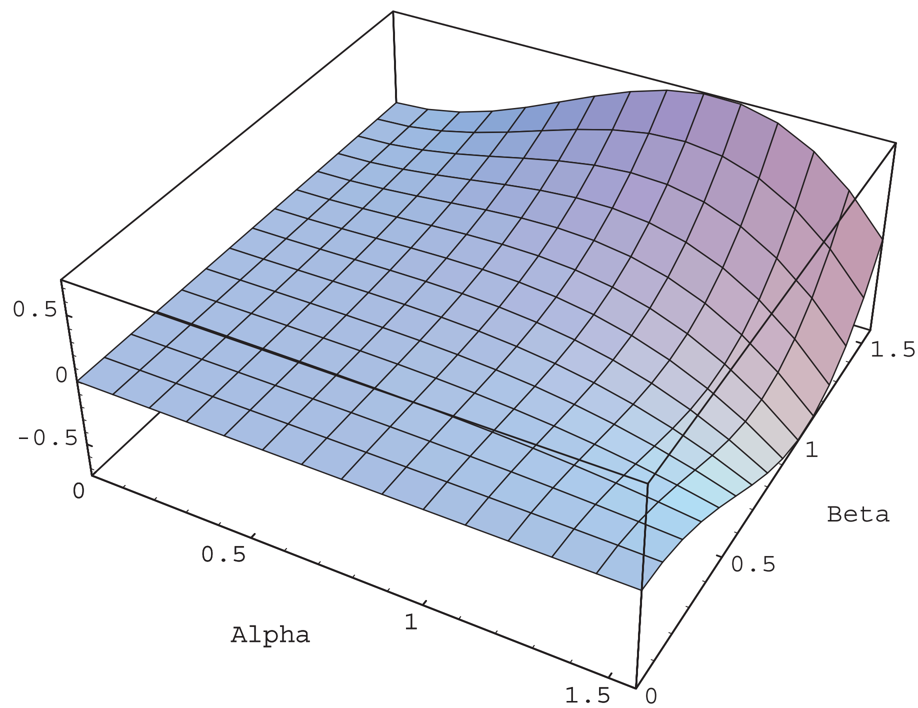


```
-SurfaceGraphics-
```

```
"Figure - 14i Hyperbolic Cosine Law of Gravity Warp"

(TGW)=23.2466
Plot3D[((ArcTan[(TGW)/(RX)]^2)/(X^2)*(Cos[X]^2))-
((TGW)^2/(RX)^2)-1,{X,-Pi/2,Pi/2},{(RX),-50,50},
PlotPoints->{50,50},PlotRange->{{-Pi/2,Pi/2},
{-50,50},{-1000,3000}},ViewPoint->{5,-2.4,2},
AxesLabel->{"Theta","Rest Distance",""}]
```

Figure - 14i Hyperbolic Cosine Law of Gravity Warp

23.2466

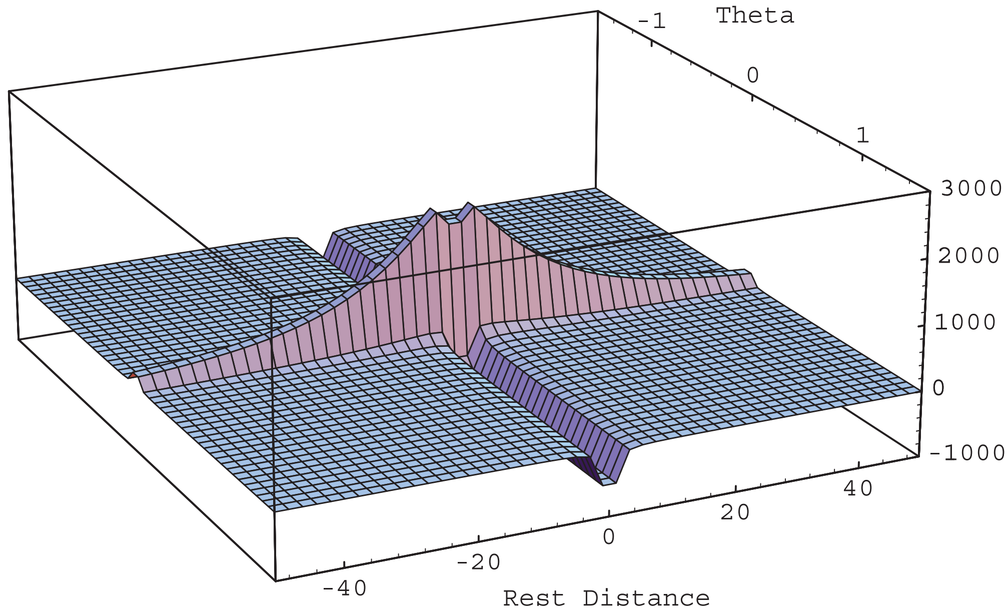

-SurfaceGraphics-

```
"Figure 15i - Quadric Surface - C8"

Plot3D[(X^2)*Cos[X]^2-(Y^2)*Cos[Y]^2,
{X,0,Pi/2},{Y,0,Pi/2},PlotRange->{{0,Pi/2},
{0,Pi/2},{-.31489,.31489}},AxesLabel->
{"Theta","Gamma",""}]

Figure 15i - Quadric Surface - C8
```

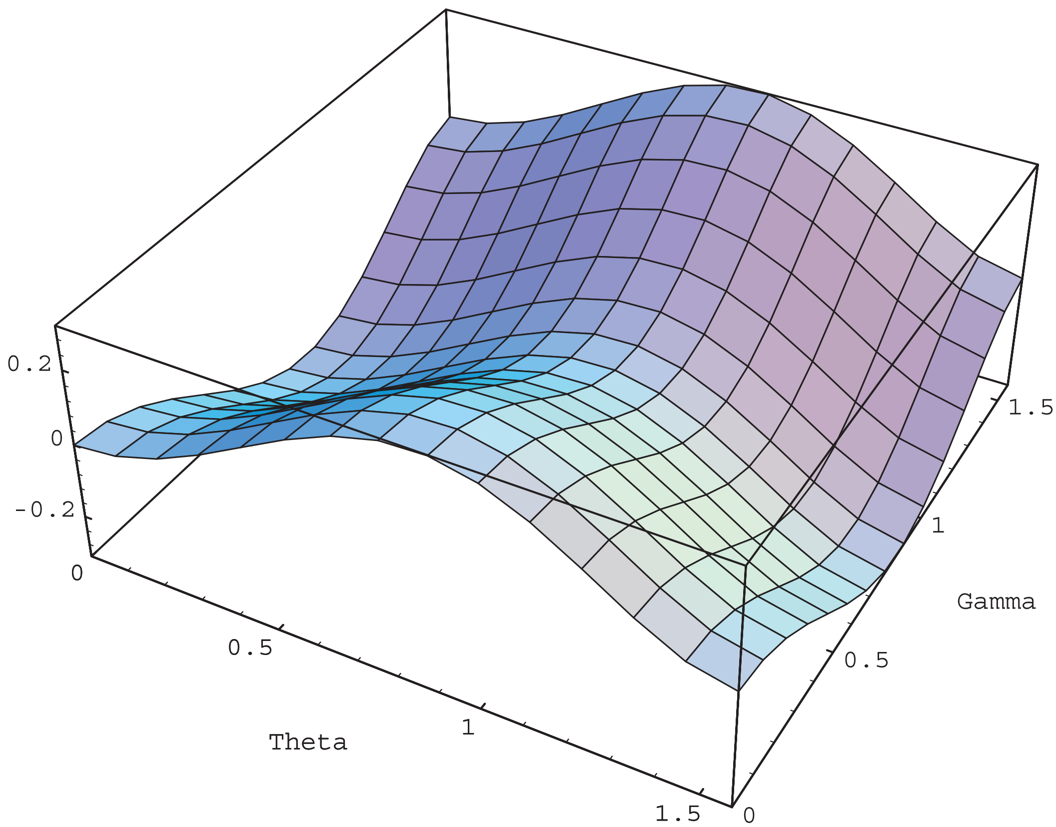

-SurfaceGraphics-

```
"Hyperbolic Paraboloid Gravity-Warp Cone"

(RX)=23.2466
Plot3D[(((14.7992*X)^2)/(ArcTan[(TGW)/(RX)]^2))-
((RX)^2)/(((RX)^2+(TGW)^2)),{X,-Pi/10.30,Pi/10.30},
{(TGW),-30,30},PlotPoints->{70,70},PlotRange->
{{-Pi/10.30,Pi/10.30},{-30,30},{-23.2466,23.2466}},
AxesLabel->{"Theta","Grav-Radius-Warp",""}]
```

Hyperbolic Paraboloid Gravity-Warp Cone

23.2466

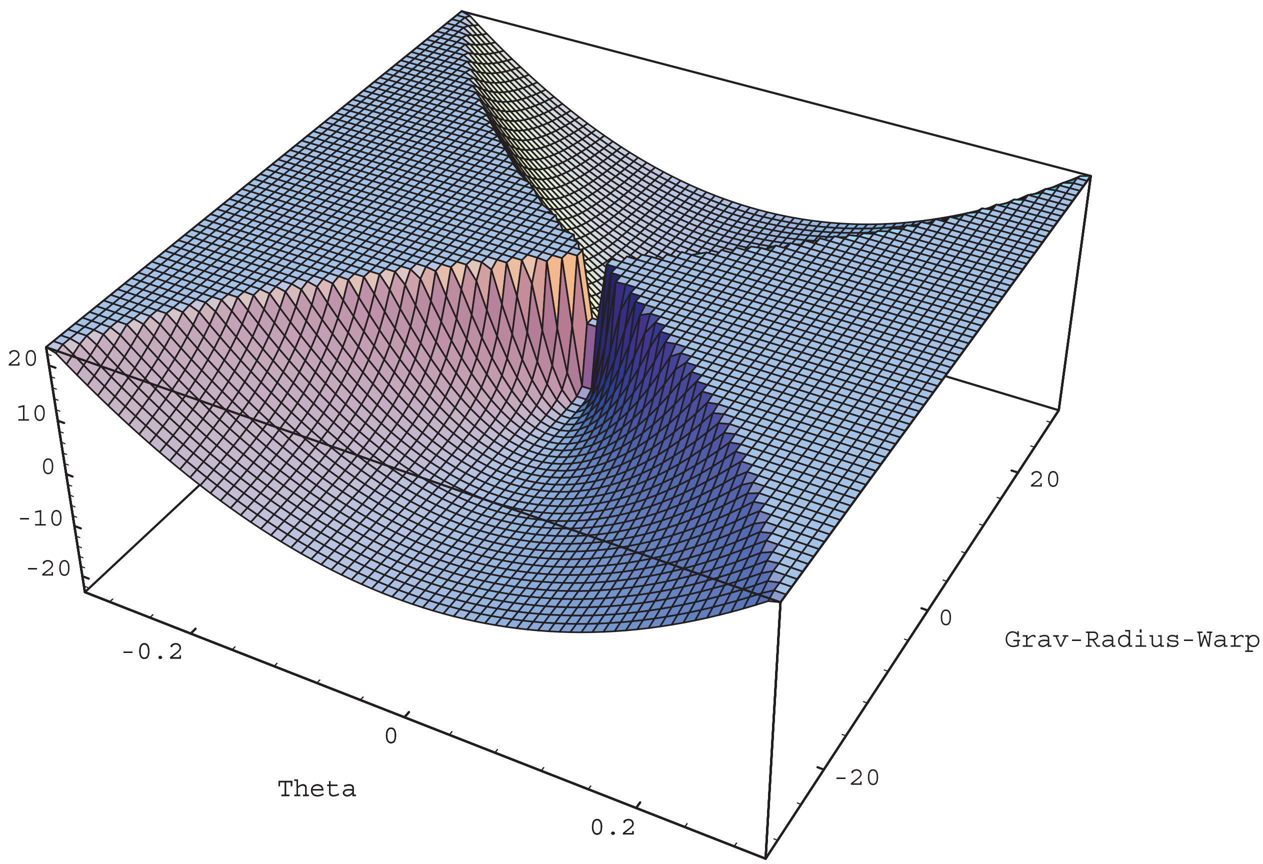

-SurfaceGraphics-

```
"Daughter Gravity Warp Equation Parabola"

(TGW)=23.2466
Plot3D[((X^2)/((RX)^2))-((ArcTan[(TGW)/(RX)]^2)/
((TGW)^2+(RX)^2)),{X,-Pi/2,Pi/2},
{(RX),-23.2466,23.2466},
PlotPoints->{72,72},PlotRange->
{{-Pi/2,Pi/2},{-23.2466,23.2466},
{-2,23.2466}},AxesLabel->
{"Theta","Rest Radius",""}]
```

Daughter Gravity Warp Equation Parabola

23.2466

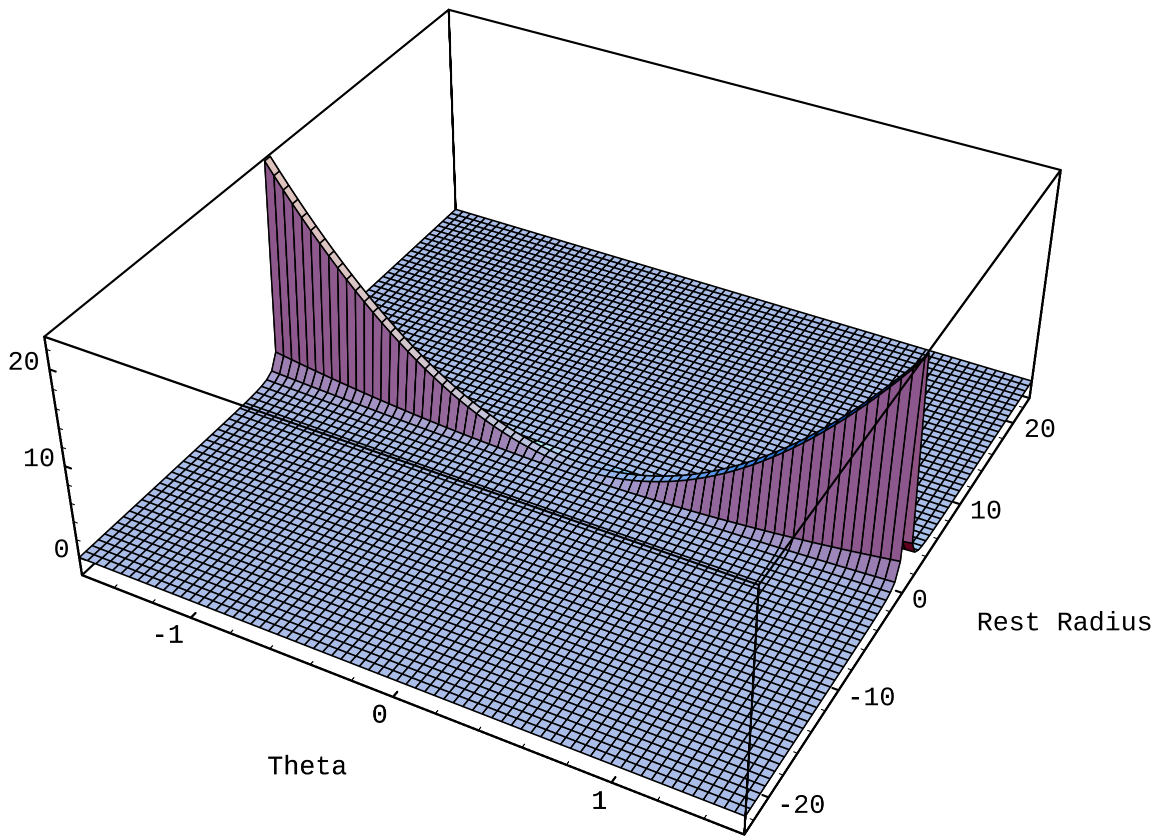

-SurfaceGraphics-

"Figure 18i - 1st Order Partial Differential"

```
TGW=11.6233
Plot3D[2*X/ArcTan[TGW/RX]^2,{X,-Pi/2,Pi/2},
{RX,-23.2466,23.2466},PlotPoints->{20,20},
PlotRange->{{-Pi/2,Pi/2},{-23.2466,23.2466},
{-14.6123,14.6123}},Axes->True,AxesLabel->
{"Theta","Rest Radius","df/d(theta)"}]
```

Figure 18i - 1st Order Partial Differential

11.6233

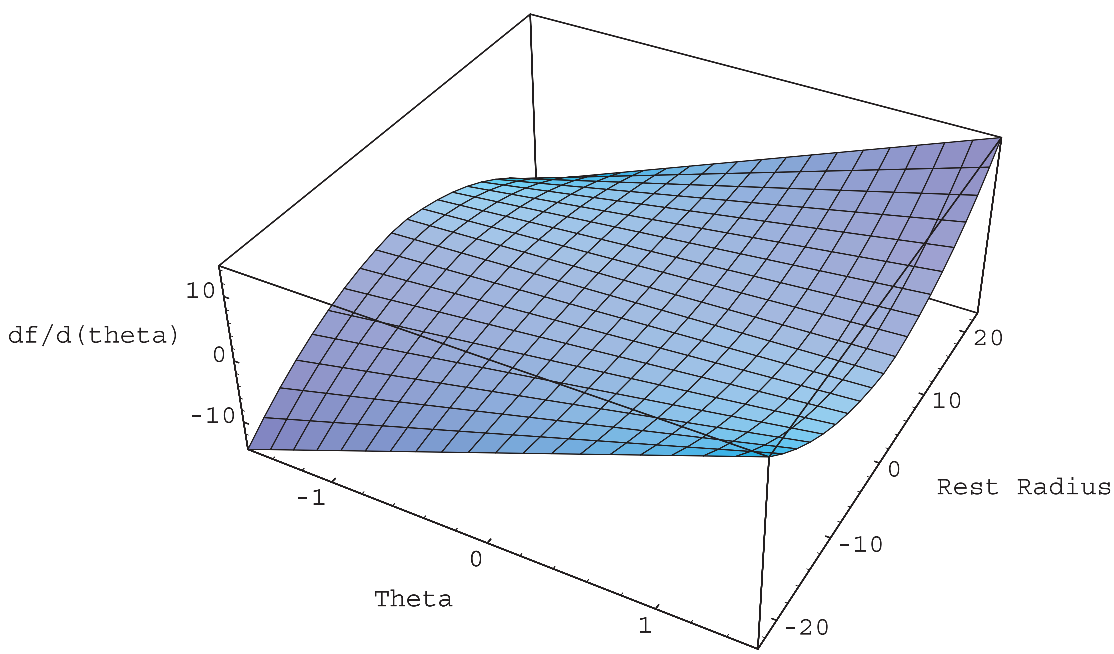

-SurfaceGraphics-

```
"HemiQuadric Surface - Q15i"

Plot3D[(B^2)*Sin[A]^2-(A^2)*Sin[B]^2,{A,0,Pi/2},
{B,0,Pi/2},PlotRange->{{0,Pi/2},{0,Pi/2},
{-.7580,.7580}},AxesLabel->{"Alpha","Beta",""}]

HemiQuadric Surface - Q15i
```

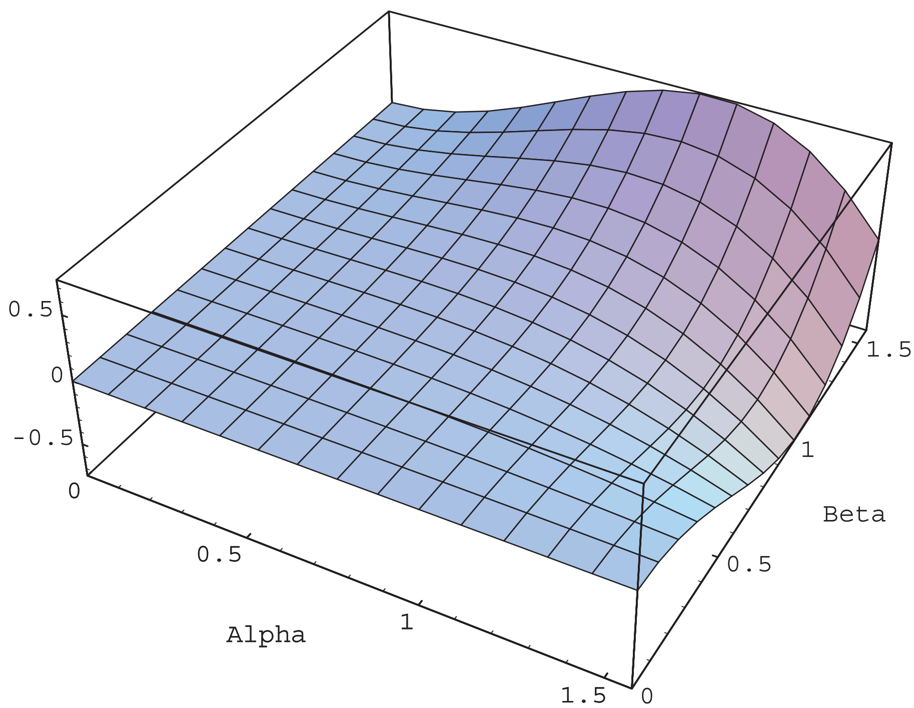


```
-SurfaceGraphics-
```